HIGH-ENERGY SEAFLOOR PROCESSES AND BIOLOGICAL REWORKING AS FIRST-ORDER CONTROLS ON MUDSTONE COMPOSITION AND GEOCHEMISTRY

A thesis submitted to the School of Graduate Studies

in partial fulfillment of the requirements for the degree of Philosophiae Doctor

Memorial University of Newfoundland

May 2014

St. John’s Newfoundland

ABSTRACT

This PhD research project aims to develop a better understanding of how physical seafloor reworking and macrofaunal bioturbation control the lithofacies variability of mudstones deposited under high-energy seafloor conditions. To address this aim, bioturbated and unbioturbated mudstones from two natural laboratories in Newfoundland, Canada and Baja California, Mexico were investigated. Sections of interest were logged at a cm-scale and organic and inorganic geochemical measurements were performed on bioturbated and unbioturbated mudstones within both successions. To improve the fidelity of paleoenvironmental reconstructions these geochemical measurements were combined with high-quality sedimentological and ichnological datasets at a range of length scales. Unbioturbated mudstones in the Early Ordovician Bell Island Group, Newfoundland, previously reported to have been deposited under anoxic conditions, instead, most likely originated as hyperpycnal flows and wave-enhanced sediment gravity flows. The proximity to a fluvial source and residence time of rock components in the near-surface zone are interpreted to be the primary control on the compositional heterogeneity of mudstones within this Ordovician mud-dominated shoreface paleoenvironment. Following this, high-energy seafloor conditions are a more realistic explanation for the high presence of unbioturbated mudstones in the heterolithic Bell Island Group. Additionally, the formation mechanism of shrinkage (‘synaeresis’) cracks, which are sedimentological prime indicators for salinity fluctuations in marginal-marine environments, has been re-evaluated. Sediment cracking is proposed to form as an exclusively intrastratal process, independent of fluctuations of pore water salinity. Spatial rheological inhomogeneities associated with microbial mat decay shortly after burial are

proposed to produce intrastratal shrinkage cracks. The effect of bioturbation on the geochemical variability of mudstones has been investigated within mudstones and fine-grained sandstones of the Rosario Formation, Mexico. The spatial distribution of organic carbon and redox-sensitive trace elements is controlled by the feeding activity of grain-size selective vermiform animals and associated in-vivo alteration of weathering-susceptible minerals. The reactivity of organic carbon is proposed to be a critical variable controlling pathways of diagenesis in bioturbated mudstones. It is imperative that paleoenvironmental analyses consider the long-term effects of bioturbation and high-energy seafloor processes to fully understand the compositional variability of mudstones within a basin-wide context.

ACKNOWLEDGEMENTS

I would like to thank my supervisor Dr. Duncan McIlroy for his guidance, support, and the chance to pursue research on such a timely and interesting topic. I have learned a great deal from you over the past few years that will continue to be invaluable as I move on through both my career and life. I also extend my gratitude to Dr. Richard Callow and Dr. Graham Layne, who both served as advisors on my supervisory committee and shared their experience and insight during challenging times that I encountered during my research. The support and love of my fiancé Kathryn has been critical to my success and to the completion of this degree. I would like to thank you for motivating me and helping me to stay focused. Finally, I would like to thank my family, my father Aleksandar, my mother Smiljana and my brother Mario, for their advice and support, which have made it possible for me to pursue this degree. Without their help I would have never been able to establish myself in Canada. When I started this degree in October 2008, many of the topics and techniques were new to me. Completing this work would not have been possible without the help from a number of colleagues. I am thankful to Malgorzata Bednarz, Florian Bulle, Lina Stolze, Elizabeth Schatz, Peter Hülse and Elisabeth Kahlmeyer, who supported me and always gave advice when it was needed. I would also like to thank the members of the MUN Ichnology Group, Chris, Robyn, Tiffany and Mary – you made the office and the lab a great experience. Your friendship is something that I will carry with me for the rest of my life. I gratefully acknowledge the financial support I received from the Natural Science and Engineering Research Council of Canada (NSERC) as well as various student grants sponsored by AAPG, SEPM, IAS and GSA.

TABLE OF CONTENTS

LIST OF TABLES

CHAPTER 2

CHAPTER 4

LIST OF FIGURES

CHAPTER 1

CHAPTER 2

CHAPTER 3

CHAPTER 4

LIST OF APPENDICES

CO-AUTHORSHIP STATEMENT

This doctoral dissertation is subdivided into five chapters. The core part of the thesis, chapters 2 to 4, is written in manuscript format. Chapter 1 provides context for the dissertation and defines the specific problems to be addressed (in the individual papers or chapters), reviews existing knowledge and describes the project significance. Additionally, the objectives are outlined and the various study areas are introduced. Chapters 2 to 4 are written as focused research papers that present the research completed as part of this doctoral dissertation. Each research paper includes an introduction, a methods and materials section, a description of the results, and a discussion and conclusion. Chapter 5 integrates the individual objectives, summarizes the overall findings of this study and outlines potential avenues for future research.

Chapters 2 to 4 have all been collaborative efforts between myself (as the thesis author) and others. For each manuscript-based thesis chapter I outline the work personally done and the contributions made by my co-authors. As the author of this thesis, the work is predominantly my own, with guidance from my supervisor Dr. Duncan McIlroy.

Chapter 2 investigates the depositional mechanisms and organic carbon characteristics within fine-grained sediments in the Cambro-Ordovician Bell Island Group. Samples have been obtained through several field trips between 2009 and 2012. I have carried out the field work and performed all the laboratory work, with the help of Kathryn Denommee, Florian Bulle, Peter Hülse and Stefanie Lode. This chapter is currently in review with the *Journal of Sedimentary Research*. Chapter 3 is a focused research paper that investigates the formation mechanisms of shrinkage cracks in shallow-marine storm-dominated systems. This chapter has been a collaborative effort between me, my supervisor, Dr. Duncan McIlroy and Dr. Richard Callow (University of Aberdeen, UK), who both have several years of experience in the field of ancient mat-building, surface-attached communities. This chapter has been published in the journal *Sedimentology*. Chapter 4 investigates the distribution of organic carbon and redox-sensitive trace elements in bioturbated sandstones and mudstones from the Pelican System, Rosario Formation, Mexico. I have performed the laboratory work and have interpreted the data. Richard Callow has provided vital information on the sedimentological context of the Rosario Formation and the majority of the sample material from this locality. Roy Wogelius, Nicholas Edwards, Phillip L. Manning (University of Manchester, UK) and Uwe Bergmann (SSRL, Palo Alto, USA) have expert knowledge on synchrotron-based elemental imaging. All of the contributing authors assisted in designing the measurement protocol and helped with processing of the XRF data. I, as the lead author, have written the manuscript with editorial assistance of all contributing co-authors.

Funding for this work was mainly provided in the form of a grant from the National Sciences and Engineering Research Council of Canada (NSERC) and the Canada Research Chair (CRC) Program, awarded to Dr. Duncan McIlroy. Additional funding has been awarded to me from the American Association of Petroleum Geologists (AAPG), International Association of Sedimentologists (IAS), Society of Sedimentary Research (SEPM) and the Geological Association of America (GSA).

CHAPTER 1

MUDSTONE SEDIMENTOLOGY: INTRODUCTION AND OVERVIEW

1. Project overview and problem statement

Mudstones (sedimentary rocks with a median grain size of < 62.5 μm; Folk 1974) are the most important part of every petroleum system (Tissot and Welte 1978). Mudstones are the volumetrically most abundant (>65%) sedimentary rock type exposed on the modern Earth surface, but the controls on their lithofacies variability are relatively poorly understood in comparison to coarse clastics and carbonates (Aplin et al. 1999). They serve as source rocks (Katz 2005), seals (Watts 1987), and even, in certain geological situations, as a regionally important reservoir (Passey et al. 2010; Aplin and Macquaker 2011 and references therein). Marine mudstones accumulate across a wide variety of water depths and hydrodynamic regimes. Thick successions of mudstones accumulate in silled basins (Demaison and Moore 1980), wave-dominated shorefaces (Plint et al. 2012) and deltaic environments (Hovikoski et al. 2008), as well as deep marine environments (Faugeres and Stow 1993).

Classic diagenetic theory emphasizes that the underlying lithofacies variability of mudstones reflects a combination of (a) the starting composition of the parent material, (b) the weathering history of the unconsolidated, highly reactive mixture of minerals and

grains (Aplin 2000) and (c) pressure- and temperature-driven mineralogical changes during deep burial (Wilson & Pittman 1977; Bjørlykke 1998). The effect of burial diagenesis is comparatively well understood because this process operates on geological time scales and is readily reconstructed from the rock record (Potter et al. 2005). A great deal of textural and compositional variability within mudstones however cannot be explained by variations in initial starting composition or burial diagenetic processes.

Studies on hydrocarbon sealing efficiency reveal that porosity relationships, mineral surface area and organic matter richness (expressed as total organic carbon, TOC wt%) all can vary by at least one order of magnitude between mudstones across wide range of water depths and paleoenvironmental settings (Schlömer and Kroos 1997; Bohacs et al. 2005; Heath et al. 2011). The impact of geologically 'instantaneous events', such as biological and physical seafloor reworking are rarely incorporated into modern conceptual models of sediment generation, diagenesis and provenance (Ingersoll 1990; Weltje 2012). Hydraulic sediment transport processes and bioturbation might in fact be an important, yet little considered 'bottleneck' that preconditions the (long-term) compositional and geochemical changes of fine-grained sediment during late burial diagenesis. To date, the role of biological and physical seafloor reworking as a potentially important modifier of mudstone composition is not well understood. As opposed to sandstones or carbonates, problems arise in almost all cases when water depth, seafloor energy regime or oxygenation state of the bottom-water are to be reconstructed. These uncertainties arise, because fine-grained sedimentary rocks often do not exhibit sufficient hand-specimen variability to determine the underlying physical and biogenic processes that led to their formation (Schieber 1998). In mudstones diagnostic sedimentary

structures as well as mudstone ichnofabrics are often very small (<1 mm in diameter) and difficult to observe if hand specimens are not polished or examined via petrographic methods (Schieber 1998; Wetzel and Uchman 1998). In order to increase the fidelity of paleoenvironmental reconstructions, and to formulate reasonable geological models for mud-dominated systems, an integrated approach is needed. The analytical approaches within this thesis encompass descriptions of sedimentological and ichnological relationships at the sub-hand specimen scale (scales of 10^{-1} to 10^{-3} m) and integrate these datasets with conventional whole-rock geochemical techniques (Potter et al. 2005; Schieber et al. 2007; Ratcliffe et al. 2012). A well-defined process-sedimentological framework combined with geochemical and petrophysical rock properties allows the development of more realistic geological models that improve exploration efforts in a wide range of depositional environments.

1.1 Lithofacies variability in fine-grained sedimentary rocks: Classic conceptual models

During recent decades, the study of mudstone petrology and geochemistry was chiefly driven by the needs of the North American petroleum industry, who sought to develop an understanding about the mechanisms that underlie organic matter production and preservation in fine-grained sedimentary rocks (Yergin 2011). In order to predict the location and basin-wide extent of petroleum source rocks (organic rich mudstones with >2 wt% total organic carbon; Tissot and Welte 1978) research efforts were targeted in

modern settings towards bottom sediments and the water column, where processes that likely control organic carbon preservation are most easily observed (reviews in Katz et al. 2005; Bohacs et al., 2005; Harris 2005). The most celebrated examples of potential modern day source rock formation include the periodically anoxic borderland basins of California (Berner 1964; Thunell 1998), the Black Sea (Demaison and Moore 1980; Pedersen and Calvert 1990), the dynamic coastal upwelling systems with seasonally well-developed oxygen minimum zones along the western margins of continents (Helly and Levin 2004), and highly productive meromictic lakes (Hollander et al. 1992). After decade-long research, converging evidence from modern as well as ancient systems indicate that the preservation of marine organic carbon is maximized when relative to inert dilution by siliciclastic particles (a) sufficient amounts of reactive organic carbon reach the sea floor and (b) when the contact time of organic carbon with potential oxidants, such as oxygen or sulfate is limited (Henrichs and Reeburgh, 1987). The importance of bottom-water anoxia was at that time rooted in the (now discredited) assumption (Pompeckj 1909; Woolnough 1937) that anaerobic bacteria, the most important decomposers of organic carbon, are less efficient in remineralizing organic carbon than aerobic bacteria (summarized in Wignall 1994).

1.2 Shallow-marine mud-dominated systems: The motivation for extending existing facies models

In the light of the above, it is often difficult to rank anoxia, salinity fluctuations and frequent physical seafloor reworking as potential reasons for unbioturbated mudstones

when the majority of mudstones within a shallow-marine depositional paleoenvironment are bioturbated. A possible solution to this problem is the rigorous sedimentological description at a range of spatial scales (as undertaken in chapter 2 and 3) could for example help to eliminate persistent water-column anoxia as one candidate for unbioturbated mudstones when sediment structures (e.g., ripples, grooves and other erosional features) instead indicate the influence of surface gravity waves and bottom currents during mud deposition (e.g., Hollister and McCave 1984).

On the modern Earth, restricted basins and truly anoxic quiet water environments make up only a very small proportion of the environments that accumulate mud (Parrish 1995; Trabucho-Alexandre et al. 2012). Instead, the volumetrically highest percentage (>50%) of organic-rich mud-grade material accumulates in shallow-marine depocenters such as estuaries, deltas and wave-dominated coastlines (Burdige 2005; Walsh and Nittrouer 2009; Blair and Aller 2012). Mud-dominated successions accumulating in the vicinity of fluvial sources with high suspended sediment load are currently not well understood and integrated into existing shallow-marine siliciclastic facies models (Plint 2010). In these environments, the accumulation of mud is highly dynamic. Weathering-derived clay minerals, which are drained in large amounts from river mouths into the world's oceans, are able to develop opposing surface charges when negatively charged clay surfaces come into contact with positive charged ions in seawater (e.g., Na^+, K^+; Potter et al. 2005). Resulting 'face to edge attraction' of clay minerals leads to formation of card house fabrics, allowing clay minerals to flocculate and deposit quickly in shallow water in close proximity to the shoreline (e.g., Windom 1976). Storm-induced, offshore-directed surge-currents operate in combination with alongshore-directed, geostrophic

currents as the main dispersal mechanism of fine-grained material (Hill et al. 2000; Mulder and Syvitski 1995; Allison et al. 2007). Furthermore, wave- and gravity-driven combined flows are capable of transporting high volumes of flocculated clay and organic carbon away from river mouths beyond the nearshore wave-induced 'littoral fence' which tends to trap sand close to the shoreline (Elliott 1989) and resuspend sediment along and oblique to the shoreline (Keil et al. 1997; Allison et al. 2000; Friedrichs & Wright 2004). On low-slope (<0.5%) wave-dominated shelves, wave-advected sediment gravity flows of fluid mud (suspended solid concentration >10g L^{-1}; Kirby & Parker 1983; Mehta & McAnally et al. 2002) are the major sediment transport mechanisms. The energy required to hinder floc and grain settling and maintain sediment in suspension is augmented by near-bed currents and the superimposed orbital motion of surface gravity waves (Traykowski et al. 2000). If the supply of sand to the shelf is restricted, the shoreface can be the locus of mud accumulation (e.g., Amazon-Orinoco coastline; Rine and Ginsburg 1985; Anthony et al. 2010).

Understanding shallow-marine depositional environments of mud has potentially significant implications for fully characterizing the facies variability of mudstones deposited on the entire margin to basin transect. Modern conceptual models of marine sediment generation predict that freshly deposited river borne sedimentary layers will exhibit a strong compositional connection to sources of mud production up-dip (Xu et al. 2009; Weltje 2012). Energetic shelves down drift from large rivers with high suspended sediment load accumulate thick successions of mud – preferentially after pulsed discharge events (i.e., flash floods; Ogston et al. 2000). Compositionally, these mud layers are dominated by the chemical breakdown products of primary Al-silicates (e.g. feldspars)

and are delivered as river borne flocculated clay from soil profiles up dip (Langmuir 1997; Nesbitt and Markovics 1997). The weathering history of the parent rock in the hinterland and its position with respect to regional climate (Milliman and Syvitski 1992) determines the grain size distribution as well as the "freshness" of the fine-grained material (e.g., Ingersoll 1990). In regions dominated by physical weathering, mud layers can contain a high contribution of unaltered feldspar, pyroxene and amphibole that are introduced as glacial rock flour or volcanic ash (Potter et al. 2005). During deep burial, unweathered high-temperature crystalline debris will produce late diagenetic quartz cement and characteristic clay mineral assemblages (e.g., higher contributions of chlorite) (Chamley 1989; Fedo et al. 1995; Kennedy et al. 2005). The importance of unweathered, highly reactive mud-grade material versus highly weathered clay-rich mud as a control on lithofacies variability is not well described in current compositional studies of ancient mud-dominated depositional environments (Potter et al. 2005).

The source composition and mixing history of the organic carbon fraction of sedimentary layers that are deposited on shorelines within the vicinity of rivers will differ systematically from mudstones that originate in offshore regions with high marine water-column productivity. The former lithologies accumulate terrestrial organic matter that is successively replaced by marine organic carbon further offshore (Goñi et al. 2003; Miserocchi et al. 2007). Seasonal and diurnal wave- and tidal reworking in nearshore muddy surface sediment results in frequent re-oxidation of anoxic sediment layers and the prevalence of microbially-mediated, suboxic diagenesis (Aller 1998). Frequent wave resuspension also causes the freshly entrained organic carbon to be exposed longer to suboxic microbial degradation (high availability of oxygen or sulfate) and potentially lose

its attractivity as a food source to macrofaunal bioturbators (Leithold and Hope 1999). Classic facies models incorporate periodic hyposaline and hypoxic bottom-water conditions as a major reason for spatio-temporal changes in bioturbation intensity in ancient marginal-marine depositional environments (Demaison and Moore 1980; Gingras et al. 2011). The chapters 2 and 3 of this thesis investigate this postulated relationship and evaluate the different potential reasons that might be responsible for the generation of unbioturbated mudstones.

1.3 Bioturbation: an important control on the composition of solids in the near surface zone

Chapter 4 of this thesis investigates the effect of bioturbation, as an important modifier of solids below the sediment-water interface. At the sediment surface the transformation of primary minerals to simpler phases occurs under low-temperature and low-pressure conditions (Aplin 2000). The processes necessary to degrade this highly reactive mixture are chiefly driven by a diverse microbial community whose catabolic activity is fueled by a mixture of bioavailable organic matter (as the most commonly occurring renewable reductant) and an assemblage of inorganic oxidizing agents such as O_2, NO_3^-, MnO_2, Fe(OH), SO_4^{2-}, PO_4^{3-} (Tyson 1995). The core of this concept, commonly referred to as early diagenesis, is that all diagenetic reactions are vertically structured (Fig. 1A), (Froelich et al. 1979; Canfield 1993). When considered in detail, however, this model is only valid for certain geological situations and highly complicated in sediments where (a) wave reworking (Aller et al. 2004), and (b) meio- and macrofaunal particle

redistribution (Zhu et al. 2006) modify primary bedding relationships. Unfortunately, the majority of classic geological models marginalize the role of animals as predominantly "physical disturbance" (e.g. Boudreau and Jorgensen 2000) of an initially vertical microbial reaction geometry that quickly re-equilibrates to stratified conditions (sensu Froelich et al. 1979) once bioturbation ceases. While this is true to some degree for the concentration of fluids and gases (Zhu et al. 2006), modern research has demonstrated that meio- and macrofauna are powerful modifiers of the mineralogical and geochemical variability of solids in fine-grained sediment (McIlroy et al. 2003; Needham et al. 2005, 2006:

a) The hostile gut environment of polychaetes accelerates the alteration of high-temperature crystalline debris and produces neo-formed clay minerals faster than naturally occurring chemical weathering reactions (McIlroy et al. 2003). Biological (in-vivo) weathering has the potential to be a significant vector in mineral transformations prior to long-term burial.

b) It is long accepted that animal feeding alters the molecular composition of organic carbon (e.g., DeNiro and Epstein 1979; Checkley and Entzeroth 1985) and imparts significant shifts on the isotopic ratios of residual organic carbon. The preservation potential of a macrofaunal (not microbial) influence on sedimentary organic matter is to date poorly understood (e.g., Pratt et al. 1986).

c) A large number of redox-sensitive divalent and trivalent transition metals are commonly applied as proxies for the reconstruction of biogeochemical processes in ancient water-columns and sediment (e.g., oxygenation state of the water column or productivity indicator for ancient seas). These elements have been demonstrated to show specific isotopic fractionation behavior or component-specific concentrations, depending on the oxygenation state, pH and Eh conditions in pore waters (Tribovillard et al. 2006). The construction and irrigation of permanent burrows by bioturbating macrofaunal invertebrates (e.g., bivalves, crustaceans and polychaetes) increases the downward diffusion of oxygen below the sediment-water interface and skews the geometry and the dynamics of a vertically stratified microbial zonation (Aller 1982; Grossmann and Reichardt 1991; McIlroy and Logan 1999; Zhu et al. 2006; Stockdale et al. 2010). To date little is known about how macrofaunal activity controls the distribution of redox sensitive trace elements in sedimentary rocks. Chapter 4 examines the spatial variability of organic carbon and trace elements in bioturbated sand- and mudstones from a well-preserved depositional environment.

1.4 Physical and biological seafloor reworking as a major control on the geochemistry and composition of fine-grained sediment: Three working hypotheses.

The contribution of physical and biological sea floor processes and their role in controlling diagenetic patterns in modern seafloor sediment is undisputed. However, the extent to which these processes control the textural and geochemical attributes of rocks has, to date, not been completely integrated into sedimentological facies models. Using two well-preserved mud-stone rich successions `from Newfoundland and Mexico, this Ph.D. thesis aims to help bridge this knowledge gap by a) investigating the vertical and lateral facies distributions of mudstones deposited under a wide range of paleo seafloor conditions; b) re-examining the role of previously postulated relationships between salinity and oxygen as a prime control on bioturbation intensity, and c) defining the ability of vermiform animals to manipulate both the organic carbon and redox-sensitive major element characteristics of fine-grained siliciclastic rocks during foraging and feeding. Within this thesis three hypotheses were tested:

a) *Laminated mudstones are commonly the depositional products of high-energy seafloor processes rather than being associated with low energy bottom water anoxia. (Chapter 2)*

Shallow-marine systems close to river mouths periodically experience high-suspended riverine sediment discharge, off-shore directed mud density flows, and

seasonal wave- and current-driven reworking of previously emplaced semi-consolidated deposits (e.g., Young and Southard 1978). These dynamic seafloor conditions can manifest themselves in stark lateral fluctuations of bioturbation intensity (*sensu* Taylor and Goldring 1993), and consequently produce a high volume of unbioturbated mud layers (Aller and Stupakoff 1996). In paleoenvironmental studies, unbioturbated mudstones are often used as critical indicator of the inability of most marine endobenthic animals to tolerate even small deviations from oxygen and salinity conditions that are 'normal' for a given species (e.g., Whitfield et al. 2012). Alternative interpretations, such as high sedimentation rate or repetitive sediment reworking, are often not employed in paleoenvironmental reconstructions as they require detailed sedimentological description of the mud-dominated interbeds. The presence of cm- and mm-scale erosional features (e.g., gutter casts, continuous mud-on-mud and mud-on-sand erosional contacts), mm-thick graded beds, and silt- and sand-sized intraclasts with variable composition are diagnostic recognition criteria for periodic wave-reworking and bed load transport of sand-sized mud aggregates (Plint et al. 2012).

Chapter 2 integrates the sedimentology and geochemistry of previously unstudied mud-dominated sections of the well-exposed Ordovician Beach Formation on the eastern Avalon Peninsula of Newfoundland. Sedimentological and lithofacies data obtained from bioturbated and unbioturbated mudstones are used to develop a combined sedimentological-geochemical facies model that accounts for high-energy seafloor processes, and allows the identification of muddy coastlines from the rock record. Specific preference was given to unbioturbated mudstones, as they were previously

interpreted as having been deposited under hypoxic and periodically hyposaline conditions (Brenchley et al. 1993).

b) *Salinity fluctuations are not necessarily a major control on the bioturbation intensity and style in marginal-marine mudstones (Chapter 3)*

The presence of intrastratal shrinkage ('synaeresis') cracks in unbioturbated marine mudstones is commonly regarded as key evidence for a salinity-stressed near-shore environment (e.g., Wightman et al. 1987; Pemberton and Wightman 1992). Intrastratal shrinkage cracks are common in shallow-marine depositional environments prior to the Devonian (Pratt 1998), and are commonly employed as marginal-marine facies indicators in the subsurface, especially when other diagnostic criteria are lacking. However, to date, their origin, formation mechanism, and relationship to paleoenvironmental conditions has not been fully and convincingly described. One popular model favors the fragmentation of semi-lithified, heterolithic strata during seismic events (Pratt 1998). Another popular model favors the cracking of mud as a result of the contraction of clay-mineral lattices under fluctuating pore-water salinities (Jüngst 1934). By integrating ichnological, sedimentological, petrographic and geochemical data chapter 3 investigates a third previously hypothesized, but to date never tested model, that describes the shrinkage of mud and subsequent sediment cracking as a passive process that occurs during organic matter decay.

c) *Bioturbation exerts a significant control on the small-scale (<10 mm) spatial distribution of organic matter and trace elements in fine-grained siliciclastic sediments (Chapter 4)*

The two-dimensional distribution of organic carbon and trace elements in moderately bioturbated mudstones is virtually unknown. Building on previous morphological studies of the common mudstone trace fossil *Phycosiphon* isp. (Bednarz and McIlroy 2009, 2012) chapter 4 chapter specifically investigates if the spatial distribution of clay minerals, organic carbon concentration, and redox-sensitive trace metals co-varies with the spatial distribution of phycosiphoniforms, and if compositional differences exist between single burrow elements (i.e., halo and core) and the unbioturbated host sediment. It is hypothesized that endobenthic, grain-size selective deposit feeders directly alter sediment composition, that goes beyond a pre-compaction disturbance of primary sedimentary fabric. Phycosiphoniform trace fossils have a wide ecological occurrence and are produced by grain size-selective deposit feeders. They are a common trace fossil in mudstones and are regularly encountered together with *Chondrites* isp. and *Zoophycos* isp. throughout a wide variety of depositional environments (e.g., Savrda and Bottjer 1991). Previous studies revealed that bioturbated mudstones contain a different organic carbon composition than unbioturbated mudstones (e.g., Pratt et al. 1986). This conclusion, deduced from whole rock biomarker analyses carried out on the cm-scale between laminated and unbioturbated mudstones, show significant differences when compared to bioturbated mudstones from the same succession. In this study Pratt et al. (1986) proposes that in bioturbated mudstones the altered organic matter is the result of

increased oxygen exposure time and enhanced microbial decomposition (Pratt et al. 1986). To date, the direct connection between bioturbation and organic carbon quality in sedimentary rocks has not been fully understood. This chapter investigates the quality of organic matter in bioturbated versus unbioturbated sediment within the same bed. In order to reconstruct all potential material fluxes between bioturbated and unbioturbated sediment, the analytical approach within this chapter also incorporates the analyses of redox-sensitive trace elements and clay-minerals.

2. Objectives and analytical approach

In order to test the hypotheses above, this PhD project was designed with two objectives: (1) to characterize the vertical and lateral facies heterogeneity of the mudstone-dominated parts of the Beach Formation in order to resolve the functioning of this ancient shallow-marine mud-dominated system; (2) to understand how common black shale bioturbators such as phycosiphoniforms control the organic carbon and the distribution of trace elements in fine-grained sandstones.

The following analytical approaches were used to address these objectives:

a) To develop a better understanding of the sea-floor conditions during deposition of mud-dominated Beach Formation, bioturbated and unbioturbated mudstones were visually examined for their sedimentary structures and grain size trends across all

available length scales. Sedimentary structures and trace fossils were described on the cm- and mm-scale from polished hand sample surfaces and polished petrographic thin sections.

b) Total organic carbon (TOC, wt %) and $\delta^{13}C_{org}$ (‰) analyses were performed, as whole-rock and as mm-scale measurements, from both bioturbated and unbioturbated intervals to test whether the organic carbon characteristics within mudstones vary as a function of sedimentological characteristics (i.e., event bed deposition versus repetitive seafloor reworking) or bioturbation.

c) To better understand the role of bioturbating animals in controlling the compositional diversity of mudstones, the composition of clay minerals and organic matter with respect to biogenic fabric were determined from both bioturbated and unbioturbated intervals. Two-dimensional trace element maps were produced for planar rock surfaces to image the spatial distribution of trace and major elements of bioturbated and unbioturbated portions of the same bed. Component-specific geochemical analyses (elemental ratios) were measured from individual phycosiphoniform burrow elements (i.e., halo and core) and compared to unbioturbated host sediment within the same bed.

3. Study areas

The best places to test these hypotheses are fine-grained sedimentary archives that contain ample evidence for mudstone deposition under periodically high-energy seafloor conditions and lateral variability in bioturbation. Two localities that meet these requirements are: 1) the Ordovician storm-dominated muddy coastline, preserved within the Beach Formation of Bell Island, Newfoundland and 2) fine-grained gravity flow deposits within an submarine channel belt exposed in the Late Cretaceous Rosario Formation (Baja California, México).

3.1 The Beach Formation, Bell Island Group, Newfoundland

Mudstone-rich rocks of the Bell Island Group outcrop on coastal exposures and in inland quarries on Bell Island on the eastern Avalon Peninsula, Newfoundland (Fig. 2). The Beach Formation is approximately 450 m thick (Ranger 1979) and consists predominantly of bioturbated, ripple-, and hummocky-cross-stratified sandstones, interbedded with bioturbated and unbioturbated silty mudstones (Ranger et al. 1979, 1984). Heterolithic, meter-thick packages of mudstones and sandstones are completely exposed along tall (~60 m) vertical cliffs around the island – with ten well-accessible outcrops that cover ~30% of the exposed stratigraphy in the Bell Island Group (Ranger et al. 1984). Previous research has focused on the geometry and lateral variability of thick shoreface sandstones. (Brenchley et al. 1993). To date, the sedimentology, ichnology and geochemistry of the mudstones have not been investigated.

Figure 1-1. A) Distribution of Cambro-Ordovician rocks on the Northeast Avalon Peninsula Newfoundland, including the working area, which is located on Bell Island (red arrow). B) Stratigraphic Column showing the Bell Island and Wabana groups. The working interval in the Beach Formation is indicated with a red arrow.

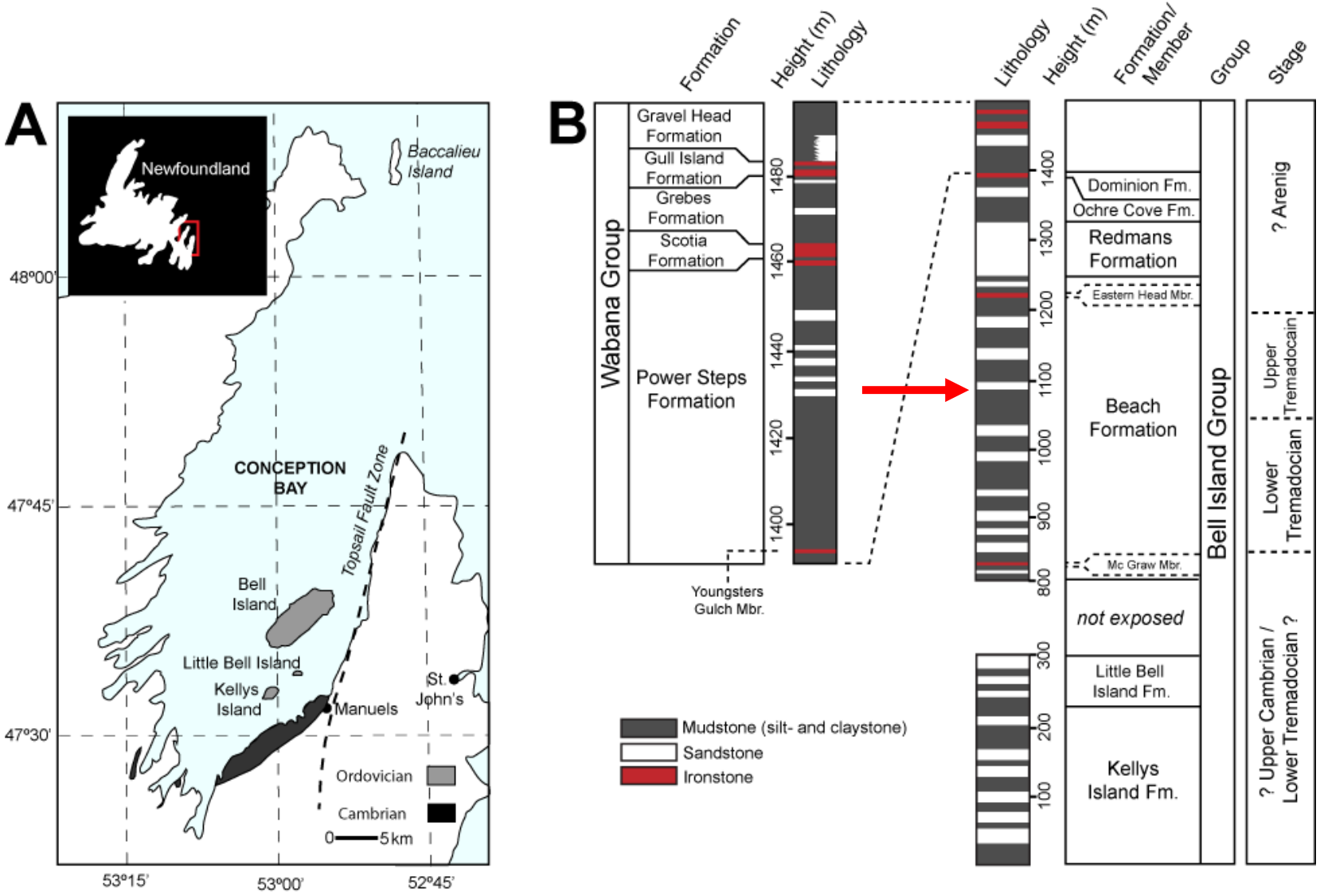
A
Newfoundland
Baccalieu Island
48°00'
47°45'
47°30'
CONCEPTION BAY
Topsail Fault Zone
Bell Island
Little Bell Island
Kellys Island
Manuels
St. John's
Ordovician
Cambrian
0 5 km
53°15'
53°00'
52°45'
B
Formation
Height (m)
Lithology
Wabana Group
Gravel Head Formation
Gull Island Formation
Grebes Formation
Scotia Formation
Power Steps Formation
Youngsters Gulch Mbr.
1480
1460
1440
1420
1400
Mudstone (silt- and claystone)
Sandstone
Ironstone
Lithology
Height (m)
Formation/ Member
Group
Stage
1400
1300
1200
1100
1000
900
800
300
200
100
Dominion Fm.
Ochre Cove Fm.
Redmans Formation
Eastern Head Mbr.
Beach Formation
Mc Graw Mbr.
not exposed
Little Bell Island Fm.
Kellys Island Fm.
Bell Island Group
? Arenig
Upper Tremadocian
Lower Tremadocian
? Upper Cambrian / Lower Tremadocian ?

3.2 The Rosario Formation, Baja California, México

Trace fossils from well-characterized deep-marine gravity flow deposits of the Late Cretaceous (Maastrichtian) Rosario Formation (Dykstra and Kneller 2009; Kane and Hodgson 2011; Callow et al. 2012) were used in this research to test the role of bioturbation in controlling organic and inorganic geochemical properties of fine-grained event deposits. The Late Cretaceous Rosario Formation is the youngest unit of a belt of Cretaceous sedimentary rocks that are exposed along the Pacific coast of southern California and Baja California (e.g., Gastil et al. 1975). The Rosario Formation comprises a deep-marine turbidite system that includes submarine channels and canyons with an overlying channel levee complex. The sedimentary units have previously been interpreted as slope deposits that were delivered as mass flows in 1500 to 3000 m water depth (Dykstra and Kneller 2009; Kane and Hodgson 2011).

At Pelican Point a small number of outcrops expose conglomerates, sandstones and mudstones belonging to the lower paleo-canyon fills of the Canyon San Fernando complex (Dykstra and Kneller 2009). Material analyzed within this study was collected from channel belt turbidites exposing cm- to dm-thick, parallel-bedded, weakly to moderately bioturbated siltstones and very fine-grained sandstones (Callow et al. 2012). These rocks contain large (up to 10 mm diameter) trace fossils suitable for geochemical analyses. The same trace fossils are also present in basinal black shales, but in much smaller size (less than 5 mm; Wetzel 1991). The deep marine, fine-grained event bed deposits at Pelican Point are therefore an ideal natural laboratory for comparison studies, because levels of late diagenetic alteration are generally low. Bioturbation constitutes

Figure 1-2. A) The Baja California peninsula in western Mexico. B) shows a simplified stratigraphic column of Cretaceous rocks exposed on the Baja California peninsula, including the Maastrichtian Rosario Formation (red arrow). C) shows the investigated outcrops north of Cajiloa (red arrow). Location map adapted from Dykstra and Kneller (2009).

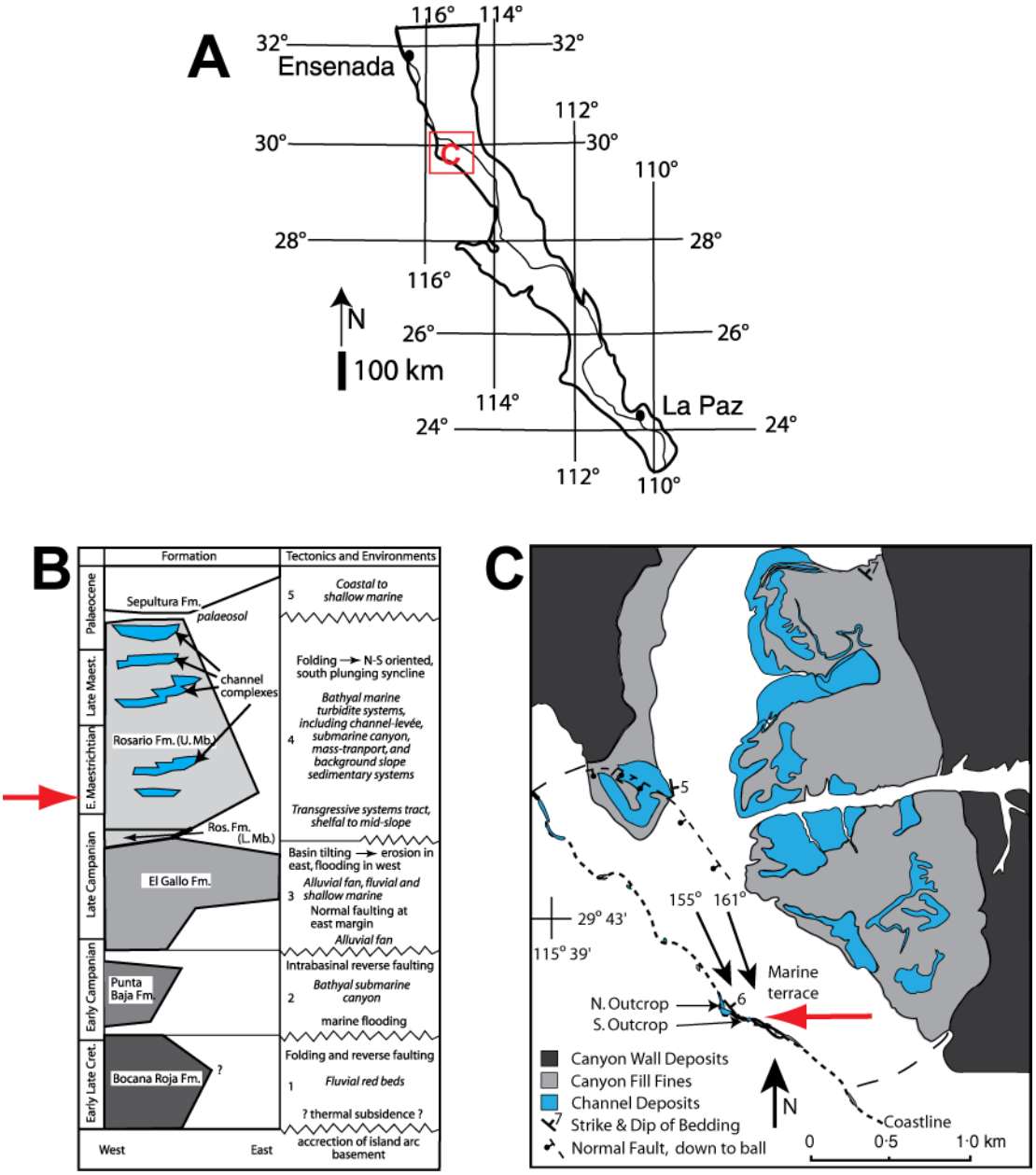
A
116°
114°
32°
Ensenada
112°
30°
C
110°
28°
116°
N
26°
100 km
114°
La Paz
24°
112°
110°
B
Formation
Tectonics and Environments
Palaeocene
Late Maest.
E. Maestrichtian
Late Campanian
Early Campanian
Early Late Cret.
Sepultura Fm.
palaeosol
channel complexes
Rosario Fm. (U. Mb.)
Ros. Fm. (L. Mb.)
El Gallo Fm.
Punta Baja Fm.
Bocana Roja Fm.
?
5 Coastal to shallow marine
Folding → N-S oriented, south plunging syncline
Bathyal marine turbidite systems, including channel-levée, submarine canyon, mass-tranport, and background slope sedimentary systems
4
Transgressive systems tract, shelfal to mid-slope
Basin tilting → erosion in east, flooding in west
Alluvial fan, fluvial and shallow marine
3
Normal faulting at east margin
Alluvial fan
Intrabasinal reverse faulting
Bathyal submarine canyon
2
marine flooding
Folding and reverse faulting
Fluvial red beds
1
? thermal subsidence ?
accretion of island arc basement
West
East
C
5
155°
161°
29° 43'
115° 39'
Marine terrace
6
N. Outcrop
S. Outcrop
Canyon Wall Deposits
Canyon Fill Fines
Channel Deposits
Strike & Dip of Bedding
Normal Fault, down to ball
N
Coastline
0
0·5
1·0 km

essentially the only post-depositional modification of primary sedimentary texture and mineralogy at Pelican Point.

4. References

ALLER, R. C., 1982, The effects of macrobenthos on chemical properties of marine sediment and overlying water. P.L. McCall, M.J.S. Tevesz (Eds.), Animal-Sediment Relations, Plenum, New York, N.Y., pp. 53–102.

ALLER, R. C., 1998, Mobile deltaic and continental shelf muds as suboxic, fluidized bed reactors: Marine Chemistry, vol. 61, 143-155.

ALLER, R.C., 2004, Conceptual models of early diagenetic processes: The muddy seafloor as an unsteady, batch reactor: Journal of Marine Research, v. 62, p. 815-835.

ALLISON, M. A., KINEKE, G. C., GORDON, E. S., AND GOÑI, M. A., 2000, Development and reworking of a seasonal flood deposit on the inner continental shelf off the Atchafalaya River: Continental Shelf Research, vol. 20, p. 2267-2294.

ALLISON, M.A., BIANCHI, T.S., MCKEE, B.A., AND SAMPER, T.P., 2007, Carbon burial on river-dominated continental shelves: impact of historical changes in sediment loading adjacent to the Mississippi River: Geophysical Research Letters, v. 34, 6 p, doi:10.1029/2006GL028362.

APLIN, A. C., 2000, Mineralogy of modern marine sediments: a geochemical framework, *in* Vaughan D. J., and Wogelius, R. A., eds., Environmental Mineralogy: Eotovos University Press, Budapest, v. 2, p. 125-172.

ANTHONY, E. J., GARDEL, A., GRATIOT, N., PROISY, C., ALLISON, M. A., DOLIQUE, F., AND FROMARD, F., 2010, The Amazon-influenced muddy coast of South America: A review of mud-bank–shoreline interactions: Earth-Science Reviews, vol. 103, p. 99-121.

APLIN, A.C., FLEET, A.J., AND MACQUAKER, J.H.S., 1999, Muds and mudstones: Physical and fluid flow properties, in Aplin, A., et al., eds., Mudstones at a basin scale: The Geological Society of London Special Publication vol. 158, p. 1–8.

APLIN, A. C., AND MACQUAKER, J. H., 2011, Mudstone diversity: Origin and implications for source, seal, and reservoir properties in petroleum systems. AAPG bulletin, vol. 95, p. 2031-2059.

BEDNARZ, M., AND MCILROY, D., 2009, Three-dimensional reconstruction of "phycosiphoniform" burrows: implications for identification of trace fossils in core: Palaeontologia Electronica, vol. 12, 13A: 15p.

BEDNARZ, M., AND MCILROY, D., 2012, Effect of phycosiphoniform burrows on shale hydrocarbon reservoir quality. AAPG Bulletin, vol. 96, p. 1957-1980.

BERNER, R. A., 1964, An idealized model of dissolved sulfate distribution in recent sediments: Geochimica and Cosmochimica Acta, vol. 28, p. 1497–1503.

BJØRLYKKE, 1998., Clay mineral diagenesis in sedimentary basins--a key to the prediction of rock properties. Examples from the North Sea Basin: Clay Minerals, v. 33, p. 15-34.

BLAIR, N.E. AND ALLER, R.C., 2012, The fate of terrestrial organic carbon in the Marine environment: Annual Review of Marine Science, v. 4, p. 401-423.

BOHACS, K. M., GRABOWSKI JR, G. J., CARROLL, A. R., MANKIEWICZ, P. J., MISKELL-GERHARDT, K. J., SCHWALBACH, J. R., ... AND SIMO, J. T., 2005, Production, destruction, and dilution – the many paths to source-rock development, in SEPM Special publication 82, p. 61.

BOUDREAU, B. P., AND JØRGENSEN, B. B., 2001, The benthic boundary layer: Transport processes and biogeochemistry: Oxford University Press, Oxford, 440 p.

BRENCHLEY, P.J., PICKERILL, R.K. AND STROMBERG, S.G., 1993, The role of wave reworking on the architecture of storm sandstone facies, Bell Island Group (Lower Ordovician), Eastern Newfoundland: Sedimentology, v. 40, p. 359-382.

BURDIGE, D. J., 2005, Burial of terrestrial organic matter in marine sediments: A re-assessment: Global Biogeochemical Cycles, vol. 19, doi: 10.1029/2004GB002368

CALLOW, R.H.T., MCILROY, D., KNELLER, B. AND DYKSTRA, M., 2012a, Integrated ichnological and sedimentological analysis of a Late Cretaceous submarine channel-levee system: The Rosario Formation, Baja California, Mexico: Marine and Petroleum Geology, vol. 41, p. 277-294.

CANFIELD, D. E., 1993, Organic matter oxidation in marine sediments. Interactions of C, N, P and S biogeochemical Cycles and Global Change, vol. 14, p. 333-363.

CHAMLEY, H., 1989, Clay sedimentology, vol. 623: Springer, New York, 623 p.

CHECKLEY, D. M., AND ENTZEROTH, L. C., 1985, Elemental and isotopic fractionation of carbon and nitrogen by marine, planktonic copepods and implications to the marine nitrogen cycle: Journal of Plankton Research, vol. 7, p. 553-568.

CUOMO, M. C., AND BARTHOLOMEW, P. R., 1991, Pelletal black shale fabrics: their origin and significance: Geological Society, London, Special Publications, vol. 58, p. 221-232.

DEMAISON, G.J. AND MOORE, G.T., 1980, Anoxic environments and oil source bed genesis: American Association of Petroleum Geologists Bulletin, v. 64, p. 1179-1209.

DENIRO, M. J., AND EPSTEIN, S., 1981, Influence of diet on the distribution of nitrogen isotopes in animals: Geochimica et Cosmochimica Acta, vol. 45, p. 341-351.

DYKSTRA, M. AND KNELLER, B., 2009, Lateral accretion in a deep-marine channel complex: Implications for channelized flow processes in turbidity currents: Sedimentology, vol. 56, p. 1411-1432.

ELLIOTT, T., 1989, Deltaic systems and their contribution to an understanding of basin-fill successions: Geological Society, London, Special Publications, vol. 41, p. 3-10.

FAUGÈRES, J. C., AND STOW, D. A., 1993, Bottom-current-controlled sedimentation: a synthesis of the contourite problem: Sedimentary Geology, vol. 82, p. 287-297.

FEDO, C. M., NESBITT, H. W., AND YOUNG, G. M., 1995, Unraveling the effects of potassium metasomatism in sedimentary rocks and paleosols, with implications for paleo weathering conditions and provenance: Geology, vol. 23, p. 921-924.

FOLK, R. L., 1974, Petrology of Sedimentary Rocks: Hemphill, Austin,182 p.

FRIEDRICHS, C. T., AND WRIGHT, L. D., 2004, Gravity-driven sediment transport on the continental shelf: implications for equilibrium profiles near river mouths: Coastal Engineering, vol. 51, p. 795-811.

FROELICH, P. N., KLINKHAMMER, G. P., BENDER, M. A. A., LUEDTKE, N. A., HEATH, G. R., CULLEN, D., ... AND MAYNARD, V., 1979, Early oxidation of organic matter in pelagic sediments of the eastern equatorial Atlantic: suboxic diagenesis: Geochimica et Cosmochimica Acta, vol. 43, p. 1075-1090.

GASTIL, R.G., PHILLIPS, R.P., AND ALLISON, E.C., 1975, Reconnaissance geology of the state of Baja California: Geological Society of America Memoir 140, 170 p.

GINGRAS, M. K., MACEACHERN, J. A., AND DASHTGARD, S. E., 2011, Process ichnology and the elucidation of physico-chemical stress: Sedimentary Geology, vol. 237, p. 115-134.

GOÑI, M. A., TEIXEIRA, M. J., AND PERKEY, D. W., 2003, Sources and distribution of organic matter in a river-dominated estuary (Winyah Bay, SC, USA): Estuarine, Coastal and Shelf Science, vol. 57, p.1023-1048.

GROSSMANN, S., AND REICHARDT, W., 1991, Impact of *Arenicola marina* on bacteria in intertidal sediments: Marine ecology progress series. Oldendorf, vol. 77, p. 85-93.

HARRIS, N. B., 2005, The deposition of organic-carbon-rich sediments: models, mechanisms, and consequences. Society for Sedimentary Geology Special Publication vol. 82, p. 1-5.

HEATH, J. E., DEWERS, T. A., MCPHERSON, B. J., PETRUSAK, R., CHIDSEY, T. C., RINEHART, A. J., AND MOZLEY, P. S., 2011, Pore networks in continental and marine mudstones: Characteristics and controls on sealing behavior: Geosphere, vol. 7, p. 429-454.

HELLY, J.J. AND LEVIN, L.A., 2004, Global distribution of naturally occurring marine hypoxia on continental margins: Deep-Sea Research Part I: Oceanographic Research Papers, vol. 51, p. 1159-1168.

HENRICHS, S. M., AND REEBURGH, W. S., 1987, Anaerobic mineralization of marine sediment organic matter: Rates and the role of anaerobic processes in the oceanic carbon economy: Geomicrobiology Journal, vol. 5, p. 191-237.

HILL, P. S., MILLIGAN, T. G., AND GEYER, W. R., 2000, Controls on effective settling velocity of suspended sediment in the Eel River flood plume: Continental shelf research, vol. 20, p. 2095-2111.

HOLLANDER, D.J., MCKENZIE, J.A. AND LO TEN HAVEN, H., 1992, A 200 year sedimentary record of progressive eutrophication in Lake Greifen (Switzerland): implications for the origin of organic-carbon- rich sediments: Geology, vol. 20, p. 825-828.

HOLLISTER, C. D., AND I. N. MCCAVE, 1984, Sedimentation under deep-sea storms: Nature v. 309, p. 220-225.

HOVIKOSKI, J., LEMISKI, R., GINGRAS, M., PEMBERTON, G., AND MACEACHERN, J. A., 2008, Ichnology and sedimentology of a mud-dominated deltaic coast: Upper Cretaceous Alderson Member (Lea Park Fm), western Canada: Journal of Sedimentary Research, vol. 78, p. 803-824.

INGERSOLL, R. V., 1990, Actualistic sandstone petrofacies: discriminating modern and ancient source rocks: Geology, vol. 18, p. 733-736.

JÜNGST, H., 1934, Geological significance of synaeresis: Geologische Rundschau, vol. 25, p. 321-325.

KANE, I. A., AND HODGSON, D. M., 2011, Sedimentological criteria to differentiate submarine channel levee subenvironments: exhumed examples from the Rosario Fm.(Upper Cretaceous) of Baja California, Mexico, and the Fort Brown Fm.(Permian), Karoo Basin, S. Africa: Marine and Petroleum Geology, vol. 28, p. 807-823.

KATZ, B. J., 2005, Controlling factors on source rock development—a review of productivity, preservation, and sedimentation rate: SEPM Special publication 82, 7.

KEIL, R. G., MAYER, L. M., QUAY, P. D., RICHEY, J. E., AND HEDGES, J. I., 1997, Loss of organic matter from riverine particles in deltas: Geochimica et Cosmochimica Acta, vol. 61, p. 1507-1511.

KENNEDY, M., DROSER, M., MAYER, L. M., PEVEAR, D., AND MROFKA, D., 2006, Late Precambrian oxygenation; inception of the clay mineral factory: Science, vol. 311, p. 1446-1449.

KIRBY, R., AND PARKER, W. R., 1983, Distribution and behavior of fine sediment in the Severn Estuary and Inner Bristol Channel, UK: Canadian Journal of Fisheries and Aquatic Sciences, vol. 40, p. 83-95.

LANGMUIR, D. AND J. I. DREVER, 1997, Environmental Geochemistry. Englewood Cliffs: Prentice-Hall.

LEITHOLD, E. L., AND HOPE, R. S., 1999, Deposition and modification of a flood layer on the northern California shelf: lessons from and about the fate of terrestrial particulate organic carbon: Marine Geology, vol. 154, p. 183-195.

LIU, Z., COLIN, C., LI, X., ZHAO, Y., TUO, S., CHEN, Z., ... AND HUANG, K. F., 2010, Clay mineral distribution in surface sediments of the northeastern South China Sea and surrounding fluvial drainage basins: Source and transport: Marine Geology, vol. 277, p. 48-60.

MACQUAKER, J.H.S. AND ADAMS, A.E., 2003, Maximizing information from fine-grained sedimentary rocks: An inclusive nomenclature for mudstones: Journal of Sedimentary Research, v. 73, p. 735-744.

MCILROY, D. AND LOGAN, G.A., 1999, The impact of bioturbation on infaunal ecology and evolution during the Proterozoic-Cambrian transition: Palaios, v. 14, p. 58-72.

MCILROY, D., WORDEN, R.H. AND NEEDHAM, S.J., 2003, Faeces, clay minerals and reservoir potential: Journal of the Geological Society, vol. 160, p. 489-493.

MEHTA, A. J., AND MCANALLY, W. H., 2002, Fine-grained cohesive sediment transport. Sedimentation engineering, ASCE manual 54, Chapter 4, vol. 2, ASCE, New York.

MILLIMAN, J. D., AND SYVITSKI, J. P., 1992, Geomorphic/tectonic control of sediment discharge to the ocean: the importance of small mountainous rivers: The Journal of Geology, vol. 100, p. 525-544.

MISEROCCHI, S., LANGONE, L., AND TESI, T., 2007, Content and isotopic composition of organic carbon within a flood layer in the Po River prodelta (Adriatic Sea): Continental Shelf Research, vol. 27, p. 338-358.

MULDER, T., AND SYVITSKI, J. P., 1995, Turbidity currents generated at river mouths during exceptional discharges to the world oceans: The Journal of Geology, vol. 103, p. 285-299.

NEEDHAM, S.J., WORDEN, R.H. AND MCILROY, D. 2005, Experimental production of clay rims by macrobiotic sediment ingestion and excretion processes: Journal of Sedimentary Research, v. 75, p. 1028-1037.

NEEDHAM, S.J., WORDEN, R.H. AND CUADROS, J. 2006, "Sediment ingestion by worms and the production of bio-clays: A study of macrobiologically enhanced weathering and early diagenetic processes", Sedimentology, vol. 53, no. 3, pp. 567-579.

NESBITT, H. W, AND MARKOVICS, G., 1997, Weathering of granodioritic crust, long-term storage of elements in weathering profiles, and petrogenesis of siliciclastic sediments: Geochimica et Cosmochimica Acta, vol. 61, p. 1653-1670.

OGSTON, A. S., CACCHIONE, D. A., STERNBERG, R. W., AND KINEKE, G. C., 2000, Observations of storm and river flood-driven sediment transport on the northern California continental shelf: Continental Shelf Research, vol. 20, p. 2141-2162.

PARRISH, J. T., 1995, Paleogeography of C_{org}-rich rocks and the preservation versus production controversy, in Paleogeography, Paleoclimate and Source Rocks, in by Huc, A. Y., ed., American Association. of Petroleum Geologists, Tulsa, pp. 1–20

PASSEY, Q. R., BOHACS, K. M., ESCH, W. L., KLIMENTIDIS, R., AND SINHA, S., 2010, From oil-prone source rock to gas-producing shale reservoir: Geologic and petrophysical characterization of unconventional shale-gas reservoirs: Chinese Petroleum Society/Society of Petroleum Engineers International Oil and Gas Conference and Exhibition in China, Beijing, China, June 8–10, 2010, SPE Paper 131350, 29 p., doi:10.2118/131350-MS.

PLINT, A.G., J.H.S. MACQUAKER AND VARBAN, B., 2012, Bedload Transport of Mud Across A Wide, Storm-Influenced Ramp: Cenomanian–Turonian Kaskapau Formation, Western Canada Foreland Basin: Journal of Sedimentary Research, v. 82, p. 801-822,

PLINT, A. G., 2010, Wave-and storm-dominated shoreline and shallow-marine systems. Facies Models, 4, 167-200.

PELTONEN, C., MARCUSSEN, Ø., BJØRLYKKE, K., AND JAHREN, J., 2009, Clay mineral diagenesis and quartz cementation in mudstones: The effects of smectite to illite reaction on rock properties. Marine and Petroleum Geology, vol. 26, p. 887-898

PEDERSEN, T.F. AND CALVERT, S.E., 1990, Anoxia vs. productivity: what controls the formation of organic- carbon-rich sediments and sedimentary rocks?: American Association of Petroleum Geologists Bulletin, v. 74, p. 454-466.

PEMBERTON, S. G., AND WIGHTMAN, D. M., 1992, Ichnological characteristics of brackish water deposits, In Applications of Ichnology to Petroleum Exploration: SEPM, Core Workshop, vol. 17, p. 141-167.

POMPECKJ, J. F., 1909, Die zoogeographischen Beziehungen zwischen den Jurameeren Nordwest- und Süddeutschlands. 1. Jb. Nieders. Geol. Ver. Hannover, 10.

POTTER, P. E., MAYNARD, J. B., AND DEPETRIS, P. J. (2005). *Mud and mudstones: Introduction and overview*. Springer Verlag. p. 297.

PRATT, L. M., CLAYPOOL, G. E., AND KING, J. D., 1986, Geochemical imprint of depositional conditions on organic matter in laminated—Bioturbated interbeds from fine-grained marine sequences: Marine Geology, vol. 70, p. 67-84.

PRATT, B. R., 1998, Syneresis cracks: subaqueous shrinkage in argillaceous sediments caused by earthquake-induced dewatering: Sedimentary Geology, vo. 117, p. 1-10.

RINE, J. M., AND GINSBURG, R. N., 1985, Depositional facies of a mud shoreface in Suriname, South America - a mud analogue to sandy, shallow-marine deposits: Journal of Sedimentary Research, vol. 55, p. 633-652.

RANGER, M. J., 1979, The stratigraphy and depositional environment of the Bell Island Group, the Wabana Group, and the Wabana iron ores, Conception Bay, Newfoundland,[unpublished M. Sc. thesis]: Memorial University of Newfoundland, St. John's, Newfoundland, 216 p.

RANGER, M.J., PICKERILL, R.K. AND FILLION, D., 1984, Lithostratigraphy of the Cambrian? - Lower Ordovician Bell Island and Wabana groups of Bell, Little Bell, and Kellys islands, Conception Bay, eastern Newfoundland: Canadian Journal of Earth Sciences, v. 21, p. 1245-1261.

RATCLIFFE, K. T., WRIGHT, A. M., AND SCHMIDT, K., 2012, Application of inorganic whole-rock geochemistry to shale resource plays: an example from the Eagle Ford Shale Formation, Texas: The Sedimentary Record, vol. 10, p. 4-9.

SCHIEBER, J., 1998, Sedimentary features indicating erosion, condensation, and hiatuses in the Chattanooga Shale of Central Tennessee: relevance for sedimentary and stratigraphic evolution, in Schieber, J., Zimmerle, W., and Sethi, P., eds., Shales and Mudstones (vol. 1): Basin Studies, Sedimentology and Paleontology: Stuttgart,Schweizerbart'sche Verlagsbuchhandlung, p. 187–215.

SCHIEBER, J., SOUTHARD, J., AND THAISEN, K., 2007, Accretion of mudstone beds from migrating floccule ripples. Science, vol. 318, p. 1760-1763.

STOCKDALE, A., DAVISON, W. AND ZHANG, H., 2010, Formation of iron sulfide at faecal pellets and other microniches within suboxic surface sediment: Geochimica et Cosmochimica Acta, vol. 74, p. 2665-2676.

STOW, D. A., AND SHANMUGAM, G., 1980, Sequence of structures in fine-grained turbidites: comparison of recent deep-sea and ancient flysch sediments: Sedimentary Geology, vol. 25, p. 23-42.

TAYLOR, A. M., AND GOLDRING, R., 1993, Description and analysis of bioturbation and ichnofabric: Journal of the Geological Society, vol. 150, p. 141-148.

THUNELL, R. C., 1998, Particle fluxes in a coastal upwelling zone: Sediment trap results from Santa Barbara Basin, California. Deep-Sea Research Part II, vol. 45, p. 1863-1884.

TISSOT, B. P., AND WELTE, D. H., 1978, Petroleum formation and occurrence: a new approach to oil and gas exploration, Springer, New York, 521 p.

TRABUCHO-ALEXANDRE, J., HAY, W. W., AND DE BOER, P. L., 2011, Phanerozoic black shales and the Wilson Cycle: Solid Earth, vol. 3, p. 29-42.

TRAYKOVSKI, P., GEYER, W. R., IRISH, J. D., AND LYNCH, J. F., 2000, The role of wave-induced density-driven fluid mud flows for cross-shelf transport on the Eel River continental shelf: Continental Shelf Research, vol. 20, p. 2113-2140.

TYSON, R. V., 1995, Sedimentary organic matter: organic facies and palynofacies. Chapman & Hall, London, 615 p.

WETZEL, A. 1991, Ecologic interpretation of deep-sea trace fossil communities: Palaeogeography, Palaeoclimatology, Palaeoecology, v. 85, p. 47-69.

WETZEL, A., AND UCHMAN, A., 1998, Biogenic sedimentary structures in mudstones—An overview: Shales and mudstones, v. 1, p. 351-369.

WALSH, J. P., AND NITTROUER, C. A., 2009, Understanding fine-grained river-sediment dispersal on continental margins: Marine Geology, vol. 263, p. 34-45.

WATTS, N. L., 1987, Theoretical aspects of cap-rock and fault seals for single-and two-phase hydrocarbon columns: Marine and Petroleum Geology, vol. 4, p. 274-307.

WELTJE, G. J., 2012, Quantitative models of sediment generation and provenance: State of the art and future developments: Sedimentary Geology, v. 280, p. 4-20.

WHITFIELD, A. K., ELLIOTT, M., BASSET, A., BLABER, S. J. M., AND WEST, R. J., 2012, Paradigms in estuarine ecology–A review of the Remane diagram with a suggested revised model for estuaries: Estuarine, Coastal and Shelf Science, vol. 97, p. 78-90.

WINDOM, H.L., 1976, Lithogenous material in marine sediments, in: Riley, J.P., and Chester, R., eds, Chemical oceanography (2nd edition) London, Academic Press, v. 5, p. 103-135.

WIGHTMAN, D.M., PEMBERTON, S.G. AND SINGH, C., 1987, Depositional modeling of the Upper Mannville (Lower Cretaceous), east-central Alberta: implications for the recognition of brackish water deposits, in Reservoir Sedimentology, eds, R.W. Tillman and K.J. Weber: SEPM Special Publication 40, 189–220.

WIGNALL, P. B., 1994, Black shales: Clarendon Press, Oxford, 127 p.

WOOLNOUGH, W. G., 1937, Sedimentation in barred basins, and source rocks of oil. AAPG Bulletin, vol. 21, p. 1101-1157.

YANG, Y. L., AND A. C. APLIN, 2004, Definition and practical application of mudstone porosity-effective stress relationships: Petroleum Geoscience, v. 10, p. 153–162, doi:10.1144/1354-079302-567.

YERGIN, D., 2011, The prize: The epic quest for oil, money & power: Free Press. 928 p.

YOUNG, R. N., AND SOUTHARD, J. B., 1978, Erosion of fine-grained marine sediments: sea-floor and laboratory experiments: Geological Society of America Bulletin, vol. 89, p. 663-672.

ZHU, Q., ALLER, R.C. AND FAN, Y., 2006, Two-dimensional pH distributions and dynamics in bioturbated marine sediments: Geochimica et Cosmochimica Acta, vol. 70, p. 4933-4949.

CHAPTER 2

Wave-advected dispersal of mud in the Cambro-Ordovician Bell Island Group: High-resolution stratigraphy and diagenetic framework

Dario Harazim[1] and Duncan McIlroy[1]

[1]Department of Earth Science, Memorial University of Newfoundland, 300 Prince Philip Drive, St. John's, NL, A1B 3X5 Canada

(In review with the Journal of Sedimentary Research)

1. Abstract

A determination of the suitability of mudstones to function as either source, reservoir or seal rocks depends on an interdisciplinary integration of all physical, biological and chemical rock attributes - preferably within a basin-wide framework. This study presents the sedimentology, ichnology and geochemistry of exceptionally preserved hyperpycnal flow and wave-enhanced sediment gravity flow deposits, the dominant depositional mechanisms of mud in the Early Ordovician Bell Island Group, Newfoundland. Seven mudstone facies are described, based on textural, compositional and ichnological characteristics. Mudstones originating from hyperpycnal flows are well-cemented, exhibit high chlorite-illite ratios, and contain well-developed grain size breaks with a tripartite-subdivision. Conversely, mudstones deposited in association with wave-enhanced sediment gravity flows exhibit decimeter-sized combined-flow structures as well as

laterally discontinuous, unbioturbated mudstone layers with abundant mud-on-mud and mud-on-sand erosional contacts. These latter mudstones are composed of predominantly illite and are poorly indurated. The compositional diversity of mudstones within this heterolithic shoreface succession is interpreted to be controlled by proximity to a fluvial source and residence time of rock components in the oxic and suboxic diagenetic zone. Low organic carbon loading from a non-vegetated Early Paleozoic hinterland, combined with a potentially high reworking frequency are inferred to result in a low preservation potential of organic carbon in this muddy shoreface environment. Two master variables, burial efficiency and availability as food for macrofaunal bioturbators, are proposed to be critical and exert a significant control on macrofaunal colonization patterns and bioturbation intensities within this mud-dominated shoreface paleoenvironment.

2. Introduction

Laminated, organic carbon-rich (>2 wt% TOC; Tissot and Welte 1978), unbioturbated mudstone successions are typically interpreted to be deposited in low-energy basinal settings, where bottom waters develop dysoxia or even persistent anoxia (Demaison and Moore 1980; Katz 2005). If unbioturbated and possibly laminated mudstones are interbedded with bioturbated and cross-laminated or cross-bedded sandstones, a reasonable interpretation is that sandstones were deposited during rare storms disrupting otherwise low energy basinal or deeper shelf systems. The precept underlying this paradigm is that mud, and associated organic matter is delivered to the sea floor by

suspension settling during times when bottom currents are weak or completely absent (Aigner and Reineck 1982; O'Brien 1990; Cuomo and Bartholomew 1991; Arthur and Sageman 1994; Pancost et al. 2004; Algeo and Lyons 2006).

Modern research in ancient mud-dominated successions has provided data that contradict these assumptions (Plint et al. 2012). Mud introduced by rivers flocculates due to electrostatic forces and settles quickly to the sea-floor as bottom-hugging layers of fluid mud, typically within a few tens of kilometers of the river mouth (e.g.,Wolanski and Gibbs 1995; McCave 1984; McIlroy 2004; Hill et al. 2007). This research demonstrates that at ocean-continent boundaries large quantities of river borne, fine-grained sediment are introduced via post-storm surge currents (Mulder and Syvitski 1995). On low-slope (<0.5%) continental shelves freshly introduced mud is advected alongshore via geostrophic currents (Wright and Friedrichs 2006). During storms, previously emplaced mud layers are resuspended by large surface gravity waves, resulting in the formation of near-bed suspensions of fluid mud (suspended solid concentration >10g L^{-1}; Kirby and Parker 1983; Mehta and McAnally et al. 2002). Such wave-advected sediment gravity flows have the ability to transport mud over low-angle shelves and effectively shift the locus of mud deposition away from the vicinity of a river mouth, to parts of the shelf which are never affected by typical deltaic processes (Keil et al., 1997; Allison et al., 1998; Friedrichs and Wright 2004; Plint et al. 2009). While en-route to offshore depocenters, multiple cycles of (seasonal) resuspension, transport and deposition are predicted to generate large volumes of mud with geochemical (Wheatcroft and Drake 2003) and sedimentological (Martin et al. 2008) characteristics that drastically differ from mudstone deposited on low-energy shelves. Mud-dominated coastlines are rarely

preserved in the stratigraphic record since they are mostly developed during sea-level high-stand and commonly removed during sea-level fall. The textural and geochemical characteristics of the resulting sedimentary layers are poorly known to date (Keen et al. 2006; Schieber 2011).

From a geological perspective one question arises: What are suitable environmental conditions for the deposition of fine-grained mud layers in heterolithic successions? Some authors have claimed that fine-grained units in heterolithic successions are the sedimentary products of low-energy suspension settling in predominantly low-energy distal offshore environments (Aigner and Reineck 1982), whereas others have proposed that muddy intervals can potentially result from high-energy seafloor processes in a storm-dominated shoreface succession (e.g. Rine and Ginsburg 1985).

Understanding the origin and dispersal mode of fine-grained sediment has implications for the origin and preservation of organic carbon as well as implications for the compositional diversity of inorganic and organic components in mudstones. For example, at presently high sea-levels approximately 50% (Blair and Aller 2012) of all terrestrially entrained and marine organic carbon is effectively deposited in near-shore position, and reworked via several classes of seafloor processes. Such processes include wave-advected sediment gravity flows, tidal processes and hyperpycnal currents that occur shortly after river floods (e.g., Hastings et al. 2012). A combination of biochemical proxies in the water column and the shallow sea bed indicate that on high-energy shelves the organic fraction is subjected to long periods of microbially-dominated decomposition under suboxic conditions, thus yielding deposits dominated by refractory terrestrial

organic matter and a relative dominance of microbial biomass (Leithold and Hope 1999; Aller 2004; Aller et al. 2010).

Investigating the origin of fine-grained mud-dominated sediment is not straightforward. The traditional, hydrodynamically controlled onshore-offshore trend of offshore fining from high-energy coastal sands to low-energy offshore mudstones (Aigner and Reineck 1982; Yoshida et al. 2007) is not always expressed in a predictable fashion close to riverine systems with high input of fine-grained sediment (Rine and Ginsburg 1985). Especially where large-scale oceanographic currents disperse fine-grained sediment alongshore, considerable stacking pattern variability can obscure classic sequence and parasequence development (e.g., Catuneanu and Zecchin 2013). The low-power (scales of 10^{-1} to 10^{-2} m) petrographic analysis (e.g., Schieber 1998) of sedimentary fabrics in mudstones can be used to unravel the physical seabed processes that operated during the dispersal and burial of fine-grained sediment and to separate mudstones deposited in nearshore regions from mudstones that were deposited further offshore in quiet water settings.

3. Aims of the study

This study aims to develop a better understanding about the compositional and textural characteristics of Lower Paleozoic mudstones that were deposited under high-energy, shallow marine conditions. It is hypothesized that the textural and compositional diversity of mudstones deposited in shallow-marine conditions differs from typical organic-rich mudstones preserved in deep-water, offshore depocenters (cf. Demaison and Moore 1980;

O'Brien 1990; Ghadeer and Macquaker 2012). The sedimentological attributes of mudstones deposited under combined-flow conditions are currently not well known (Plint et al. 2012). Establishing an understanding of the seafloor conditions that govern sediment transport is key to developing a reasonable geological model that accounts for the shelf-wide distribution of silt- and clay-sized rock components and to understand the underpinning controls on the preservation of kerogen along the entire onshore-offshore gradient.

The Cambro-Ordovician Beach Formation is an ideal natural setting to investigate these research questions, because it contains meter-thick packages of weakly bioturbated to unbioturbated mudstones (with up to 3.4 wt% TOC; Harazim et al. 2013) interbedded with bioturbated, ripple- and hummocky cross-stratified sandstones (Ranger et al., 1984; Fillion and Pickerill 1990). The periodic absence of bioturbation in some mud-rich, but demonstrably shallow-marine parts of the succession has been attributed to either periodically anoxic bottom-water conditions or salinity fluctuations (Ranger 1979; Fillion and Pickerill 1990).

This study investigates the sedimentological processes responsible for the deposition of heterolithic strata, and investigates the relationships between mudstone dispersal mechanisms, burial conditions, organic carbon characteristics and bioturbation style / intensity.

4. Geological Framework of the Beach Formation

The Lower Ordovician (Tremadocian, ~485 Ma) Beach Formation (Fig. 2-1) is well-exposed in sea cliffs around Bell Island. Cambrian-Ordovician sediments of Bell Island are organized into the Bell Island and Wabana groups. The whole succession is approximately 1500 m thick in total, of which the Beach Formation of the Bell Island Group comprises approximately 440 m (Ranger et al. 1984). The Beach Formation at Freshwater Cove (47°35'49.53"N; 53° 0'43.98"W) is composed of stacked upward thickening and upward coarsening parasequences of mudstones and interbedded sandstones. Previous research has proposed eustatically-controlled parasequence-scale cyclicity at several localities (Brenchley et al. 1993). Each of the shallowing upward shoreface cycles has dark grey mudstones at its base and partially amalgamated hummocky-cross stratified sandstones at its top. The associated vertical changes in diversity of trace fossil assemblages have been interpreted to indicate a bathymetric shift from a deep-shelfal, anoxic environment to one above storm-wave base (Fillion and Pickerill 1990).

5. Material and Methods

5.1 Characterization of sedimentary fabric

To obtain rock descriptions at the necessary resolution, and to characterize the mud-dominated lithologies of the heterolithic Beach Formation, mudstones at Freshwater Cove

Figure 2-1. (A) Early Ordovician (~485.0 Ma) paleogeographic reconstruction of the northern margin of Gondwana. Avalonian terranes and studied section (labeled with green star) are located at ~65° S during Tremadocian times (modified from Stämpfli et al., 2002) (B) Stratigraphic position of the Beach Formation within the Bell Island Group (simplified after Ranger et al., 1984). (C) Simplified geological map of Bell Island with study location at Freshwater Cove (green star) (modified after Ranger et al., 1984).

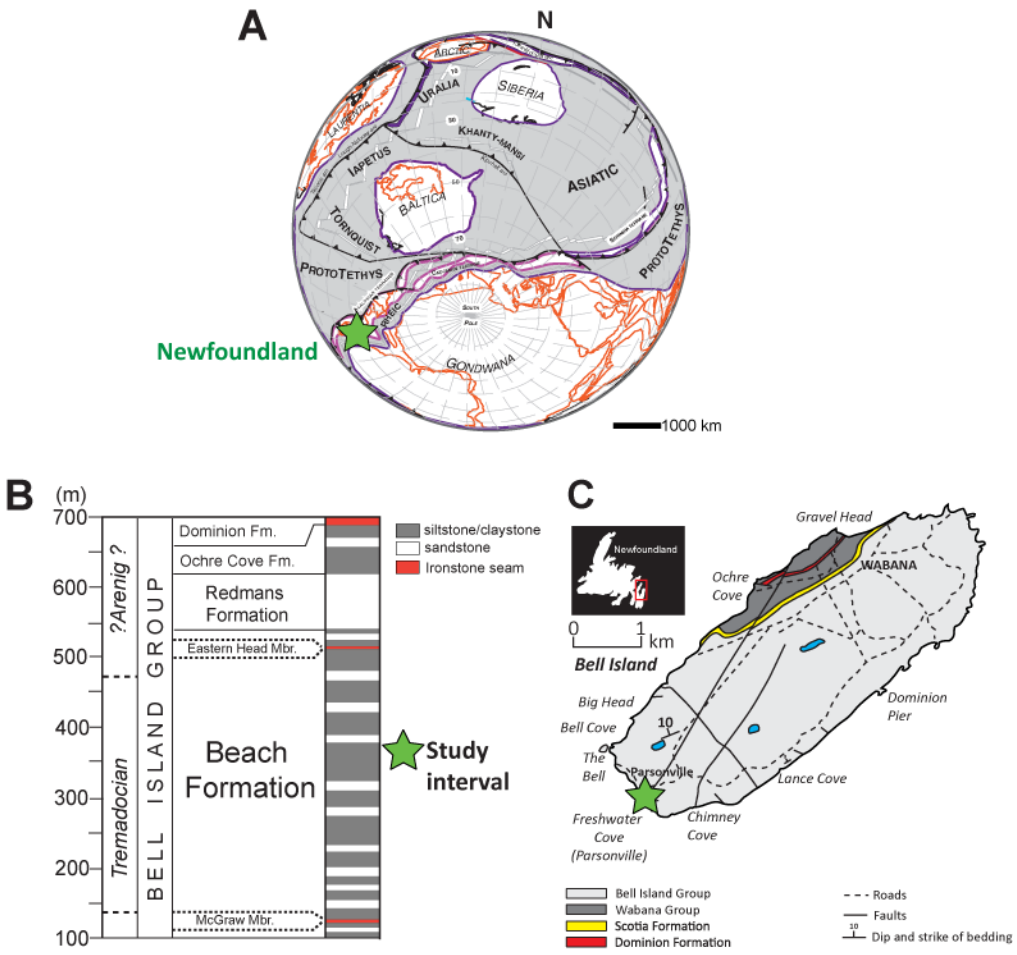
A
N
Newfoundland
1000 km
B
(m)
700
600
500
400
300
200
100
?Arenig ?
Tremadocian
BELL ISLAND GROUP
Dominion Fm.
Ochre Cove Fm.
Redmans Formation
Eastern Head Mbr.
Beach Formation
McGraw Mbr.
siltstone/claystone
sandstone
Ironstone seam
Study interval
C
Newfoundland
0
1
km
Bell Island
Gravel Head
Ochre Cove
WABANA
Big Head
Bell Cove
The Bell
Parsonville
Dominion Pier
Lance Cove
Freshwater Cove (Parsonville)
Chimney Cove
Bell Island Group
Wabana Group
Scotia Formation
Dominion Formation
Roads
Faults
Dip and strike of bedding

(Parsonville) were logged at cm-scale (Fig. 2-2). Oriented, unweathered samples collected from the logged sections were slabbed in the laboratory perpendicular to bedding to study the variability of sedimentary textures, mineralogy and ichnology. The burrowed area within one bed was described using the bioturbation index (BI; Taylor and Goldring 1993). The BI has six grades. Each grade is allocated a numerical value ranging from BI 1 (no bioturbation and sharp bed boundaries, 0%) to BI 6 (complete homogenization of bed boundaries, 100%). The BI classifies bioturbation in terms of burrow density, amount of burrow overlap and sharpness of the original sedimentary fabric (Reineck 1963). These hand-specimen descriptions were supplemented by petrographic descriptions (summarized in Table 1). The mineralogical characteristics of the individual rock components were imaged using a FEI Quanta FEG 650 ESEM equipped with an energy dispersive X-Ray microanalytical system (EDS). Field, hand-specimen, petrographic and mineralogical data were combined to produce composite facies descriptions of mudstones (Table 2-1; following Folk, 1980; Macquaker and Adams 2003). The scheme of Campbell (1967) has been employed to describe the geometry of bounding surfaces of beds and bedsets. Textural observations made from polished slabs and thin sections form the base of this facies classification.

5.2 Geochemical measurements

Samples were also collected for bulk rock TOC and $\delta^{13}C_{org}$ analyses (Fig. 2-2). Approximately 5 to 10 mg of unweathered, carbonate-free sample material (determined thorugh a combination of XRD, FTIR, and ESEM analyses) were analyzed for weight

Figure 2-2. Generalized stratigraphic log and whole-rock record of TOC and $\delta^{13}C_{org}$ as measured from sedimentary organic matter in the Beach Formation at Freshwater Cove (Parsonville) (discussion see text).

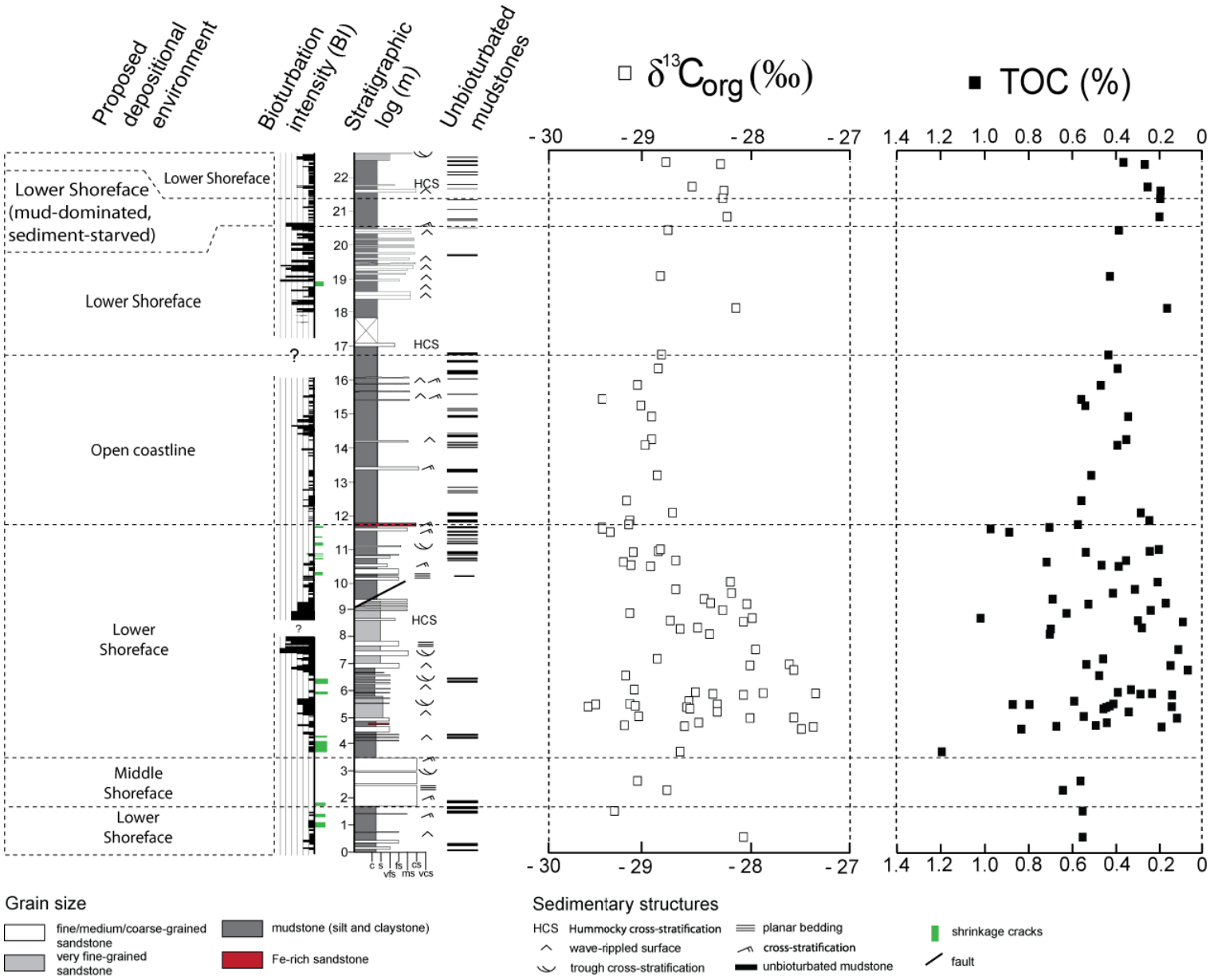
Proposed depositional environment
Bioturbation intensity (BI)
Stratigraphic log (m)
Unbioturbated mudstones
□ δ13Corg (‰)
■ TOC (%)
Lower Shoreface
Lower Shoreface (mud-dominated, sediment-starved)
Lower Shoreface
Open coastline
Lower Shoreface
Middle Shoreface
Lower Shoreface
HCS
HCS
HCS
- 30
- 29
- 28
- 27
1.4 1.2 1.0 0.8 0.6 0.4 0.2 0
c s fs ms cs
vfs vcs
Grain size
fine/medium/coarse-grained sandstone
very fine-grained sandstone
mudstone (silt and claystone)
Fe-rich sandstone
Sedimentary structures
HCS Hummocky cross-stratification
wave-rippled surface
trough cross-stratification
planar bedding
cross-stratification
unbioturbated mudstone
shrinkage cracks
fault

percentage (wt%) of Total Organic Carbon (TOC) using a Carlo Erba Elemental Analyzer. A Gas Bench II® (Thermoquest) connected to the continuous flow inlet system of a Delta V plus gas source mass spectrometer (Thermo Fisher Scientific, Waltham, MA, USA) has been used to run $\delta^{13}C_{org}$ analyses. Certified reference material (G-33/MUN Sulfanilamide, MUN-CO-1, MUN-CO-2, B2153; Coplen et al. 2006) was analyzed with the samples to demonstrate accuracy and precision. Samples and standards reproduced within ±0.18‰ for $\delta^{13}C_{org}$ analyses and ±0.01% for TOC analyses. Carbon isotope values are reported relative to the Vienna Pee Dee Belemnite standard (V-PDB ‰).

6. Facies descriptions

6.1 Facies M1 – Stratified mudstone

Mudstones of this facies comprise dm-thick, unbioturbated to weakly bioturbated (BI 1-2; 0-30%) sand-, silt- and clay-bearing mudstones interbedded with decimeter-thick, fine- to medium-grained sandstones of facies S2. Mudstone beds contain distinct grain-size breaks with either bi- or tripartite subdivision (Fig. 2-3). Decimeter-wide, mud-filled gutters are common within this facies. Ichnofabrics comprise shallow tier, sand-filled *Planolites, Trichophycus* and rare *Arenicolites* (Fig. 3A). The framework is comprised of moderately sorted, subrounded fine-grained quartz and feldspar, whereas the matrix is dominated by chlorite and illite cement, with accessory biotite and muscovite (Figs 2-3C and D). Average TOC is 0.56% and $\delta^{13}C_{org}$ values are on average -28.7‰ within this facies.

Table 2-1. This table summarizes the sedimentological, ichnological and geochemical attributes of mudstones and sandstones within the Beach formation at Freshwater Cove (Parsonville) (see text for detailed explanation).

Facies code	Facies name	Lithology	Sedimentary structures	Composition and mineralogy	Ichnology	Average TOC content (wt%)	Interpreted depositional environment
M1	**Stratified mudstone**	Sand-, silt-, and clay-bearing mudstone	Centimeter to decimeter-thick continuous beds; Sandstone/mudstone contact in most cases developed sharp with at least one distinct grain-size break; graded bedding uncommon	Chlorite-cement matrix with subordinate detrital illite; subrounded, floating quartz and albite; replacement of grains by chlorite; scattered rutile in matrix	Millimeter to centimeter-sized, shallow-tier *Planolites* ; centimeter-sized T*richophycus;* rare *Arenicolites* (BI 1-2; 10-30%), simple cross cutting relationships	0.56	Lower shoreface
M2	**Dark mudstone**	Silt-bearing, clay-rich mudstone	Centimeter-thick continuous beds; structureless, ungraded	Subrounded quartz grains in matrix of Fe-rich chlorite (chamosite?); post-compaction replacement of feldspar by chlorite cement; scattered Ti-rich minerals and framboidal pyrite	Millimeter-sized, shallow *Planolites* ; BI 1; <10%); Shallow tiering; no cross-cutting	0.37	Upper/Middle shoreface
M3	**Sandy mudstone**	Sandy mudstone	Centimeter-thick continuous beds; internally structureless, abundant erosional surfaces, sporadically developed shrinkage cracks	Quartz, plagioclase feldspar and altered lithic components in a matrix of Fe-rich chlorite; illite and biotite are common; rare clusters of siderite and framboidal pyrite; authigenic post-compaction replacement (chloritization) of unstable lithic (mafic?) grains/clasts	Burrow-mottled; BI 4-5 (61-99%)	0.60	Lower/Middle shoreface
M4	**Thick, unbioturbated mudstone**	Silt- and Clay-rich mudstone	Centimeter-thick even continuous beds; common mud-on-mud erosional contacts	Quartz, feldsoar and altered grains in a chlorite/illite matrix; biotite and muscovite common; framboidal pyrite and firely dispersed Ti-rich minerals in matrix	Rare soft- and firmground burrows infilled with mud and sand from overlying unit; (BI 0-1; <10%); simple cross-cutting relationships	0.30	Mud-dominated coastline, lower shoreface
M5	**Thin-bedded mudstone**	Sand-bearing, silt- and clay-rich mudstone	Millimeter-thick even continuous, normally-graded and ungraded, erosionally-based beds; cm-sized, combined-flow structures with tripartite subdivision (i.e., starved sandstone ripples with with laminated siltstone and draped by unbioturbated clay-dominated mudstone)	Subrounded quartz grains in illite and chlorite matrix with subborcinate biotite, silt- and sand-sized lithic fragments common	Millimeter-sized, sand-filled shallow-tier *Planolites* (P); (BI 1; <10%); Shallow tiering; No cross-cutting relationships; Escape traces common; simple cross-cutting relationships	0.53	Lower shoreface, offshore transition, mud-dominated coastline
M6	**Sediment-starved mudstone**	Silt-bearing, clay-rich mudstone	Centimeter-thick, erosionally based beds and bedsets; non-parallel, curved and discontinuous mud-on-sand and mud-on-mud erosional contacts at a range of scales; high lateral variability in bedding thickness at all scales; abundant interbedded starved sandstone combined-flow ripples	Quartz, feldsoar and altered grains in a chlorite/illite matrix; biotite and muscovite common; framboidal pyrite and firely dispersed Ti-rich minerals in matrix	Shallow-tier *Planolites* ; BI 0-3 (0-60%); high lateral varaibility, low tiering depth; simple cross-cutting relationships	0.28	Mud-dominated coastline, lower shoreface, (sediment-starved)
M7	**Bioturbated mudstone**	Sand-bearing, silt- and clay-rich mudstone	Centimeter-thick, graded and ungraded beds, erosionally based mudstones	Quartz, feldsoar and altered grains in a chlorite/illite matrix; common biotite and muscovite; framboidal pyrite, finely dispersed rutile in matrix	Shallow-tier *Planolites* , *Trichophycus, Gyrolithes;* BI 1-4 (1-90%), complex cross-cutting relationships	0.23	Mud-dominated coastline

S1	**Thick-bedded sandstone**	Moderately sorted, subrounded, fine- to coarse-grained sandstone	Beds and bedsets continuous; High-wavelength (m scale), very low-angle cross-stratified and planar bedded sandstones in base; upper part of this facies contains low-angle bedforms with mm-spaced, tabular or sigmoidal cross-sets	Well-cemented quartz arenite	*Arenicolites;* BI 0-1 (0-4%); no cross-cutting relationships	*not determined*	Middle shoreface
S2	**Thin-bedded sandstone**	Poorly to moderately sorted, fine- to medium-grained sandstone, interbedding with mudstone of various composition	Beds and bedsets continuous; HCS sandstones common; lenticular bedding locally devloped; thin-bedded (10 cm-thick) sandstones are planar bedded with wave- and interference ripples; bedding planes often contain Microbially-Induced Sedimentary Structures (MISS), sandstones originating as tempestites contain layers with broken, poorly rounded inarticulate brachiopod shell debris	Quartz and lithic fragments embedded in non-resolvable pseudo matrix composed of silt-sized detrital mica and illite; quartz grains well-cemented via point and long contacts; inter-granular porosity infilled with post-compaction Fe-chlorite cement, subordinate phosphate and isolated patches of ferroan carbonate	Shallow-tier *Planolites, Trichophycus, Cruziana, Diplocraterion, Schaubcylindrichnus, Skolithos;* weakly to intensely-bioturbated (BI 2-5; 5-99%); variable tiering depth, simple cross-cutting relationships, rare sandstone bedding planes monogeneric suites of mud-filled *Skolithos;* common arthropod scratch marks (*Monomorphichnus*) and *Cruziana* on bedding planes.	*not determined*	Lower shoreface, offshore transition
S3	**Bioturbated sandstone**	Poorly to moderately sorted, fine- to medium-grained sand- and mudstone	Beds and bedsets continuous; sedimentary sructures rarely visible due to high bioturbation intensity	Quartz and lithic fragments embedded in matrix composed of silt-sized detrital mica and illite; quartz grains mostly floating in illite matrix and subordinate, isolated patches of ferroan carbonate	Shallow-tier *Planolites, Trichophycus, Skolithos;* well-bioturbated (BI 5-6; 91-100%); variable tiering depth, complex cross-cutting relationships	0.29	Lower shoreface, offshore transition; less influenced by lateral sediment transport dynamics

6.2 Facies M2 – Dark grey mudstone

Dark grey mudstones are relatively uncommon (<5 % of the beds) and have only been observed in the lower and middle part of the studied succession (Fig. 2-4). The mudstones are interbedded with thick-bedded, coarse-grained sandstones of Facies S1 (Fig. 2-4A). The bioturbation intensity in this unit is low (BI 1; <10 %), comprising sand-filled compressed, shallow-tier burrows with elliptical cross section up to 3 mm wide (Fig 5A – white arrows). Facies M2 consist of structureless, centimeter-thick ungraded, silt-bearing, clay-rich mudstones with subrounded, 'floating' grains of silt-sized quartz and minor feldspar (Figs 2-4B and C). The mudstones are well-cemented by post-compaction chlorite cement. The chlorite-dominated matrix contains subordinate illite and pyrite (Fig. 2-4D). This facies has an average TOC value of 0.37%, and $\delta^{13}C_{org}$ values are -28.8‰ on average.

6.3 Facies M3 – Sandy mudstone

Sandy mudstones are composed of cm-thick beds with eroded tops (Fig. 2-5A – yellow dashed line). In some cases bedding interfaces are siderite-cemented (Fig. 2-6A). This facies is burrow-mottled and highly (BI 4-5; 61-99%) bioturbated (Fig. 2-5B). The framework components include predominantly quartz, plagioclase and altered mafic grains, embedded in a Fe-rich chlorite matrix with minor contributions of illite/muscovite and biotite (Figs 2-5C and D). Framboidal pyrite is a common authigenic accessory mineral. Average TOC is 0.60% and $\delta^{13}C_{org}$ values are on average -28.9‰.

Figure 2-3. Facies M1 is regularly interbedded with facies S2. Graded bedding is uncommon this facies; instead, at least one grain-size break is developed in almost all cases through the sandstone-siltstone-mudstone transition; (*P*, *Planolites*; *Tr*, *Trichophycus*) (B) Thin- section scan (perpendicular to bedding) showing the tripartite subdivision characteristic for this facies (red arrows). (C) shows a low-power thin section micrograph (plane-polarized light). Mudstones of facies M1 are composed of predominantly illite/chlorite matrix with floating silt- and very-fine sand grains. (D) Backscattered SEM image of a representative region of facies M3 (Qz, quartz; Py, pyrite; Bio, biotite; Fsp, feldspar).

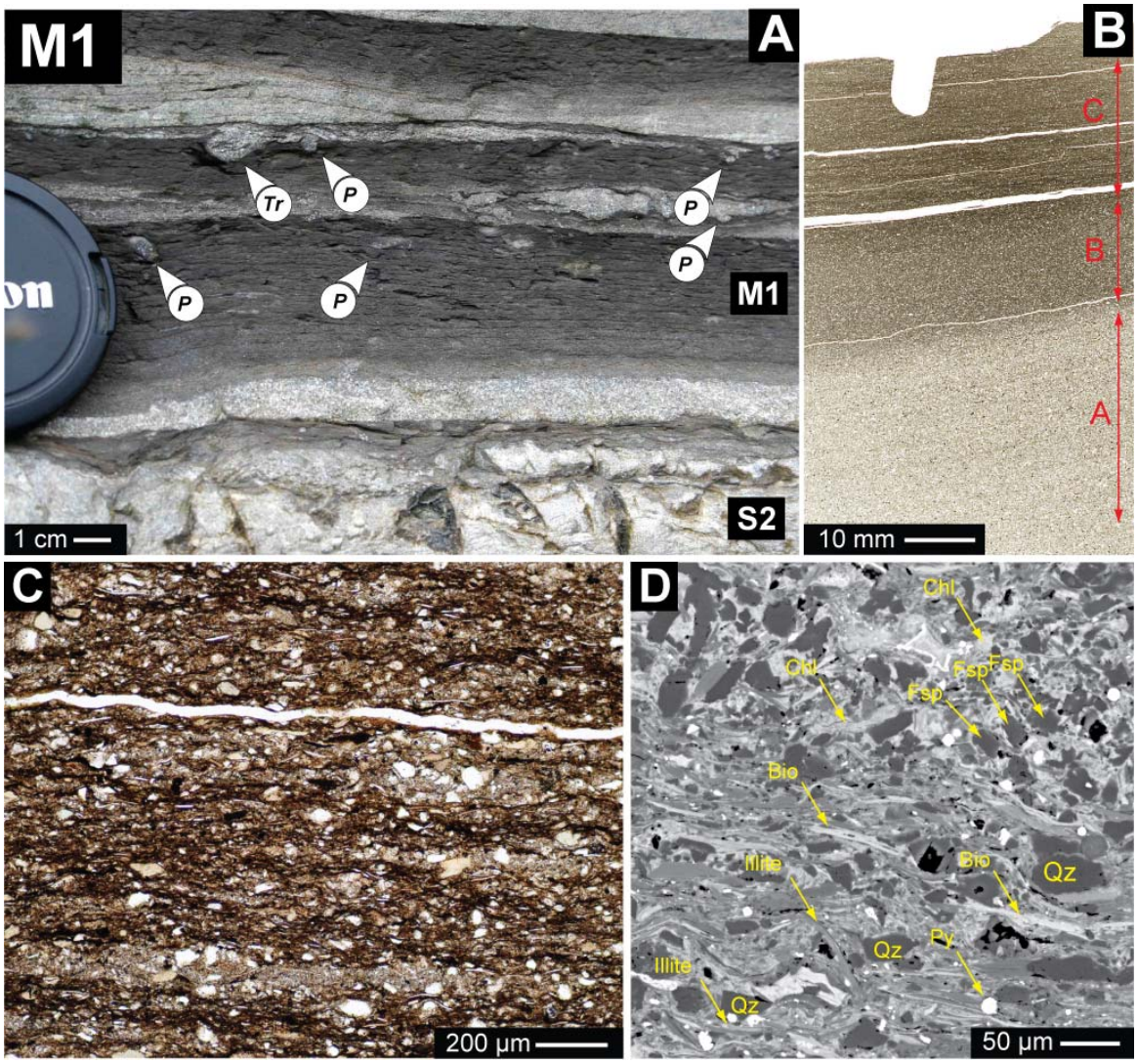
M1
A
Tr
P
P
P
P
P
M1
S2
1 cm
B
C
B
A
10 mm
C
200 µm
D
Chl
Chl
Fsp
Fsp
Fsp
Bio
Illite
Bio
Qz
Qz
Py
Illite
Qz
50 µm

Figure 2-4. Facies M2 comprises structureless and ungraded silt-bearing, clay-rich mudstones. The upper mudstone-sandstone contact is uneven (yellow dashed line), and muddy and flattened rip-up clasts are incorporated into the overlying sandstone of facies S1 (red arrows). (B) Thin section scan, perpendicular to bedding. (C) Low-power thin-section micrograph showing floating silt-grains (Qz) within clay-dominated matrix (illite/chlorite); plane-polarized light. (D) Backscatter SEM image showing composition of rock components within this facies (Qz, quartz; Chl, Chlorite; Py, Pyrite).

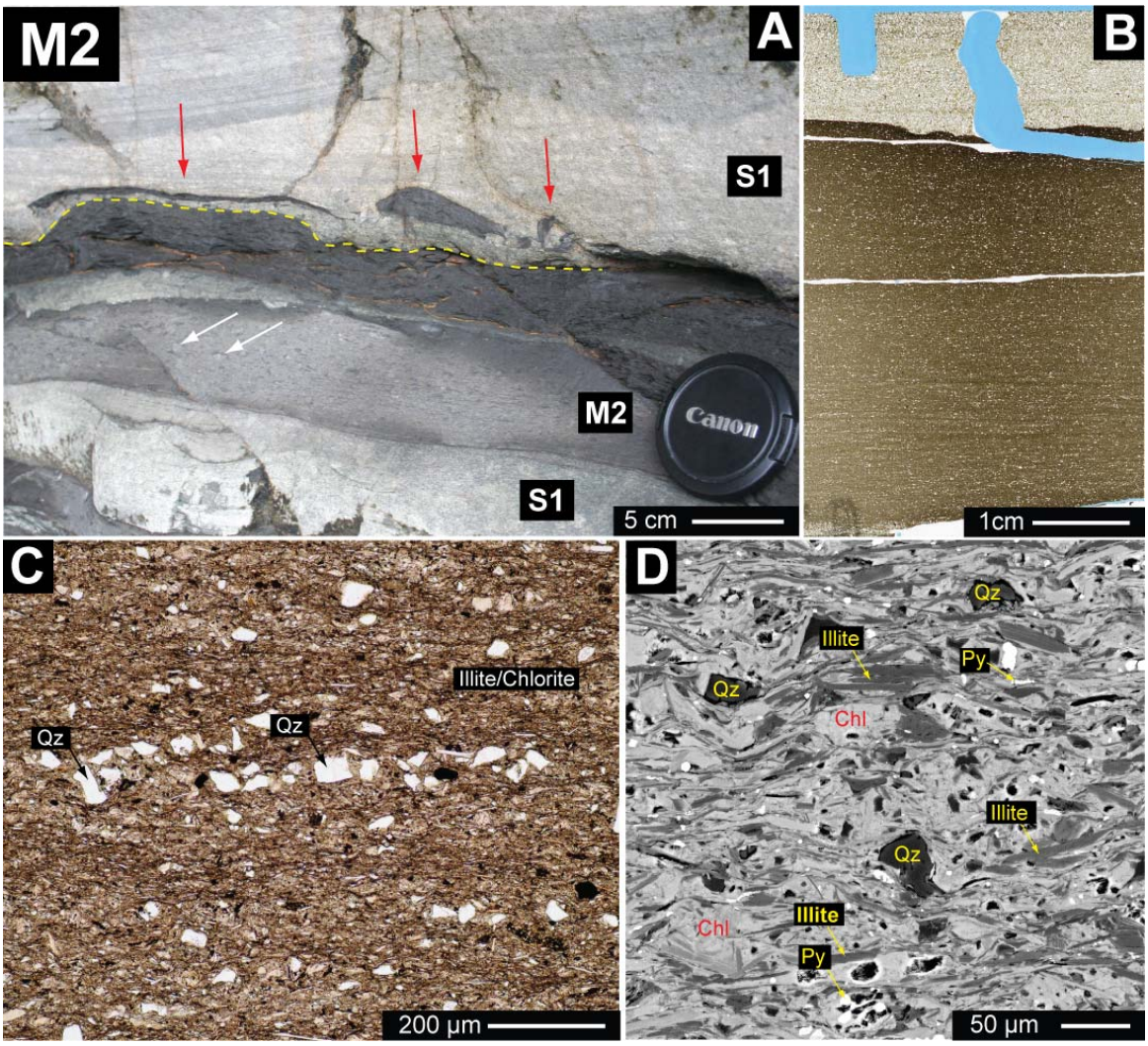
M2
A
S1
M2
S1
5 cm
B
1cm
C
Illite/Chlorite
Qz
Qz
200 µm
D
Qz
Illite
Py
Qz
Chl
Illite
Qz
Chl
Illite
Py
50 µm

Figure 2-5. This figure shows sandy mudstones of facies M3. These mudstones contain cm-thick, wavy and even continuous beds. Sandy mudstones are commonly bioturbated; the tops contain occasionally small shrinkage cracks (sc). (B) Thin section scan of facies M3, showing burrow-mottled fabric of sandy mudstones. (C) Thin section micrograph, perpendicular to bedding; plane-polarized light. This facies shows very fine-grained and fine-grained sand grains floating in a clay-dominated matrix. (D) Backscatter SEM image shows floating quartz grains (Qz), partially replaced Feldspar (Fsp) as well as abundant chloritized lithic (mafic?) clasts in an iron-rich chlorite matrix (Fe-chl). Authigenic pyrite (Py) and detrital mica (Biotite; Bio) and illite occur within the matrix.

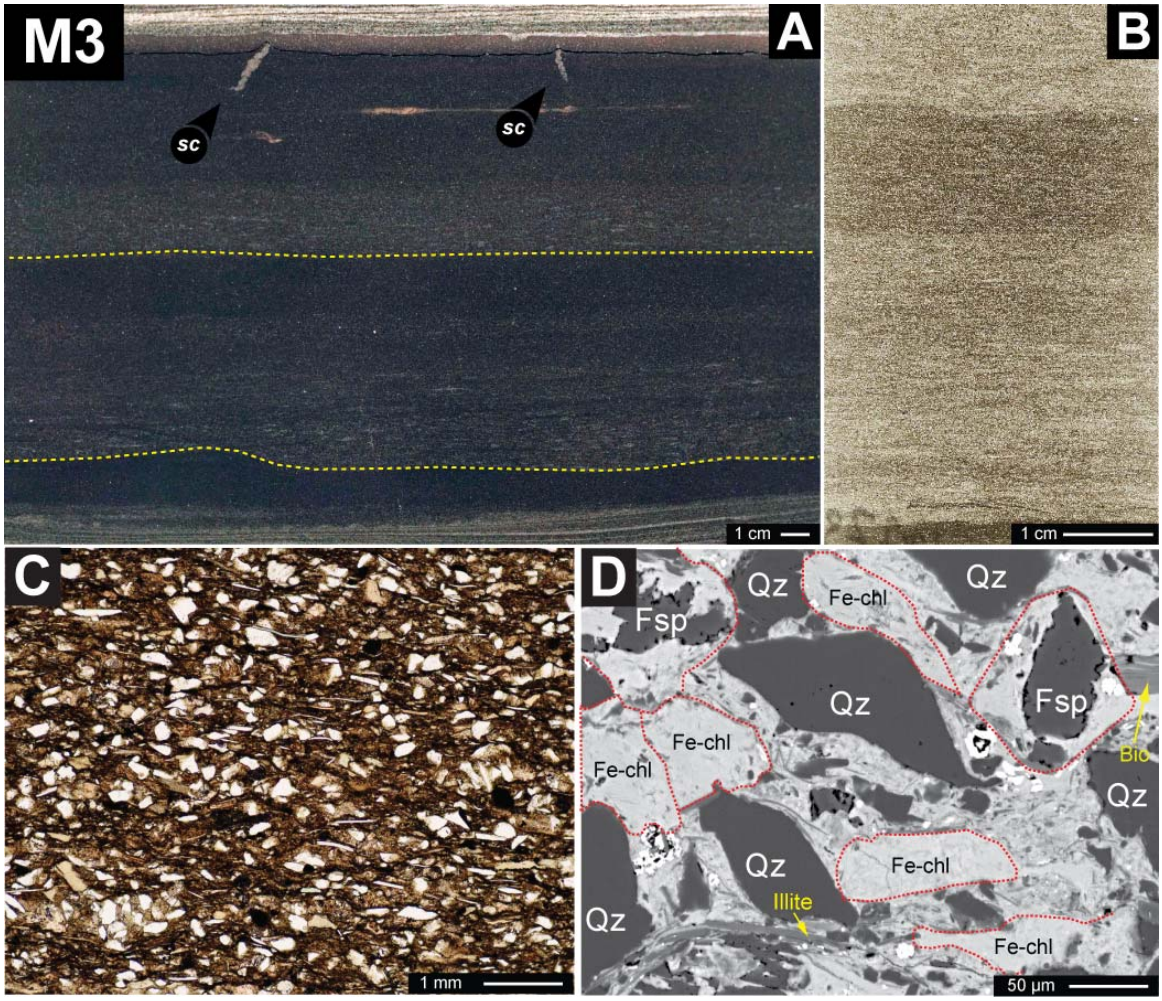
M3
A
sc
sc
1 cm
B
1 cm
C
1 mm
D
Qz
Fsp
Fe-chl
Qz
Qz
Fsp
Fe-chl
Fe-chl
Bio
Qz
Qz
Fe-chl
Illite
Qz
Fe-chl
50 µm

6.4 Facies M4 – Thick, unbioturbated mudstone

This facies contains silt- and clay-rich mudstones. Unbioturbated mudstones are up to 15 cm-thick and interbedded with minor, cm-thick, discontinuous sandstone lenses. Mud-on-mud erosional contacts are common in this facies. This facies is usually unbioturbated, except by deep tier burrows that originate from other facies (Fig. 2-6A and B). The silt-sized fraction includes quartz, lithic fragments and minor feldspar in a chlorite/illite matrix which contains biotite, muscovite, and framboidal pyrite and finely dispersed Ti-rich minerals as accessory components (Figs. 2-7C and D). Average TOC is 0.30% and $\delta^{13}C_{org}$ values are approximately 28.7‰ within this facies.

6.5 Facies M5 – Thin-bedded mudstone

This facies is composed of sand-bearing, silt- and clay-rich mudstone. The mud-dominated units contain centimeter-long starved, combined-flow ripples of fine-grained sandstone with erosional bases (Fig. 2-7A unit I). The starved ripples are sharply overlain by laminated silt (Fig. 7A unit II), and draped by unbioturbated mudstone (Fig. 2-7A unit III). A cross section 30° oblique to surface shown in Fig. 2-7A shows in unit I centimeter-sized, vertically stacked starved ripples with elongated, biconvex flanks (Fig. 2-7B). In this facies the majority of beds are mm-thick, discontinuous and normally graded with occasionally mm-sized starved ripples with erosional bases (Fig. 8A). This facies contains millimeter-sized, sand-filled, unlined, shallow-tier *Planolites (P)* and *Diplocraterion (D)* as well as mm- to cm-sized, funnel-shaped traces (aff. *Rosselia, Ro*) cross-cutting several

Figure 2-6. (A) This figure shows a slab of thick, unbioturbated mudstone (facies M4). Mudstones of this facies comprise centimeter-thick unbioturbated to sparsely bioturbated beds (indicated as arrowed intervals), which sometimes contain thin, normally-graded lags composed of silt and very fine-grained sand (yellow dashed line). (B) Thin-section scan perpendicular to bedding. Mudstones of this facies contain silty bases and tops are usually unbioturbated and contain mm-sized (diameter) occurrences of pyrite (blue arrows). (C) shows a thin-section micrograph (perpendicular to bedding; plane-polarized light) of M4 mudstones. Floating silt-sized quartz and feldspar are in clay-dominated matrix. Bioturbation comprises post-depositionally emplaced soft-ground burrows with elliptical cross-section. (D) Backscatter-SEM image of the clay-dominated matrix of facies M4 (Qz, quartz; Fsp, feldspar; Chl, chlorite; Py, pyrite).

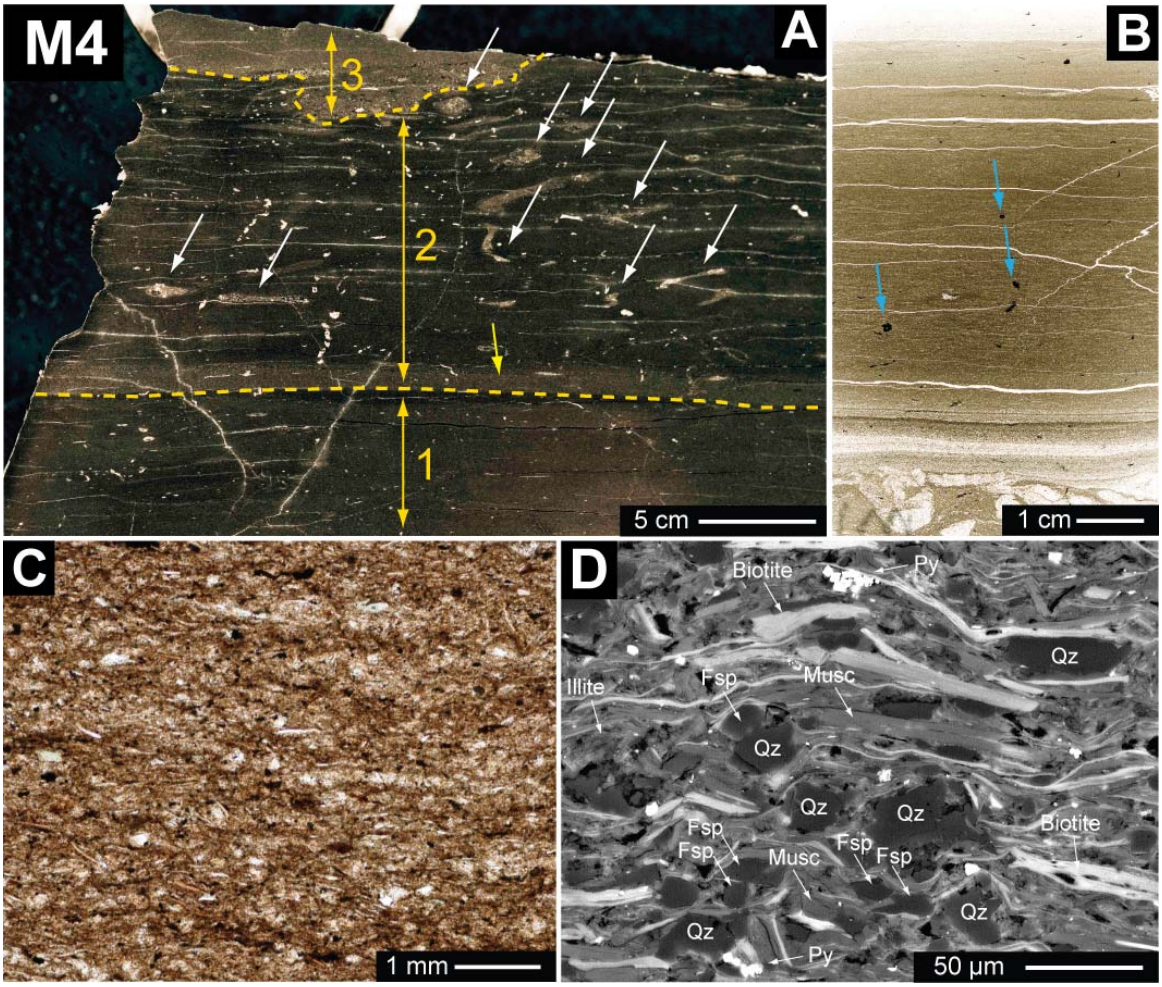
M4
A
3
2
1
5 cm
B
1 cm
C
1 mm
D
Biotite
Py
Qz
Illite
Fsp
Musc
Qz
Qz
Qz
Biotite
Fsp
Fsp
Musc
Fsp
Fsp
Qz
Qz
Py
50 µm

Figure 2-7. (A) Hand sample of facies M5, interbedded with facies S2. Mudstones contain starved combined-flow ripples, truncated by overlying silt- and clay-rich mudstone Yellow dashed lines outline either gas escape structures or vertical escape burrows. Locations for figures 9A and B are indicated with yellow bars. (B) Mudstones of this facies show combined flow structures with tripartite subdivision (I,II and III) and small *Planolites*, P. (C) shows an oblique cross section (30°) to imaged sample surface (A). This view shows vertically stacked and laterally displaced cross-ripples (green arrows) interpreted to be sand-clay combined flow deposits. This latter unit is underlain by previously reworked deposits containing palimpsest ichnofabrics (Ro, *Rosselia;* P, *Planolites*).

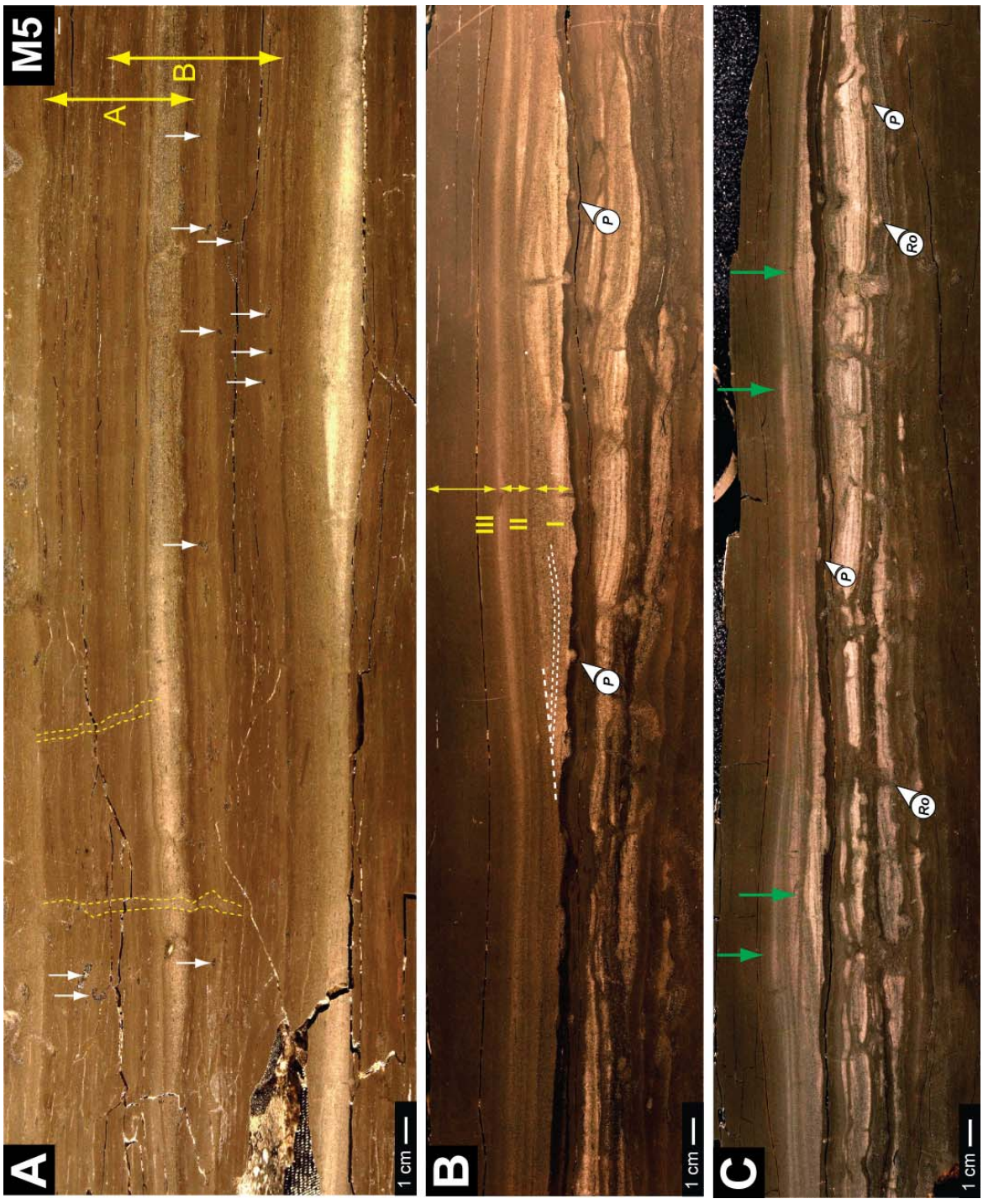
M5
A
B
A
B
III
II
I
P
Ro
1 cm
1 cm
1 cm

Figure 2-8. (A) Thin section scan (perpendicular to bedding) showing sparsely bioturbated (BI 1; 1-4%), mm-thick, normally graded beds with mm-sized starved ripples of siltstone in the base (white arrow). (B) Thin-section scan (perpendicular to bedding) showing mm-sized traces (P, *Planolites*; Ro, *Rosselia*; D, *Diplocraterion*) in thin-bedded mudstones from Fig. 8A.

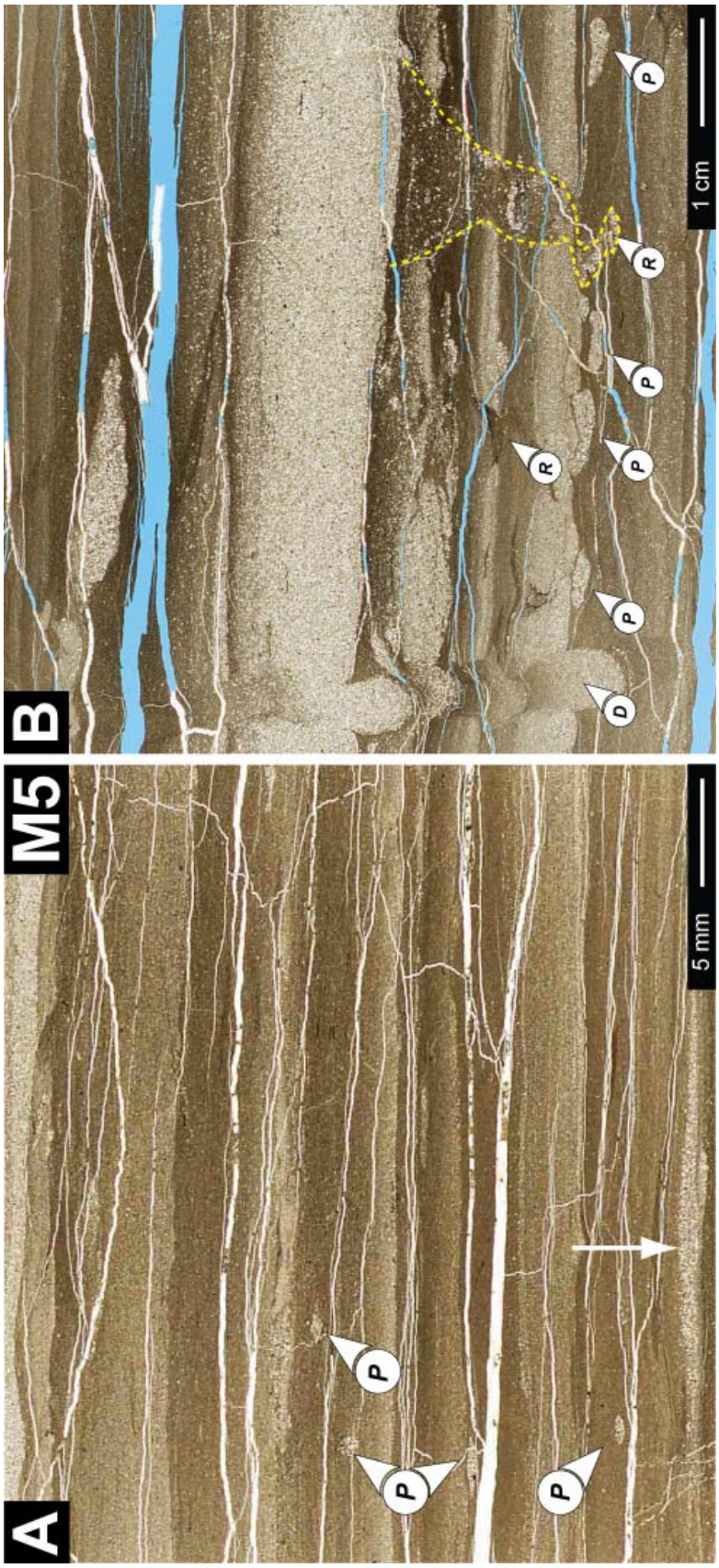
A
M5
P
P
P
5 mm
B
P
R
P
P
P
R
D
1 cm

thin beds (Fig 2-8B – yellow dashed line). Within this facies the overall bioturbation intensity is low (<10%) and depth of infaunal tiering is less than 5 cm. Mudstones within this facies contain "floating", subrounded grains of quartz and feldspar, embedded in a illite/chlorite matrix with subordinate biotite, muscovite and finely-dispersed aggregates of pyrite. Sand- and silt-sized lithic fragments and altered volcanic clasts are common. Average TOC values recorded from this facies are 0.53% and $\delta^{13}C_{org}$ values are on average -28.8‰.

6.6 Facies M6 – Sediment-starved mudstone

The cm-thick, laterally discontinuous, curved and non-parallel silt- and clay-rich mudstones of this facies contain sharp, irregular bases that cut into underlying beds of mudstone and sandstone. Interbedded sandstones contain discontinuous sediment-starved, combined-flow ripples (Fig. 2-9A). Bioturbation is sparse (BI 0-2; 0-30%), and where present consists of millimeter-sized, shallow-tier, sand-filled burrows (Fig. 2-9B). The chlorite- and illite-dominated mudstones of this facies contain accessory biotite and muscovite and silt-sized quartz, feldspar, framboidal pyrite, Ti-bearing minerals and dispersed siderite cement (Figs 2-9C and D). Within this facies the average TOC values are 0.28% and average $\delta^{13}C_{org}$ values are -28.6‰.

Figure 2-9. Mudstones of facies M6 are interbedding with cm-thick, starved combined-flow ripples. Bedding contacts contain abundant evidence for erosional events (red arrows) and shallow-tier bioturbation with high lateral variability. (B) shows a thin section scan of facies M6. The mudstones in this facies are composed of mm-thick beds with silty bases (dashed lines) and contain mm-sized sand-filled gutters (red arrows). Bedding tops are bioturbated by mm-sized, shallow-tier *Planolites (P)*. (C) Thin-section micrograph showing a silt-bearing, clay-rich matrix with sand-sized, authigenically-formed siderite (yellow arrows). (D) Backscatter SEM image of illite and chlorite-dominated portion of facies M6 showing silt grains (Qz) and microconcretions of siderite (Sd), closely associated with Fe-rich mica (Bio). Pyrite (Py) is not common within this facies.

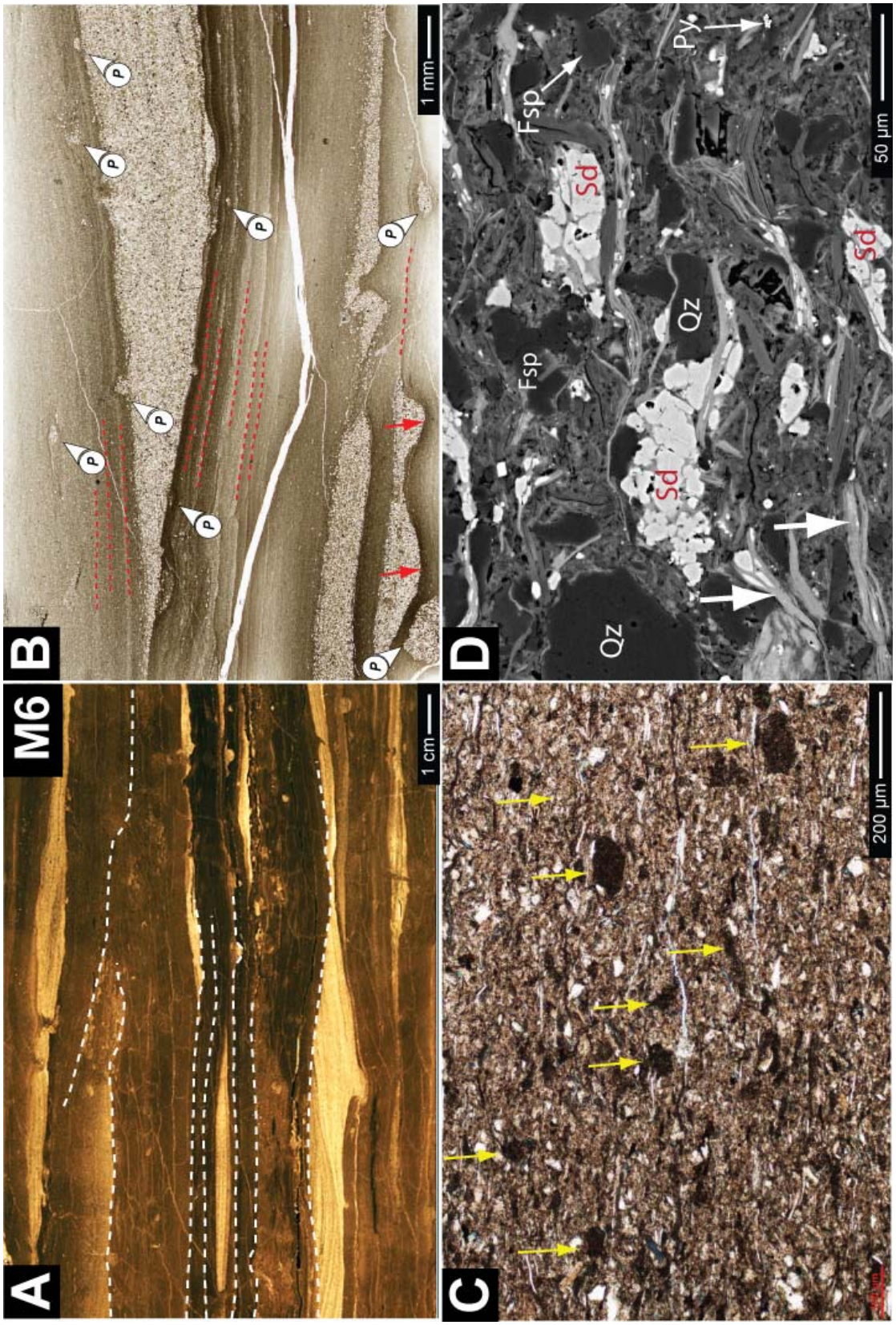
A
M6
1 cm
B
P
1 mm
C
200 µm
D
Qz
Fsp
Sd
Qz
Sd
Fsp
Py
Sd
50 µm

6.7 Facies M7 – Bioturbated mudstone

The centimeter-thick, bioturbated silty mudstones of this facies are interbedded with erosionally based sandstones. Trace fossils include *Planolites, Trichophycus, Gyrolites* and escape traces (Figs. 2-10A and B). Several sediment layers within facies M7 are burrow-mottled under soft-ground conditions. Mudstones of facies M7 are chlorite and illite dominated, with dispersed biotite, muscovite, pyrite and Ti-bearing minerals. This facies has TOC values averaging at 0.23% and average $\delta^{13}C_{org}$ values of -28.5‰.

6.8 Facies S1 – Thick-bedded sandstone

Sandstones of this facies consist of moderately sorted, subrounded, coarse-grained well-cemented quartz arenite. This facies contains continuous beds and bedsets of long-wavelength (m-scale) bedforms which contain very low-angle cross-stratified and planar bedded sandstones at the base. The upper part of the majority of beds within this facies contains low-angle bedforms with mm-spaced, tabular or sigmoidal cross-lamination. Sandstones of facies S1 are commonly unbioturbated (0-5%) and only contain rare *Arenicolites*.

Facies 2-10. This figure shows two representative polished slabs of facies M7. This facies contains highly variable sedimentary textures and mudstone of variable clay content. It is characterized by higher bioturbation intensities and more complicated tiering patterns. (B) Slab showing thin, even, discontinuous beds of facies M7 with shallow, sand-filled *Planolites* (*P*).

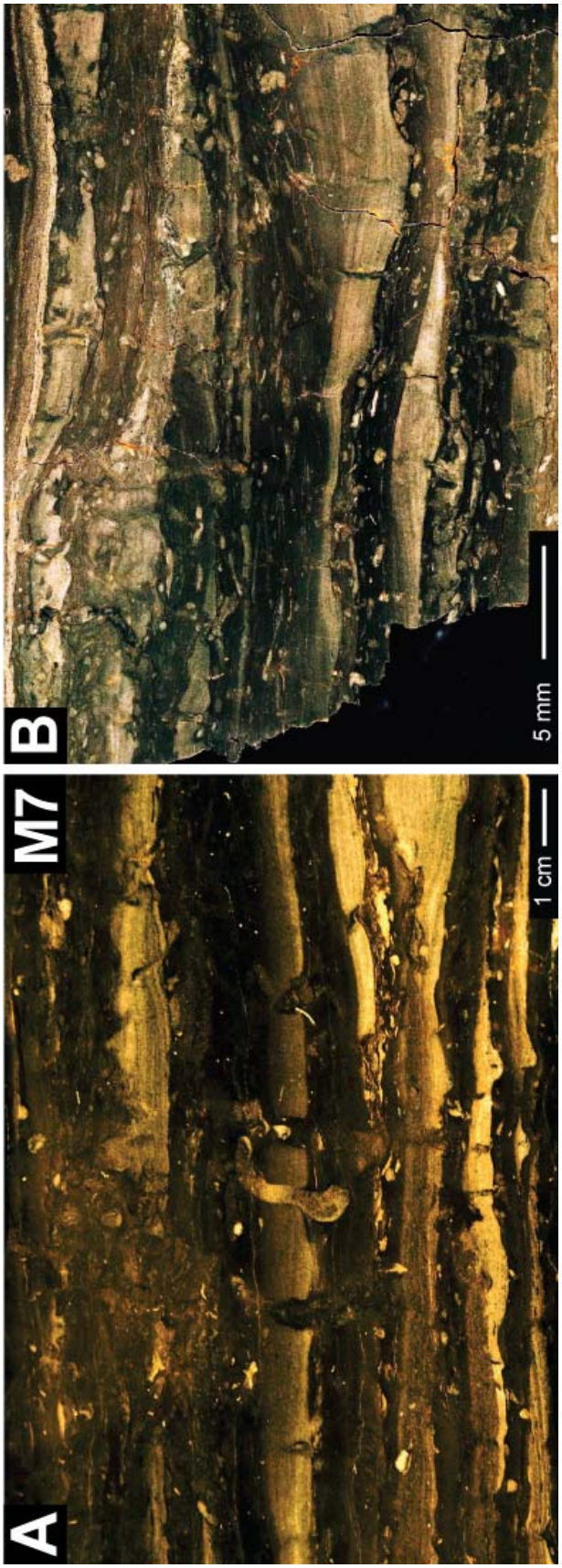
A
M7
1 cm
B
5 mm

6.9 Facies S2 – Thin-bedded sandstone

This facies makes up the majority of the sand-dominated lithologies within the Beach Formation at Freshwater Cove (Parsonville). This facies consist of poorly to moderately sorted, fine- to medium-grained sandstone, interbedding with mudstones of Facies M1 to M7. Thin-bedded (~10 cm-thick) sandstones are planar bedded with wave- and interference ripples at bedding tops. Beds and bedsets are discontinuous. This facies may also be composed of laterally continuous, 10 cm-thick hummocky cross-stratified sandstones. Bedding planes often contain Microbially-Induced Sedimentary Structures (Hagadorn and Bottjer 1997; Harazim et al. 2013) and internally, layers with broken and poorly rounded inarticulate brachiopod shell debris. Sandstones of this facies sandstones are composed of quartz and lithic fragments embedded in a matrix of silt-sized detrital mica (muscovite and biotite). Quartz grains are well-cemented via point and long contacts. The preserved inter-granular porosity is infilled with post-compaction chlorite and illite cement (Table 1). In rare cases thin-bedded sandstones contain thin layers of phosphate cement and isolated patches of inter-granular ferroan carbonate. This facies contains shallow-tier *Planolites, Trichophycus, Diplocraterion, Schaubcylindrichnus* and *Skolithos*. Sandstones of this facies are weakly to well-bioturbated (BI 2-6; 5-100%). The tiering depth is variable and cross-cutting relationships are simple. In rare cases sandstone bedding planes contain monogeneric suites of mud-filled *Skolithos.* Arthropod scratch marks (*Monomorphichnus*) and *Cruziana* are common on sandstone bedding planes (Fillion and Pickerill 1990; Harazim et al. 2013).

6.10 Facies S3 – Bioturbated sandstone

Bioturbated sandstones are composed of poorly to moderately sorted, fine- to medium-grained sand- and mudstone. Beds and bedsets are continuous and sedimentary structures are rarely preserved due to high bioturbation intensity. Mineralogically this facies is composed of quartz and lithic fragments and contains abundant silt-sized detrital mica and illite. Quartz grains are predominantly floating within an illite matrix and subordinate isolated patches of ferroan carbonate. Bioturbation consists of shallow-tier *Planolites, Trichophycus* and *Skolithos.* The facies is well-bioturbated (BI 5-6; 91-100%) and cross-cutting relationships are complex. The average TOC values are 0.29 wt% and $\delta^{13}C_{org}$ values average at -28.5‰.

7. Discussion

7.1 Mechanisms of mud transport in the Beach Formation

At the sub-cm scale the mudstones investigated within this study are non-homogeneous. The presence of normally-graded beds with erosive bases, small burrows and ripple-lamination (Figs 2-3 to 2-9; Table 1) is inconsistent with deposition by suspension fall-out from buoyant plumes or hemipelagic settling. Instead, based on grain size trends and fabrics, mudstones M1 to M4 are proposed to be deposits resulting from various classes of river borne density flows with varying deceleration times and clay concentrations. During storm events combined with significant fluvial discharge, large

quantities of fine-grained sediment can be discharged from rivers and estuaries to the shallow-marine shelf as dense, hyperpycnal flows that range from being turbulent to laminar (Hill et al. 2001; Baas et al. 2009; Kane and Ponten 2012). Even small amounts of cohesive mud can significantly influence flow rheology and settling dynamics since it affects the yield strength (Coussot 1997) and modulates turbulence (Baas et al. 2004). Within this study it has therefore been regarded as reasonable to focus on the interaction of high-density flows with the substrate and classify deposits based on their fraction of mud, bed boundary geometry and nature of sedimentary structures.

Facies M1 is characterized by stratified mudstones that often contain a tripartite subdivision (Fig. 2-3). Stratified mudstones exhibit a laterally continuous basal lag of coarse- to medium-grained sand, which is overlain by a largely unsorted, silt-rich mudstone. The grain size distributions result from turbulence modulation and differential settling of non-cohesive sand, silt and flocculated clay. The presence of coarse sand in the base and well-preserved, continuous grain size contacts has previously been inferred to represent the sedimentary products of rapidly decelerating, hyperconcentrated flows (Sumner et al. 2009; van Maren et al. 2009). Longer deceleration times would necessarily involve the formation of coarse- to medium-grained sand ripples and subsequent incorporation of clay into the sand ripple (Baas et al. 2011). This has not been observed within facies M1. Additionally, the fact that the top within M1 contains “floating” silt and fine sand within a clay-rich matrix, indicates that during the waning phase, a reduction in particle support in the top layer (as both, coarse and fine sand settle out of the flow) is, in turn, compensated by increased cohesive matrix strength that prevents silt from settling out of the flow. Bipartite beds form under transitional flow conditions where the vast

majority of flocculated clay and silt and a small amount of sand were in suspension and were deposited without developing a graded bed (Baas et al. 2011).

It appears that bedform development during flow deceleration is strongly controlled by the grain-size distribution of material in suspension as well as the density of the flow (Ozdemir et al. 2011). This part of the Beach Formation also contains rare occurrences of silt-bearing, clay-rich mudstones, interbedded with cross-stratified sandstones (facies S1 and S2; Table 1). Mudstones of facies M2 were most likely deposited as cohesive, near-shore marine muds via pulsed discharge events from rivers and estuaries that contained less sand (Fig. 2-4). In Facies M3 sand-sized grains are incorporated into a clay-rich matrix. A grain size break is less well developed, although grain separation is clearly visible at the hand specimen scale (Fig. 2-5A). The latter mudstones might have resulted as quickly decelerated, river borne, hyperpycnal flows that contained a relatively low clay concentration (cf Baas et al. 2011). Given the high number of chloritized grains it might be possible that a large abundance of clay minerals have formed during deep diagenetic in-situ alteration of unstable mafic minerals (cf. Hower et al. 1976). Given the lateral continuity of bounding surfaces, well-developed grain-size contacts and absence of ripple bedding and lamination, mudstones of facies M1 to M4 most likely originate as deposits of flood events with less evidence for wave-influenced processes during deposition (cf. Mulder et al. 2003; Bhattacharya and MacEachern 2009; Chang and Chun 2012; Figs 2-3 to 6).

Another class of mudstones with contrasting sedimentary structures and a different inferred mode of deposition is represented by Facies M5. The sedimentary structures (i.e., muddy beds with basal erosion surfaces), observed in facies M5 (Fig. 2-7A) are

comparable with structures that have previously been interpreted as the distal deposits of wave-enhanced sediment gravity flows of fluid mud (Bentley and Nittrouer 2003; Keen et al. 2006; Macquaker et al. 2010a). Such combined flow deposits show a distinct succession of sedimentary structures from pronounced erosionally-based units, initially overlain by upward-curved laminae, and capped by normally-graded laminae of silt- and clay-rich mudstone (Fig. 7). Exceptionally large discharge events in shallow-marine conditions can coincide with wave reworking of the sea floor (Mulder and Syvitski 1995; Kineke et al., 1996; Lamb and Parsons 2005). It is predicted, that under the combined force of large, shore-parallel surface gravity waves and gravity (as the down-slope component), sediment can be transported offshore on very low-gradient slopes via combined wave- and gravity-driven flows (cf. Traykovski et al. 2000; Friedrichs and Wright 2004; Ozdemir et al. 2011). The presence of combined-flow structures in muddy lithologies of the Beach Formation (Fig. 2-7C) indicates that mud was dispersed advectively, possibly as concentrated near-bed slurry at the sediment-water interface via combined flows and did not just accumulate as a continuous rain of particles from buoyant plumes. The presence of sedimentary structures indicating high-energy sea-floor processes are inconsistent with all previously proposed paleoenvironmental models for the Beach Formation, that relate these mudstones to anoxic and low-energy conditions at the sediment-water interface (cf. Fillion and Pickerill 1990).

Mudstones belonging to facies M6 are more common above 15 m stratigraphic height. Based on a high lateral variability of bedding geometry (e.g., starved combined-flow ripples) and bedding thickness in sand- and mudstones, it is possible to infer that mudstones in facies M6 indicate less frequent deposition of fine-grained sediment and a

comparatively higher importance of wave-reworking of previously deposited mud. Mud-on-mud erosional surfaces (Figs 2-9A and B) in facies M6 indicate physical reworking of pre-existing, partially consolidated mud deposits. Modern experiments have demonstrated that temporal modulation of shear-generated turbulence in unidirectional sand-mud flows on muddy sand often results in scours which are often 'healed' by triangular patches of sand (Baas et al. 2013). Additionally, in these latter experiments sandstone ripples are deposited on the mud-dominated bed. However, these experimentally produced sandstone ripples mostly occur on mudstone tops and exhibit angle-of-repose cross-lamination. Within this study winnowed patches of sand also have the tendency to heal mud scours (Fig. 2-9B – red arrow); however, the sandstones internally exhibit combined-flow structures instead of current lamination. The occurrence of sand-sized aggregates of siderite (Figs 9C and D) is only confined to this facies and indicates both periodic reworking and wave-dominated dispersal of previously semi-consolidated mudstone with early diagenetic crusts, or, alternatively in situ, diagenetic growth of siderite under prolonged conditions of anoxic diagenesis (Curtis et al. 1986).

Bioturbated mudstones (M7) are interpreted to represent sufficiently long bed exposure times. Palimpsest ichnofabrics indicate that exposure times are long enough to allow for sediment to become completely colonized. Cross-cutting relationships reveal that most of the trace fossils pre-date the deposition of overlying sandstone beds. Even though most of the mudstones contain ample evidence for bioturbation (i.e., partial homogenization of entire beds by predominantly shallow-tier *Planolites*; Fig. 2-10), compelling evidence for fluid sediment swimming (i.e., 'mantle and swirl' structures; Lobza and Schieber 1999), is absent. This relationship indicates that the soupground stage

was either not preserved (as a result of winnowing), or that the mudstones became re-colonized at later stage after the mud was partially dewatered. Well-bioturbated, heterolithic beds of facies M7 and S3 (Bioturbated sandstones) indicate that these beds experienced lower accumulation rate and were most likely not within the range of frequent down-drift supply of fine-grained sediment.

7.2 Organic matter characteristics

Stratigraphic intervals that are inferred to have been deposited by gravity-dominated flow types under low net reworking rates (facies M1, M2, M3, M4) have overall slightly higher TOC values (~0.5%), whereas mudstones that have spend longer periods in a wave-dominated regime (facies M5, M6 and M7) close to the sediment surface (M5, M6) exhibit overall lower (~0.2%) TOC values (Fig. 2-11). The latter mudstones however contain isolated beds that exhibit peak TOC values of up to 3.4% (Table 1; Harazim et al. 2013).

Given the overall evidence that mud-dispersal occurred above storm-wave base, it can be argued that exposure time to oxygenated bottom-water, reworking frequency of bottom sediment and frequency of fine-grained sediment deposition played a significant role in the preservation of organic carbon. The entire whole-rock $\delta^{13}C_{org}$ dataset reveals a relatively narrow isotopic range (-27.5 to -29.5‰; Figs 2-2 and 2-11A) with only a weak facies-dependent correlation (Fig. 2-11C). Facies M1 records $\delta^{13}C_{org}$ values which span this entire range, whereas other facies plot in a narrower window never exceeding 1‰ (Fig. 2-11C). The reasons for this low spread might be due to mixing of different organic

Figure 2-11. (A) shows a cross-plot of TOC and $\delta^{13}C_{org}$ values for whole-rock measurements. (B) Box-and-whisker plots displaying maximum, minimum, median and 1st and 3rd quartile (if available) for whole-rock TOC values within a facies at Freshwater Cove. Note the light positive correlation between TOC values measured from event beds (M1, M2, M3, M4 and M5) versus TOC values measured from units that experienced more reworking prior to burial (M6 and M7). Bioturbated sandstones (facies S3) have been included in this correlation and show equally low TOC values. (C) Box-and-whisker plots for $\delta^{13}C_{org}$ values show similar values for all mudstone facies M1, M4, M5, M6, M7, and S3. The wide range of data within facies M1 seems to indicate a modified organic matter composition (see text for discussion).

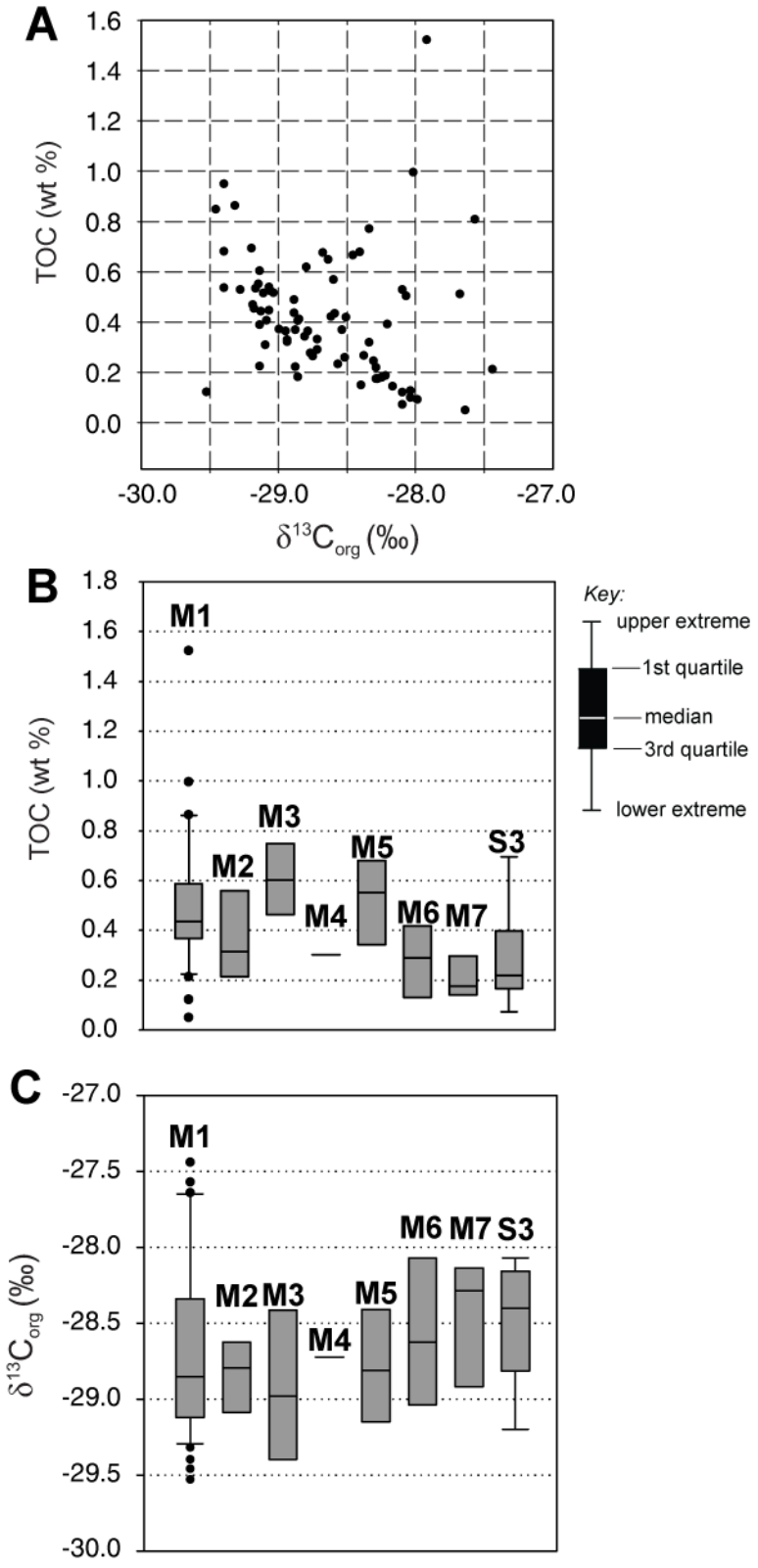
A
TOC (wt %)
1.6
1.4
1.2
1.0
0.8
0.6
0.4
0.2
0.0
-30.0
-29.0
-28.0
-27.0
δ13Corg (‰)
B
TOC (wt %)
1.8
1.6
1.4
1.2
1.0
0.8
0.6
0.4
0.2
0.0
M1
M2
M3
M4
M5
M6
M7
S3
Key:
upper extreme
1st quartile
median
3rd quartile
lower extreme
C
δ13Corg (‰)
-27.0
-27.5
-28.0
-28.5
-29.0
-29.5
-30.0
M1
M2
M3
M4
M5
M6
M7
S3

carbon sources, or alternatively mirror the residual remineralized end-member buried within a higher-energy seafloor regime. Petrological assessment of the preserved organic fraction (Harazim et al. 2013) revealed little net preservation of the common constituents of modern sedimentary organic matter, such as fecal pellets (Rhoads and Boyer 1982; Cuomo and Bartholomew 1991) or marine snow (Arthur et al. 1994). Instead, the visible organic carbon fraction of shallow-marine mudstones consists of benthic microbial kerogen within both sandstone- (Hagadorn and Bottjer, 1997) and mudstone-dominated facies (Harazim et al., 2013). This latter organic carbon has been demonstrated to be generated at or below the sea-floor under conditions of suppressed bioturbation resulting in locally elevated TOC values (>1%) preferably in facies M1 (Figs 2-2 and 2-11). The possible contribution of a land-dominated portion of organic carbon is considered to be unlikely given the (a) old geological age of this succession and (b) no conclusive petrological evidence for cellular woody or plant remains within any of the studied material. The high presence of unbioturbated mudstones might therefore not only be attributed to the quick removal of event beds out of the zone of bioturbation (facies M1 to M4), but also to the remineralization efficiency of sedimentary organic matter within a high-energy sea-floor regime. Since any entrained bioavailable organic carbon is quickly remineralized through microbial reworking in a wave-dominated seafloor regime, the residual organic matter is proposed to be altered and progressively unattractive to bioturbating infauna the longer its residence time in the oxic and suboxic zone (cf. Aller 2004).

7.3 Pore-water conditions during sediment burial

The petrological analysis of inorganic rock components reveals that mudstones of facies M1 to M4 were initially immature and contained a significant contribution of unstable mafic minerals and feldspar (Fig. 2-5D). The unusual thickness (>10cm) of unbioturbated mudstone beds within facies M1 (Fig. 2-3), combined with a high abundance of post-compaction grain alteration and replacement, preferably in facies M2 and M3 (Figs 2-4 and 2-5) lends to support a relatively short time period between production of fine-grained sediment up-dip (i.e., via mechanical weathering), transport and burial. The rock components susceptible to weathering (e.g., mafic minerals, Ca-rich feldspar) were probably delivered to the shelf via pulsed discharge events (i.e., as flash floods from a non-vegetated early Paleozoic hinterland) that were not subjected to significant weathering along the terrestrial portion of the dispersal path (cf. Hillier 1995).

Evidence for sea-floor reworking in mudstone facies M6 suggests that the reactivity of organic carbon exerted an important control on the early diagenetic mineral inventory. Specifically, the formation of significant amounts of siderite, instead of pyrite, within open-marine facies M6 (Fig. 2-9D) is taken as evidence to infer episodic non-steady diagenetic conditions that favor the formation of Fe-rich minerals other than pyrite (cf. Aller 2004). Previous research has demonstrated that in shallow-marine, mud-dominated environments with high supply of iron oxides and iron (oxy) hydroxides microbial iron reduction is the energetically more favorable diagenetic pathway (instead of sulfate reduction; Berner 1984) and might result in the precipitation of iron-rich phases from

Figure 2-12. Conceptual summary diagram showing important parameters considered for the generation of unbioturbated mudstones and the role of waves and gravity-dominated processes. In order to preserve unbioturbated mudstones within a shallow-marine, heterolithic environment three master variables are considered. Those are (a) frequency of disturbance, (b) duration of low-energy intervals, and (c) reworking depth (see text for discussion).

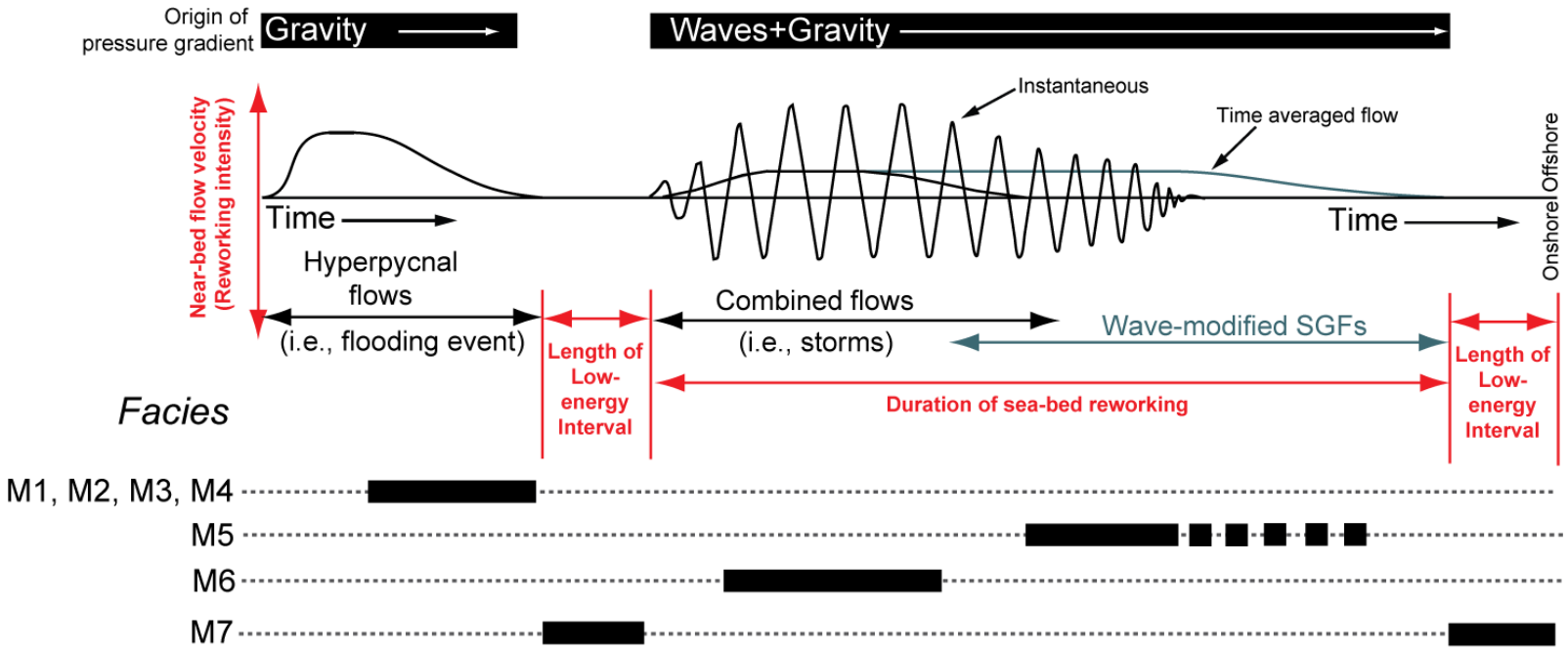
Origin of pressure gradient
Gravity
Waves+Gravity
Instantaneous
Time averaged flow
Near-bed flow velocity (Reworking intensity)
Time
Time
Onshore
Offshore
Hyperpycnal flows
(i.e., flooding event)
Combined flows
(i.e., storms)
Wave-modified SGFs
Length of Low-energy Interval
Duration of sea-bed reworking
Length of Low-energy Interval
Facies
M1, M2, M3, M4
M5
M6
M7

pore waters (Aller et al. 1986; Raiswell 2011). The frequent remobilization of the sea-floor under relatively slow net accumulation and presumably low organic carbon reactivities is significant in these systems. First, the low amounts of liberated hydrogen sulfide produced by bacterial sulfate reduction might not be sufficient to remove all reactive ferrous iron from pore waters in the form of pyrite. Secondly, prolonged periods of microbial iron reduction result in net acid-consumption followed by a relative increase of pore water pH (Taylor and Curtis 1995). Within the Beach Formation siderite might have preferably precipitated in regions of the shelf that experienced frequent wave reworking and persistently high pH conditions. Mudstones of facies M1, instead, contain locally elevated TOC values (>1 wt%) and higher contributions of framboidal pyrite and an absence of siderite (Harazim et al. 2013). The exact origin of these microconcretions requires further research, because at present it is not possible to determine if ferroan carbonate precipitated as products of suboxic diagenesis or if these microconcretions represent are the result of methanogenesis later during burial (Taylor and Curtis 1995; Taylor and Macquaker 2000).

The well-bioturbated beds of facies M7 and S3 (Bioturbated sandstone) most likely represent depositional environments that experienced less frequent reworking by wave- and gravity-driven processes and probably experienced more intense nutrient cycling (cf. McIlroy and Logan 1999) and therefore more ideal paleo-environmental conditions that allowed bioturbators to rework sediment completely (Fig. 2-12).

Combining sedimentological, ichnological and geochemical evidence is of paramount importance to understand the first-order controls on organic carbon preservation and compositional diversity in mudstones that were deposited from high-energy sea-bed

processes. Early Paleozoic shallow-marine, muddy depositional environments are under-represented in the geological literature. Integrated sedimentological and geochemical approaches provide more realistic models on the preservation of organic carbon in heterolithic depositional environments and a more complete picture on the first-order controls on compositional and textural diversity of mudstones and black shales deposited along the entire margin-to-basin transect.

8. Conclusions

1. Combined sedimentological, ichnological and geochemical evidence reveals that hyperpycnal flows were the primary delivery process for fine-grained sediment in the Tremadocian Beach Formation of Bell Island. Mud layers investigated shoreface setting also contain textural evidence for subsequent reworking by wave-enhanced sediment gravity flows.
2. This interpretation contrasts with previous interpretations of the Beach Formation, which explained the preservation of unbioturbated mudstone beds by a combination of periodically anoxic, low-energy conditions, or by periodic salinity fluctuations in a tidal paleoenvironment. Instead, it is proposed that shoreface mudstones in the Beach Formation accumulated in a high-energy seafloor regime, under fully oxygenated, normal marine bottom waters.
3. The retention of organic carbon in this Early Ordovician muddy shoreface environment is most likely a function of residence time of organic material in the

oxic and suboxic zone of the sediment. A delicate interplay between the three master variables (a) frequency of physical disturbance, (b) duration of exposure, and (c) depth of erosion will most likely be the first-order control on the preservation potential of organic carbon in the Beach Formation.

4. Burial efficiency and bioavailability of organic matter is inferred to be a critical variable that might control bioturbation intensities within wave-reworked mudstones in the Beach Formation than oxygen or salinity changes.

9. Acknowledgements

DH acknowledges financial support via student grants sponsored by AAPG, IAS, GSA and SEPM. DMc acknowledges the financial support of the Canada Research Chair program and a NSERC discovery grant. Dr. Richard Callow and Dr. Rick Hiscott are both thanked for sharing their experience on gravity flow deposits and critical reading of a previous version of this manuscript. Kathryn Denommee, Peter Hülse, Florian Bulle and Tiffany Miller are thanked for helpful discussions and for assisting during field work on Bell Island.

10. References

AIGNER, T. AND REINECK, A., 1982, Proximality trends in modern storm sands from the Helgoland Bight (North Sea) and their implications for basin analysis: Senckenbergiana Maritima, v. 14, p. 183-215.

ALGEO, T.J. AND LYONS, T.W., 2006, Mo-total organic carbon covariation in modern anoxic marine environments: Implications for analysis of paleoredox and paleohydrographic conditions: Paleoceanography, v. 21, PA1016

ALLER, R.C., MACKIN, J.E. AND COX JR., R.T.,1986, Diagenesis of Fe and S in Amazon inner shelf muds: apparent dominance of Fe reduction and implications for the genesis of ironstones: Continental Shelf Research v. 6, p. 263-289.

ALLER, R.C., 2004, Conceptual models of early diagenetic processes: The muddy seafloor as an unsteady, batch reactor: Journal of Marine Research, v. 62, p. 815-835.

ALLER, R.C., MADRID, V., CHISTOSERDOV, A., ALLER, J.Y. AND HEILBRUN, C., 2010, Unsteady diagenetic processes and sulfur biogeochemistry in tropical deltaic muds: Implications for oceanic isotope cycles and the sedimentary record: Geochimica et Cosmochimica Acta, v. 74, p. 4671-4692.

ALLISON, M.A., KUEHL, S.A., MARTIN, T.C. AND HASSAN, A, 1998, Importance of flood-plain sedimentation for river sediment budgets and terrigeneous input to the oceans: Insights from the Brahmaputra-Jamuna River: Geology, v. 26, p. 175-178.

ALLISON, M.A., DELLAPENNA, T.M., GORDON, E.S., MITRA, S. AND PETSCH, S.T., 2010, Impact of Hurricane Katrina (2005) on shelf organic carbon burial and deltaic evolution: Geophysical Research Letters v. 37, L21605

ARTHUR, M.A. AND SAGEMAN, B.B., 1994, Marine black shales: depositional mechanisms and environments of ancient deposits: Annual Review of Earth and Planetary Sciences v. 22, p. 499-551.

BAAS, J.H., VAN KESTEREN,W. AND POSTMA, G., 2004, Deposits of depletive high-density turbidity currents: a flume analogue of bed geometry, structure and texture. Sedimentology, 51, 1053–1088.

BAAS, J.H., BEST, J.L., PEAKALL, J. AND WANG, M., 2009, A phase diagram for turbulent, transitional, and laminar clay suspension flows: Journal of Sedimentary Research, v. 79, p. 162-183.

BAAS, J. H., BEST, J. L., AND PEAKALL, J., 2011, Depositional processes, bedform development and hybrid bed formation in rapidly decelerated cohesive (mud–sand) sediment flows: Sedimentology, v. 58, p. 1953-1987.

BAAS, J.H., DAVIES, A.G. AND MALARKEY, J., 2013, Bedform development in mixed sand-mud: The contrasting role of cohesive forces in flow and bed: Geomorphology, v. 182, p. 19-32.

BENTLEY, S.J. AND NITTROUER, C.A., 2003, Emplacement, modification, and preservation of event strata on a flood-dominated continental shelf: Eel shelf, Northern California: Continental Shelf Research, v. 23, p. 1465-1493.

BERNER, R.A., 1984, Sedimentary pyrite formation: An update: Geochimica et Cosmochimica Acta, v. 48, p. 605-615.

BHATTACHARYA, J.P. AND MACEACHERN, J.A., 2009, Hyperpycnal rivers and prodeltaic shelves in the cretaceous seaway of North America: Journal of Sedimentary Research v. 79, p. 184-209.

BLAIR, N.E. AND ALLER, R.C., 2012, The fate of terrestrial organic carbon in the Marine environment: Annual Review of Marine Science, v. 4, p. 401-423.

BRENCHLEY, P.J., PICKERILL, R.K. AND STROMBERG, S.G., 1993, The role of wave reworking on the architecture of storm sandstone facies, Bell Island Group (Lower Ordovician), Eastern Newfoundland: Sedimentology, v. 40, p. 359-382.

CAMPBELL, C. V., 1967, Lamina, laminaset, bed, and bedset. Sedimentology, v. 8, p. 7-26.

CATUNEANU, O. AND ZECCHIN, M., 2013, High-resolution sequence stratigraphy of clastic shelves II: Controls on sequence development: Marine and Petroleum Geology, v. 39, p. 26-38.

CHANG, T.S. AND CHUN, S.S., 2012, Micro-characteristics of sustained, fine-grained lacustrine turbidites in the Cretaceous Hwangsan Tuff, SW Korea: Geosciences Journal, v. 16, p. 409-420.

COPLEN, T.B., BRAND, W.A., GEHRE, M., GRÖNING, M., MEIJER, H.A.J., TOMAN, B. AND VERKOUTEREN, R.M., 2006, After two decades a second anchor for the VPDB $\delta^{13}C$ scale: Rapid Communications in Mass Spectrometry v. 20, p. 3165-3166.

CUOMO, M.C. AND BARTHOLOMEW, P.R., 1991, Pelletal black shale fabrics: their origin and significance: Modern and ancient continental shelf anoxia, pp. 221-232.

COUSSOT, P., 1997, Mudflow Rheology and Dynamics. IAHR Monograph, Balkema, Rotterdam, 272 pp.

CURTIS, C.D., COLEMAN, M.L., AND LOVE, L.G., 1986, Pore water evolution during sediment burial from isotopic and mineral chemistry of calcite, dolomite and siderite concretions: Geochimica et Cosmochimica Acta, v. 50, p. 2321–2334.

DEMAISON, G.J. AND MOORE, G.T., 1980, Anoxic environments and oil source bed genesis: American Association of Petroleum Geologists Bulletin, v. 64, p. 1179-1209.

FILLION, D. AND PICKERILL, R.K., 1990, Ichnology of the Upper Cambrian? to Lower Ordovician Bell Island and Wabana groups of eastern Newfoundland, Canada: Palaeontographica Canadiana, v. 7, p. 1-119.

FOLK, R.L., 1980, Petrology of Sedimentary Rocks: Austin, Texas, Hemphill Publishing Company, 182 p.

FRIEDRICHS, C.T. AND WRIGHT, L.D., 2004, Gravity-driven sediment transport on the continental shelf: Implications for equilibrium profiles near river mouths Coastal Engineering, v. 51, p. 795-811.

GHADEER, S.G. AND MACQUAKER, J.H.S., 2012, The role of event beds in the preservation of organic carbon in fine-grained sediments: Analyses of the sedimentological processes operating during deposition of the Whitby Mudstone Formation (Toarcian, Lower Jurassic) preserved in northeast England. Marine and Petroleum Geology, v. 35, p. 309-320.

HAGADORN, J.W. AND BOTTJER, D.J., 1997, Wrinkle structures: Microbially mediated sedimentary structures common in subtidal siliciclastic settings at the Proterozoic-Phanerozoic transition: Geology, v. 25, p. 1047-1050.

HARAZIM, D., CALLOW, R.H.T. AND MCILROY, D., 2013, Microbial mats implicated in the generation of intrastratal shrinkage (‘synaeresis’) cracks. Sedimentology, in press.

HASTINGS, R.H., GOÑI, M.A., WHEATCROFT, R.A. AND BORGELD, J.C., 2012, A terrestrial organic matter depocenter on a high-energy margin: The Umpqua River system, Oregon: Continental Shelf Research, v. 39-40,p. 78-91.

HAUGHTON, P., DAVIS, C., MCCAFFREY, W. AND BARKER, S., 2009, Hybrid sediment gravity flow deposits - Classification, origin and significance: Marine and Petroleum Geology, v. 26, p. 1900-1918.

HEDGES, J.I. AND KEIL, R.G., 1995, Sedimentary organic matter preservation: an assessment and speculative synthesis: Marine Chemistry, v. 49, p. 81-115.

HILL, P.R., PETER LEWIS, C., DESMARAIS, S., KAUPPAYMUTHOO, V. AND Rais, H., 2001, The Mackenzie Delta: Sedimentary processes and facies of a high-latitude, fine-grained delta: Sedimentology, v. 48, p, 1047-1078.

HILL, P. S., FOX, J. M., CROCKETT, J. S., CURRAN, K. J., FRIEDRICHS, C. T., GEYER, W. R., MILLIGAN, T. G., OGSTON, A. S., PUIG, P., SCULLY, M. E., TRAYKOVSKI, P. A. AND WHEATCROFT, R. A., 2009, Sediment Delivery to the Seabed on Continental Margins, in Continental Margin Sedimentation: From Sediment Transport to Sequence Stratigraphy, eds., C. A. Nittrouer, J. A. Austin, M. E. Field, J. H. Kravitz, J. P. M. Syvitski and P. L. Wiberg), Blackwell Publishing Ltd., Oxford, UK. doi: 10.1002/9781444304398.ch2

HILLIER, S., 1995, Erosion, sedimentation and sedimentary origin of clays, in B. Velde, ed., Origin and mineralogy of clays: Berlin, Germany, Springer-Verlag, p. 162–219.

HOWER J., ESLINGER E.V., HOWER M.E. AND PERRY E.A., 1976, Mechanism of burial metamorphism of argillaceous sediments I. Mineralogical and chemical evidence: Geological Society of America Bulletin, vol. 87, p. 725-737.

KANE, I.A. AND PONTÉN, A.S.M., 2012, Submarine transitional flow deposits in the Paleogene Gulf of Mexico: Geology, v. 40, p. 1119-1122.

KATZ, B.J., 2005, Controlling factors on source rock development: a review of productivity, preservation, and sedimentation rate. In: Harris, N.B. (Ed.), The Deposition of Organic Carbon-rich Sediments: Models, Mechanisms, and Consequences. (SEPM) Society for Sedimentary Geology, Special Publication, pp. 7e16.

KEEN, T.R., FURUKAWA, Y., BENTLEY, S.J., SLINGERLAND, R.L., TEAGUE, W.J., DYKES, J.D. AND ROWLEY, C.D., 2006, Geological and oceanographic perspectives on event bed formation during Hurricane Katrina: Geophysical Research Letters, v. 33, L23614.

KLEMME, H.D. AND ULMISHEK, G.F., 1991, Effective petroleum source rocks of the world: stratigraphic distribution and controlling depositional factors: American Association of Petroleum Geologists Bulletin, v. 75, p. 1809-1851.

KEIL, R.G., MAYER, L.M., QUAY, P.D., RICHEY, J.E. AND HEDGES, J.I., 1997, Loss of organic matter from riverine particles in deltas: Geochimica et Cosmochimica Acta, v. 61, p. 1507-1511.

KINEKE, G.C., STERNBERG, R.W., TROWBRIDGE, J.H. AND GEYER, W.R., 1996, Fluid-mud processes on the Amazon continental shelf: Continental Shelf Research v. 16, p. 667-696.

KIRBY, R. AND PARKER, W.R., 1983, Distribution and behavior of fine sediment in the Severn Estuary and inner Bristol Channel, U.K. Canadian Journal of Fisheries and Aquatic Sciences v. 40, p. 83–95.

LEITHOLD, E.L. AND HOPE, R.S.,1999, Deposition and modification of a flood layer on the northern California shelf: Lessons from and about the fate of terrestrial particulate organic carbon: Marine Geology, v. 154, p. 183-195.

LOBZA, V. AND SCHIEBER, J., 1999, Biogenic sedimentary structures produced by worms in soupy, soft muds: observations from the Chattanooga shale (Upper Devonian) and experiments: Journal of Sedimentary Research, v. 69, p. 1041-1049.

LAMB, M.P. AND PARSONS, J.D., 2005, High-density suspensions formed under waves, Journal of Sedimentary Research, v. 75, p. 386-397.

MACQUAKER, J.H.S. AND ADAMS, A.E., 2003, Maximizing information from fine-grained sedimentary rocks: An inclusive nomenclature for mudstones. Journal of Sedimentary Research, v. 73, p. 735-744.

MACQUAKER, J.H.S., BENTLEY, S., AND BOHACS, K.M., 2010a, Wave enhanced sediment-gravity flows and mud dispersal across continental shelves: reappraising sediment transport processes operating in ancient mudstone successions. Geology, v. 38, p. 947-950.

MARTIN, D.P., NITTROUER, C.A., OGSTON, A.S. AND CROCKETT, J.S., 2008, Tidal and seasonal dynamics of a muddy inner shelf environment, Gulf of Papua. Journal of Geophysical Research, v. 113, F01S07.

MCCAVE, I.N., 1984, Erosion, transport and deposition of fine-grained marine sediments: Geological Society Special Publication, v. 15, p. 35-69.

MCILROY, D., 2004, Ichnofabrics and Sedimentary Facies of a Tide-Dominated Delta: Jurassic Ile Formation of Kristin Field, Haltenbanken, Offshore Mid-Norway: Geological Society Special Publication., v. 228, p. 237-272.

MCILROY, D. AND LOGAN, G.A., 1999, The impact of bioturbation on infaunal ecology and evolution during the Proterozoic-Cambrian transition: Palaios, v. 14, p. 58-72.

MCKEE, B.A., ALLER, R.C., ALLISON, M.A., BIANCHI, T.S. AND KINEKE, G.C., 2004, Transport and transformation of dissolved and particulate materials on continental margins influenced by major rivers: Benthic boundary layer and seabed processes: Continental Shelf Research, v. 24, p. 899-926.

MEHTA, A.J. AND MCANALLY, W.H., 2002, Fine-grained cohesive sediment transport. In: Sedimentation Engineering: Processes, Measurements, Modeling

and Practice. ASCE manual 54, ed., Marcelo Garcia, P.E.: American Society of Civil Engineers, New York, p. 253-306.

MULDER, T. AND SYVITSKI, J.P.M., 1995, Turbidity currents generated at river mouths during exceptional discharges to the world oceans: Journal of Geology v. 103, p. 285-299.

MULDER, T., SYVITSKI, J.P.M., MIGEON, S., FAUGÈRES, J.-. AND SAVOYE, B., 2003, Marine hyperpycnal flows: Initiation, behavior and related deposits. A review: Marine and Petroleum Geology, v. 20, p. 861-882.

OZDEMIR, C.E., HSU, T.J., AND BALACHANDAR, S., 2011, A numerical investigation of lutocline dynamics and saturation of fine sediment in the oscillatory boundary layer. Journal of Geophysical Research, v. 116, C09012, doi: 10.1029/2011JC007185, 2011.

PLINT, A.G., TYAGI, A., HAY, M.J., VARBAN, B.L., ZHANG, H. AND ROCA, X., 2009, Clinoforms, paleobathymetry, and mud dispersal across the Western Canada cretaceous foreland basin: Evidence from the Cenomanian Dunvegan formation and Contiguous Strata: Journal of Sedimentary Research, v. 79, p. 144-161.

PLINT, A.G., J.H.S. MACQUAKER AND VARBAN, B., 2012, Bedload Transport of Mud Across A Wide, Storm-Influenced Ramp: Cenomanian–Turonian Kaskapau Formation, Western Canada Foreland Basin: Journal of Sedimentary Research, v. 82, p. 801-822,

O'BRIEN, N.R., 1990, Significance of lamination in Toarcian (Lower Jurassic) shales from Yorkshire, Great Britain: Sedimentary Geology, v. 67, p. 25-34.

PANCOST, R.D., CRAWFORD, N., MAGNESS, S., TURNER, A., JENKYNS, H.C. AND MAXWELL, J.R., 2004, Further evidence for the development of photic-zone euxinic conditions during Mesozoic oceanic anoxic events: Journal of the Geological Society, v. 161, p. 353-364.

PEDERSEN, T.F. AND CALVERT, S.E., 1990, Anoxia vs. productivity: what controls the formation of organic- carbon-rich sediments and sedimentary rocks?: American Association of Petroleum Geologists Bulletin, v. 74, p. 454-466.

RAISWELL, R., 2011, Iron transport from the continents to the open ocean: The aging–rejuvenation cycle: Elements, v. 7, p. 101-106.

RANGER, M.J., 1979, The stratigraphy and depositional environment of the Bell Island Group, the Wabana Group and the Wabana Iron Ores, Conception Bay, Newfoundland. M. Sc. thesis, Memorial University of Newfoundland, Canada. 216 pp.

RANGER, M.J., PICKERILL, R.K. AND FILLION, D., 1984, Lithostratigraphy of the Cambrian? - Lower Ordovician Bell Island and Wabana groups of Bell, Little Bell, and Kellys islands, Conception Bay, eastern Newfoundland: Canadian Journal of Earth Sciences, v. 21, p. 1245-1261.

REINECK, H.-E, 1963, Sedimentgefüge im Bereich der südlichen Nordsee. Abhandlungen der Senckenbergischen naturforschenden Gesellschaft, v. 505, pp. 138.

RINE, J.M. AND GINSBURG, R.N., 1985, Depositional facies of a mud shoreface in Suriname, South America - a mud analogue to sandy, shallow-marine deposits: Journal of Sedimentary Petrology, v. 55, p. 633-652.

RHOADS, D.C. AND BOYER, L.F., 1982. The effects of marine benthos on physical properties of sediments: a successional perspective, in P.L. McCall and M. Tevesz, eds., Animal-Sediment Relations: Plenum, New York, p. 3-52.

SCHIEBER, J., 1998, Deposition of Mudstones and Shales: Overview, Problems, and Challenges. In: J. Schieber, W. Zimmerle, and P. Sethi (editors), Shales and Mudstones (vol. 1): Basin Studies, Sedimentology and Paleontology, Schweizerbart'sche Verlagsbuchhandlung, Stuttgart, p. 131-146.

SCHIEBER, J., SOUTHARD, J.B. AND SCHIMMELMANN, A., 2010, Lenticular shale fabrics resulting from intermittent erosion of water-rich muds - Interpreting the rock record in the light of recent flume experiments: Journal of Sedimentary Research, v. 80, p. 119-128.

SCHIEBER, J., 2011, Reverse engineering mother nature - Shale sedimentology from an experimental perspective: Sedimentary Geology, v. 238, p. 1-22.

STÄMPFLI, G. M., VON RAUMER, J. F., AND BOREL, G. D., 2002, Paleozoic evolution of pre-Variscan terranes: from Gondwana to the Variscan collision. Special papers, Geological Society of America, p. 263-280.

SUMNER, E.J., TALLING, P.J. AND AMY, L.A., 2009, Deposits of transitional flows between turbidity current and debris flow: Geology, v. 37, p. 991-994.

TALLING, P.J., MASSON, D.G., SUMNER, E.J. AND MALGESINI, G., 2012, Subaqueous sediment density flows: Depositional processes and deposit types: Sedimentology, v. 59, p. 1937-2003.

TAYLOR, K. G. AND CURTIS, CD, 1995, Stability and facies association of early diagenetic mineral assemblages; an example from a Jurassic ironstone-mudstone succession, U.K: Journal of Sedimentary Research, v. 65, p. 358-368

TAYLOR, A. M., AND GOLDRING, R., 1993, Description and analysis of bioturbation and ichnofabric: Journal of the Geological Society, v. 151, p. 141-148.

TAYLOR, K.G. AND MACQUAKER, J.H.S., 2000, Spatial and temporal distribution of authigenic minerals in continental shelf sediments: implications for sequence stratigraphic analysis. In: Glenn, C.R., Prévôt-Lucas, L., Lucas, J, eds., Marine Authigenesis: From Global to Microbial. SEPM (Soc. Sedim. Geol.) Spec. Publ., vol. 66. SEPMSSG,Tulsa, Oklahoma, p. 309–323.

TISSOT, B. P., AND WELTE, D. H., 1978, Petroleum formation and occurrence: a new approach to oil and gas exploration, Springer, New York, 521 p.

TRAYKOVSKI, P., GEYER, W.R., IRISH, J.D. AND LYNCH, J.F., 2000, The role of wave-induced density-driven fluid mud flows for cross-shelf transport on the Eel River continental shelf: Continental Shelf Research, v. 20, p. 2113-2140.

TURNER, J.T., 2002, Zooplankton fecal pellets, marine snow and sinking phytoplankton blooms: Aquatic Microbial Ecology, v. 27, p. 57-102.

VAN MAREN, D.S., WINTERWERP, J.C., WU, B.S. AND ZHOU, J.J., 2009, Modeling hyperconcentrated flow in the Yellow River. Earth Surface Processes and Landforms, v. 34, p. 596-612.

WHEATCROFT, R.A. AND DRAKE, D.E., 2003, Post-depositional alteration and preservation of sedimentary event layers on continental margins, I. The role of episodic sedimentation: Marine Geology, v. 199, p. 123-137.

WRIGHT, L.D. AND FRIEDRICHS, C.T., 2006, Gravity-driven sediment transport on continental shelves: A status report: Continental Shelf Research, v. 26, p. 2092-2107.

WOLANSKI, E. AND GIBBS, R.J., 1995, Flocculation of suspended sediment in the Fly River Estuary, Papua New Guinea: Journal of Coastal Research, v. 11, p. 754-762.

YOSHIDA, S., STEEL, R.J. AND DALRYMPLE, R.W., 2007, Changes in depositional processes - An ingredient in a new generation of sequence-stratigraphic models: Journal of Sedimentary Research, v. 77, p. 447-460.

CHAPTER 3

Microbial mats implicated in the generation of intrastratal shrinkage ("synaeresis") cracks

Dario Harazim, Richard Callow, Duncan McIlroy

(Published in *Sedimentology* 6 JUN 2013)

1. Abstract

Intrastratal shrinkage (often termed 'synaeresis') cracks are commonly employed as diagnostic environmental indicators for ancient salinity-stressed, transitional fluvial-marine or marginal-marine depositional environments. Despite their abundance and use in facies interpretations, the mechanism of synaeresis crack formation remains controversial and widely-accepted explanations for their formation have hitherto been lacking. Sedimentological, ichnological, petrographic and geochemical study of shallow marine mudstone beds from the Ordovician Beach Formation of Bell Island, Newfoundland has revealed that crack development (cf. synaeresis cracks) on the upper surface of mudstone beds is correlated with specific organic, geochemical and sedimentological parameters. Contorted, sinuous, sand-filled cracks are common at contacts between unbioturbated mudstone and overlying sandstone beds. Cracks are absent in highly bioturbated mudstone, and are considered to pre-date firmground assemblages of trace fossils that include *Planolites* and *Trichophycus*. The tops of

cracked mudstone beds contain up to 2.1 wt% Total Organic Carbon (TOC, wt%), relative to underlying mudstone beds which contain around 0.5 wt% TOC. High-resolution carbon isotope analyses reveal low $\delta^{13}C_{org}$ values (-27.6‰) on bed tops, compared to sandy intervals lacking cracks (-24.4 to -24.9‰). Cracked mudstone facies show evidence for microbial matgrounds, including microbially induced sedimentary structures on bedding planes and carbonaceous laminae and tubular carbonaceous microfossils in thin section. Non-cracked mudstone lacks evidence for development of microbial mats. Microbial mat development is proposed as an important prerequisite for intrastratal shrinkage crack formation. Both microbial mats and intrastratal shrinkage cracks have broad palaeoenvironmental distributions in the Precambrian and early Phanerozoic. In later Phanerozoic strata, matgrounds are restricted to depositional environments that are inhospitable to burrowing and surface-grazing macrofauna. Unless evidence of synaeresis (i.e. contraction of clay mineral lattices in response to salinity change) can be independently demonstrated, the general term 'intrastratal shrinkage crack' is proposed to describe sinuous and tapering cracks in mudstone beds.

2. Introduction

The process of synaeresis is defined as a loss of volume and shrinkage of a material as a function of dehydration or phase change. Synaeresis is well-documented in a variety of non-geological materials such as foams, polymers and cement pastes (Tanner, 2003). The first geological investigations of synaeresis processes invoked crack generation by

changing the pore-water salinity of artificial clay–cement mixtures ("Synäretische Prozesse"; Jüngst 1934). The term synaeresis has since become entrenched within the geological literature, where it used to describe vertically compacted, sand-filled cracks ('synaeresis cracks') in vertical cross-section, that show sinuous, doubly tapering geometries on bedding planes. Such cracks typically occur in successions of alternating sandstone and mudstone and are mostly developed at mudstone–sandstone interfaces within siliciclastic successions deposited in subaqueous depositional environments (e.g., Tanner 2003). The irregular network pattern that is characteristic of 'synaeresis cracks' in plan-view, along with their highly contorted vertical cross-sections, distinguishes them from desiccation cracks, which are polygonal, and have straight sides in vertical cross-section (Peron et al. 2009). Desiccation cracks form exclusively in subaerial settings. Intrastratal shrinkage cracks (a generalized term for sediment-filled cracks regardless of origin), and the similar crack-like structures in sandstone, including "Rhysonetron" and "Manchuriophycus" (Endo, 1933; Hofmann, 1967, 1971; Parizot et al. 2005; Eriksson et al. 2007) are well documented from a range of subaqueous siliciclastic palaeoenvironments throughout the rock record (Tanner, 2003). They are most common during the Proterozoic and Cambrian, and decrease in abundance after the Early Ordovician (Pratt 1998).

Two principal hypotheses have been proposed to explain subaqueous crack formation in heterolithic sediments. The first model is based on the contraction of the mineral lattice in swelling clay (smectite) in response to a change in pore-water salinity (i.e., synaeresis;

Jüngst 1934; Weiss 1958; White 1961; Burst 1965). The second model suggests that seismic shock can cause the rapid dewatering and upward injection of water-laden sand into overlying unconsolidated mud-rich sediment (Pratt 1998; Cowan and James 1992). Given the uncertainty surrounding the mechanism of crack formation, the generic term 'intrastratal shrinkage crack' should be used to avoid implying a mechanism of crack generation in fine-grained, siliciclastic sediment.

The salinity change and seismic shock models do not easily explain a number of geological observations. For example:

1) Intrastratal shrinkage cracks are not known from modern salinity-stressed environments (Allen 1984; Tanner 2003).

2) Intrastratal shrinkage cracks exist in ancient successions that lack independent evidence for salinity change (cf. Bhattacharya and MacEachern 2009).

3) The comparatively low recurrence frequency of seismic events does not account for the presence of abundant intrastratal shrinkage cracks in tectonically stable cratonic settings (Fyson 1962; Hughes and Hesselbo 1997).

4) The seismic shock model, as proposed by Pratt (1998), predicts the upward-injection of sand into unlithified mud. However, observations of intrastratal shrinkage cracks from many shallow-marine facies suggest that the cracks are more commonly filled by sand from above.

5) Despite good evidence throughout the geologic record for sand injection in association with seismic shock (in the form of seismites), structures resembling synaeresis cracks have not been unambiguously linked to either modern seismites (Obermeier 1996) or their ancient equivalents (Hurst et al. 2011).

'Synaeresis cracks' are commonly used as indicators for marginal-marine facies and are regularly employed as diagnostic environmental indicators for salinity-stressed, transitional fluvial-marine, or marginal-marine depositional environments (e.g., Wightman et al. 1987; Pemberton and Wightman 1992; Bhattacharya and MacEachern 2009; Buatois et al. 2011). Despite their abundance and importance in palaeoenvironmental interpretations, the sedimentary prerequisites and mechanisms for shrinkage crack formation in subaqueous environments remain controversial (Donovan and Foster 1972; Plummer and Gostin, 1981; Astin and Rogers 1991; Cowan and James 1992; Pratt 1998; Tanner 1998, 2003).

Since no single model is able to explain unequivocally the formation of contorted intrastratal shrinkage cracks, a detailed study of their sedimentological context was undertaken. This case study of Lower Ordovician strata from Bell Island, Newfoundland includes the study of cracks at the scale of the 'deformational event' itself (millimetre to centimetre scales), and focuses on the distribution of cracked mudstone with respect to: i) ancient depositional environment; ii) ichnology; iii) the biogeochemical characteristics of preserved organic matter; and iv) distribution of microbially induced sedimentary structures (MISS; *sensu* Noffke et al. 2001).

3. Sedimentological and stratigraphic context

The Lower Ordovician (Tremadocian, ~ 485 Ma) Beach Formation at Freshwater Cove, Bell Island, Newfoundland (Fig. 3-1), is a storm-dominated, heterolithic succession characterized by alternations between thin (~10 cm) beds of hummocky cross-stratified

Figure 3-1. (A) Location map of Bell Island, Newfoundland. (B) Stratigraphic position of the studied interval of the Beach Formation within the Bell Island Group (simplified after Ranger et al. 1984). (C) Simplified geological map of Bell Island with study location at Freshwater Cove (red arrow).

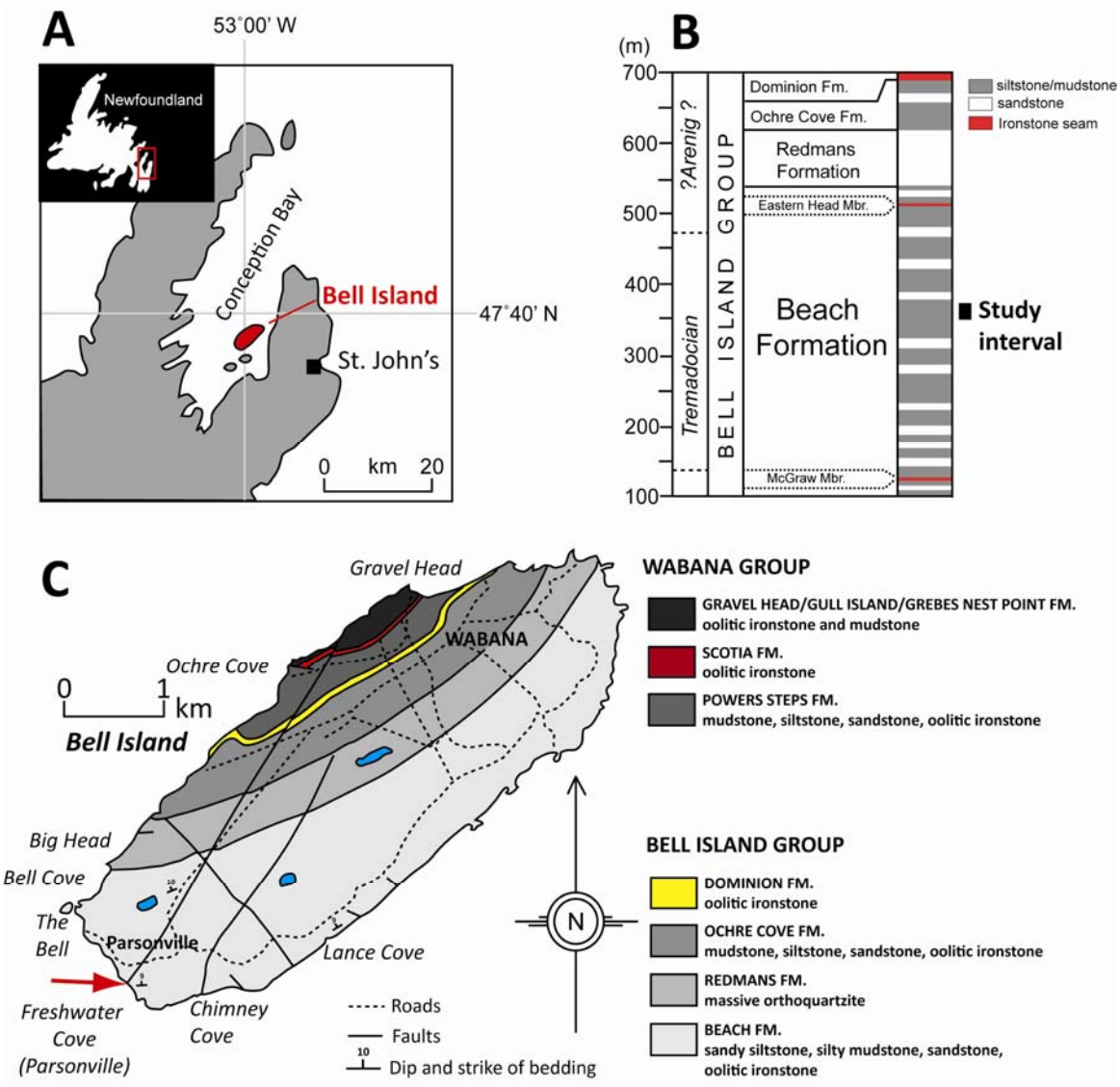
A
53°00' W
Newfoundland
Conception Bay
Bell Island
47°40' N
St. John's
0 km 20
B
(m)
700
600
500
400
300
200
100
?Arenig ?
Tremadocian
BELL ISLAND GROUP
Dominion Fm.
Ochre Cove Fm.
Redmans Formation
Eastern Head Mbr.
Beach Formation
McGraw Mbr.
siltstone/mudstone
sandstone
Ironstone seam
Study interval
C
Gravel Head
WABANA
Ochre Cove
0 1 km
Bell Island
Big Head
Bell Cove
The Bell
Parsonville
Lance Cove
Freshwater Cove (Parsonville)
Chimney Cove
Roads
Faults
Dip and strike of bedding
N
WABANA GROUP
GRAVEL HEAD/GULL ISLAND/GREBES NEST POINT FM.
oolitic ironstone and mudstone
SCOTIA FM.
oolitic ironstone
POWERS STEPS FM.
mudstone, siltstone, sandstone, oolitic ironstone
BELL ISLAND GROUP
DOMINION FM.
oolitic ironstone
OCHRE COVE FM.
mudstone, siltstone, sandstone, oolitic ironstone
REDMANS FM.
massive orthoquartzite
BEACH FM.
sandy siltstone, silty mudstone, sandstone, oolitic ironstone

Figure 3-2. (A) Field photograph showing the study locality at Freshwater Cove (see Fig. 3 for stratigraphic log). The studied succession shows a change from lower shoreface to offshore transition zone environments. (B) A representative interval exhibiting abundant intrastratal shrinkage cracks (white arrows), overlain by wave-rippled storm sandstones. (C) A representative interval containing abundant muddy sediment-gravity flow deposits. Rapid mud deposition and frequent reworking of the seafloor is indicated by discontinuous lenses of sandstones and erosional mud-on-sand and mud-on-mud contacts (yellow dashed lines).

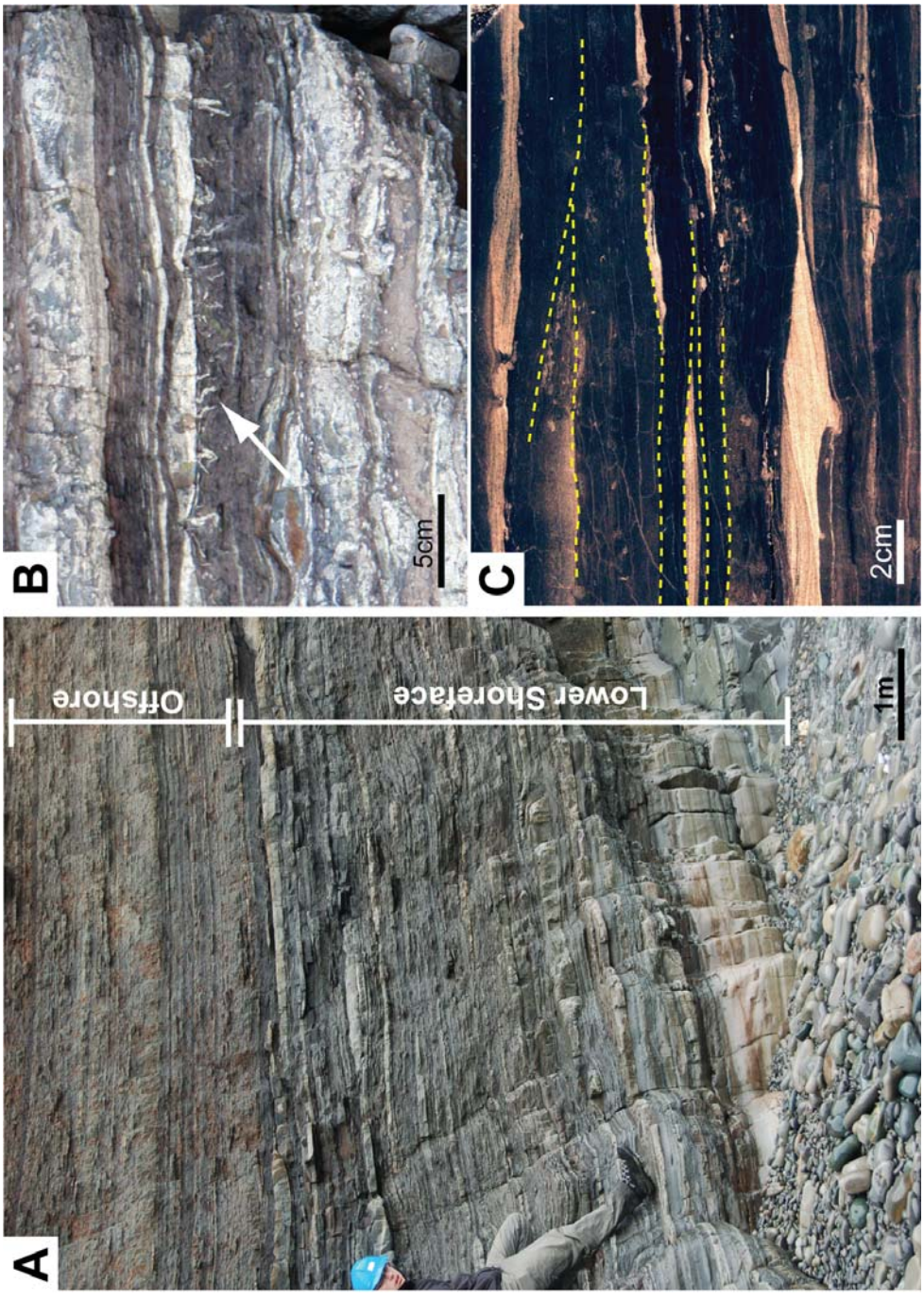
A
Offshore
Lower Shoreface
1m
B
5cm
C
2cm

and planar-stratified sandstone and mudstone. The succession has been interpreted as lower shoreface and offshore transition zone deposits (Fillion and Pickerill 1990; Brenchley et al. 1993). The studied interval is 9 m thick, and consists of two mudstone-rich, upward-coarsening successions, interpreted to represent the distal expression of shoreface parasequences (Figs 3-2 and 3-3). The interval was selected for detailed study due to the abundance of mudstone units with well-developed cracks, in a succession otherwise dominated by similar mudstones lacking cracks. The ichnodiversity and bioturbation intensity throughout the studied interval are low relative to other parts of the Beach Formation (Fillion and Pickerill 1990).

The lower parasequence consists of medium-to coarse-grained, cross-stratified and planar-stratified sandstone with oscillation ripples. The interbedded mudstone units consist of three distinct facies: i) unbioturbated dark mudstone without intrastratal shrinkage cracks; ii) unbioturbated, sharp-based dark mudstone with intrastratal shrinkage cracks and wrinkle-marked upper surfaces, the latter interpreted as evidence for microbial matgrounds (Fig. 3-4A; e.g., Hagadorn and Bottjer 1997); and iii) bioturbated grey silty mudstone without intrastratal shrinkage cracks.

The upper parasequence has a lower sandstone-to-mudstone ratio, compared with the lower parasequence and is interpreted to record a more-distal lower shoreface palaeoenvironment (Figs 3-2 and 3-3). Field observations provide no sedimentological or ichnological evidence to suggest deposition in anything but fully-marine depositional environments (Ranger et al. 1984; Fillion and Pickerill 1990). The studied succession contains hummocky cross-stratification (HCS) and interbedded mudstone, indicating a storm-dominated subtidal depositional setting (Brenchley et al. 1993). Post-storm

Figure 3-3. Generalized stratigraphic log and bulk geochemical data (TOC and $\delta^{13}C_{org}$) from the studied interval at Freshwater Cove. Bulk $\delta^{13}C_{org}$ values plot between -27.4‰ and -29.5‰. TOC values are usually below 1.0 wt%, but outliers from intervals containing shrinkage cracks show TOC values up to 3.4 wt%. Bioturbation index (BI; see Taylor and Goldring, 1993) is generally low within the lower shoreface of this succession (BI 0-2), while sediments in the offshore transition zone facies are more intensely bioturbated (BI 5-6) (c = claystone, s = siltstone, vfs = very fine-grained sandstone, fs = fine-grained sandstone, ms = medium-grained sandstone, cs = coarse-grained sandstone). Mudstones are all lithologies with a median grain size finer than 62.5 μm (i.e., siltstone and claystone) (Folk 1954, 1956).

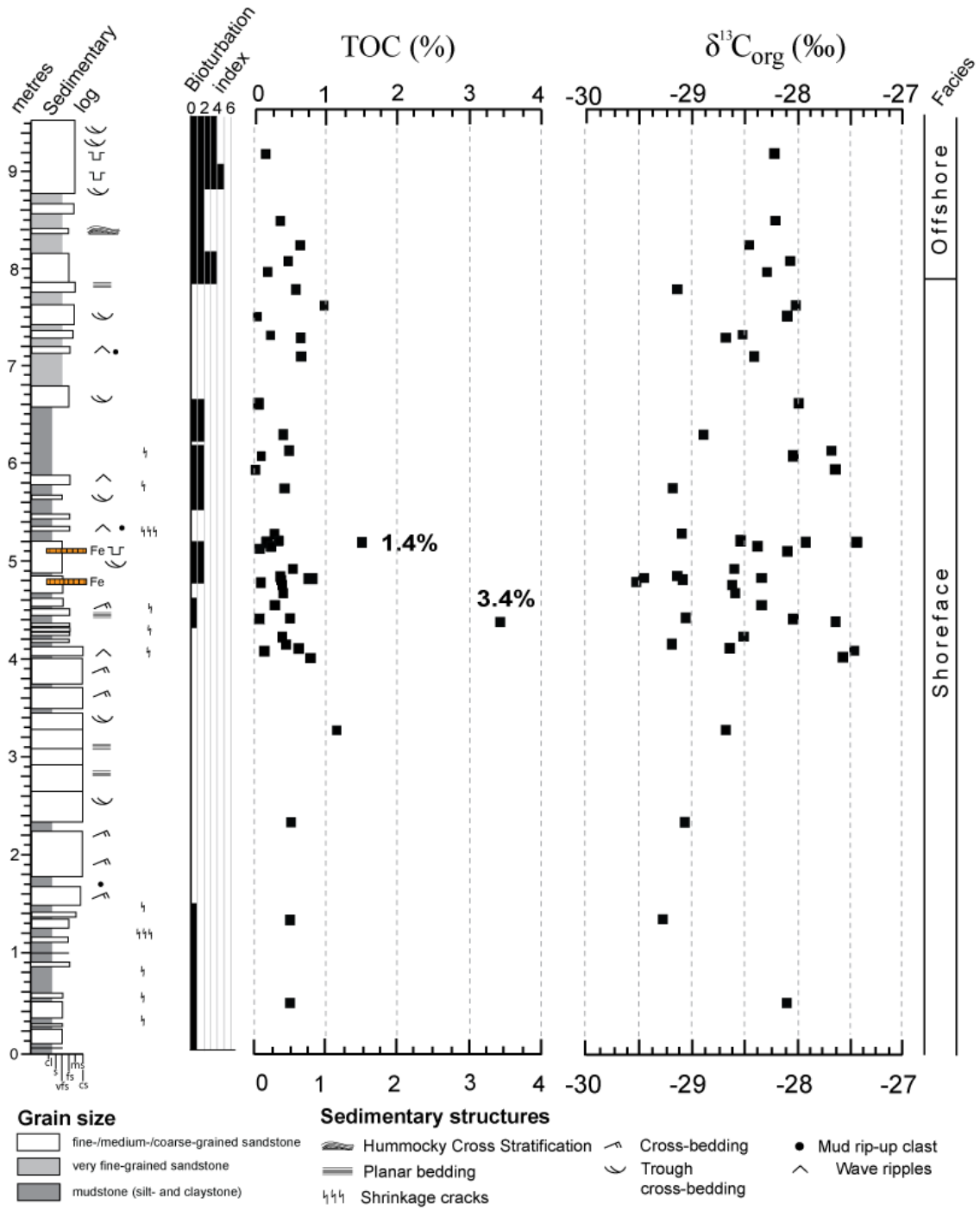
metres
Sedimentary log
Bioturbation index
0 2 4 6
TOC (%)
0 1 2 3 4
δ13Corg (‰)
-30 -29 -28 -27
Facies
Offshore
Shoreface
1.4%
3.4%
Fe
Fe
cl
s
fs
vfs
ms
cs
Grain size
fine-/medium-/coarse-grained sandstone
very fine-grained sandstone
mudstone (silt- and claystone)
Sedimentary structures
Hummocky Cross Stratification
Planar bedding
Shrinkage cracks
Cross-bedding
Trough cross-bedding
Mud rip-up clast
Wave ripples

deposition of mud from suspension during the slack-water stage of a tidally influenced environment has previously been invoked as the main sediment delivery mechanism for the mudstones of the Bell Island Group (Ranger et al. 1984; Fillion and Pickerill 1990). However, close observation of mudstone facies of the Beach Formation reveals abundant erosion surfaces within, and at the base of, unbioturbated mudstone beds (Fig. 3-2C). New paradigms for mudstone deposition suggest that dense suspensions of 'fluid mud' (suspended sediment concentration >10 g l^{-1}; Kirby and Parker 1983; Mehta and McAnally 2002), sourced from estuarine systems, can be rapidly deposited in shallow marine settings via hyperpycnal currents and dispersed via wave-advected, cross-shelf transport (Wolanski and Gibbs 1995; McIlroy 2004; Macquaker et al. 2010). Input of mud as fluid mud is therefore considered likely in the Beach Formation.

Independent evidence for syn-sedimentary tectonic activity (which would help corroborate a seismic model for the formation of intrastratal shrinkage cracks; Pratt 1998) has not been documented in the Bell Island and Wabana Groups. Neither sand-injection features parallel to bedding, nor multilayered sand intrusions (Obermeier 1996; Hurst et al. 2011) were observed in the succession.

4. Methodology

An integrated sedimentological, petrographic and geochemical approach is used herein to study mudstone facies with intrastratal shrinkage cracks. The studied section at Freshwater Cove (Fig. 3-2) was logged on a cm scale and both physical sedimentological and ichnological fabrics were documented through the section. Samples were collected

for bulk rock TOC and $\delta^{13}C_{org}$ analysis, as well as for laboratory study of sedimentological and ichnological fabrics (Figs 3-2 and 3-3). The sampling strategy incorporated collection of material from both crack-bearing and non-crack-bearing beds.

4.1 Analysis of sedimentary fabric

Oriented, unweathered samples of heterolithic facies were collected from the field and slabbed in the laboratory. Thin sections were manufactured perpendicular to bedding to study mineralogy and sedimentary fabrics, and to determine the relative chronology of biological and physical sedimentary processes. Bedding-parallel/oblique thin sections were also prepared to search for bedding-parallel microbial filaments that were suspected from the observation of MISS on bedding planes (Fig. 3-4A). Thin sections were studied using both a flatbed 35 mm film scanner and a petrographic microscope to study cm-scale to mm-scale fabrics. Detailed study of sedimentary fabrics was undertaken using a FEI Quanta FEG 650 Environmental Scanning Electron Microscope (SEM) equipped with an energy dispersive X-Ray micro-analytical system (EDX). The SEM was also operated in backscattered mode to image the distribution of clay and kerogen.

4.2 Geochemical measurements

Unweathered, carbonate-free mudstone samples (*ca* 10 mg) were analysed for weight percentage of TOC and $\delta^{13}C_{org}$ using a Carlo Erba Elemental Analyser, connected to the continuous-flow inlet system of a Delta V plus gas-source mass spectrometer (TERRA

facility, Memorial University of Newfoundland). The USGS 24 standard was analysed with the samples to demonstrate accuracy and precision (Coplen et al. 2006). The values reported herein are relative to the Vienna Pee Dee Belemnite standard (V-PDB ‰).

5. Results

5.1 Ichnology

Mudstone beds with intrastratal shrinkage cracks are characterized by a near-absence of softground trace fossils (<1% bioturbated) in an otherwise bioturbated succession (Fig. 3-3). Bioglyphs (scratch marks preserved in partially indurated or cohesive sediment) are common at mudstone–sandstone interfaces, and define trace fossils such as *Cruziana* and *Monomorphichnus* that were produced at the sediment–water interface (Fig. 3-4D). These surficial trace fossils post-date deposition of the mudstone, but pre-date deposition of the overlying sandstone. Similarly, bioglyphs are also found on the burrow walls of deeper-tier, post-compaction (and post-cracking) *Trichophycus*/*Planolites* assemblages (Figs 3-4C and 3-5C) developed in buried mudstone (concealed firmgrounds; Bromley 1996).

5.2 Crack morphology

Bedding plane expressions of intrastratal shrinkage cracks consist of straight to curved,

Figure 3-4. (A) Abundant wrinkle structures in fine sandstones and siltstones that are interpreted as microbially-induced sedimentary structures (MISS). (B) Bedding plane exposure of intrastratal shrinkage cracks. Note the absence of polygonal patterns. (C) Bioturbated facies from the Beach Formation showing a *Planolites* (P) and *Trichophycus* (Tr) ichnofabric, characteristic of non-crack-bearing mudstones. (D) Surficial trace fossils *Cruziana* (Cr) and *Monomorphichnus* (M) preserved in convex hyporelief associated with shallow-tier *Planolites* (P) and *Lockeia* (L), attesting to the fully marine, euryhaline character of the succession.

A
1 cm
B
10 cm
C
P
P
P
Tr
Tr
5 cm
D
Cr
L
P
L
L
L
M
M
M
L
L
2 cm

often doubly-tapering structures, which are typically between 1 and 5 mm in width (Fig. 3-4B) and around 10 mm in depth. Unlike polygonal desiccation cracks, sand-filled intrastratal shrinkage cracks do not form regular polygons, but instead produce irregular, poorly-organized networks with limited lateral connectivity, which are 10 to 20 cm in length (Fig. 3-4B). Due to a common lack of bedding plane exposure it is difficult to give a range of values for crack length. Observations of cracks in cross-section on polished slabs and thin sections demonstrate that the cracks are typically filled with siltstone and/or very fine-grained sandstone derived from the overlying bed. Cracks that vertically connect sandstone layers (as inferred by Pratt, 1998) are very rare (Figs 3-5 and 3-6).

5.3 Mudstone fabric

The upper surfaces of sandstone-mudstone interfaces are commonly covered by a variety of wrinkle structures that are comparable with the suite of microbially induced sedimentary structures (Fig. 3-4A; Hagadorn and Bottjer, 1997; Noffke et al. 2001; Schieber et al. 2007). The inference of ancient microbial matgrounds at the sediment-water interface is also supported by observations of an array of microstructures in petrographic thin section and SEM (Figs 3-6 and 7). Thin sections perpendicular to bedding show that all of the studied crack-bearing mudstone horizons contain wavy to anastomosing laminae of amorphous organic matter with abundant ‘floating’ silt- and sand-sized quartz grains in a fine-grained, clay-dominated matrix (Fig. 3-6A and B). Other microtextures at mudstone to sandstone interfaces include abundant vertically-aligned mica flakes and convex upward-domed clay minerals in wavy, clay-dominated

matrix (Fig. 3-7). Pyrite framboids are common at mudstone–sandstone interfaces, and may provide evidence for sulphate reduction and decay of organic matter at shallow depths within the sediment, possibly beneath a microbial matground (Fig. 7; cf. Gehling 1999).

Thin sections from cracked mudstones prepared parallel to bedding contain carbonaceous, tubular, filamentous structures (~5 μm in diameter and 300 to 400 μm in length), at and immediately below the interface between shrinkage cracked mudstone and the overlying sandstone (Fig. 3-6C and D). These organic filaments are comparable with published examples of fossil and modern microbial sheaths (Fig. 3-6C and D; Visscher and Stolz 2005; Franks and Stolz 2009).

SEM-EDX analyses demonstrate that the clay mineral assemblage of all the studied mudstone is predominantly chlorite and illite, with a detrital contribution of biotite and muscovite (Fig. 3-7C and D). SEM backscatter imaging confirms observations made from thin sections, that, relative to uncracked mudstone, intrastratal shrinkage cracks have increased abundances of: ii) detrital mica; ii) amorphous organic matter (in the form of elongated, anastomosing layers); iii) 'floating' silt and sand grains; and iv) vertically oriented clay minerals (Fig. 3-7).

Figure 3-5. Thin-section micrographs showing the cross-cutting relationships between sandstones, mudstones and shrinkage cracks, vertical to bedding; plane-polarized light. (A) Highly contorted sand-filled cracks indicate bed shortening of up to 80%. (B) Intrastratal, sand-filled shrinkage cracks cross-cutting originally emplaced sand laminae (arrowed). (C) Association of deformed intrastratal shrinkage cracks and undeformed burrow indicates that the mud dewatered prior to bioturbation by shallow-tier burrows, such as *Planolites* (P) (see also Noffke, 2000).

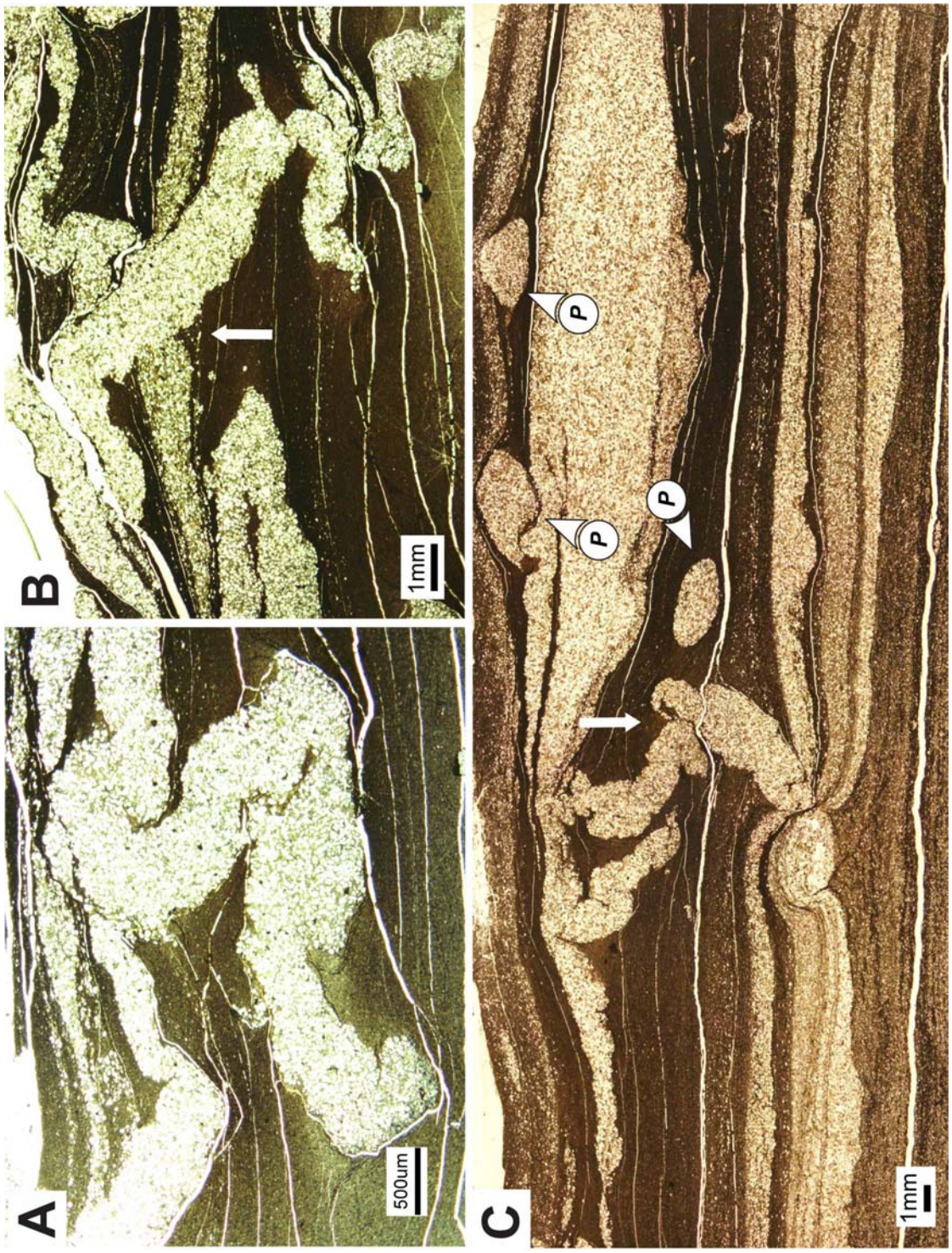
A
500um
B
1mm
C
P
P
P
1mm

Figure 3-6. Thin-section micrographs of microbial fabrics in the Beach Formation, vertical and parallel to bedding; plane-polarized light. (A) Cross-section through a microbial mat in the Beach Formation, showing typical wavy, anastomosing fabric with characteristic alternations between silt-rich layers (S) and layers composed of organic matter and clay minerals (org). (B) High-magnification view of mudstone-sandstone interface from a shrinkage crack-bearing horizon. Note the presence of similar microbial fabrics to (A), with scattered silt grains and aggregates of framboidal pyrite (Py). (C and D) Bedding-parallel thin sections from an interval containing shrinkage cracks containing elongated, hollow, tubular sheaths that are interpreted as microfossil (cyanobacterial?) remains (arrowed).

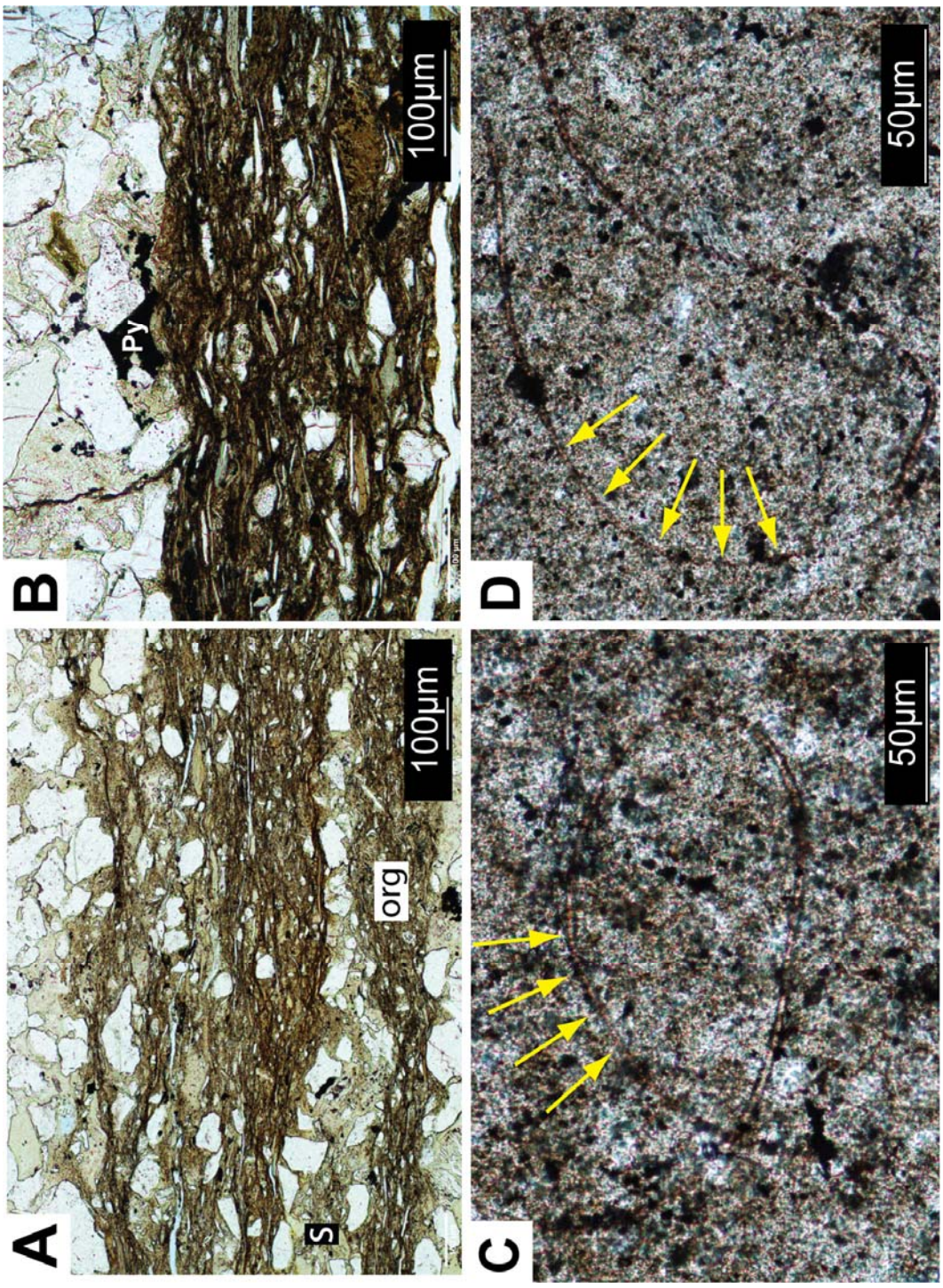
A
100µm
org
S
B
Py
100µm
C
50µm
D
50µm

5.4 Geochemistry (TOC and $\delta^{13}C$)

Total organic carbon contents (TOC as wt%) were measured from 32 unweathered samples, collected from throughout the whole studied succession (Fig. 3). TOC values from mudstone beds are typically 0.5 wt%, with two outliers of 1.4 wt% and 3.4 wt%. Both outliers were from crack-bearing mudstone. One oriented sample was selected from the latter horizon, and sampled for high-resolution, millimetre-scale geochemical analysis (TOC and $\delta^{13}C_{org}$; Fig. 3-8).

Total organic carbon values were found to vary significantly within this single mudstone bed. The TOC values are 2.1 wt% TOC at the top of the bed, relative to the lower part of the mudstone bed which only contains TOC values of around 0.5 wt% (Fig. 3-8). The $\delta^{13}C_{org}$ values were also found to vary through the studied mudstone horizon. The most positive $\delta^{13}C_{org}$ values (-24.4‰) were recorded immediately above the upper mudstone to sandstone interface, while the most negative values (-27.6‰) were measured from a sample a few millimetres below the top sandstone-mudstone contact (Fig. 3-8). The top of the mudstone bed thus has an elevated TOC content, with an isotopically light carbon isotope composition.

6. Discussion of petrographic and geochemical evidence for microbial mats in the Beach Formation.

6.1 Petrographic evidence for microbial mats

The observed association of sedimentological and biogenic (organic) components/fabrics confirms the presence of ancient microbial mats (in accordance with the criteria of Schieber 1998; Noffke 2009). Following this, it is considered that matgrounds formed on a mud-rich sea floor at, and just beneath, the sediment-water interface, prior to being smothered by the deposition of sand.

Petrographic analysis has demonstrated both the presence of filamentous organic microfossils and the presence of non-hydrodynamically oriented grains (e.g., micas) in the shrinkage crack-bearing mudstone of the Beach Formation (Noffke et al. 1997; Figs 3-6 and 3-7). Such fabrics are conventionally interpreted to result from sediment baffling and trapping of detrital grains in microbial matgrounds (Gerdes 2007).

Textural evidence from observations in siliciclastic successions elsewhere demonstrate that the presence of ancient microbial mats can be inferred from observations of distinctive MISS, such as wrinkle structures on sandstone bedding planes (cf. Pflüger 1999; Schieber 1999; Gerdes et al. 2000; Noffke et al. 2001; Schieber et al. 2007; Noffke 2010). MISS have also been described in association with microbial sheaths and organic-rich laminae in petrographic thin sections, further reinforcing the inference of ancient microbial matgrounds (cf. Peat 1984; Pflüger 1999; Noffke et al. 1997, 2006;

Callow and Brasier 2009a, b).

Wrinkle structures were described from sandstone bedding planes of the Beach Formation by Hagadorn and Bottjer (1997; figs 3-1D to F). The wrinkly carbonaceous laminae and tubular microfossils identified from Beach Formation thin sections, are described here for the first time. Taken together, the assemblage of wrinkle structures (Fig. 4A) and microbial sheaths (Figs 3-6 and 3-7) provide strong evidence that the upper surface of the cracked mudstone beds were bound by microbial mats prior to smothering by the overlying sandstone.

6.2 Geochemical evidence for microbial mats

Light organic carbon isotope compositions (-21.5‰ to -35‰) have been used to support a microbial interpretation of putative MISS from Proterozoic strata (Noffke et al. 2006). A negative isotopic signal is the expected result of microbial degradation of organic matter and the selective preservation of resistant, isotopically light, bacterial cellular remains (the 'carbohydrate effect'; Dean et al. 1984; Parkes et al. 1993; Tyson 1995; Pacton et al. 2007, 2008). Phytodetritus falling onto the same sediment-water interface would be remineralized within the water column, a process that would most likely result in higher carbon isotope values. The elevated TOC values immediately below the upper mudstone-sandstone interface (Fig. 3-8) indicate that the increase in organic matter was most likely post-depositional (i.e. grown at the sediment-water

interface). Negative $\delta^{13}C_{org}$ values provide evidence for post-depositional growth of microbes (e.g., Logan et al. 1999).

Very isotopically light organic carbon could also be a product of sulphide oxidation by sulfur bacteria close to the sediment–water interface ('dark CO_2 fixation'). This microbially-mediated, anaerobic redox reaction can generate significant amounts of microbial organic carbon in the form of microbial mats and microbially-bound surface layers at the sediment–water interface (Tuttle and Janasch 1973; Sarbu et al. 1996; Taylor et al. 2001; Gilhooly et al. 2007; Bailey et al. 2009; Glaubitz et al. 2010), which may also contribute to the organic matter preserved in units dominated by intrastratal shrinkage cracks. High concentrations of organic carbon with isotopically low $\delta^{13}C_{org}$ values, MISS, and associated microbial filaments in the upper part of cracked mudstone beds confirm the development of microbial mats upon and within the mud prior to its burial by storm-transported sand.

Figure 3-7. (A) Thin section micrograph perpendicular to bedding through interbedded fine siltstones and sandstones containing intrastratal shrinkage cracks (Sc); plane-polarized light. Evidence for microbial binding is shown by mudstone rip-up clasts incorporated within the sandstone (R). (B) High magnification image of microbially-bound siltstone from the same interval as in previous figure (A). Filament-like textures, i.e., black anastomosing, continuous stringers - yellow arrows, engulf larger silt and mica grains (see also Noffke 2000; Noffke et al. 2002; 2003; 2006; 2008). The black regions are interpreted as the carbonaceous remnants of microbial mats. (C and D) SEM backscattered images taken from a mudstone containing contorted shrinkage cracks. Convex, upward-domed clay minerals and vertically-stacked micas, which are common within the sediment prior to compaction (red arrows). Organic matter (black regions), typically consists of elongated, wavy stringers which may represent remnants of horizontally organized microbial films (yellow arrows). Vertically oriented biotite (Bio) with wavy layering of illite/chlorite minerals (Chl) between floating silt grains (Qz) and muscovite (Mu). Pyrite (Py) and rutile (Ru) are dispersed throughout the matrix as minor components.

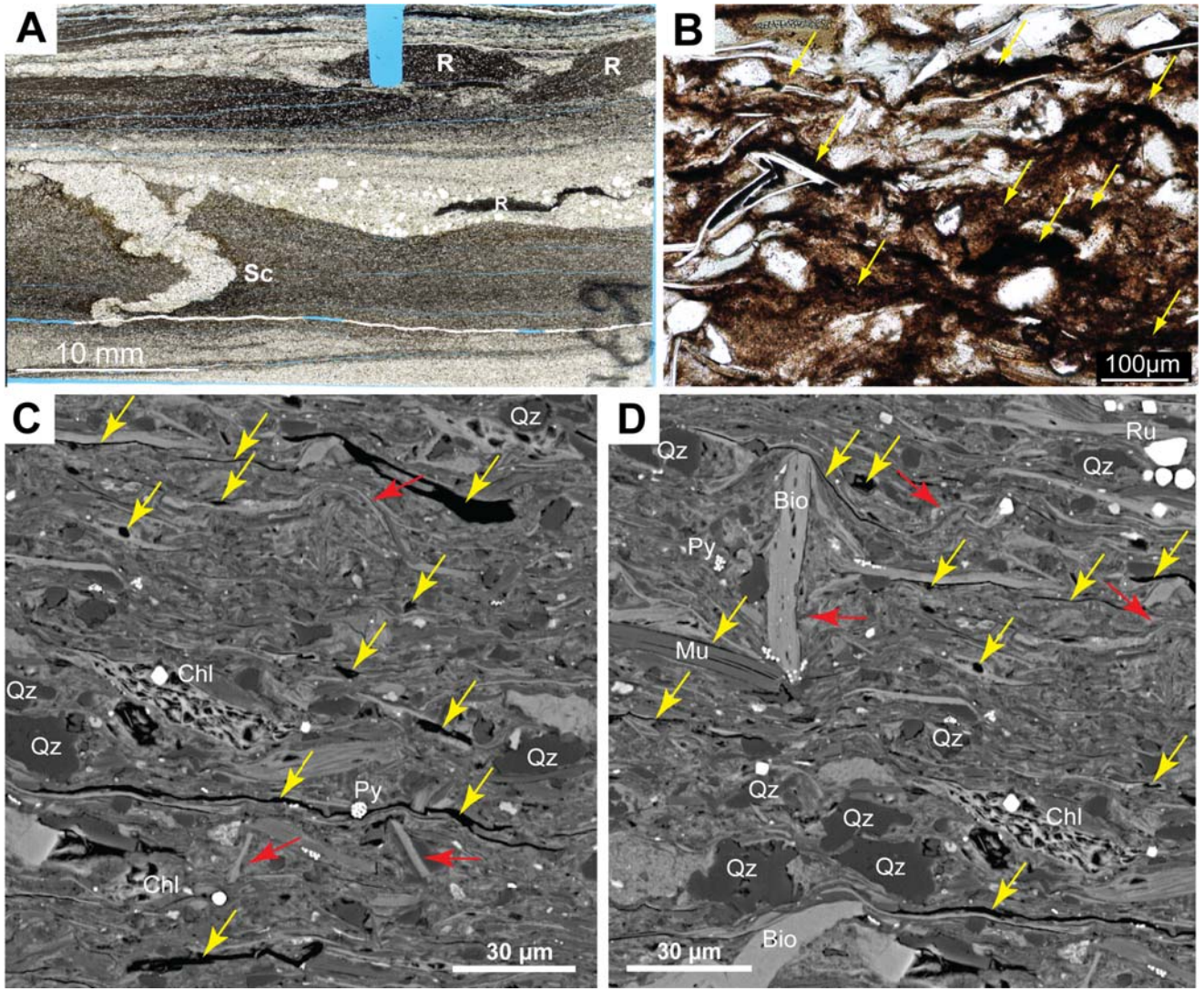
A
R
R
R
Sc
10 mm
B
100μm
C
Qz
Chl
Qz
Qz
Qz
Py
Chl
30 μm
D
Qz
Ru
Qz
Bio
Py
Mu
Qz
Qz
Qz
Chl
Qz
Qz
30 μm
Bio

Figure 3-8. Millimeter-scale variations in TOC and $\delta^{13}C_{org}$ from a vertical profile through a cracked interval. Enriched values of TOC (2.1 wt%) are recorded from the top of mudstone beds, and low TOC values (<1 wt%) are measured from the base of the mudstone and from sandstones. $\delta^{13}C_{org}$ data indicate the concentration of isotopically light organic carbon in mudstone bed tops (associated with high TOC values), and isotopically heavier organic carbon in sands and in the base of the mudstone.

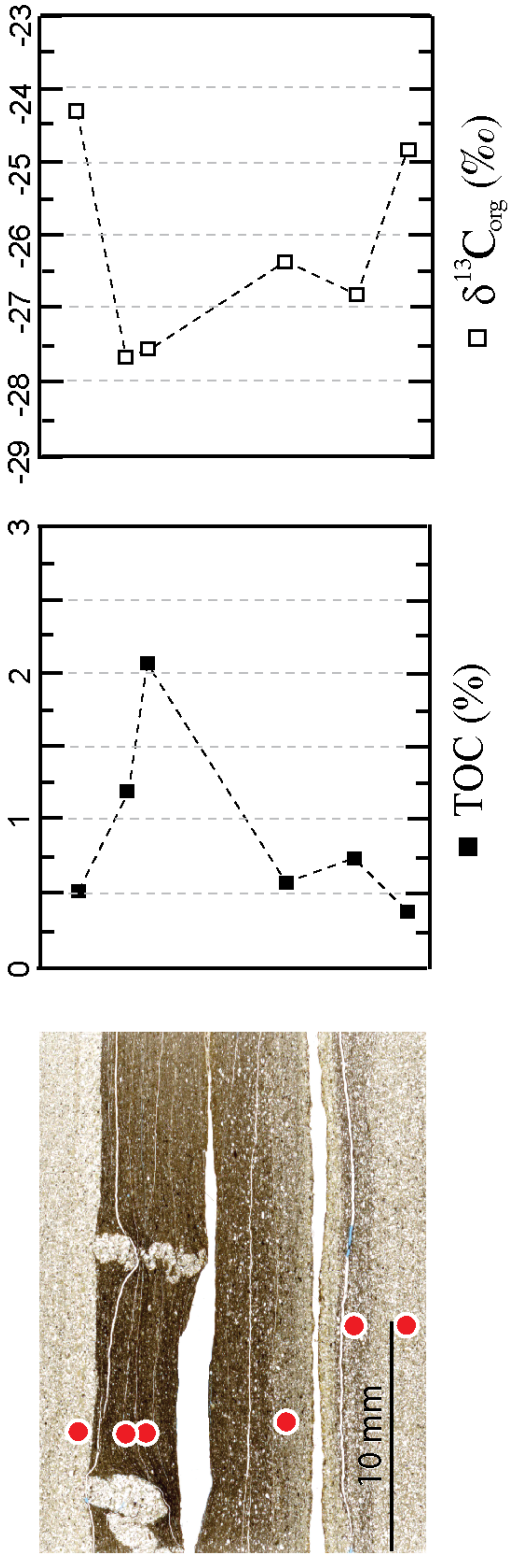
-23
-24
-25
-26
-27
-28
-29
□ δ13Corg (‰)
3
2
1
0
■ TOC (%)
10 mm

7. Matground development in mud-rich marine settings

Microbial matgrounds will naturally develop wherever: i) the substrate is stable and not subject to erosion; ii) the rate of sediment accumulation is not so fast that it smothers the mat and kills the microbes; iii) the rate of metazoan grazing is less than the productivity of the microbiota; and iv) there is a continuously replenished source of nutrients (Madrid, 2006).

The combination of ichnological observations indicates that:

1 The absence of compacted trace fossils indicates that little, if any, deposit-feeding activity was present in the mud-rich substrate below the firmground/matground after deposition of the mud and before lithification. Surficial scratch-rich trace fossils (Fig. 3-4D) do not penetrate deeply into the underlying mud-rich substrate, but are preserved on what is considered to be a surficial firmground, which was possibly microbially-bound (*sensu* Seilacher 2008).

2 The surficial firmground rested on water-rich mud. This is evidenced by the compaction and contraction of the originally broadly vertical and planar cracks (Figs 3-2B and 3-5). The compression is estimated to have been up to 80%, based on the deconvolution of the sand-filled cracks.

3 After shrinkage crack development, a later firmground trace fossil assemblage was developed in the previously pore-water rich mud (Figs 3-4C and 3-5C). These burrows cut the surface microbial matground, and were excavated into a firm mud, as evidenced

by the preserved bioglyphs on *Trichophycus* and *Planolites* burrows. Since this last assemblage of burrows is not compressed (Figs 3-4C and 3-5C), this assemblage is considered to have formed after the mud was already dewatered/compacted.

Microbial mats were common in normal-marine settings until intense bioturbation became widespread in the late Cambrian to Ordovician (Seilacher and Pflüger 1994; McIlroy and Logan, 1999; Seilacher 1999). From the Ordovician onwards, microbial mats in marine settings are increasingly confined to sedimentary facies with some evidence of palaeoenvironmental stress (Hagadorn and Bottjer, 1999). Proterozoic and lower Palaeozoic shallow-marine deposits, such as the Beach Formation, are thus non-uniformitarian in nature (e.g., Jensen et al. 2005). No suitable modern analogue exists in which marine matgrounds exist in normal marine facies, such as storm-influenced continental shelves.

Most mud in marine depositional settings is deposited along with abundant terrigeneous organic matter, and thus becomes the substrate upon which endobenthic deposit feeders thrive. Macrofaunal reworking of upper sediment layers increases oxygen levels through irrigation and particle movement, thus promoting nutrient cycling and bacterial activity in deeper sediment layers. Following this, bioturbation has been considered to create a positive feedback loop, which further increases endobenthic productivity (McIlroy and Logan 1999). Consequently, mudstones in the rock record are seldom completely unbioturbated, except when they were deposited under extreme environmental stress (e.g., persistent anoxia, hyposalinity and hypersalinity). An important exception to this norm is fluid mud deposited in well-oxygenated estuaries and fluvially influenced nearshore environments (McIlroy 2004; Ichaso and Dalrymple 2009).

Comparison with modern mud-dominated coastlines, such as the Amazon Shelf (e.g., Aller and Blair 2006), indicates that a lack of bioavailable nutrients may be the reason for a lack of bioturbation, rather than environmental stresses such as hypersaline events or hypoxia.

In general, if metazoan grazing/bioturbation is suppressed for any reason in marine settings, micro-organisms can develop into a surface-attached community (i.e., microbial mat or biofilm). Mat development is facilitated by the production of a cohesive matrix of extracellular polymeric substances (EPS; Decho 1990; Bhaskar and Bhosle 2005). The binding effects of microbial filaments and EPS between sediment grains play an important role in the ecology and physiology of mat-building organisms by increasing the shear strength and rigidity of the microbially-stabilized sediment layer (Wachendörfer et al. 1994; Yallop et al. 1994, 2000; Mayer et al. 1999; Tolhurst et al. 2002, 2008).

Microbial matgrounds present numerous challenges to burrowing macrofauna. The sediment-binding effects of filamentous microbial mats are a significant biomechanical and biogeochemical (i.e., sporadically elevated H_2S) challenge to infaunal bioturbation (Meyers 2007). Furthermore, the abundant organic matter associated with microbial mats encourages surface and near-surface grazing activity (e.g., Seilacher 1999), rather than bulk sediment deposit feeding. This form of amensalism further excludes the development of burrowing macrofauna.

8. Discussion

It has been demonstrated that MISS and elevated levels of isotopically light, organic carbon are associated with unbioturbated Early Ordovician mudstones containing intrastratal shrinkage cracks. Beds without MISS have low organic carbon contents and are devoid of cracks. Thus, microbial matgrounds likely played a key role in the formation of ancient intrastratal shrinkage cracks. Observations of deformed cracks and undeformed trace fossils enable us to propose a sequence of events for mud that developed intrastratal shrinkage cracks (Fig. 3-9):

Sediment was rapidly deposited as a nutrient-poor fluid mud (Fig. 9A; cf. Aller and Blair, 2006). Following deposition of the mud, the sediment-water interface was stabilized by microbial mats (Fig. 3-9B). While at the sediment-water interface, the cohesive surface of the mats was marked or scratched by organisms, producing surficial trace fossils (e.g., *Monomorphichnus*). It is proposed here that the underlying mud then underwent volume reduction without significant compaction as a consequence of the removal of fluids (e.g., pore water) or perhaps microbially generated gas. This allowed the mud to become more cohesive by partitioning particulate grains and fluids (i.e., gas and water). Two possible scenarios are proposed for the timing of shrinkage crack development. In the first scenario, internal volume reduction is predicted to have generated irregular, planar, sub-vertical, fluid-filled vacuities prior to burial by sand (Fig. 9C). After burial by sand (Fig. 9D) the matground was smothered and began to decay.

The decaying matground then ruptured and the pre-existing sub-vertical vacuities (shrinkage cracks) were filled with sand from the overlying bed (Fig. 9E).

In the second scenario, it is proposed that the internal vacuities (shrinkage cracks) were not present prior to burial by sand (Fig. 9F). In this model, the vacuities formed as the matground became compromised by mat decay during burial (Fig. 9F), and then became filled by the overlying sand. In both scenarios, continued burial led to compaction of the crack-bearing mudstone. During compaction the less-compressible, sand-filled cracks became sinuous and contorted due to plastic deformation of the surrounding mud (Fig. 9G). The dewatered mud was subsequently colonized by infaunal bioturbating organisms that penetrated downwards from the overlying sand. Firmground burrows (e.g., *Trichophycus* and *Planolites*) with rather low aspect ratios attest to the cohesive nature of the mud prior to bioturbation (Fig. 5C).

It is important to note that our observations of cracks in thin section indicate that the process of cracking must have been largely passive and without creation of overpressure such as can be created by burial or seismic shocking underneath an impermeable 'topseal'. Creation of overpressure would likely have resulted in the creation of mud-volcanoes and fragmentation of sedimentary layers rather than generation of shrinkage cracks (Pratt 1998; Hurst et al. 2011), and such features were not observed. Although dewatering would reduce total volume of the fluid-rich mud, this would not be sufficient to generate intrastratal shrinkage cracks unless sediment cohesiveness was increased by microbial binding.

Figure 3-9. Summary diagram showing the geological pre-requisites for the generation of intrastratal shrinkage cracks within microbially-bound mudstones. The stages shown here allow us to consider the effects of sediment exposure time, bioturbation intensity, and the binding effects of microbial mats on the generation of cracks. A) Sediment is delivered as nutrient-poor fluid mud. B) The upper surface of the mud is stabilized by microbial mats and organisms marked the mat to generate surficial trace fossils (e.g. *Monomorphichnus*). C) Volume reduction occurs within the mud, either prior to, or shortly after sand deposition. This volume reduction produces irregular, planar, sub-matground vacuities. D) Burial by sand smothers the matground. E) During matground decay sand fills the linear vacuities (shrinkage cracks) from above. Alternatively, shrinkage cracks might have formed after burial by sand during mat decay. (F). Continued burial leads to mudstone compaction of up to 80%, while incompressible, sand-filled cracks become sinuous and contorted (G). Colonization by firmground burrows (e.g. *Trichophycus*) occurs after mudstone compaction, prior to burial below the maximum burrowing depth of *Trichophycus* (c. 10 cm).

A
unbioturbated non-cohesive mud
x
erosionally based mud
B
Monomorphichnus
microbially stabilized surface layer
x
C
microbially stabilized surface layer
x
D
Storm-sand
x
smothered matground
E
Storm-sand
x
decaying matground and formation of shrinkage cracks
F
Storm-sand
x
smothered matground
G
Trace fossils
Storm-sand
0.2x

Microbial mat development is a common feature of all the studied examples of mudstone with intrastratal shrinkage cracks, but absent in mudstone beds that lack such features. It is therefore likely that matground formation is a necessary precursor to the preservation of the intrastratal shrinkage cracks that subsequently developed. It is hypothesized that matgrounds are important in stabilizing the upper parts of mud deposits. Furthermore, matgrounds isolate underlying mud from contact with the water column, thus protecting it from the erosive action of currents caused by shear stress at the sediment-water interface (Tolhurst et al. 2002, 2008).

In cross-section, cracks exhibit contorted morphology and are typically filled by sand sourced from the overlying bed. It is therefore possible to infer cracking and subsequent filling by sand at a very early stage, namely prior to burial and lithification. Irregular fractures of variable length develop where inhomogeneities in the sediment composition and rheology allow the horizontal stresses to exceed material strength (see Figs 3-4A and 3-5).

Microbial mats develop in marine settings where metazoan bioturbation is suppressed either by ambient palaeoenvironmental conditions such as persistent anoxia, a lack of available organic matter, or, in extreme cases, salinity stress. Whether microbial mats were present in association with fluid mud deposits containing intrastratal shrinkage cracks during deposition of younger Phanerozoic deposits remains to be determined.

9. Conclusions

1. Contorted, sinuous, sand-filled cracks are common at the junction between unbioturbated mudstone and overlying storm sandstone beds in the Early Ordovician Beach Formation, Bell Island, Newfoundland. Integrated sedimentological, ichnological, petrographic and geochemical study of shallow marine mudstone reveals that crack development (cf. synaeresis cracks) on the upper surface of mudstone beds occurs in conjunction with specific organic biogeochemical and sedimentological parameters.

2. Cracks are absent in highly bioturbated mudstones. In sparsely bioturbated mudstones, cross-cutting relationships indicate that the cracks pre-date firmground assemblages of trace fossils that include horizontally to obliquely oriented *Trichophycus*. The tops of cracked mudstone horizons show evidence of microbial matground development, including microbially-induced sedimentary structures on bedding planes and carbonaceous laminae and tubular carbonaceous microfossils visible in thin sections. Non-cracked mudstones lack evidence for development of microbial mats. It is proposed that microbial-binding of surface sediment is an important prerequisite for intrastratal shrinkage crack formation.

3. Data from the Ordovician of Bell Island indicate that cracking may develop during: i) rapid deposition of a nutrient-poor fluid mud; ii) stabilization of the upper part of the mud by microbial communities to form a cohesive surface layer (microbial mat); iii)

volume reduction of the microbially stabilized mud via fluid removal. iv) The volume reduction might occur prior or during subsequent burial of the matground by storm-generated sands. This stage is followed by degradation of the matground, causing passive infill of cracks by sand from the overlying bed. v) The subsequent compaction of the mudstone that hosts the sand-filled cracks produces the typical contorted morphologies of intrastratal shrinkage cracks. While the term 'synaeresis crack' is commonly used to describe sinuous and tapering cracks in mudstone beds, the use of the non-genetic term 'intrastratal shrinkage crack' is proposed, unless evidence of synaeresis (i.e. contraction of clay mineral lattices in response to salinity change) can be unequivocally demonstrated.

Future work to determine the mechanism by which mud undergoes intrastratal shrinkage should focus on experimental studies of clay–pore water mixtures in sub-matground conditions and varying composition of microorganisms involved (cf. Ross et al. 2011). Such work would be challenging, but is going to be key to unravelling the conundrum of intrastratal shrinkage crack ("synaeresis crack") formation. Until such a time as the mechanism is fully understood, it is recommended that sedimentologists and ichnologists refrain from using intrastratal shrinkage cracks as indications of palaeoenvironmental settings with fluctuating pore water salinity.

10. Acknowledgements

DH acknowledges financial support from the Grant-in-Aid scheme of AAPG and student grants sponsored by IAS and GSA. RC acknowledges the support of a postdoctoral fellowship at Memorial University from the Slopes 2 Consortium funded by BG Group, BP, ConocoPhillips, DONG, GDF Suez, Hess, Petrobras, RWE Dea, Statoil and Total. DMc acknowledges the financial support of a Canada Research Chair and an NSERC discovery grant. Alex Liu is thanked for helpful discussion and suggestions on a previous version of this manuscript. The suggestions of Paul Myrow and one anonymous reviewer helped to improve the manuscript. Editors Stephen Lokier and Tracy Frank are gratefully acknowledged for editorial assistance and helpful suggestions.

11. References

ALLEN, J.R.L., 1982, Sedimentary Structures, Volume II: Their Character and Physical Basis. Elsevier, Amsterdam. p. 663

ALLER, R.C. AND BLAIR, N.E., 2006, Carbon remineralization in the Amazon-Guianas tropical mobile mud belt: A sedimentary incinerator: Continental Shelf Research, v. 26, p. 2241-2259.

ASTIN, T.R. AND ROGERS, D.A., 1991, 'Subaqueous shrinkage cracks' in the Devonian of Scotland reinterpreted: Journal of Sedimentary Petrology, v. 61, p. 850-859.

BAILEY, J.V., ORPHAN, V.J., JOYE, S.B. AND CORSETTI, F.A., 2009, Chemotrophic microbial mats and their potential for preservation in the rock record: Astrobiology, v. 9, p. 843-859.

BHASKAR, P.V. AND BHOSLE, N.B., 2005, Microbial extracellular polymeric substances in marine biogeochemical processes: Current Science, v. 88, p. 45-53.

BHATTACHARYA, J.P. AND MACEACHERN, J.A., 2009, Hyperpycnal rivers and prodeltaic shelves in the cretaceous seaway of North America: Journal of Sedimentary Research, v. 79, p. 184-209.

BRENCHLEY, P.J., PICKERILL, R.K. AND STROMBERG, S.G., 1993, The role of wave reworking on the architecture of storm sandstone facies, Bell Island Group (Lower Ordovician), Eastern Newfoundland. Sedimentology, 40, 359-382.

BROMLEY, R.G., 1996, Trace fossils; biology, taphonomy and applications. Chapman and Hall, London, United Kingdom.

BUATOIS, L. A., SACCAVINO, L.L. AND ZAVALA, C., 2011, Ichnological signatures of hyperpycnal flow deposits in Cretaceous river-dominated deltas, Austral Basin, southern Argentina, in R. M. Slatt and C. Zavala, eds., Sediment transfer from shelf to deep water—Revisiting the delivery system: AAPG Studies in Geology v. 61, p. 153-170.

BURST, J.F., 1965, Subaqueously formed shrinkage cracks in clay: Journal of Sedimentary Petrology, v. 35, p. 348-353.

CALLOW, R. AND BRASIER, M., 2009a, A solution to Darwin's dilemma of 1859: exceptional preservation in Salter's material from the late Ediacaran Longmyndian Supergroup: England. Journal of the Geological Society, London, v. 166, p. 1-4.

CALLOW, R. AND BRASIER, M., 2009b, Remarkable preservation of microbial mats in Neoproterozoic siliciclastic settings: Implications for Ediacaran taphonomic models: Earth-Science Reviews, v. 96, p. 207-219.

COPLEN, T.B., BRAND, W.A., GEHRE, M., GRÖNING, M., MEIJER, H.A.J., TOMAN, B. AND VERKOUTEREN, R.M., 2006, After two decades a second anchor for the VPDB $\delta^{13}C$ scale: Rapid Communications in Mass Spectrometry, v. 20, p. 3165-3166.

COWAN, C.A. AND JAMES, N.E., 1992, Diastasis cracks: mechanically generated synaeresis-like cracks in Upper Cambrian shallow water oolite and ribbon carbonates: Sedimentology, v. 39, p. 1101-1118.

DEAN, W.E., CLAYPOOL, G.C. AND THIEDE, J., 1984, Accumulation of organic matter in Cretaceous oxygen-deficient depositional environments in the central Pacific Ocean: Organic Geochemistry, v. 7, p. 39-51.

DECHO A.W., 1990, Microbial exopolymer secretions in ocean environments: their role(s) in food webs and marine processes: Oceanography and Marine Biology, v. 28, p. 73-153

DONOVAN, R.N. AND FOSTER, R.J., 1972, Subaqueous shrinkage cracks from the Caithness Flagstone series (Middle Devonian) of northeast Scotland: Journal of Sedimentary Petrology, v. 42, p. 309-317.

ENDO, R., 1933, *Manchuriophycus* nov. gen., from a Sinian formation of South Manchuria: Journal of Geology and Geography, v. 11, p. 43-48.

ERIKSSON, P.G., PORADA, H., BANERJEE, S., BOUOUGRI, E., SARKAR, S. AND BUMBY, A.J., 2007, Mat-destruction features. In: Atlas of microbial mat features preserved within the siliciclastic rock record, eds., J. Schieber, P.K. Bose, S. Eriksson, S. Banerjee, S. Sarkar, W. Altermann and O. Catuneanu): Atlases in Geoscience 2, Elsevier, Amsterdam, p. 76-105.

FILLION, D. AND PICKERILL, R.K., 1990, Ichnology of the Upper Cambrian? to Lower Ordovician Bell Island and Wabana groups of eastern Newfoundland, Canada: Palaeontographica Canadiana, v. 7, p. 1-119.

FOLK, R.L., 1954, The distinction between grain size and mineral composition in sedimentary rock nomenclature: Journal of Geology, v. 62, p. 344–359.

FOLK, R.L., 1956, The role of texture and composition in sandstone classification: Journal of Sedimentary Petrology 26, 166–171.

FRANKS, J. AND STOLZ, J.F., 2009, Flat laminated microbial mat communities: Earth-Science Reviews, v. 96, p. 163-172.

FYSON, W.K., 1962, Deadwood and Winnipeg stratigraphy in south-western Saskatchewan: Saskatchewan Department of Mineral Resources Report, v. 64, 37 p.

GEHLING, J.G., 1999, Microbial mats in terminal Proterozoic siliciclastics: Ediacaran death masks: Palaios, v. 14, p. 40-57.

GERDES, G., 2007, Structures left by modern microbial mats in their host sediments. In: Atlas of microbial mat features preserved within the siliciclastic rock record, eds., J. Schieber, P.K. Bose, S. Eriksson, S. Banerjee, S. Sarkar, W. Altermann and O. Catuneanu: Atlases in Geoscience 2, Elsevier, Amsterdam, p. 5-38.

GERDES, G., KLENKE, T. AND NOFFKE, N., 2000, Microbial signatures in peritidal siliciclastic sediments: a catalogue: Sedimentology, v. 47, p. 279-308.

GILHOOLY, W.P., CARNEY, R.S. AND MACKO, S.A., 2007, Relationships between sulfide-oxidizing bacterial mats and their carbon sources in northern Gulf of Mexico cold seeps: Organic Geochemistry, v. 38, p. 380-393.

GLAUBITZ, S., LABRENZ, M., JOST, G. AND JÜRGENS, K., 2010, Diversity of active chemolithoautotrophic prokaryotes in the sulfidic zone of a Black Sea pelagic redoxcline as determined by rRNA-based stable isotope probing: FEMS Microbiology Ecology, v. 74, p. 32-41.

HAGADORN, J.W. AND BOTTJER, D.J., 1997, Wrinkle structures: Microbially mediated sedimentary structures common in subtidal siliciclastic settings at the Proterozoic-Phanerozoic transition: Geology, v. 25, p. 1047-1050.

HAGADORN, J.W. AND BOTTJER, D.J., 1999, Restriction of a Late Neoproterozoic biotope: suspect-microbial structures and trace fossils at the Vendian-Cambrian transition. Palaios, v. 14, p. 73-85.

HOFMANN, H.J., 1967, Precambrian fossils (?) near Elliot Lake, Ontario: Science, v. 156, p. 500-504.

HOFMANN, H.J., 1971, Precambrian fossils, pseudofossils, and problematica in Canada: Geological Survey of Canada Bulletin, v. 189, p. 1-146.

HUGHES, N.C. AND HESSELBO, S.R., 1997, Stratigraphy and sedimentology of the St. Lawrence Formation, Upper Cambrian of the northern Mississippi Valley: Milwaukee Public Museum Contributions to Biology and Geology, v. 91, p. 1-50.

HURST, A., SCOTT, A. AND VIGORITO, M., 2011, Physical characteristics of sand injectites: Earth-Science Reviews, v. 106, p. 215-246.

ICHASO, A.A. AND DALRYMPLE, R.W., 2009, Tide- and wave-generated fluid mud deposits in the Tilje Formation (Jurassic), offshore Norway: Geology, v. 37, p. 539-542.

JENSEN, S., DROSER, M.L. AND GEHLING, J.G., 2005, Trace fossil preservation and the early evolution of animals: Palaeogeography, Palaeoclimatology, Palaeoecology, v. 220, p. 19-29.

JÜNGST, H., 1934, Zur geologischen Bedeutung der Synärese. Ein Beitrag zur Entwässerung der Kolloide im werdenden Gestein: Geologische Rundschau, v. 25, p. 312-325.

KIRBY, R. AND PARKER, W.R., 1983, Distribution and behavior of fine sediment in the Severn Estuary and inner Bristol Channel, U.K: Canadian Journal of Fisheries and Aquatic Sciences, v. 40, p. 83–95.

LOGAN, G.A., CALVER, C.R., GORJAN, P., SUMMONS, R.E., HAYES, J.M. AND WALTER, M.R., 1999, Terminal Proterozoic mid-shelf benthic microbial mats in the Centralian Superbasin and their environmental significance: Geochimica et Cosmochimica Acta, v. 63, p. 1345-1358.

MACQUAKER, J.H.S., BENTLEY, S.J. AND BOHACS, K., 2010, Wave-enhanced sediment-gravity flows and mud dispersal across continental shelves: Reappraising sediment transport processes operating in ancient mudstone successions: Geology, v. 38, p. 947-950.

MADRID, V.A., 2006, The role of microbial communities in the biogeochemistry of nonsulfidic, tropical deltaic mobile sediments. PhD dissertation: Stony Brook University, 347 p.

MAYER, C., MORITZ, R., KIRSCHNER, C., BORCHARD, W., MAIBAUM, R., WINGENDER, J. AND FLEMMING, H., 1999, The role of intermolecular interactions: Studies on model systems for bacterial biofilms: International Journal of Biological Macromolecules, v. 26, p. 3-16.

MCILROY, D., 2004, Ichnofabrics and sedimentary facies of a tide-dominated delta: Jurassic Ile Formation of Kristin Field, Haltenbanken, offshore Mid-Norway. In: McIlroy, D., ed., The Application of Ichnology to Palaeoenvironmental and Stratigraphic Analysis: Geological Society of London Special Publication, v. 228, p. 237-272.

MCILROY, D. AND LOGAN, G.A., 1999, The impact of bioturbation on infaunal ecology and evolution during the Proterozoic-Cambrian transition: Palaios, v. 14, p. 58-72.

MEHTA, A.J. AND MCANALLY, W.H., 2002, Fine grained cohesive sediment transport. In: Sedimentation Engineering: Processes, Measurements, Modeling and Practice. ASCE manual 54. (Ed P.E. Marcelo Garcia), American Society of Civil Engineers, New York, p. 253-306.

MEYERS, S.R., 2007, Production and preservation of organic matter: The significance of iron: Paleoceanography 22, PA4211.

NOFFKE, N., 2000, Extensive microbial mats and their influences on the erosional and depositional dynamics of a siliciclastic cold water environment (Lower Arenigian, Montagne Noire, France): Sedimentary Geology, v. 136, p. 207-215.

NOFFKE, N., 2009, The criteria for the biogenicity of microbially induced sedimentary structures (MISS) in Archean and younger, sandy deposits: Earth-Science Reviews, v. 96, p. 173-180.

NOFFKE N., 2010, Geobiology: Microbial Mats in Sandy Deposits from the Archean Era to Today. Springer, Berlin. p. 194.

NOFFKE, N., GERDES, G., KLENKE, T. AND KRUMBEIN, W.E., 1997, A microscopic sedimentary succession of graded sand and microbial mats in modern siliciclastic tidal flats: Sedimentary Geology, v. 110, p. 1-6.

NOFFKE, N., GERDES, G., KLENKE, T. AND KRUMBEIN, W.E., 2001, Microbially induced sedimentary structures-a new category within the classification of primary sedimentary structures: Journal of Sedimentary Research, v. 71, p. 649-656.

NOFFKE, N., KNOLL, A.H. AND GROTZINGER, J., 2002, Sedimentary controls on the formation and preservation of microbial mats in siliciclastic deposits: a case study from the upper Neoproterozoic Nama Group, Namibia: Palaios, v. 17, p. 1-14.

NOFFKE, N., HAZEN, R.M. AND NHLEKO, N., 2003, Earth's earliest microbial mats in a siliciclastic marine environment (Mozaan Group, 2.9 Ga, South Africa): Geology, v. 31, p. 673-676.

NOFFKE, N., ERIKSSON, K.A., HAZEN, R.M. AND SIMPSON, E.L., 2006, A new window into Early Archean life: Microbial mats in Earth's oldest siliciclastic tidal deposits (3.2 Ga Moodies Group, South Africa): Geology, v. 34, p. 253-256.

NOFFKE, N., BEUKES, N., BOWER, D., HAZEN, R.M., AND SWIFT, D.J.P., 2008, An actualistic perspective into Archean worlds — (cyano-)bacterially induced sedimentary structures in the siliciclastic Nhlazatse Section, 2.9 Pongola Supergroup, South Africa: Geobiology, v. 6, p. 5-20.

OBERMEIER, S.F., 1996, Use of liquefaction-induced features for paleoseismic analysis - An overview of how seismic liquefaction features can be distinguished from other features and how their regional distribution and properties of source

sediment can be used to infer the location and strength of Holocene paleo-earthquakes: Engineering Geology, v. 44, p. 1-76.

PACTON, M., FIET, N. AND GORIN, G.E., 2007, Bacterial activity and preservation of sedimentary organic matter: The role of exopolymeric substances. Geomicrobiology Journal, v. 24, p. 571-581.

PACTON, M., GORIN, G.E. AND FIET, N., 2008, Unravelling the origin of ultralaminae in sedimentary organic matter: The contribution of bacteria and photosynthetic organisms: Journal of Sedimentary Research, v. 78, p. 654-667.

PARIZOT, M., ERIKSSON, P.G., AIFA, T., SARKAR, S., BANERJEE, S., CATUNEANU, O., ALTERMANN, W., BUMBY, A.J., BORDY, E.M., VAN ROOY, J.L. AND BOSHOFF, A.J., 2005, Suspected microbial mat-related crack-like structures in the Palaeoproterozoic Magaliesberg Formation sandstones, South Africa: Precambrian Research, v. 138, p. 274-296.

PARKES, R.J., CRAGG, B.A., GETLIFF, J.M., HARVEY, S.M., FRY, J.C., LEWIS, C.A. AND ROWLAND, S.J., 1993, A quantitative study of microbial decomposition of biopolymers in Recent sediments from the Peru Margin: Marine Geology, v. 113, p. 55-66.

PEAT, C.J., 1984, Precambrian Microfossils from the Longmyndian of Shropshire. Proceedings of the Geologists Association, v. 95, p. 17-22.

PEMBERTON, S.G. AND WIGHTMAN, D.M., 1992, Ichnological characteristics of brackish water deposits: In: Applications of ichnology to petroleum exploration, a core workshop, ed., S.G. Pemberton: Society of Economic Paleontologists and Mineralogists, Core Workshop v. 17, p. 141-167.

PERON, H., HUECKEL, T., LALOUI, L. AND HU, L.B., 2009, Fundamentals of desiccation cracking of fine-grained soils: Experimental characterisation and mechanisms identification: Canadian Geotechnical Journal, v. 46, p. 1177-1201.

PFLÜGER, F., 1999, Matground structures and redox facies: Palaios, v. 14, p. 25-39.

PLUMMER, R.S. AND GOSTIN, V.A., 1981, Shrinkage cracks: desiccation or synaeresis: Journal of Sedimentary Petrology, v. 51, p. 1147-1156.

PRATT, B.R., 1998, Syneresis cracks: Subaqueous shrinkage in argillaceous sediments caused by earthquake-induced dewatering: Sedimentary Geology, v. 117, p. 1-10.

RANGER, M.J., PICKERILL, R.K. AND FILLION, D., 1984, Lithostratigraphy of the Cambrian? - Lower Ordovician Bell Island and Wabana groups of Bell, Little Bell, and Kellys islands, Conception Bay, eastern Newfoundland: Canadian Journal of Earth Sciences, v. 21, p. 1245-1261.

ROSS, J.A., PEAKALL, J. AND KEEVIL, G.M., 2011, An integrated model of extrusive sand injectites in cohesionless sediments: Sedimentology, v. 58, p. 1693-1715.

SARBU, S.M., KANE, T.C. AND KINKLE, B.K., 1996, A chemoautotrophically based cave ecosystem: Science, v. 272, p. 1953-1954.

SCHIEBER, J., 1998, Possible indicators of microbial mat deposits in shales and sandstones: examples from the Mid-Proterozoic Belt Supergroup, Montana, USA: Sedimentary Geology, v. 120, p. 105-124.

SCHIEBER, J., 1999, Microbial mats in terrigeneous clastics: The challenge of identification in the rock record: Palaios, v. 14, p. 3-12.

SCHIEBER, J., BOSE, P.K., ERIKSSON, P.G., BANERJEE, S., SARKAR, S., ALTERMANN, W. AND CATUNEANU, O., 2007, Atlas of microbial mat features preserved in the siliciclastic rock record: Atlases in Geoscience 2. Elsevier, Amsterdam. p. 324.

SEILACHER, A., 1999, Biomat-related lifestyles in the Precambrian: Palaios, v. 14, p. 86-93.

SEILACHER, A., 2008, Biomats, biofilms, and bioglue as preservational agents for arthropod trackways: Palaeogeography, Palaeoclimatology, Palaeoecology, v. 270, p. 252-257.

SEILACHER, A. AND PFLÜGER, F., 1994, From biomats to benthic agriculture: A biohistoric revolution. In: Biostabilization of Sediments, eds., W.E. Krumbein, D.M. Paterson, and L.J. Stal: Bibliotheks und Informationssystem der Carl von Ossietzky Universität Oldenburg, p. 97-105.

TANNER, P.W.G., 1998, Interstratal dewatering origin for polygonal patterns of sand-filled cracks: A case study from late Proterozoic metasediments of Islay, Scotland. Sedimentology, v. 45, p. 71-89.

TANNER, P.W.G., 2003, Syneresis. In: Encyclopedia of sediments and sedimentary rocks (Ed. G.V. Middleton), Kluwer Academic Publishers, The Netherlands, p. 718-720.

TAYLOR, A.M. AND GOLDRING, R., 1993, Description and analysis of bioturbation and ichnofabric: Journal of the Geological Society, London, v. 150, p. 141-148.

TAYLOR, G.T., IABICHELLA, M., HO, T., SCRANTON, M.I., THUNELL, R.C., MULLER-KARGER, F. AND VARELA, R., 2001, Chemoautotrophy in the redox transition zone of the Cariaco Basin: A significant midwater source of organic carbon production: Limnology and Oceanography, v. 46, p. 148-163.

TOLHURST, T.J., GUST, G. AND PATERSON, D.M., 2002, The influence of an extracellular polymeric substance (EPS) on cohesive sediment stability. In: Fine Sediment Dynamics in the Marine Environment, eds., J.C. Winterwerp and C. Kranenburg: Elsevier, Amsterdam, p. 409-426.

TOLHURST, T.J., CONSALVEY, M. AND PATERSON, D.M., 2008, Changes in cohesive sediment properties associated with the growth of a diatom biofilm: Hydrobiologia, v. 596, p. 225–239.

TUTTLE, J. H. AND JANASCH, H. W., 1973, Sulfide and thiosulfate-oxidizing bacteria in anoxic marine basins: Marine Biology, v. 20, p. 64-70.

TYSON, R.V., 1995, Sedimentary organic matter: Organic facies and palynofacies. Kluwer Academic Publishers, The Netherlands, p. 615.

VISSCHER, P.T. AND STOLZ, J.F., 2005, Microbial mats as bioreactors: Populations, processes, and products: Palaeogeography, Palaeoclimatology, Palaeoecology, v. 219, p. 87-100.

WACHENDÖRFER, V., RIEGE, H. AND KRUMBEIN, W.E., 1994, Parahistological sediment thin sections. In: Biostabilization of Sediments, eds., W.E. Krumbein, D.M. Paterson, and L.J. Stal: Bibliotheks und Informationssystem der Carl von Ossietzky Universität Oldenburg, p. 257-277.

WEISS, A., 1958, Die innerkristalline Quellung als allgemeines Modell für Quellungsvorgänge: Chemische Berichte, v. 91, p. 481-502.

WHITE, W.A., 1961, Colloid phenomena in sedimentation of argillaceous rocks: Journal of Sedimentary Research, v. 31, p. 560-570.

WIGHTMAN, D.M., PEMBERTON, S.G. AND SINGH, C., 1987, Depositional modelling of the Upper Mannville (Lower Cretaceous), east-central Alberta: Implications for the recognition of brackish water deposits. In: Reservoir

Sedimentology, eds., R.W. Tillman and K.J. Weber: Society of Economic Paleontologists and Mineralogists, Special Publication, v. 40, p. 189-220.

WOLANSKI, E. AND GIBBS, R.J., 1995, Flocculation of suspended sediment in the Fly River Estuary, Papua New Guinea: Journal of Coastal Research, v. 11, p. 754-762.

YALLOP, M.L., DE WINDER, B., PATERSON, D.M. AND STAL, L.J., 1994, Comparative structure, primary production and biogenic stabilization of cohesive and non cohesive marine sediments inhabited by microphytobenthos: Estuarine, Coastal and Shelf Science, v. 39, p. 565-582.

YALLOP, M.L., PATERSON, D.M. AND WELLSBURY, P., 2000, Interrelationships between rates of microbial production, exopolymer production, microbial biomass, and sediment stability in biofilms of intertidal sediments: Microbial Ecology, v. 39, p. 116-127.

CHAPTER 4

Vermiform deposit feeders control the spatial distribution of organic carbon and redox-sensitive trace elements in fine-grained siliciclastic rocks

Dario Harazim, Duncan McIlroy, Nicholas Edwards, Roy Wogelius, Phillip L. Manning, Uwe Bergmann

1. Abstract

The distribution of organic matter and partitioning of trace elements in fine-grained siliciclastic rocks is here demonstrated to be systematically controlled by trace making organisms. Detailed petrographic analyses of well-connected silty, illitic/chloritic burrow halo and illite/smectite bearing clay-rich fecal core at a range of spatial scales reveal that phycosiphoniform trace makers sort sediment grains irrespective of both mineralogy and shape. Illite/smectite enrichment of the burrow core is inferred to result from a combination of selective physical sorting and biological (in-vivo) weathering. The fecal burrow core is composed of a dense organo-clay matrix critically enriched in TOC (1.8 wt%) compared to host sediment TOC values (0.6 wt%). A newly developed synchrotron rapid scanning x-ray fluorescence (SRS-XRF) technique combined with conventional inductively coupled plasma mass spectrometry (ICP-MS) revealed that some redox-sensitive elements (Mn, Fe, Co, Cu, Zn and S) are enriched by several orders of

magnitude in the burrow core compared to unbioturbated host sediment. Some biologically important elements (e.g. Sr and Ba) are depleted in both the burrow halo and core relative to the host sediment. Elements (i.e., Zr and Rb) which have no known function in biological systems show simple redistribution with depletion in the burrow halo being equivalent to enrichment in the burrow core. Despite a significant enrichment in organic matter by ~1.1 wt%, the absence of high amounts of early diagenetic pyrite in close association with organic matter indicates that the fecal organic carbon in bioturbated mudstone was of potentially low reactivity.

2. Introduction

This research aims to unravel the effects of deposit feeding organisms on the spatial patterns and characteristics of organic carbon and trace elements within bioturbated siliciclastic mudstones. Understanding the biogeochemistry of deposit feeding is of importance, because of its prevalence in marine sediments and the effect of bioturbation on the balance of solutes and gases in the bioturbated zone (Aller 1982; Jørgensen 2000). Bioturbation is a first order control on all microbially-mediated biogeochemical reactions below the sediment-water interface (Aller 1982; Grossmann and Reichardt 1991; Seilacher and Pflüger 1994; McIlroy and Logan 1999) and influences the reaction geometry, rate and intensity of both solid (Herringshaw and McIlroy 2013) and dissolved pore-water species (Zhu et al. 2006; Cao et al. 2010; Volkenborn et al. 2012). Bioturbation affects early diagenesis and authigenesis and regulates the formation rates and chemical composition of the earliest formed diagenetic minerals associated with

biogenic fabric (Aller et al. 2010; Virtasalo et al. 2010, 2012). Bioturbation has previously been considered predominantly as a "physical disturbance" that leads to the oxidation of organic matter and reduces previously formed metal sulfides, thereby putting trace elements into solution (Aller and Rude 1988). The dissolved, inorganic by-products of organic matter remineralization (i.e., Mn^{2+}, Fe^{2+}, HCO_3^-, S^{2-}) accumulate in early diagenetic minerals such as carbonates, silicates, phosphates and metal sulfides (e.g., Froehlich et al. 1979). Popular box models (e.g., Canfield 2004) incorporating the repartitioning of both major and trace elements between all biological and geological reservoirs insufficiently account for reflux relationships, rates and geometries at complex, three-dimensional boundaries associated with biogenic structures (Aller et al. 2010).

Incorporating the impact of deposit feeding into diagenetic modeling suffers from a lack of data, perhaps because geochemical data are difficult to collect from trace fossils preserved in the rock record. Many mudstone trace fossils are morphologically complex and small (<5 mm; Wetzel 1991). Most researchers gather “whole-rock” data using sampling techniques that homogenize sedimentary components of dissimilar origin, thus producing mixed “whole-rock” datasets without appreciation of the heterogeneities imparted on the sediment by bioturbating organisms (see Stockdale et al. 2010).

While the mineralogical products of early diagenesis are diverse, they can be identified via electron beam imaging and quantified via non-destructive spectroscopic measurements and (Wogelius et al. 2011; Edwards et al. 2012). This work focuses on the impact of grain size-selective deposit-feeding with respect to: 1) sediment mineralogy; 2)

the composition and abundance of organic matter; and 3) the distribution of major and trace elements.

The incomplete knowledge on the role of bioturbation that acts to control the compositional diversity of organic-rich mudstones (e.g., black shales) on a range of scales is a major shortcoming in geological models regularly used in the study of hydrocarbon systems and ancient oceanic anoxic events (Demaison and Moore 1980; Pedersen and Calvert 1990; Klemme and Ulmishek 1991; Arthur and Sageman 1994; Pancost et al. 2004; Jarvis et al. 2011; Owens et al. 2012). The chemical properties of sediments are commonly documented as one-dimensional geochemical measurements from logged sedimentological sections (e.g., Berner 1964; Froelich et al. 1979; Berner 1980; Jenkyns 2010). Sedimentary microenvironments are characterized by complex redox conditions and competing bacterial populations (Jørgensen and Boudreau 2001; Zhu et al. 2006). The geometry and duration of these microbially mediated biogeochemical redox reactions (and their mineralogical products) in bioturbated sediments are strongly controlled by infaunal organisms (Aller 1994; McIlroy & Logan 1999), but their distribution and effect on long-term storage of geochemical information in fine-grained sedimentary rocks remains poorly understood to date. This study investigates in detail the geochemistry of mm-scale trace fossils of deposit-feeding organisms that are homogenized by most bulk-sampling techniques.

3. Material and Methods

3.1. Background to sample material and sampling strategy

Phycosiphoniform trace fossils (including *Phycosiphon* isp. and *Nereites* isp.) are common in mudstones and sandstones in a wide variety of post-Ordovician marine paleoenvironments (Ekdale and Lewis 1991; Wetzel and Uchman 2001; Taylor et al. 2003; Bednarz and McIlroy 2009). The makers of phycosiphoniform burrows are considered to be opportunistic, grain-selective deposit feeders that colonize and ingest freshly deposited sediment (e.g., Goldring et al. 1991; Savrda et al. 2001; Wetzel and Uchman 2001; McIlroy 2004; Bednarz and McIlroy 2009).

The samples used in this study were collected from Late Cretaceous (Maastrichtian) age turbidites of the Rosario Formation, Baja California, Mexico. Within the Rosario Formation phycosiphoniform burrows occur within several ichnofabric associations containing phycosiphoniform traces, which are regularly found together with *Chondrites*, *Planolites* and *Paleophycus* (Callow et al. 2012). The typical 'frogspawn' ichnofabric of Phycosiphoniform burrows has been observed to be the earliest ichnofabric developed within a turbidite event bed in the Rosario Formation (Callow et al. 2012).

Large-scale sedimentological and ichnological characteristics and patterns of the deep-marine Canyon San Fernando channel-levee complex have previously been described by Dykstra and Kneller (2007) and Callow et al. (2013). Coastal outcrops of a submarine slope channel system at Pelican Point (Dykstra and Kneller 2009) reveal evidence for laterally migrating and sinuous submarine channels, and their channel-

Figure 4-1. The study area near Cajiloa, located on the Pacific Coast of Baja California, Mexico. The major roads are marked in red, dashed lines indicate unpaved roads. Dry river valleys are shown as continuous blue lines. Adapted from Callow et al. (2013). (B) shows the investigated outcrops north of Cajiloa. Location map adapted from Dykstra and Kneller (2009).

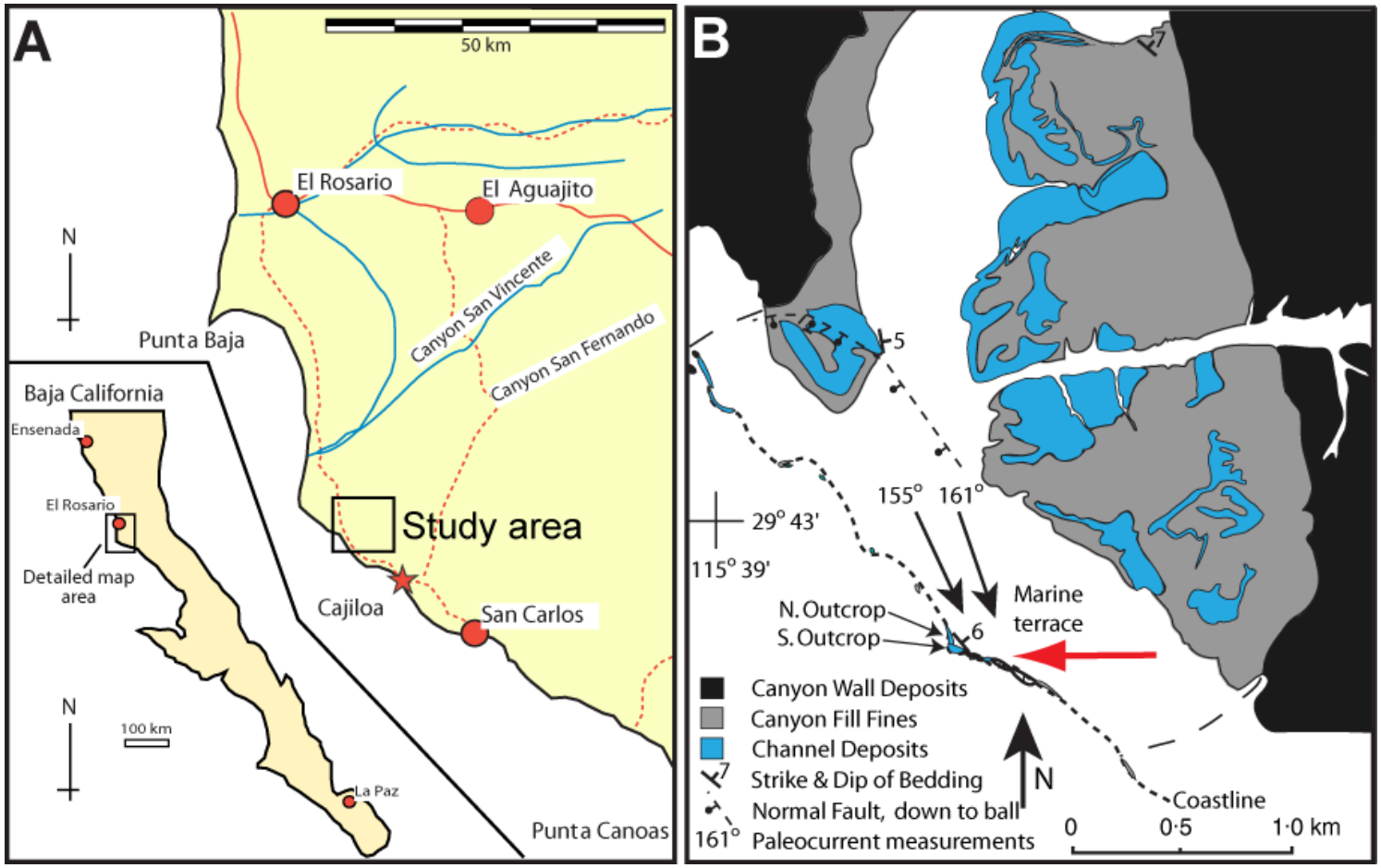
A
50 km
El Rosario
El Aguajito
N
Punta Baja
Canyon San Vincente
Canyon San Fernando
Baja California
Ensenada
El Rosario
Detailed map area
Study area
Cajiloa
San Carlos
N
100 km
La Paz
Punta Canoas
B
5
155°
161°
29° 43'
115° 39'
N. Outcrop
S. Outcrop
6
Marine terrace
Canyon Wall Deposits
Canyon Fill Fines
Channel Deposits
Strike & Dip of Bedding
Normal Fault, down to ball
161°
Paleocurrent measurements
N
Coastline
0
0·5
1·0 km

associated, thin bedded overbank sediments (Fig. 4-1B) at this locality contain very fine-grained sandstone and mudstone interbedded with coarse-grained (partly conglomeratic) lithologies. Large (ca. 5 kg) hand samples containing phycosiphoniform trace fossils were collected from fresh sandstone and mudstone outcrops from channel overbank facies just south of the locality Pelican Point (see Bednarz and McIlroy 2009; Dykstra and Kneller 2009; Fig. 4-1B). Rocks containing phycosiphoniform burrows from Pelican Point (Fig. 4-2A) were slabbed to remove weathering artifacts. Additionally, trace fossils are of sufficient size (~5 mm burrow core diameter; Fig. 4-2). To allow sampling of sufficient amounts of material from bioturbated and unbioturbated sediment for compositional analyses, powder samples were obtained for geochemical measurements using a rotary, handheld sampling device (DREMEL® 4000). All geochemical analyses (except ICP-MS analyses) were carried out on the same aliquot. Powder samples were obtained from fresh surfaces with sub-millimeter precision using a stationary high-precision Merchantek Micromill (New Wave®) microsampling device. Sample powder collected from host sediment, burrow halo and burrow core was analyzed separately using well-established laboratory techniques (see below).

3.2 Petrographic description

Polished thin sections were prepared from host sediment, burrow halo and core. Thin sections were examined via a petrographic microscope in transmitted and reflected light. The composition of framework and matrix components was examined with a FEI Quanta 650 Environmental Scanning Electron Microscope (SEM), equipped with an energy

Figure 4-2. (A) Representative outcrop from the Pelican System showing terrace sediments. The sandstone beds show little bioturbation, while the fine-grained beds are dominated by phycosiphoniform traces. (B) Photograph of planar surface showing a representative sample including Phycosiphon ichnofabric and its characteristic burrow elements halo and core that were analyzed with respect to host sediment. The light, sand-rich halo is usually located beneath the dark, clay-rich fecal core. The diameter of the burrow core is ~5 mm. (C) Schematic sketch showing the foraging mechanism and production of halo and core by an unknown vermiform organism (schematically represented in red) (modified from Bednarz and McIlroy 2009).

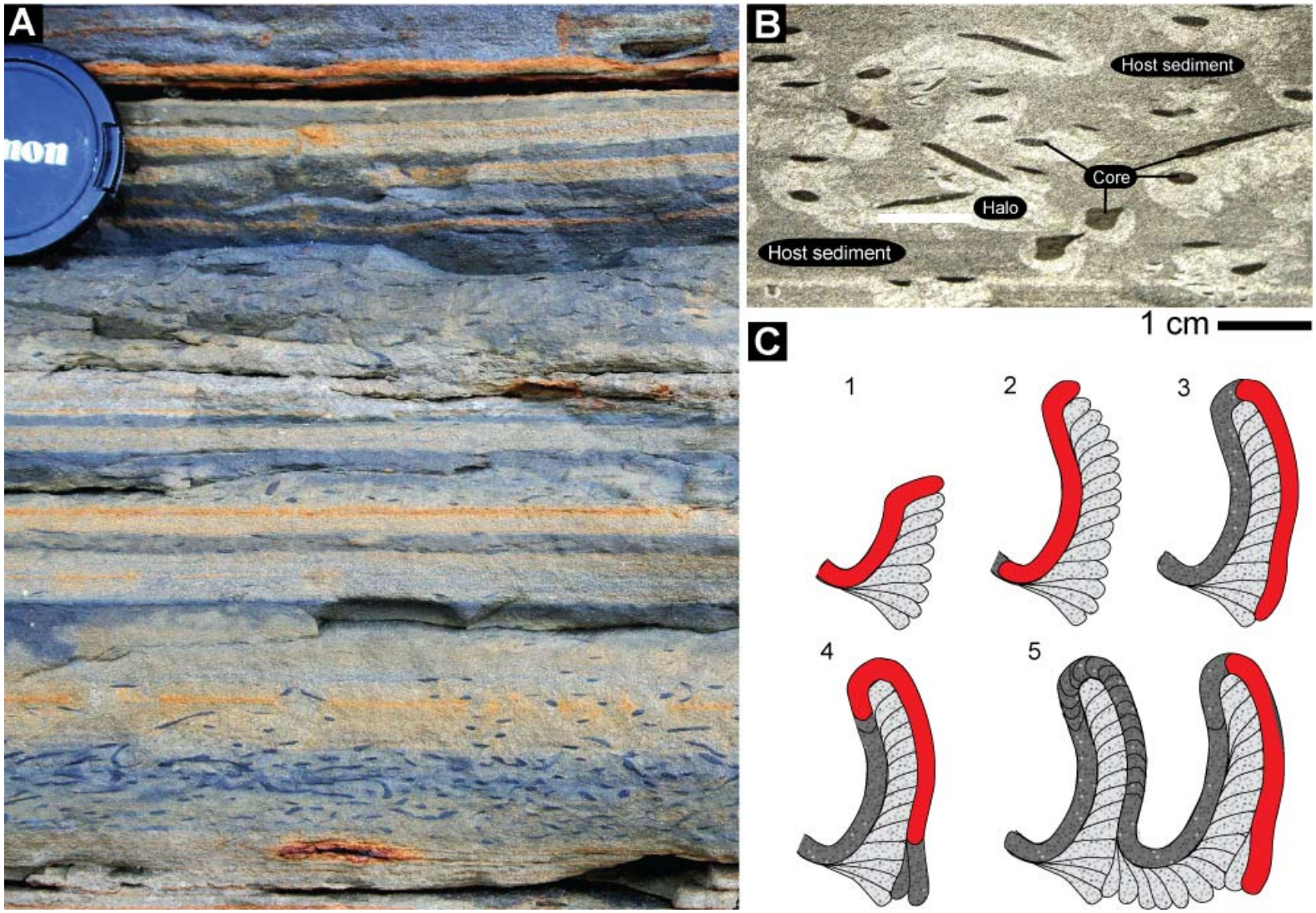
A
B
Host sediment
Core
Halo
Host sediment
1 cm
C
1
2
3
4
5

dispersive X-Ray (EDX) analytical system. The SEM was operated in backscatter mode.

3.3 Chemical Imaging via Synchrotron Rapid Scanning X-Ray Fluorescence (SRS-XRF)

Non-destructive synchrotron X-Ray fluorescence imaging was performed to reveal the elemental distributions within the samples. Analyses were performed at wiggler beam line 6-2 at the Stanford Synchrotron Radiation Lightsource (SSRL, CA, USA). Elemental maps were acquired with incident beam energies of 12 and 3.15 KeV for imaging of high and low atomic weight elements (respectively) and a beam spot size of 100 microns. For low atomic weight elements element imaging, samples were enclosed within a helium atmosphere to avoid the X-Ray absorption and scattering effects of air at lower incident beam energy. Photon flux was within10^{10} and 10^{11} photons s^{-1}. Samples were mounted on a computer-controlled x-y raster stage (see Popescu et al. 2008 and Bergmann et al. 2010) which rasters the sample in front of the fixed X-Ray beam. The elemental intensities were plotted for each element as two dimensional maps using Interactive Data Language™ (ITT Visual Information Systems). The fluorescence was normalized during measurements to account for fluctuations in the intensity of the X-ray beam.

Elemental maps have been quantified using both ICP-MS and SRS-XRF point analyses. For element quantification, point data were obtained from host sediment, halo and burrow core by driving the rapid scanning stage to locations of interest defined by the previously acquired maps. A full energy dispersive spectrum was obtained for 100

Figure 4-3. (A) Shows a thin section micrograph (crossed polarizers) of primary rock components typical for the host-sediment. The feldspar-quartz ratio is approximately 2:1 (see text for discussion). (B) shows a backscatter SEM image of the host sediment. Qz = Quartz; K-Fsp = K-Feldspar; Na-Fsp = Na-Feldspar; M = Mica. (C) Thin section micrograph (plane-polarized light) of the burrow halo-host sediment boundary. Note the sharp boundary between the burrow halo and host sediment. (D) Backscatter SEM image of the burrow halo. Note the significantly increased porosity within the burrow halo and rare presence of pyrite (green arrows). The halo is predominantly composed of feldspar and quartz. (E) Shows a thin section micrograph (plane-polarized light) of the burrow core. Note the high concentration of clay-sized components and organic matter. (F) Backscatter SEM image of the burrow core. The burrow core contains predominantly grains with components smaller than 40 μm (see text for discussion) and a larger (> 50 μm in length) dense mass of organic carbon (yellow arrows).

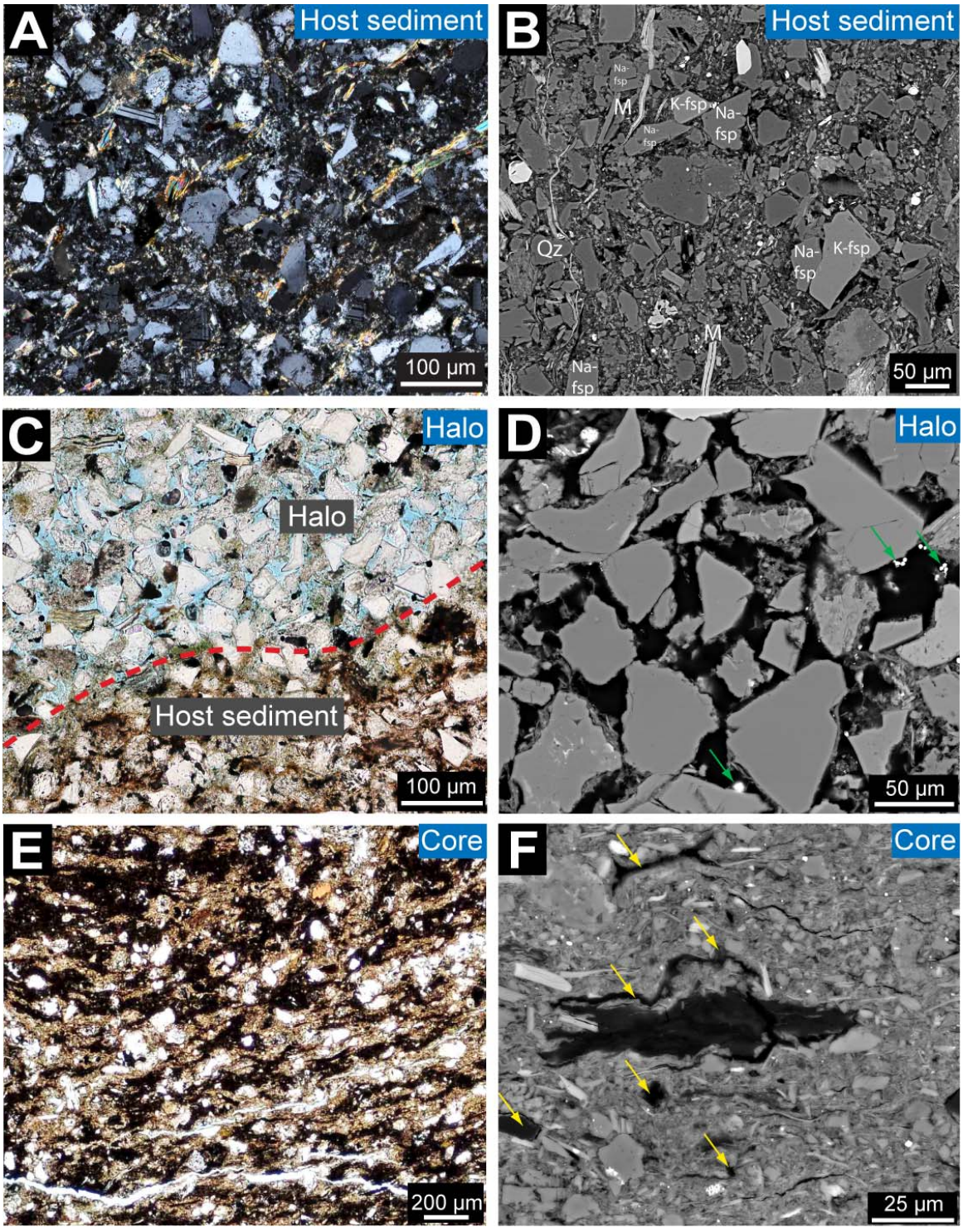
A
Host sediment
100 µm
B
Host sediment
Na-fsp
M
K-fsp
Na-fsp
Na-fsp
Qz
Na-fsp
K-fsp
M
Na-fsp
50 µm
C
Halo
Halo
Host sediment
100 µm
D
Halo
50 µm
E
Core
200 µm
F
Core
25 µm

seconds at points of interests. Due to the significant compositional heterogeneity of most geological materials errors are ~30 % for high atomic number elements and ~50 % for light elements. The measured point analyses are comparable to yields at the same pixel for Mn, Fe, Co, Cu, Zn, As and S. Elemental concentration obtained through SRS-XRF point measurements are listed in Appendix G. Given the large uncertainties associated with the spatial distribution of elements in geological materials, these latter point measurements were only treated qualitatively.

3.4 Elemental quantification

Point analyses were obtained from host sediment, halo and burrow core by driving the rapid scanning stage to locations of interest defined by the previously acquired maps. Separate counts were obtained (~200 seconds) acquiring a full energy dispersive spectrum. Elemental maps have been quantified using both ICP-MS and SRS-XRF point analyses. The quantification of individual point spectra performed post scanning using the newly collected elemental images as a guide. Due to the significant compositional heterogeneity of most geological materials errors are ~30 % for high atomic number elements and ~50 % for light elements. The measured point analyses are comparable to yields at the same pixel for Mn, Fe, Co, Cu, Zn, As and S (see supplementary information).

Figure 4-4. (A) Altered (green arrows) ferromagnesian minerals (biotite) in co-occurrence with feldspar-dominated, very fine-grained sand of the burrow halo. (B) Shows illite/chlorite-coated (green arrows) feldspar grains. (C) The halo shows high abundances of threadlike, curvilinear assemblages of silt- and clay-sized rock fragments and clay minerals (red arrows) (cf. Needham et al., 2005) coating and occupying pore space within the burrow halo. (D) Shows altered lithic grains (white arrows) within a dense clay matrix containing higher amounts of organic matter (yellow arrows). (E) shows lithic grains (possibly feldspar) within an illitic/chloritic matrix (a) which are partially replaced (red arrow) replaced by fibrous illite/smectite (b).

A
Halo
Biotite
Fsp
25 µm
B
Halo
Fsp
Fsp
L
25 µm
C
Halo
L
5 µm
D
Core
100 µm
E
Core
Fsp
a
b
a
10 µm

3.5 X-Ray Diffraction (XRD)

In order to identify the mineral phases present in different portions of the burrowed sediment, samples were obtained from the host sediment, halo and core and analysed with a Rigaku Ultima IV X-Ray diffractometer (Rigaku Systems®, Tokyo, Japan) using monochromatic Cu–Kα radiation. The X-Ray diffractometer was operated at 40 kV and 44 mA current, using a scintillation counter (1 mm divergent slit, 0.6 mm detector slit, 1.0 mm anti-scatter slit and a graphite monochromator). Samples were scanned with a step size of 0.03° and a count time of 2 s per step. All samples were analyzed in air-dried state.

3.6 Organic geochemistry (TOC and $\delta^{13}C_{org}$)

Unweathered, carbonate-free samples (5 to 10 mg) of host sediment, halo and core were analyzed for weight percentage (wt%) of Total Organic Carbon (TOC) using a Carlo Erba Elemental Analyzer. A Gas Bench II® (Thermoquest) connected to the continuous flow inlet system of a Delta V plus gas source mass spectrometer (Thermo Fisher Scientific, Waltham, MA, USA) has been used to run $\delta^{13}C_{org}$ analyses. Certified reference material (Coplen et al. 2006) was analyzed with the samples to demonstrate accuracy and precision. Samples and standards reproduced within ±0.1‰ for $\delta^{13}C_{org}$ analyses and ±0.02% for Total Organic Carbon (TOC) analyses. Carbon isotope values herein are reported relative to the Vienna Pee Dee Belemnite standard (V-PDB ‰) (Fig. 4-4).

3.7 Fourier Transform Infrared Spectroscopy

Fourier Transform Infrared Spectroscopy (FTIR) was performed on powder samples of host sediment, halo and core (Fig.4-7). Samples were ground in an agate mortar for ~1 minute. The sample material was diluted with KBr (Sigma Aldrich, FTIR-grade). The sample-KBr mixture was then pressed at 10 tons to allow KBr and sample to crystallize as an IR transparent matrix (see Blanch et al. 2007 and Poduska et al. 2011). Infrared spectra have been obtained using a Bruker® Alpha FT-IR Spectrometer (Bruker Corporation, Billerica, MA, USA). The FT-IR measurements were carried out in transmission geometry (Nicolet 380, 4 cm^{-1} resolution).

3.8 Inductively coupled Plasma-Mass Spectrometry (ICP-MS)

Approximately 0.1 g of sample were dissolved using HF and HNO_3 in a screw-top Teflon® bomb (Savillex®) to ensure complete dissolution of resistant silicate and oxide minerals. After evaporation of the HF-HNO_3 mixture, the sample was dissolved in HNO_3. After having evaporated to dryness, the sample was taken up in 2-3 ml of 8 N HNO_3, transferred to a 125-ml bottle and diluted with water to 90 g. Reagent acids were prepared in two-bottle Teflon® stills and diluted with either quartz-distilled or high-quality Millipore®-prepared water. The sample solution was sprayed into the inductively coupled argon plasma (~8000°C) of a HP 4500 plus mass-spectrometer, allowing all analyte

species to be atomized, ionized and thermally excited in order to be detected (see also Jenner et al. 1990 for detailed procedure).

4. Compositional analyses of bioturbated sandstones and mudstones from the Pelican System (Rosario Formation)

4.1 Unbioturbated host sediment

Compositional analyses determined the unbioturbated host sediment as a fine- to medium-grained feldspathic wacke (*sensu* Folk 1965) with ~50% clay-sized components of various composition (Fig. 4-3A). The framework grains are poorly-sorted and subangular to angular. Combined SEM (Fig. 4-4), XRD (Fig. 4-5) and FTIR (Fig. 4-6) analyses reveal that the framework grains are composed at equal proportions of Ca- and Na-rich plagioclase, comprising together each ~20% of the total composition. K-feldspar and quartz make up less than 20% of the total composition. The host sediment is matrix-supported and is predominantly composed of illite and iron- and magnesium-rich chlorite (Fig. 3B). Combined XRD and FTIR analyses did not detect significant amounts of kaolinite. EDX-based elemental mapping also revealed quartz and feldspar in the clay-sized fraction. The sediment does not contain any post-compaction carbonate or silica cement. Detrital zircon, titanium-bearing minerals and minor amounts of small (<10 μm), dispersed framboidal pyrite are common within the clay mineral-dominated matrix (Fig. 4-3B). Visible organic matter is rare and occurs together with clay-minerals located in pore

Figure 4-5. X-Ray diffractograms of host sediment, burrow halo and core from phycosiphoniform burrows analyzed in this study (see text for discussion). Each burrow element was analyzed in triplicates. Within this figure all three triplicate measurements are presented for the burrow core (core, core d1, core d2).

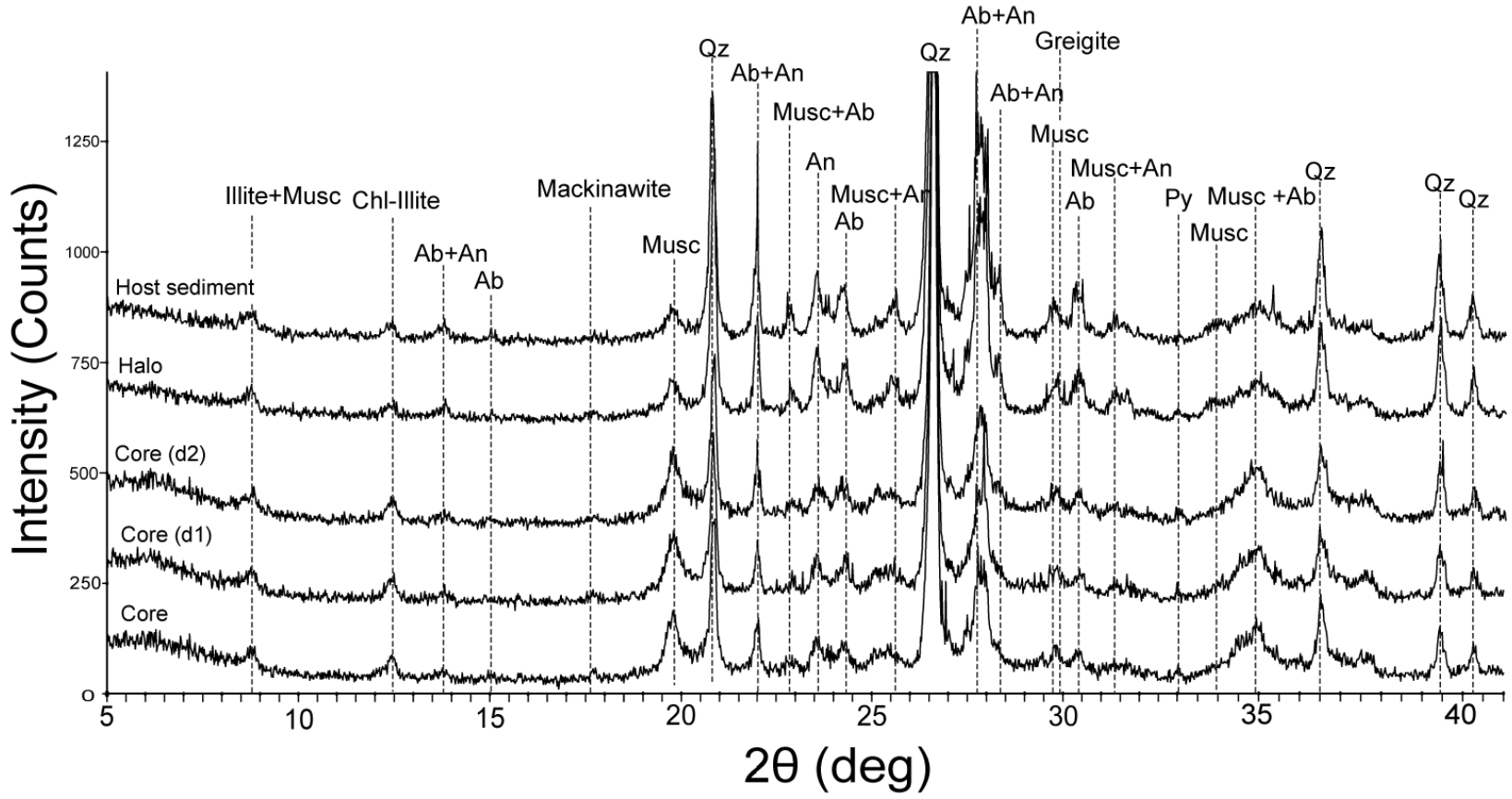
Intensity (Counts)
2θ (deg)
Host sediment
Halo
Core (d2)
Core (d1)
Core
Illite+Musc
Chl-Illite
Ab+An
Ab
Mackinawite
Musc
Qz
Ab+An
Musc+Ab
An
Musc+An
Ab
Qz
Ab+An
Ab+An
Greigite
Musc
Ab
Musc+An
Py
Musc
Musc +Ab
Qz
Qz
Qz

Figure 4-6: Shows FTIR measurements of host sediment, burrow halo and core of phycosiphoniform burrows analyzed within this study (see text for discussion).

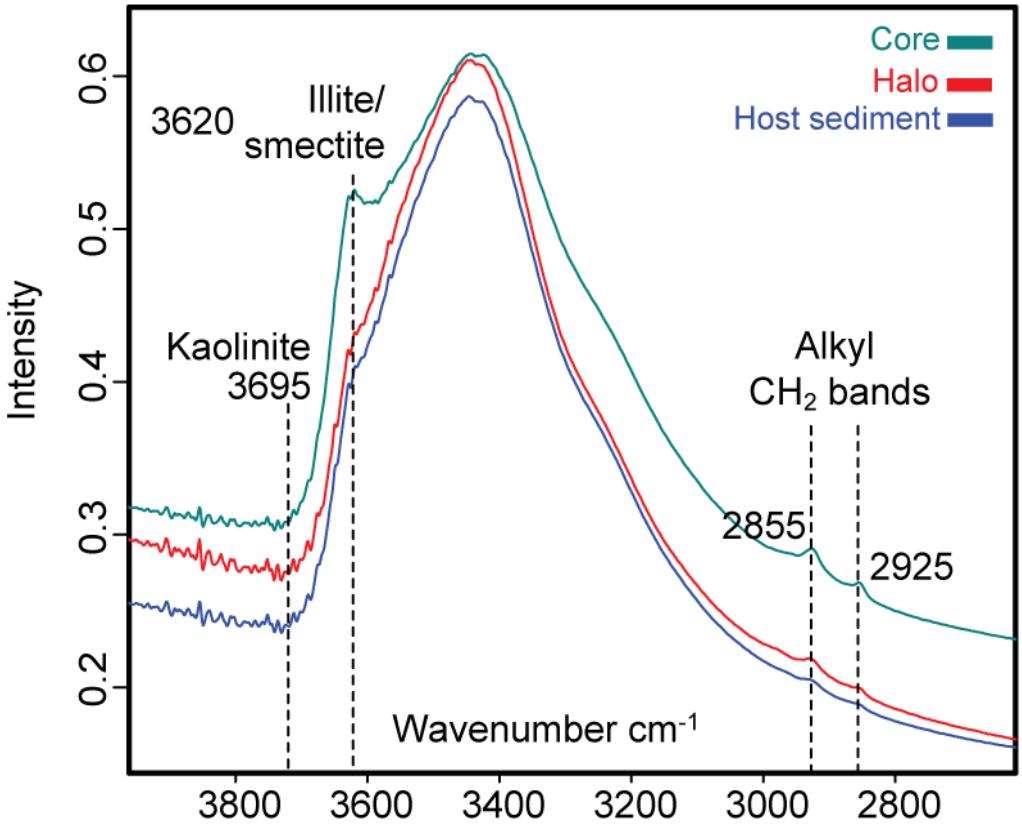
Core
Halo
Host sediment
3620
Illite/
smectite
Kaolinite
3695
Alkyl
CH2 bands
2855
2925
Intensity
0.2
0.3
0.4
0.5
0.6
Wavenumber cm-1
3800
3600
3400
3200
3000
2800

spaces between grains. The visually estimated porosity is very low (0-5%; Fig. 4-3A). The average $\delta^{13}C_{org}$ values are -24.1‰ (n = 2) and average TOC values of 0.73 wt% (n = 2) (Fig. 4-7). Combined SRS-XRF (Fig. 8) and ICP-MS quantification are presented in Fig. 4-9 and Table 4-1.

4.2 Burrow halo

The burrow halo is composed of very fine-grained and silt-sized Ca- and Na-Feldspar at approximately equal proportions (20%). K-Feldspar and quartz are both present at ~20% each. The grains are subangular to angular and moderately to well-sorted (Fig. 4-3C). The burrow halo shows no evidence for post-compaction cementation. The halo is compositionally a feldspathic arenite (*sensu* Folk, 1965) with minor amounts (<10%) of clay-sized components (Fig 3D). Combined SEM and XRD analyses reveal that the composition of the clay-sized components is illite and iron- and magnesium-rich chlorite, which are coating the majority of silt- and sand-sized framework grains, irrespective of mineralogy (Fig. 3D). Combined XRD (Fig. 4-5) and FTIR analyses (Fig. 4-6) do not reveal any significant amounts of kaolinite within the burrow halo and show a high compositional similarity. Detrital Zr and Ti-bearing minerals occur as accessory components within the fine-grained fraction of the burrow halo. Intergranular pores are filled with minor (<5%) framboidal pyrite as well as single pyrite microcrysts (Figs 4-4C and D). The burrow halo does not contain structured organic matter. The average TOC values from the halo are 0.58 wt% (n = 2) and average $\delta^{13}C_{org}$ values are -23.8‰ (n = 2) (Fig. 4-6). Combined SRS-XRF and ICP-MS analyses reveal that the burrow halo is

depleted in iron by 0.2 wt% compared to unbioturbated host sediment. The redox-sensitive trace elements are depleted by ~30 ppm compared to host sediment. Rb and Zr are depleted by ~20 ppm compared to host sediment. The concentration of Sr and Ba are ~60 ppm below host sediment values (Table 1). Visual estimates of porosity from backscatter SEM images shows visually estimated post-compaction porosities of up to 30% in the burrow halo (Figs 3D).

4.3 Burrow core

The burrow core is composed of predominantly clay-sized components, mainly illite and Fe- and Mg-rich chlorite (Figs 4-3E, F and Figs 4-4D, E). XRD data show a slight increase in peak-height and breadth in the 5 to 10° as well as a significant increase in peak intensity in the 12.4° and the 18-19° 2θ region indicates an enrichment in chlorite and possibly hydrated dioctahedral mica within the core (Fig. 4-5). A well-developed peak at 3622 cm^{-1} (Fig. 4-6) confirms the presence of illite/smectite in the core relative to host sediment. Disappearance of peaks in the core region (26.5 and 28° 2θ) mirror most likely the absence of Ca-rich feldspar in the burrow region as a combination of either in-vivo weathering (Fig. 4-4E) or grain size selective separation of clay-sized components. Combined XRD, FTIR and SEM analyses did not reveal any kaolinite within the core. No significant enrichment of pyrite and its precursor phases mackinawite and greigite has been recorded. The TOC values for the core were determined to be on average 1.8 wt% (n

Figure 4-7. TOC (wt%) and $\delta^{13}C_{org}$ values for host sediment, burrow halo and core, analyzed within this study. Samples were analyzed as duplicates. Error bars report the analytical precision. Samples were obtained from an entire hand sample. The aliquot comprised ~20 burrows.

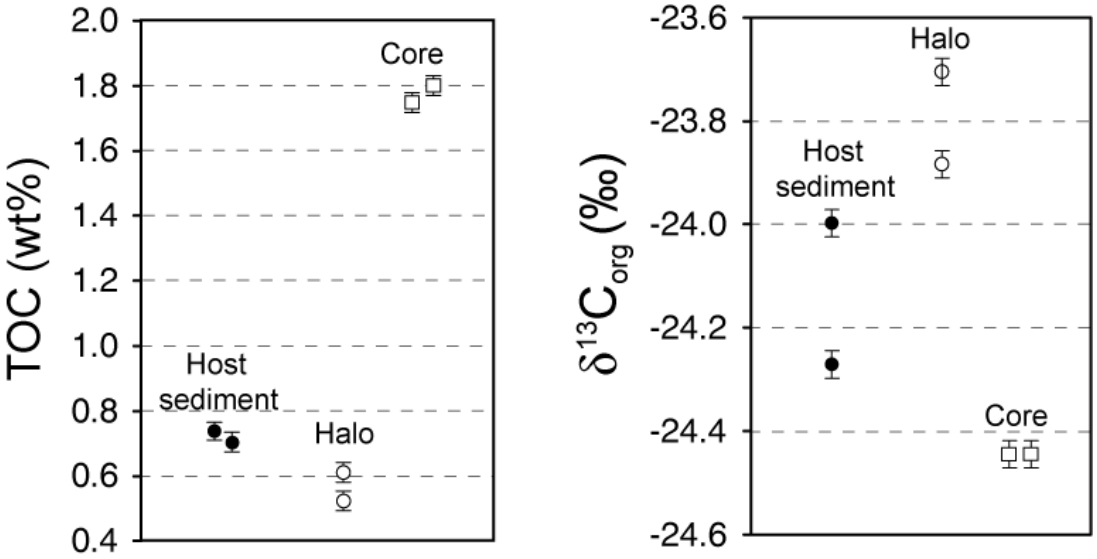
TOC (wt%)
2.0
1.8
1.6
1.4
1.2
1.0
0.8
0.6
0.4
Core
Host sediment
Halo
$\delta^{13}C_{org}$ (‰)
-23.6
-23.8
-24.0
-24.2
-24.4
-24.6
Halo
Host sediment
Core

= 2) and average $\delta^{13}C_{org}$ values were found to be -24.4‰ (n = 2) (Table 4-1). Combined SRS-XRF and ICP-MS analyses indicate a significant enrichment in Fe by ~15,300 ppm, Ca by ~10,000 ppm and Ti by ~1800 ppm compared to values measured for unbioturbated host sediment (Table 4-1). The measured suite of the redox-sensitive elements shows significant enrichment (Fig. 4-8) between 10 to 100 ppm whereas the high atomic number elements Sr and Ba are depleted by ~50 ppm compared to values measured for host sediment and burrow halo (Fig. 4-9). SRS-XRF measurements also indicate higher amounts of sulfur in the burrow core (Fig. 4-8). Backscatter SEM analysis reveals that the clay-dominated burrow core has higher concentrations of organic matter including larger, wavy to elongated aggregates of concentrated organic matter, ranging 10 to 300 μm in length (Figs 4-3F and 4-4D). EDX analyses indicate that at least some of these larger aggregates have higher amounts of sulfur (Fig 4-10F).

5. Discussion

5.1 Modification of primary texture and mineralogy by the trace maker

The preferential removal of silt- and clay-sized components <40 μm from the host sediment and concentration within the burrow core has two implications for sediment texture. First, it produces burrow halo with a higher porosity (Bednarz and McIlroy, 2012) that exhibits significantly higher permeability. Second, previous research has

Figure 4-8. SRS-XRF elemental scans resolving details of elemental distributions with respect to biogenic structures. (A) shows optical photograph of a prominent sample containing large (>5 mm) phycosiphoniform traces as well as *Paleophycus* isp. containing well-preserved phycosiphoniform traces. SRS-XRF map of (B) iron, (C) copper, D), manganese (E), calcium and (F) sulfur (G). (B) to (F) Data collected at beam line 6-2 at SSRL; beam energy/size/flux/detector distance = 12 keV/100 microns/ 10^{11} photons s^{-1}/ ~120 mm. (G) Data collected at beam line 6-2 at SSRL; beam energy/size/flux/detector distance = 3keV/100 micron/10^{9} photons s^{-1}/ ~10 mm. Active area ~800 mm^2.

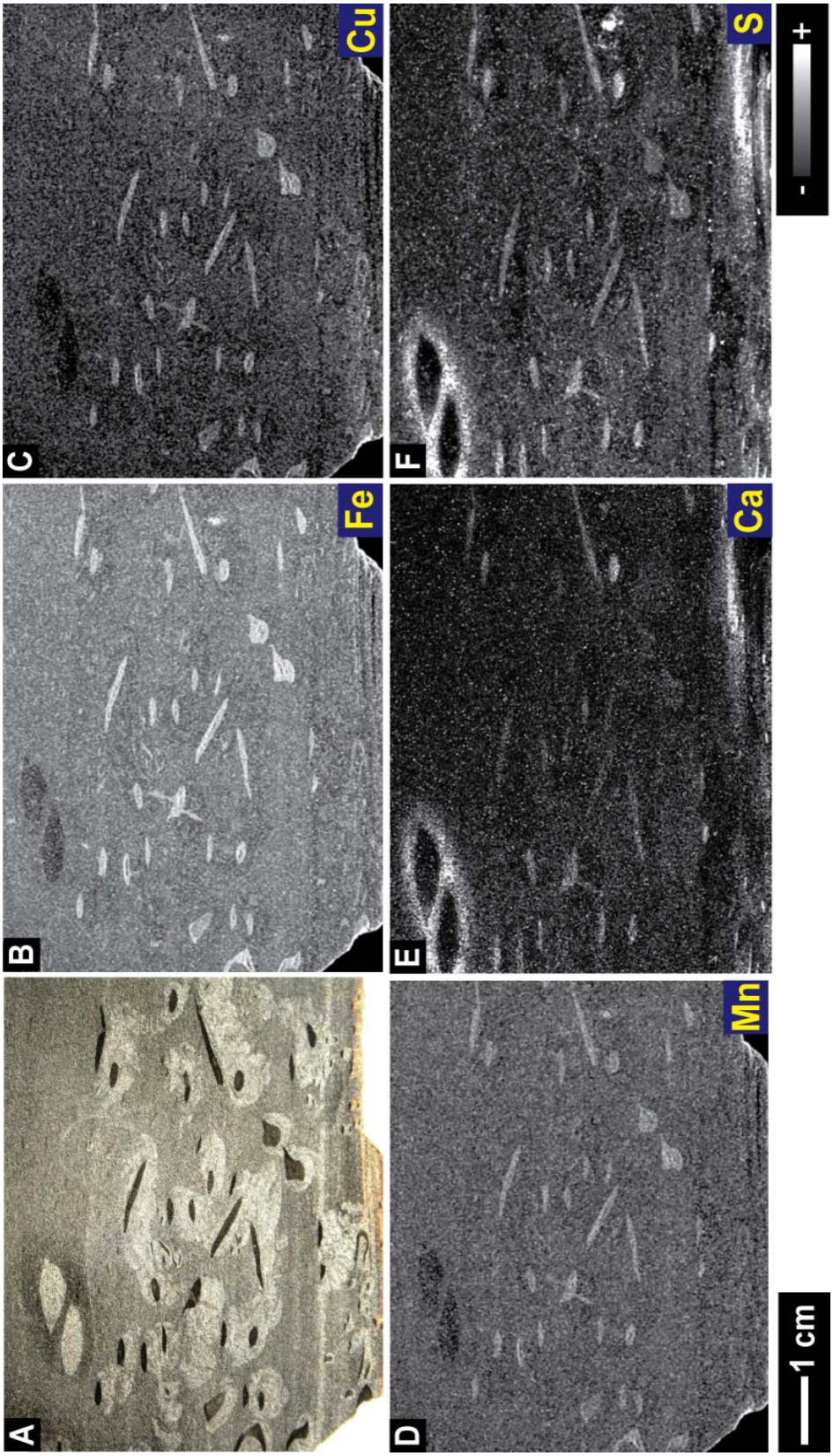
A
B
Fe
C
Cu
D
Mn
E
Ca
F
S
+
-
1 cm

Figure 4-9. (A) Whole-rock ICP-MS data collected from host sediment (sample A and B), showing the absolute concentration of Ca, Ti and Fe. (B) is showing the concentration of Ca, Ti and Fe as difference between host sediment and burrow halo and core. (C) This figure shows the absolute concentration of redox-sensitive elements measured within this study. (D) This figure shows the concentration of the same elements as in (C) for the burrow halo and core, plotted as difference between host sediment. Concentrations are given as ppm values. Error is presented as 1σ. Open and closed circles represent two analyses of the unbioturbated host sediment (Sample 1 and 2, see Appendix D for sample locations).

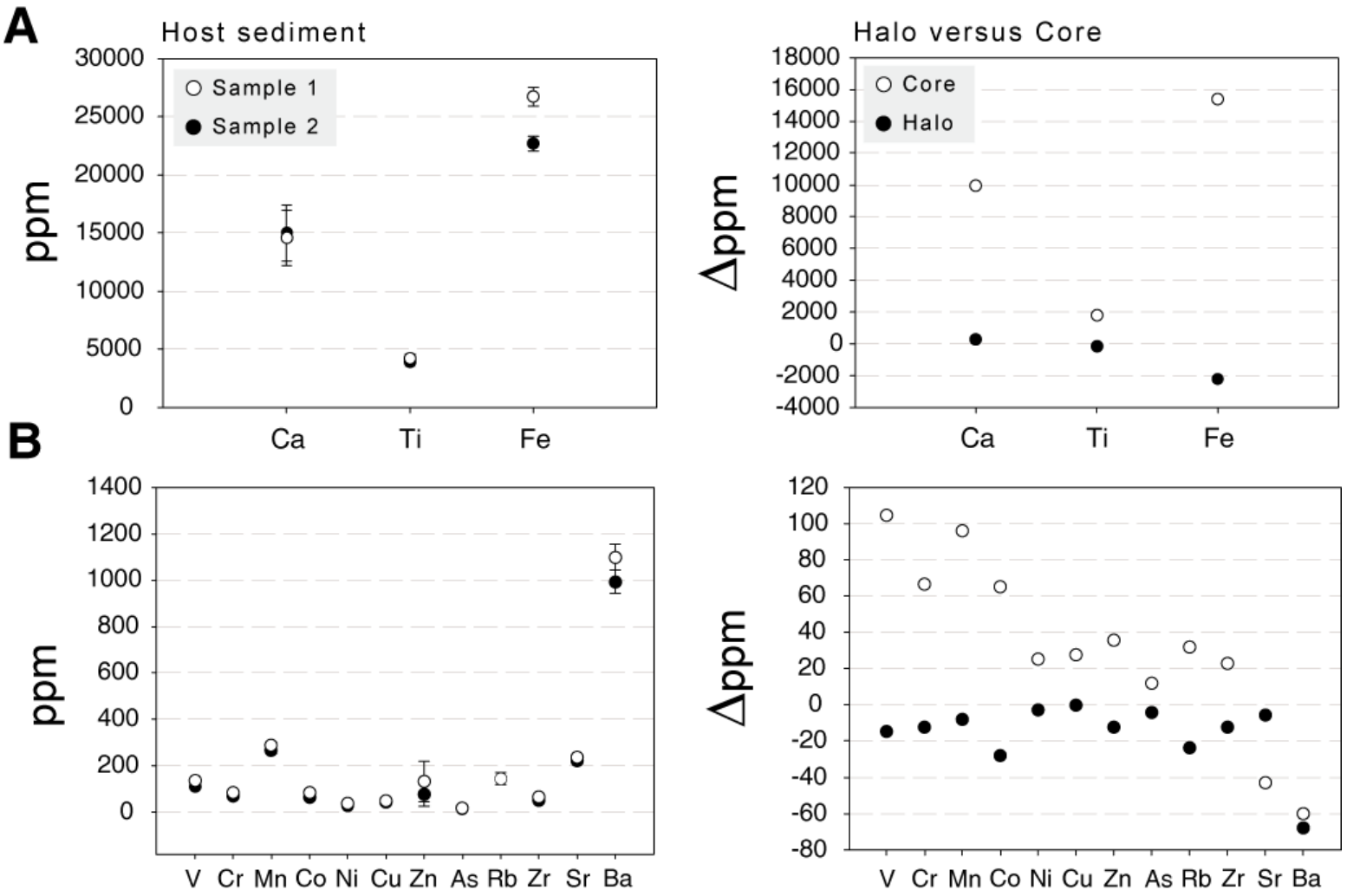
A
Host sediment
ppm
30000
25000
20000
15000
10000
5000
0
Sample 1
Sample 2
Ca
Ti
Fe
Halo versus Core
Δppm
18000
16000
14000
12000
10000
8000
6000
4000
2000
0
-2000
-4000
Core
Halo
Ca
Ti
Fe
B
ppm
1400
1200
1000
800
600
400
200
0
V Cr Mn Co Ni Cu Zn As Rb Zr Sr Ba
Δppm
120
100
80
60
40
20
0
-20
-40
-60
-80
V Cr Mn Co Ni Cu Zn As Rb Zr Sr Ba

Table 4-1: ICP-MS and SRS-XRF point quantification for analyzed host sediment (Host sediment 1-open circle and 2-closed circle), halo and burrow core. All elements were quantified via SRS-XRF point analyses (see Appendix) and ICP-MS (except sulfur). Analyses for sulfur were obtained from the halo of *Paleophycus* isp. via SRS-XRF point analyses (*). For details see Appendix.

Element	Host sediment 1	1σ	Host sediment 2	1σ	Halo	1σ	Core	1σ	*Paleophycus* isp. Halo	1σ*
Ca	14593	(2342)	15001	(2408)	15089	(2422)	24746	(3972)		
Ti	4230	(370)	3886	(340)	3897	(341)	5863	(513)		
Fe	26736	(780)	22691	(662)	22529	(657)	40077	(1169)		
V	135	(12)	111	(10)	108	(10)	227	(21)		
Cr	82	(2)	68	(2)	63	(2)	142	(4)		
Mn	286	(15)	266	(14)	268	(14)	372	(20)		
Co	82	(3)	62	(2)	44	(2)	137	(5)		
Ni	37	(3)	26	(2)	28	(2)	57	(5)		
Cu	48	(11)	42	(9)	45	(10)	72	(16)		
Zn	131	(87)	75	(50)	90	(60)	139	(92)		
As	16	(<1)	12	(<1)	10	(<1)	26	(1)		
Rb	144	(13)	144	(13)	120	(11)	175	16		
Zr	66	(4)	49	(3)	45	(3)	80	(5)		
Sr	235	(4)	222	(3)	223	(3)	185	(3)		
Ba	1098	(27)	992	(25)	977	(24)	985	(25)		
S					35*	(6)*			977*	(162)*

demonstrated that the feeding activity of macrobiota such as worms is capable of degrading unstable ferromagnesian minerals, such as chlorite and muscovite (McIlroy et al. 2003). This process results in the formation of grain coating iron- and magnesium-rich minerals such as berthierine, which upon burial can be replaced by chlorite and inhibit the cementation of quartz grains up to anomalously high burial depths (Aagaard et al. 2000; Gould et al. 2009; Karim et al. 2010). The presence of abundant illite- and chlorite-coated grains (Figs 4-3D and 4-7C) in close associations with polymineralic, threadlike curvilinear structures might modify porosity-permeability relationships upon deeper burial (cf. Needham et al. 2005). The organo-clay dominated core (Figs 4-3 and 4-4) highlights the contribution of biological in-vivo weathering and authigenic formation of illite/smectite (Fig. 4-4E). Integration of the XRD and FTIR data from the host sediment versus core lends support to infer that at least some of the authigenesis is attributed to the feeding activity of the phycosiphoniform trace maker. This observed in-situ replacement of feldspar and unstable lithic clasts by probably mixed-layer illite/smectite in the burrow core is very common and highlights the production of new clay minerals in close association with phycosiphoniform ichnofabric. Given that lattice expansion experiments were not performed in this study due to small available sample amounts, it currently remains difficult to estimate the overall contribution of neo-formed 'bio-clays' to overall clay-mineral production. Biogenic alteration of primary rock components is virtually absent in the burrow halo and the unbioturbated host sediment. It appears that although the majority of clay-grade material in the burrow core has been mechanically enriched by grain-selective deposit feeding, there is most likely also a to date unknown contribution to clay mineral content that can be attributed to the role of infaunal deposit feeding

organisms (Fig. 4-4E). At present it remains unknown whether this biological contribution results from in-situ weathering within the animal's gut or from post-defecation weathering in the burrow core microenvironment. Regardless of timing of formation this research demonstrates the universal relationship between animal feeding activity and clay mineral production and extends the concept of biogenic weathering (McIlroy et al. 2003) to fine-grained siliciclastic rocks containing phycosiphoniform burrows.

5.2 Organic carbon in bioturbated mudstones

Phycosiphoniform trace makers are among the first endobenthic colonizers of turbidite beds of inner levee/terrace settings in the Rosario Formation (Callow et al. 2013). Given that the phycosiphoniform trace maker is found to have only ingested selectively particles smaller than 40 μm (Fig. 4-3D), it is considered that organic particles bound to the clay- and silt-sized fraction were the food sought by the trace maker (Fig. 4-3E).

There is typically a close relationship between grain size of siliciclastic material and organic matter content in depositional settings dominated by upwelling and seasonally high water column productivity (e.g., Deuser et al. 1983). In such environments the organic carbon content of settling particles and their size are inversely correlated to each other (Oliveira et al. 2007; Kennedy and Wagner 2011). Organic matter adsorbed onto clay-sized siliciclastic particles and clay minerals, increases the burial efficiency of organic carbon (Hedges and Keil 1995; Wetzel 2010; Kennedy et al. 2002; Blair and Aller 2012).

In experimental food web studies biogeochemists have demonstrated that a relationship exists between $\delta^{13}C_{org}$ composition of ingested food, animal body and residual feces (DeNiro and Epstein 1979). It is predicted that kinetic fractionation operating during remineralization of ingested organic matter, ^{12}C preferably bound to CO_2, resulting in relative enrichment of ^{13}C in the residual organic carbon (Hayes et al. 1993). In some copepods (Checkley and Entzeroth 1985) and small terrestrial animals such as milkweed bugs (DeNiro and Epstein 1979) the predicted metabolic effect has been proven to yield residual fecal matter with significantly heavier $\delta^{13}C_{org}$ values of +1 to +2‰. However, the opposite is just as common and indicates kinetic fractionation by a variety of fractionation processes along the metabolic path. Food web experiments with copepods (Breteler et al. 2002), shrimp (Landrum and Montoya 2009) as well as amphipods (Macko et al. 1982) demonstrated that fecal organic matter is persistently lighter by -0.5 to -2‰ compared to the ingested food (phototrophic algae). Utilizing compound-specific isotope analyses (Breteler et al. 2002) it has been recognized that the selective digestion of compounds with different $\delta^{13}C_{org}$ values can in certain situations yield lighter residual organic matter with compositions that deviate from values expected from kinetic isotope fractionation effects alone (cf. Hayes 1993).

The use of stable isotope ratios is a powerful tracer to establish trophic level and track changes in organic matter composition in complex food webs, but it also requires detailed knowledge of all underlying conditions (i.e., length of digestion) (Harris 1993; McCutchan et al. 2003). Within this study only isotopic fractionation between bioturbated and unbioturbated portions of the same bed have been considered. A fractionation of -0.3‰ between host sediment and core might indicate a relative loss of CO_2-bound ^{12}C

from host sediment organic matter during digestive processes. Alternatively, a physical separation of two distinct organic carbon sources (background marine organic carbon versus mineral surface-bound microbial films) is supported by the fact that the value of isotopic depletion in the core (~ -0.3‰) mirrors the amount of enrichment within the halo (~ +0.3‰) (Fig. 4-7). To date it is not known if this fractionation between host sediment, halo and core might be amplified or reduced in beds with higher bioturbation intensity and/or trace fossil diversity. Three-dimensional reconstructions of phycosiphoniform burrows from the same locality demonstrate that fecal material is not reingested or cross-cut by other phycosiphoniform trace makers (cf. Bednarz and McIlroy 2012). The most likely reason for avoidance of already bioturbated, carbon-rich sediment is that the bioavailable portion of the mineral-hosted organic matter has previously been utilized (Deming and Baross 1993) and therefore rendered unattractive to bioturbators. The absence of significant amounts of pyrite within the burrow core and specifically at the halo-core boundary (cf. Stockdale et al. 2010), provides additional evidence that the reactivity of this residual, core-hosted organic carbon most likely was too low to fuel the formation of pyrite during early diagenesis (cf. Jørgensen 1977; Widerlund and Davison 2007).

5.3 The spatial organization of trace elements in bioturbated mudstones

The formation of pyrite (and its precursor minerals mackinawite and greigite) marks the final stage of iron cycling in surficial sediment (Berner 1984; Schoonen 2004). A higher abundance of pyrite in the burrow core correlates with a relative enrichment of Co, Ni, Cu

and Zn. These latter elements are known to be preferably incorporated into the pyrite lattice by the common process of trace metal pyritization (Tribovillard et al. 2006). It remains however unclear how much pyrite has been formed within the core and how much pyrite has been added from the host sediment by mechanical grain size separation. Given the low reactivity of the residual organic carbon in the burrow core (Fig. 4-6B); trace metal pyritization is unlikely to have been the dominant pathway of trace metal enrichment within the burrow core. High concentrations of Fe in the burrow core (Fig. 4-8B) are mainly associated with the presence of chlorite and some smectite. Since ferrous Fe-bearing silicate minerals are known to be least reactive with H_2S (Canfield 1989a; Canfield et al. 1992), they are regarded unlikely to constitute an important source of Fe for the neo-formation of pyrite in the burrow core. Elements like V and Cr could alternatively be located in V- and Cr-rich phyllosilicates, possibly as roscoelite (Brigatti et al. 2003) and fuchsite (Reddy et al. 2003). Preferable enrichment of mica and illite in the burrow core is indicated by the XRD and SEM data (Fig 4-5). This process is also used to explain the relative enrichment of elements Zr and Rb, which have no known biological importance. These latter elements show an enrichment within the burrow core that roughly matches the amount (in ppm) of depletion of those same elements in the burrow halo (Fig. 4-9). This relationship is taken to indicate simple physical redistribution of Zr and Rb in association with a mineral phase during grain-size selective deposit feeding.

The measured distribution of Sr and Ba reveals a significant negative mass balance of 60 to 80 ppm for both burrow core and halo relative to the host sediment (Figs 4-8B and D) that cannot be explained by simple spatial re-distribution or neo-formation of new

Figure 4-10: Combined Backscatter SEM images and EDX elemental maps of iron and sulfur within host sediment, burrow halo and core. The color yellow is a false color overlay of sulfur (red), and iron (green). (A) Shows the transition between host sediment and burrow halo. (B) shows the sulfur and iron distribution for the same region. (C) Backscatter SEM image of the transition between burrow halo and core. (D) The same region as EDX elemental map. (E) Magnified backscatter SEM image of structured organic carbon (F) EDX elemental map of the same small region showing that sulfur does not only occur as pyrite, but seems to be incorporated within kerogen to some degree (see text for discussion).

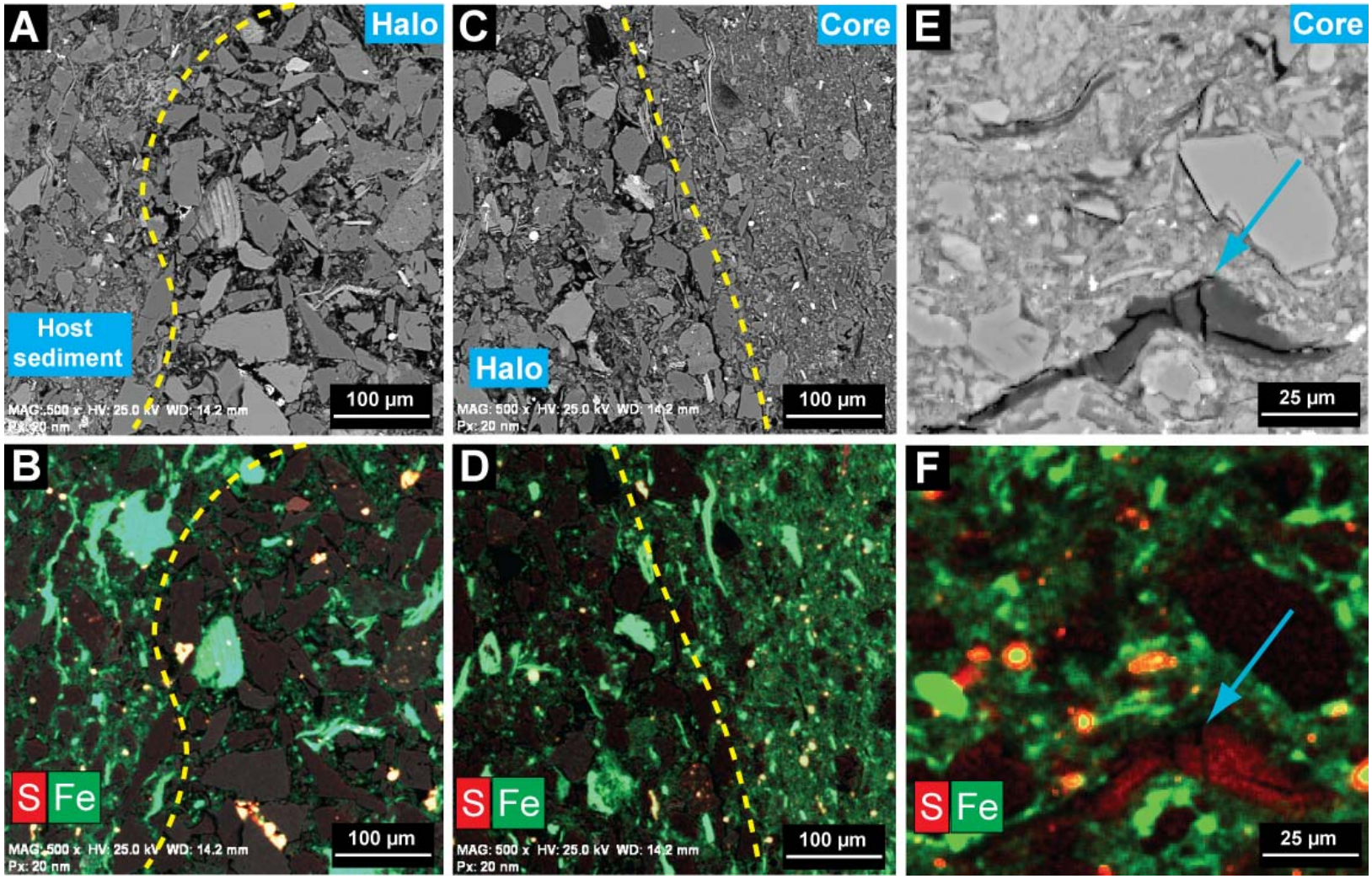
A
Halo
Host sediment
MAG: 500 x HV: 25.0 kV WD: 14.2 mm
Px: 20 nm
100 µm
C
Core
Halo
MAG: 500 x HV: 25.0 kV WD: 14.2 mm
Px: 20 nm
100 µm
E
Core
25 µm
B
S Fe
MAG: 500 x HV: 25.0 kV WD: 14.2 mm
Px: 20 nm
100 µm
D
S Fe
MAG: 500 x HV: 25.0 kV WD: 14.2 mm
Px: 20 nm
100 µm
F
S Fe
25 µm

minerals. In paleoceanographic studies Ba is used as an important paleoproductivity proxy (Martin et al. 2010). Ba is important in the metabolism of planktonic algae and its abundance is linked to the flux of Ba-hosted particulate organic matter to the sea floor in association with algal bloom events (Lea and Boyle 1989; Dymond and Collier 1996). The relative depletion of Ba and Sr within the burrow halo and core might be explained by the fact that the vermiform trace maker potentially utilizes these latter elements as essential micronutrients for secondary metabolic processes (e.g. biomineralization; Lowenstam 1981). Alternatively, feldspar grains are the only plausible inorganic storage site for Sr and Ba (Drake and Weill 1975). Given the high amount of altered lithic fragments to chlorite and smectite within the burrow core, Sr and Ba might have been released to pore waters during alteration (weathering) within the burrow core. Such a scenario is supported by decreasing peak intensities and poor peak definitions of characteristic plagioclase peaks within the 20° to 30° 2θ region (Fig. 5).

Spatial elemental mapping at a range of scales (Figs 8 and 11) indicates an abundance of sulfur within large organic matter aggregates that do not contain any pyrite (Figs 3E and F). In such organic material, sulfur might be preserved as organically-bound sulfur (Sinninghe Damste and De Leeuw 1990; Sinninghe et al. 1998).

The relationship between bioturbation and diagenetic processes, as proposed in this study of course only provides a glimpse into the potential impact of animal-sediment interactions on diagenetic pathways in mudstones. In order to build sound geological models future work should include high-resolution analysis of the organic fraction at a molecular level with respect to different trace fossils not just phycosiphoniform traces. Subsequently such data could be integrated into models to understand the effect of a

variety of traces in different sedimentary facies and could be related to relative abundances as well. Subsequently such data need to be upscaled onto the bedset and the formation scale. With increasing experience, researchers will gain further insight into how animal behavior not only translates into a measurable compositional modification, but also how this impacts, for example, the elastic and petrophysical properties of fine-grained sedimentary rocks (e.g., Dewhurst et al. 2008). An integrated sedimentological and geochemical approach will create a more complete understanding on how bioturbation controls the lithofacies variability of mudstones - the rock type that makes up >65% of all rocks exposed on the surface of the modern earth (Aplin 2000).

6. Conclusions

A. Geochemical analysis revealed that producers of phycosiphoniform burrows influence the sorting rock of components irrespective of mineralogy or shape. Particles smaller than ~40 μm are partitioned from the sediment matrix and mechanically concentrated within the burrow core. The mineralogical composition of the burrow core varies from host sediment and burrow halo, and is proposed to be a combination of weathering of primary rock components through gut and authigenic weathering in the burrow microenvironment.

B. Carbon isotope and elemental analyses reveal that the burrow core is significantly enriched in organic carbon by ~1.1 wt% TOC above background values from the host sediment, which only contains ~0.6 wt% TOC. Changes in $\delta^{13}C_{org}$ values of ~0.6‰

between the burrow core and host sediment might indicate some modification of the core-hosted organic matter. The absence of cross-cutting by other individuals indicates that the organic carbon is of low reactivity and unattractive to other individuals or the same individual producing phycosiphoniform trace fossils.

C. The significant enrichment of Ca, Ti, and redox-sensitive transition metals found in the burrow core compared to the halo and the host sediment suggest that the main storage site of these elements are Fe-bearing silicates, pyrite and possibly organic matter. To date it is not clear if the core-hosted pyrite represents neo-formed pyrite or simply relative mechanical concentration. Given the largely unreactive nature of residual, core-hosted organic matter the latter scenario is regarded as more realistic.

D. Sr and Ba are depleted within both the burrow halo and core with respect to host sediment. This net deficiency might be explained by two processes: Sr and Ba are incorporated into the vagile endobenthic organism itself and are used by the trace marking organism in biomineralization. Alternatively, the selective removal of these elements from the burrow core is might result from accelerated in-vivo weathering of unstable feldspar and release of Sr and Ba to pore waters.

7. Acknowledgements

DH acknowledges additional financial support through AAPG, IAS, SEPM and GSA. DMc acknowledges the support through an NSERC Discovery grant and the Canada Research Chair Program. All authors thank the scientists and support engineers at

SSRL for their advice and support during measurements on Beamline 6-2. Kris Poduska is thanked for her support and advice with FTIR measurements.

8. References

AAGAARD, P., JAHREN, J.S., HARSTAD, A.O., NILSEN, O. AND RAMM, M. 2000, Formation of grain-coating chlorite in sandstones. Laboratory synthesized vs. natural occurrences: Clay Minerals, v. 35, p. 261-269.

ALLER, R.C., 1982. The effects of macrobenthos on chemical properties of marine sediment and overlying water. In: McCall, P.L., Tevesz, M.J.S., eds., Animal–Sediment Relations. Plenum, New York, p.53–102.

ALLER, R.C., AND RUDE, P.D., 1988, Complete oxidation of solid phase sulfides by manganese and bacteria in anoxic sediments: Geochimica et Cosmochimica Acta, v. 52, p. 751–765, doi: 10.1016/0016-7037(88)90335-3.

ALLER, R.C., 1994, Bioturbation and remineralization of sedimentary organic matter: effects of redox oscillation: Chemical Geology, vol. 114, p. 331-345.

ALLER, R.C., MADRID, V., CHISTOSERDOV, A., ALLER, J.Y. AND HEILBRUN, C. 2010, Unsteady diagenetic processes and sulfur biogeochemistry in tropical deltaic muds: Implications for oceanic isotope cycles and the sedimentary record: Geochimica et Cosmochimica Acta, v. 74, p. 4671-4692.

APLIN, A. C., 2000, Mineralogy of modern marine sediments: a geochemical framework, *in* Vaughan D. J., and Wogelius, R. A., eds., Environmental Mineralogy: Eotovos University Press, Budapest, v. 2, p. 125-172.

ARTHUR, M.A. AND SAGEMAN, B.B., 1994, Marine black shales: depositional mechanisms and environments of ancient deposits: Annual Review of Earth & Planetary Sciences, v. 22, p. 499-551.

BERNER, R.A., 1964, Distribution and diagenesis of sulfur in some sediments from the Gulf of California: Marine Geology, v. 1, p. 117-140.

BERNER, R.A., 1980, Early diagenesis: A theoretical approach: Princeton University Press, Princeton, N.J., p. 256.

BERNER, R.A., 1984, Sedimentary pyrite formation: An update: Geochimica et Cosmochimica Acta, v. 48, p. 605–615, doi: 10.1016/0016-7037(84)90089-9.

BEDNARZ, M., AND MCILROY, 2009, Three-dimensional reconstruction of "phycosiphoniform" burrows: Implications for identification of trace fossils in core: Paleontologia Electronica v. 12, p. 3

BEDNARZ, M. AND MCILROY, D. 2012, Effect of phycosiphoniform burrows on shale hydrocarbon reservoir quality: AAPG Bulletin, v. 96, p. 1957-1980.

BERGMANN, U., MORTON, R.W., MANNING, P.L., SELLERS, W.I., FARRAR, S., HUNTLEY, K.G., WOGELIUS, R.A. AND LARSON, P. 2010, Archaeopteryx feathers and bone chemistry fully revealed via synchrotron imaging: Proceedings of the National Academy of Sciences of the United States of America, v. 107, p. 9060-9065.

BLAIR, N.E. AND ALLER, R.C. 2012, The fate of terrestrial organic carbon in the Marine environment: Annual Review of Marine Science, v. 4, p. 401-423.

BLANCH, A.J., QUINTON, J.S., LENEHAN, C.E. AND PRING, A. 2007, Autocorrelation infrared analysis of mineralogical samples: The influence of user controllable experimental parameters, Analytica Chimica Acta, v. 590, p. 145-150.

BRETELER, W.C.M., GRICE, K., SCHOUTEN, S., KLOOSTERHUIS, H.T. AND SINNINGHE DAMSTÉ, J.S., 2002, Stable carbon isotope fractionation in the marine copepod Temora longicornis: Unexpectedly low δ13C value of faecal pellets: Marine Ecology Progress Series, v. 240, p. 195-204.

BRIGATTI, M. F., CAPRILLI, E., MARCHESINI, M., AND POPPI, L., 2003, The crystal structure of roscoelite-1M: Clays and clay minerals, v.51, p. 301-308.

CANFIELD, D. E., 1989, Reactive iron in marine sediments: Geochimica et Cosmochimica Acta, v. 53, p. 619-632.

CANFIELD, D. E., RAISWELL, R., AND BOTTRELL, S., 1992, The reactivity of sedimentary iron minerals toward sulfide: American Journal of Science, v. 292, p. 659-659.

CANFIELD, D.E. 2004, The evolution of the Earth surface sulfur reservoir: American Journal of Science, v. 304, p. 839-861.

CALLOW, R.H.T., MCILROY, D., KNELLER, B. AND DYKSTRA, M. 2012a, Integrated ichnological and sedimentological analysis of a Late Cretaceous submarine channel-levee system: The Rosario Formation, Baja California, Mexico: Marine and Petroleum Geology, v. 41, p. 277-294.

CALLOW, R.H.T., MCILROY, D., KNELLER, B. AND DYKSTRA, M., 2013b, Ichnology of Late Cretaceous Turbidites from the Rosario Formation, Baja California, Mexico. Ichnos: an International Journal of Plant and Animal, v. 20, p. 1-14.

CAO, Z., 2010, A fluorosensor for two-dimensional measurements of extracellular enzyme activity in marine sediments: Marine Chemistry., doi: 10.1016/j.marchem. 2010.09.002

CHECKLEY, D.M. AND ENTZEROTH, L.C., 1985, Elemental and isotopic fractionation of carbon and nitrogen by marine, planktonic copepods and implications to the marine nitrogen cycle: Journal of Plankton Research, v. 7, p. 553-568.

COPLEN, T.B., BRAND, W.A., GEHRE, M., GRÖNING, M., MEIJER, H.A.J., TOMAN, B. AND VERKOUTEREN, R.M. 2006, New guidelines for $\delta^{13}C$ measurements: Analytical Chemistry, v. 78, p. 2439-2441.

DRAKE, M. J., AND WEILL, D. F., 1975, Partition of Sr, Ba, Ca, Y, Eu^{2+}, Eu^{3+}, and other REE between plagioclase feldspar and magmatic liquid: an experimental study: Geochimica et Cosmochimica Acta, v. 39, p. 689-712.

DYMOND, J. AND COLLIER, R. 1996, Particulate barium fluxes and their relationships to biological productivity: Deep-Sea Research Part II: Topical Studies in Oceanography, v. 43, p. 1281-1308.

DEMAISON, G.J. AND MOORE, G.T., 1980, Anoxic environments and oil source bed genesis: American Association of Petroleum Geologists Bulletin, v. 64, p. 1179-1209.

DEMING, J. W., AND BAROSS, J. A., 1993, The early diagenesis of organic matter: bacterial activity: Organic geochemistry, v. 6, 119-144.

DENIRO, M.J. AND EPSTEIN, S. 1978, Influence of diet on the distribution of carbon isotopes in animals: Geochimica et Cosmochimica Acta, v. 42, p. 495-506.

DEWHURST, D. N., SIGGINS, A. F., KUILA, U. N., CLENNELL, M. B., RAVEN, M. D., AND NORDGA RD-BOLAS, H. M., 2008, Elastic, geomechanical and petrophysical properties of shales. In: The 42nd US Rock Mechanics Symposium *(USRMS)*.

DEUSER,W.G., BREWER, P.G., JICKELLS, T.D. AND COMMEAU, R.F., 1983, Biological control of the removal of abiogenic particles from the surface ocean: Science, v. 219, p. 388–391.

DYKSTRA, M. AND KNELLER, B., 2009, Lateral accretion in a deep-marine channel complex: Implications for channelized flow processes in turbidity currents: Sedimentology, v. 56, p. 1411-1432.

EDWARDS, N.P., WOGELIUS, R.A., BERGMANN, U., LARSON, P., SELLERS, W.I. AND MANNING, P.L., 2012, Mapping prehistoric ghosts in the synchrotron, Applied Physics A: Materials Science and Processing, p. 1-9.

EKDALE, A. A., AND D. W. LEWIS, 1991, Trace fossils and paleoenvironmental control of ichnofacies in a late quaternary gravel and loess fan-delta complex, New Zealand: Paleogeography, Paleoclimatology, Paleoecology, v. 81, p. 253–279, doi:10.1016/0031-0182(91)90150-P.

FOLK, R.L., 1965, The role of texture and composition in sandstone classification: Journal of Sedimentary Petrology **26**, 166–171.

FROELICH, P.N., KLINKHAMMER, G.P., BENDER, M.L., LUEDTKE, N.A., HEATH, G.R., CULLEN, D., DAUPHIN, P., HAMMOND, D., HARTMAN, B. AND MAYNARD, V., 1979, Early oxidation of organic matter in pelagic sediments of the eastern equatorial Atlantic: suboxic diagenesis: Geochimica et Cosmochimica Acta, v. 43, p. 1075-1090.

GOULD, K., PE-PIPER, G. AND PIPER, D.J.W., 2010, Relationship of diagenetic chlorite rims to depositional facies in Lower Cretaceous reservoir sandstones of the Scotian Basin: Sedimentology, v. 57, p. 587-610.

GOLDRING, R., J. E. POLLARD, AND A. M. TAYLOR, 1991, *Anconichnus horizontalis*: A pervasive ichnofabric-forming trace fossil in post-Paleozoic offshore siliciclastic facies: Palaios v. 6, p. 250–263, doi:10.2307/3514905.

HARRIS, J.M., 1993, The presence, nature, and role of gut microflora in aquatic invertebrates: A synthesis: Microbial ecology, vol. 25, p. 195-231.

HAYES, J.M.,1993, Factors controlling ^{13}C contents of sedimentary organic compounds: Principles and evidence: Marine Geology, v. 113, p. 111-125.

HEDGES, J.I. AND KEIL, R.G., 1995, Sedimentary organic matter preservation: an assessment and speculative synthesis: Marine Chemistry, v. 49, p. 81-115.

HERRINGSHAW, L. G. AND MCILROY, D. 2013. Bioinfiltration: irrigation-driven transport of clay particles through bioturbated sediments. Journal of Sedimentary Research (in press).

JARVIS, I., LIGNUM, J.S., GRCKE, D.R., JENKYNS, H.C. AND PEARCE, M.A. 2011, Black shale deposition, atmospheric CO 2 drawdown, and cooling during the Cenomanian-Turonian Oceanic Anoxic Event: Paleoceanography, v. 26, no. 3.

JENNER, G.A., LONGERICH, H.P., JACKSON, S.E. AND FRYER, B.J. 1990, ICP-MS - A powerful tool for high-precision trace-element analysis in Earth sciences: Evidence from analysis of selected U.S.G.S. reference samples: Chemical Geology, v. 83, p. 133-148.

JENKYNS, H.C., 2010, Geochemistry of oceanic anoxic events: Geochemistry, Geophysics, Geosystems, v. 11, no. 3.

JØRGENSEN, B.B., 1977, Bacterial sulfate reduction within reduced microniches of oxidized marine sediments: Marine Biology, v. 41, p. 7-17.

JØRGENSEN, B.B. AND BOUDREAU, B.P., 2001, Diagenesis and Sediment-Water Exchange. In: Boudreau, B.P, Jørgensen, B.B., eds., The Benthic Boundary Layer: Oxford University Press, 404 p.

KANE, I. A., AND HODGSON, D. M., 2011, Sedimentological criteria to differentiate submarine channel levee subenvironments: exhumed examples from the Rosario Fm. (Upper Cretaceous) of Baja California, Mexico, and the Fort Brown Fm.(Permian), Karoo Basin, S. Africa: Marine and Petroleum Geology, v. 28, p. 807-823.

KARIM, A., PE-PIPER, G. AND PIPER, D.J.W., 2010, Controls on diagenesis of Lower Cretaceous reservoir sandstones in the western Sable Sub basin, offshore Nova Scotia: Sedimentary Geology, v. 224, p. 65-83.

KENNEDY, M.J., PEVEAR, D.R. AND HILL, R.J., 2002, Mineral surface control of organic carbon in black shale: Science, v. 295, p. 657-660.

KENNEDY, M.J. AND WAGNER, T., 2011, Clay mineral continental amplifier for marine carbon sequestration in a greenhouse ocean: Proceedings of the National Academy of Sciences of the United States of America, v. 108, p. 9776-9781.

KLEMME, H.D. AND ULMISHEK, G.F., 1991, Effective petroleum source rocks of the world: stratigraphic distribution and controlling depositional factors: American Association of Petroleum Geologists Bulletin, v. 75, p. 1809-1851.

LANDRUM, J.P. AND MONTOYA, J.P., 2009,Organic matter processing by the shrimp Palaemonetes sp.: Isotopic and elemental effects", Journal of experimental marine biology and ecology, v. 380, p. 20-24.

LEA, D. AND BOYLE, E., 1989, Barium content of benthic foraminifera controlled by bottom-water composition: Nature, v. 338, p. 751-753.

LOWENSTAM, H. A., 1981, Minerals formed by organisms: Science, v. 211, p. 1126-1131.

MACKO, S.A., WEN YUH LEE AND PARKER, P.L., 1982, Nitrogen and carbon isotope fractionation by two species of marine amphipods: Laboratory and field studies: Journal of experimental marine biology and ecology, v. 63, p. 145-149.

MARTIN, P., ALLEN, J.T., COOPER, M.J., JOHNS, D.G., LAMPITT, R.S., SANDERS, R. AND TEAGLE, D.A.H., 2010, Sedimentation of acantharian cysts in the Iceland Basin: Strontium as a ballast for deep ocean particle flux, and implications for acantharian reproductive strategies: Limnology and Oceanography, v. 55, p. 604-614.

MCILROY, D. AND LOGAN, G.A., 1999, The impact of bioturbation on infaunal ecology and evolution during the Proterozoic-Cambrian transition: Palaios, v. 14, p. 58-72.

MCILROY, D., WORDEN, R.H. AND NEEDHAM, S.J., 2003, Faeces, clay minerals and reservoir potential: Journal of the Geological Society, v. 160, p. 489-493.

MCILROY, D., 2004, Some ichnological concepts, methodologies, applications and frontiers, in D. McIlroy, ed., The application of ichnology to paleoenvironmental and stratigraphic analysis: Geological Society (London) Special Publication 228, p. 3–29.

MCCUTCHAN JR., J.H., LEWIS JR., W.M., KENDALL, C. AND MCGRATH, C.C., 2003, Variation in trophic shift for stable isotope ratios of carbon, nitrogen, and sulfur: Oikos, v. 102, p. 378-390.

NEEDHAM, S.J., WORDEN, R.H. AND MCILROY, D., 2005, Experimental production of clay rims by macrobiotic sediment ingestion and excretion processes: Journal of Sedimentary Research, v. 75, p. 1028-1037.

NEEDHAM, S.J., WORDEN, R.H. AND CUADROS, J., 2006, Sediment ingestion by worms and the production of bio-clays: A study of macrobiologically enhanced weathering and early diagenetic processes", Sedimentology, vol. 53, no. 3, pp. 567-579.

OLIVEIRA, A., SANTOS,A.I., RODRIGUES,A. AND VITORINO, J., 2007, Sedimentary particle distribution and dynamics on the Nazaré canyon system and adjacent shelf (Portugal): Marine Geology, v. 246, p. 105–122.

OWENS, J.D., LYONS, T.W., LI, X., MACLEOD, K.G., GORDON, G., KUYPERS, M.M.M., ANBAR, A., KUHNT, W. AND SEVERMANN, S., 2012, Iron isotope and trace metal records of iron cycling in the proto-North Atlantic during the

Cenomanian-Turonian oceanic anoxic event (OAE-2): Paleoceanography, v. 27, no. 3.

PANCOST, R.D., CRAWFORD, N., MAGNESS, S., TURNER, A., JENKYNS, H.C. AND MAXWELL, J.R., 2004, Further evidence for the development of photic-zone euxinic conditions during Mesozoic oceanic anoxic events: Journal of the Geological Society, v. 161, p. 353-364.

PEDERSEN, T.F. AND CALVERT, S.E., 1990, Anoxia vs. productivity: what controls the formation of organic- carbon-rich sediments and sedimentary rocks?: American Association of Petroleum Geologists Bulletin, v. 74, p. 454-466.

PODUSKA, K.M., REGEV, L., BOARETTO, E., ADDADI, L., WEINER, S., KRONIK, L. AND CURTAROLO, S. 2011, Decoupling local disorder and optical effects in infrared spectra: Differentiating between calcites with different origins: Advanced Materials, v. 23, p. 550-554.

POPESCU, B.F.G., GEORGE, M.J., BERGMANN, U., GARACHTCHENKO, A.V., KELLY, M.E., MCCREA, R.P.E., LÜNING, K., DEVON, R.M., GEORGE, G.N., HANSON, A.D., HARDER, S.M., CHAPMAN, L.D., PICKERING, I.J. AND NICHOL, H. 2009, Mapping metals in Parkinson's and normal brain using rapid-scanning x-ray fluorescence: Physics in Medicine and Biology, vol. 54, no. 3, pp. 651-663.

REDDY, S. L., SUBBA REDDY, R. R., REDDY, G. S., RAO, P. S., AND REDDY, B. J., 2003, Optical absorption and EPR spectra of fuchsite: Spectrochimica Acta Part A: Molecular and Biomolecular Spectroscopy, v. 59, p. 2603-2609.

SAVRDA, C. E., H. KRAWINKEL, F. M. G. MCCARTHY, C. M. G. MCHUGH, H. C. OLSON, AND G. MOUNTAIN, 2001, Ichnofabrics of a Pleistocene slope succession, New Jersey margin: Relations to climate and sea level dynamics: Paleogeography, Paleoclimatology, Paleoecology, v. 171, p. 41–61, doi:10.1016/S0031-0182(01)00266-8.

SCHOONEN, M.A.A., 2004, Mechanisms of sedimentary pyrite formation, *in* Amend, J.P., Edwards, K.J., and Lyons, T.W., eds., Sulfur biogeochemistry—Past and present: Boulder, Colorado, Geological Society of America Special Paper 379, p. 117–134.

SEILACHER, A., AND PFLÜGER, F., 1994, From biomats to benthic agriculture: a biohistoric revolution, in Biostabilization of Sediments, in Krumbein, W.E., Paterson, D.M., and Sal, L.J., eds., Bibliotheks und Informationssystem der Universitat Oldenburg, p. 97-105.

STOCKDALE, A., DAVISON, W. AND ZHANG, H., 2010, Formation of iron sulfide at faecal pellets and other microniches within suboxic surface sediment: Geochimica et Cosmochimica Acta, v. 74, p. 2665-2676.

SCHIEBER, J. 2002a. The role of an organic slime matrix in the formation of pyritized burrow trails and pyrite concretions. Palaios, 17, 104–109.

SEILACHER, A. AND PFLÜGER, F., 1994, From biomats to benthic agriculture: a biohistoric revolution. In: Biostabilization of Sediments, eds., W.E. Krumbein, D.M. Paterson and L.J. Stal), Bibliotheks und Informationssystem der Carl von Ossietzky Universität Oldenburg, Oldenburg, Germany. p. 97–105.

SINNINGHE DAMSTE, J.S. AND DE LEEUW, J.W., 1990, Analysis, structure and geochemical significance of organically-bound sulphur in the geosphere: State of the art and future research: Organic Geochemistry, v. 16, p. 1077-1101.

SINNINGHE DAMSTÉ, J.S., KOK, M.D., KÖSTER, J. AND SCHOUTEN, S., 1998, Sulfurized carbohydrates: An important sedimentary sink for organic carbon: Earth and Planetary Science Letters, v. 164, p. 7-13.

TAYLOR, A., R. GOLDRING, AND S. GOWLAND, 2003, Analysis and application of ichnofabrics: Earth-Science Reviews, v. 60, p. 227–259, doi:10.1016/S0012 8252(02)00105-8.

TRIBOVILLARD, N., ALGEO, T.J., LYONS, T. AND RIBOULLEAU, A., 2006, Trace metals as paleoredox and paleoproductivity proxies: An update: Chemical Geology, v. 232, p. 12-32.

VIRTASALO, J.J., LÖWEMARK, L., PAPUNEN, H., KOTILAINEN, A.T. AND WHITEHOUSE, M.J., 2010, Pyritic and baritic burrows and microbial filaments in postglacial lacustrine clays in the northern Baltic sea: Journal of the Geological Society, v. 167, p. 1185-1198.

VIRTASALO, J.J., WHITEHOUSE, M.J. AND KOTILAINEN, A.T., 2013, Iron isotope heterogeneity in pyrite fillings of Holocene worm burrows: Geology, v. 41, p. 39-42.

VOLKENBORN, N., POLERECKY, L., WETHEY, D.S., DEWITT, T.H. AND WOODIN, S.A., 2012, Hydraulic activities by ghost shrimp *Neotrypaea californiensis* induce oxic-anoxic oscillations in sediments: Marine Ecology Progress Series, v. 455, p. 141-156.

WETZEL, A., 1991, Ecologic interpretation of deep-sea trace fossil communities: Palaeogeography, Palaeoclimatology, Palaeoecology, v. 85, p. 47-69.

WETZEL, A., AND A. UCHMAN, 2001, Sequential colonization of muddy turbidites in the Eocene Beloveza Formation, Carpathians, Poland: Paleogeography, Paleoclimatology, Paleoecology, v. 168, p. 171–186, doi:10.1016/S0031-0182(00)00254-6.

WETZEL, A. 2010, Deep-sea ichnology: observations in modern sediments to interpret fossil counterparts: Acta Geologica Polonica, v. 60, p. 125–138.

WIDERLUND, A. AND DAVISON, W., 2007, Size and density distribution of sulfide-producing microniches in lake sediments: Environmental Science and Technology, v. 41, p. 8044-8049.

WOGELIUS, R.A., MANNING, P.L., BARDEN, H.E., EDWARDS, N.P., WEBB, S.M., SELLERS, W.I., TAYLOR, K.G., LARSON, P.L., DODSON, P., YOU, H., DA-QING, L. AND BERGMANN, U. 2011, Trace metals as biomarkers for eumelanin pigment in the fossil record: Science, v. 333, p. 1622-1626.

ZHU, Q., ALLER, R.C. AND FAN, Y., 2006, Two-dimensional pH distributions and dynamics in bioturbated marine sediments: Geochimica et Cosmochimica Acta, v. 70, p. 4933-4949.

CHAPTER 5

SUMMARY

To better integrate the role of physical and biogenic sea-floor reworking into modern conceptual models of sediment generation and diagenesis, two fine-grained sedimentary successions have been investigated for their sedimentology and geochemical composition, using a combination of well-established and novel analytical techniques. To date, there is a knowledge gap on how physical sea-floor processes and bioturbation control the compositional characteristics of mudstones that were deposited under a wide variety of seafloor energy regimes. This study helps to close this gap by testing the hypotheses that high-energy sea-floor processes and bioturbation were the dominant control on the lithofacies variability in the mudstone-rich Beach Formation, Newfoundland and in the Rosario Formation, Mexico.

1. Review of objectives

a) Sedimentological and ichnological analyses were utilized at a range of spatial scales to establish a better understanding of the paleoenvironmental conditions within unbioturbated mudstones in the Beach Formation, Newfoundland. In addition, it was examined if unbioturbated mudstones in the Beach Formation

have accumulated under high-energy seafloor conditions with the aim to develop a facies model that is adaptable to other similar mud-rich, marginal-marine shoreface successions that contain stark fluctuations in bioturbation intensity.

b) A facies description of mudstones has been combined with petrographic and geochemical analyses to investigate the concentration, and origin of organic carbon in the Beach Formation, Newfoundland. Combined $\delta^{13}C_{org}$ analyses and petrographic techniques have been employed to investigate if organic carbon is of benthic microbial origin.

c) The possible influence of grain-size selective deposit feeding as a modifier of rock composition was tested from very fine-grained sandstones and siltstones in the Rosario Formation, Mexico. Here, it was hypothesized that bioturbation does not only represent 'physical disturbance', but also accounts for systematic spatial variability in organic carbon concentration and distribution of redox sensitive trace elements.

2. Summary of methods

The following analytical approaches were used to achieve the above stated objectives:

1) Sedimentary structures and trace fossils in mudstones were described and characterized on hand-sample and thin-section scale to assess the environment of deposition and seafloor energy regime.
2) Integrated Scanning Electron Microscopy (SEM), X-Ray diffractometry (XRD) and Fourier Transform Infrared Spectroscopy (FTIR) were used to determine if significant variability exists between the mineralogical composition of bioturbated and unbioturbated sand- and mudstones.
3) Organic carbon content (TOC, wt %) and quality ($\delta^{13}C_{org}$, ‰) were measured to assess the origin of organic matter and to investigate the distribution of organic matter between bioturbated and unbioturbated sediment.
4) Synchrotron Rapid Scanning X-Ray Fluorescence (SRS-XRF) and Inductively coupled Plasma Mass Spectrometry (ICP-MS) were integrated to image and quantify the spatial distribution of major and trace elements between bioturbated and unbioturbated sediments in the Rosario Formation, Mexico.

3. Summary of conclusions

3.1 *Sedimentological and ichnological evidence for high-energy sea floor processes within mudstones of the Beach Formation, Newfoundland and its implications for shallow-marine facies models*

Shoreface mudstones from the Beach Formation contain ample textural evidence for high-energy seafloor reworking. Sedimentological analysis of the unbioturbated mudstones revealed that most likely both hyperpycnal flows and wave-enhanced sediment gravity flows were the primary delivery mechanism for fine-grained sediment. Decision making has been based on diagnostic sedimentary structures and ichnological characteristics. The rapid mode of sediment delivery contrasts with previous interpretations of the Beach Formation that explained the deposition of unbioturbated mudstone beds by a combination of bottom-water anoxia and periodic salinity fluctuations in a tidal paleoenvironment (Ranger et al. 1984; Fillion and Pickerill 1990; Brenchley et al. 1993). The preservation potential of organic carbon in this Early Ordovician muddy shoreface environment is most likely controlled by a combination of residence time of organic material in the suboxic zone of the sediment. A delicate interplay between the three key variables (a) frequency of physical disturbance, (b) duration of exposure and (c) depth of erosion, is most likely the first-order control on the burial efficiency of organic matter and is inferred to be a critical variable controlling bioturbation intensity and style.

3.2 *The significance of intrastratal shrinkage cracks as indicators for salinity fluctuations and the role of organic carbon decay after microbial mat burial*

It is proposed that microbial-binding of surface sediment is an important prerequisite for the formation of intrastratal shrinkage ("synaeresis") cracks in the Beach Formation. Formation of intrastratal shrinkage cracks in mudstones is proposed to be the result of

rheological heterogeneities that develop during organic matter decay within the partially dewatered mud. While the term ‘synaeresis crack’ is commonly used to describe sinuous and tapering cracks in mudstone beds, the use of the non-genetic term ‘intrastratal shrinkage crack’ is proposed, unless evidence of synaeresis (i.e. contraction of clay mineral lattices in response to salinity change) can be unequivocally demonstrated. Within the Beach Formation it is proposed that bioturbation intensity is most likely controlled by a combination of organic carbon availability and sporadically elevated H_2S in pore-waters of sedimentary layers rather than oxygen deficiency of bottom water or higher salinity levels.

3.3 *Bioturbation as a prime modifier of organic carbon trace element concentration in fine-grained siliciclastics*

Integrated geochemical and petrographic analyses revealed that phycosiphoniform trace makers redistribute grain-bound sedimentary organic matter irrespective of mineralogy or shape. This process coevally increases porosity within the burrow halo. High concentrations of Ca, Ti and some redox-sensitive trace elements were found in the burrow core, and are most likely associated with pyrite, Fe-bearing silicates (mica) and possibly organic matter. Despite organic matter enrichment quantities of neo-formed pyrite in the burrow core are relatively low. The absence of cross-cutting by other phycosiphoniform producers provides additional evidence that the fecal organic matter was of low reactivity and largely refractory. The potentially low reactivity of organic

matter is inferred to explain the low rate of microbial iron reduction and subsequent formation of pyrite. Elements such as Sr and Ba are depleted within the burrow halo and core with respect to the host sediment. The significant deficiency of these latter two elements might be explained by the fact that the vermiform trace maker used these elements for biomineralization processes. Alternatively, the loss of Sr and Ba might be explained by accelerated biological weathering of unstable lithic fragments and feldspar in the burrow core (as observed in this study), and loss of these two elements to pore waters.

4. Significance of research

Effective decision making on how hydrocarbon recovery can be maximized from a reservoir requires not only knowledge about the chemical interactions of fluids within the rock-pore system, but also a thorough understanding of all petrophysical attributes, such as effective porosity, pore-throat aperture size distribution, fluid saturation, mineral surface area, wettability and composition of the pore lining (Varva et al. 1992; Bliefnick and Kaldi 1996; Standnes and Austad 2003). All these parameters exhibit significant heterogeneity on a basin-wide scale (Heath et al. 2011; Day-Stirrat et al. 2012) which cannot be explained by the compositional diversity of sediment alone, or its burial diagenetic history.

The underlying problem during field appraisal is that critical elastic and petrophysical rock properties (e.g. Young's modulus) are easily quantified in routine core

analyses (Dewhurst et al. 2008; Schlömer and Kroos 1997) but rarely correlated with the underlying lithofacies variability. Sedimentological and ichnological datasets are readily integrated into facies associations with (broadly) predictable spatiotemporal, basin-wide distributions. A multi-disciplinary approach that integrates sedimentological, ichnological and petrophysical approaches allows an extrapolation of petrophysical properties towards geological situations that are less well known or difficult to directly access. Recent studies are just beginning to integrate the effect of physical and biological seafloor reworking on the composition of mudstones into modern siliciclastic facies models (e.g., Plint 2010). Petrophysical properties need to be supplemented with rock descriptions at all available scales and integrated into a predictive chronostratigraphic framework. With this approach a realistic geological model can be developed that allows a (careful) extrapolation of properties relevant to the basin modeler and reservoir engineer, before exploitation is undertaken.

5. Open questions and avenues for future research

- *Significance for shallow-marine, siliciclastic facies models.* All data presented from Bell Island, Newfoundland were recovered from a ~23 m thick interval at Freshwater Cove. At this locality, the investigated succession did not exhibit a significant basin-ward facies shift, but highlights rather autocyclic variability (cf. Catuneanu and Zecchin 2013) as the dominant control on the stratigraphic distribution of mudstone-rich intervals. If high-energy sea floor processes are the

dominant depositional mode for mudstones in the Bell Island Group, then this might have broader implications for existing sequence stratigraphic models that propose that thick unbioturbated mudstones represent late transgressive and early highstand deposits (Brenchley et al. 1993). In the future a larger-scale study is needed, that investigates how widely distributed high-energy seafloor processes are in unbioturbated mudstones within the Bell Island Group.

- *Independent recognition criteria for high-energy seafloor processes*. The sedimentary record of storm-dominated, sand-rich successions is well established (e.g., Aigner and Reineck 1982; Cheel 1990; Duke et al. 1991; Brenchley et al. 1993; Myrow & Southard 1996; Dumas & Arnott 2005; Yoshida et al. 2007). However, to date only a relatively small number of studies investigated the diagnostic sedimentary structures and trace fossil characteristics in fine-grained deposits that accumulated under gravity-driven and combined-flow processes (Bentley and Nittrouer 2003; McIlroy 2004; Aller et al. 2010; Plint 2010). Critical hydrodynamic parameters, such as floc settling velocity (Hill et al. 2000) and critical dimensionless in-flow variables, such as the flow Reynolds number (Baas et al. 2009, 2011), are currently difficult to accurately estimate from the rock record (Paola et al. 2009; Talling et al. 2012). It is clear, however, that necessary conditions for the preservation of unbioturbated mud layers involve discharge of high amounts of river-borne suspended solids during short-lived storm floods and high fluxes of flocculated sediment to the wave boundary layer (Gonzalez-Hidalgo et al. 2010). Shorelines adjacent to small rivers that drain high mountain ranges

(e.g., Hastings et al. 2012) are first-class candidates for future sedimentological studies which might provide a modern analogue for the mud-dominated Beach Formation. These small, 'dirty' systems discharge high volumes of immature silt- and clay-sized material with a wide grain size distribution to an energetic wave-boundary layer. A more quantitative understanding about the formation conditions and the underlying factors that enhance preservation of the various classes of shelf-wide wave- and gravity-driven currents is needed before the sedimentary products originating from these flows can be used as "stand alone" facies indicators (Schieber 2011).

- *Bioturbation as first-order control on geochemical heterogeneity*. Within this study grain-size selective deposit feeding was examined as a potential spatial modifier of sedimentary organic matter and trace elements in fine-grained siliciclastics. The small sample amounts (by weight) extracted from the burrow core unfortunately did not allow for characterization of the organic fraction at a molecular level (e.g., biomarker analysis). Future studies should also integrate different trace fossils throughout a broader range of depositional environments and sediment compositions. A high priority research target is the potential ability of other vermiform trace makers, such as the still unknown producer of *Chondrites* to permanently alter the spatial geochemical characteristics of fine-grained sedimentary rocks, as individuals and as a community.

Energetic seafloor processes and bioturbation are the volumetrically most important modifiers of fluids, gases and solids in the modern shallow seabed. This work has demonstrated that visualizing 'hard-to-see' features indicative for seafloor reworking (i.e., small burrows and erosional contacts) allows discrimination of a broader range of environmental conditions (e.g., water depths and seafloor oxygenation) in shales and mudstones with only limited hand-specimen variability. Combining detailed rock descriptions with petrographic and geochemical datasets significantly increases the fidelity of paleoenvironmental reconstructions in mudstones and allows the formulation of more realistic geological models in time and space. A good geological model can be used to predict the petrophysical and geochemical heterogeneity for mud-dominated regions of the shelf, which are not readily accessible for direct analyses.

6. References

ALLER, R. C., MADRID, V., CHISTOSERDOV, A., ALLER, J. Y., AND HEILBRUN, C., 2010, Unsteady diagenetic processes and sulfur biogeochemistry in tropical deltaic muds: implications for oceanic isotope cycles and the sedimentary record: Geochimica et Cosmochimica Acta, vol. 74, p. 4671-4692.

BAAS, J.H., BEST, J.L., PEAKALL, J. AND WANG, M., 2009, A phase diagram for turbulent, transitional, and laminar clay suspension flows: Journal of Sedimentary Research, v. 79, p. 162-183.

BAAS, J. H., BEST, J. L., AND PEAKALL, J., 2011, Depositional processes, bedform development and hybrid bed formation in rapidly decelerated cohesive (mud–sand) sediment flows: Sedimentology, vol. 58, p. 1953-1987.

BENTLEY, S. J., AND NITTROUER, C. A., 2003, Emplacement, modification, and preservation of event strata on a flood-dominated continental shelf: Eel shelf, Northern California: Continental Shelf Research, vol. 23, p. 1465-1493.

BLIEFNICK, D. M., AND KALDI, J. G., 1996, Pore geometry: control on reservoir properties, Walker Creek Field, Columbia and Lafayette counties, Arkansas. AAPG bulletin, vol. 80, p. 1027-1044.

BRENCHLEY, P.J., PICKERILL, R.K. AND STROMBERG, S.G., 1993, The role of wave reworking on the architecture of storm sandstone facies, Bell Island Group (Lower Ordovician), Eastern Newfoundland: Sedimentology, v. 40, p. 359-382.

CATUNEANU, O., AND ZECCHIN, M., 2012, High-resolution sequence stratigraphy of clastic shelves II: Controls on sequence development: Marine and Petroleum Geology, vol. 39, p. 26-38.

CHEEL, R. J., 1991, Grain fabric in hummocky cross-stratified storm beds: genetic implications: Journal of Sedimentary Research, vol. 61, p. 102-110.

DAY-STIRRAT, R. J., FLEMINGS, P. B., YOU, Y., APLIN, A. C., AND VAN DER PLUIJM, B. A., 2012, The fabric of consolidation in Gulf of Mexico mudstones: Marine Geology, vol. 295, p. 77-85.

DEWHURST, D. N., SIGGINS, A. F., KUILA, U. N., CLENNELL, M. B., RAVEN, M. D., AND NORDGÅRD-BOLÅS, H. M., 2008, Elastic, geomechanical and petrophysical properties of shales. In The 42nd US Rock Mechanics Symposium (USRMS).

DUKE, W. L., ARNOTT, R. W. C., AND CHEEL, R. J., 1991, Shelf sandstones and hummocky cross-stratification: new insights on a stormy debate: Geology, vol. 19, p. 625-628.

DUMAS, S., AND ARNOTT, R. W. C., 2006, Origin of hummocky and swaley cross-stratification – The controlling influence of unidirectional current strength and aggradation rate: Geology, vol. 34, p. 1073-1076.

FILLION, D. AND PICKERILL, R.K., 1990, Ichnology of the Upper Cambrian? to Lower Ordovician Bell Island and Wabana groups of eastern Newfoundland, Canada. Palaeontographica Canadiana, v. 7, p. 1-119.

GONZALEZ-HIDALGO, J. C., BATALLA, R. J., CERDÀ, A., AND DE LUIS, M., 2010, Contribution of the largest events to suspended sediment transport across the USA. Land Degradation and Development, vol. 21, p. 83-91.

HASTINGS, R. H., GOÑI, M. A., WHEATCROFT, R. A., AND BORGELD, J. C., 2012, A terrestrial organic matter depocenter on a high-energy margin: The Umpqua River system, Oregon. Continental Shelf Research, vol. 39, p. 78-91.

HILL, P. S., MILLIGAN, T. G., AND GEYER, W. R., 2000, Controls on effective settling velocity of suspended sediment in the Eel River flood plume. Continental shelf research, vol. 20, p. 2095-2111.

MCILROY, D., 2004, Ichnofabrics and sedimentary facies of a tide-dominated delta: Jurassic Ile Formation of Kristin field, Haltenbanken, offshore mid-Norway. Geological Society, London, Special Publications, vol. 228, p. 237-272.

MYROW, P. M., AND SOUTHARD, J. B., 1996, Tempestite deposition. Journal of Sedimentary Research, vol. 66,

PAOLA, C., STRAUB, K., MOHRIG, D., AND REINHARDT, L., 2009, The "unreasonable effectiveness" of stratigraphic and geomorphic experiments. Earth-Science Reviews, vol. 97, p. 1-43.

PLINT, A. G., 2010, Wave-and storm-dominated shoreline and shallow-marine systems. Facies Models, 4, 167-200.

RANGER, M.J., PICKERILL, R.K. AND FILLION, D., 1984, Lithostratigraphy of the Cambrian? - Lower Ordovician Bell Island and Wabana groups of Bell, Little Bell, and Kellys islands, Conception Bay, eastern Newfoundland: Canadian Journal of Earth Sciences, v. 21, p. 1245-1261.

SCHIEBER, J., 2011, Grading phenomena in mudstones – ancient shales and modern shelf muds in the context of recent flume studies. Geological Association of America Annual Meeting, Minneapolis, 9-12 October 2011.

SCHLÖMER S AND KROOS BM, 1997, Experimental characterisation of the hydrocarbon sealing efficiency of cap rocks. Marine and Petroleum Geology, vol. 14, p. 565–580

STANDNES, D. C., AND AUSTAD, T., 2003, Wettability alteration in carbonates: Interaction between cationic surfactant and carboxylates as a key factor in wettability alteration from oil-wet to water-wet conditions: Colloids and Surfaces A: Physicochemical and Engineering Aspects, vol. 216, p. 243-259.

TALLING, P. J., MASSON, D. G., SUMNER, E. J., AND MALGESINI, G., 2012, Subaqueous sediment density flows: Depositional processes and deposit types: Sedimentology, vol. 59, p. 1937-2003.

VAVRA, C. L., KALDI, J. G., AND SNEIDER, R. M., 1992, Geological Applications of Capillary Pressure: A Review: AAPG Bulletin, vol. 76, p. 840-850.

YOSHIDA, S., STEEL, R. J., AND DALRYMPLE, R. W., 2007, Changes in depositional processes – an ingredient in a new generation of sequence-stratigraphic models: Journal of Sedimentary Research, vol. 77, p. 447-460

APPENDIX A

Whole rock elemental and isotopic data, Bell Island 2009-2012

Appendix A contains whole rock geochemical data obtained from the Bell Island study site Freshwater Cove (Parsonville). These data are presented in my second and my third thesis chapter. The table lists sample number, facies code, stratigraphic height, as well as isotopic value ($\delta^{13}C_{org}$, ‰) and Total Organic Carbon TOC (wt%). Stratigraphic height is given in cm. TOC was measured using a Carlo Erba NA 1500 Series 2 elemental analyzer and $\delta^{13}C_{org}$ was measured using a Thermo Electron Delta V Plus mass spectrometer.

Sample number	Stratigraphic height (cm)	Facies code	$\delta^{13}C_{org}$ (‰)	TOC (wt%)
FC1242	2247.0	M5	-28.81	0.34
FC1241	2240.0	M6	-28.31	0.25
FC1238	2167.0	M4	-28.57	0.23
FC1237	2154.0	M7	-28.28	0.18
FC1236	2135.0	M7	-28.29	0.18
FC1235	2074.0	M2	-28.25	0.18
FC1234	2041.0	M2	-28.79	0.37
FC1231	1904.0	M1	-28.86	0.41
FC1230	1816.0	M7	-28.17	0.15
FC1229	1677.0	M1	-28.85	0.41
FC1228	1627.0	M4	-28.88	0.37
FC1227	1586.0	M6	-29.07	0.45
FC1111	1540.0	M1	-29.40	0.54
FC1226	1523.0	M7	-29.04	0.52
FC1224	1494.0	M1	-28.94	0.32
FC1223	1436.0	M6	-28.94	0.33
FC1218	1410.0	M1	-29.00	0.37
FC1217	1334.0	M1	-28.89	0.49
FC1216	1256.0	M1	-29.17	0.54
FC1215	1206.0	M2	-28.75	0.27
FC1214	1191.0	M2	-29.14	0.23
FC1213	1178.0	M5	-29.15	0.55
FC1212	1169.0	M3	-29.40	0.68
FC1210	1164.0	M3	-29.40	0.95
FC1208	1153.0	M1	-29.32	0.87
FC12-E	1088.0	M1	-29.11	0.52
FC12-D	1061.0	M1	-28.72	0.33
FC12-C	1046.0	M1	-29.13	0.44
FC12-B	1042.0	M1	-28.95	0.37
FC12-A	980.0	M7	-28.88	0.22
FC1206	945.0	S3	-29.20	0.70
FC1205	897.0	S3	-28.86	0.18
D21	880.0	S3	-28.22	0.19
D20	844.0	M1	-28.21	0.39
FC1204	856.0	S3	-28.72	0.29
D19	824.0	M1	-28.46	0.67
FC1203	811.0	S3	-28.40	0.15
D18	808.0	S3	-28.07	0.50
FC0811	788.0	S3	-28.29	0.22
D17	778.0	M1	-29.14	0.60

D16	762.0	M1	-28.02	1.00
FC1201	754.0	S3	-28.77	0.28
FC0810	750.0	S3	-28.10	0.07
AD11	731.0	M3	-28.52	0.26
D15	727.0	M3	-28.68	0.68
FC0809	710.0	M5	-28.41	0.68
FC0808	660.0	M6	-27.99	0.09
D14	630.0	M1	-28.89	0.44
FC0807	612.0	M1	-27.68	0.51
FC0806	608.0	M7	-28.04	0.13
FC0805	593.0	M1	-27.64	0.05
D13	575.0	M1	-29.18	0.46
D12	529.0	M1	-29.10	0.31
D11	521.0	M1	-28.54	0.37
FC0804_2	518.0	M1	-27.92	1.52
FC0804_1	517.0	M1	-27.44	0.21
D10	515.0	M1	-28.38	0.27
FC0803	512.0	M1	-28.10	0.12
FC0812b	492.0	M1	-28.60	0.57
FC0813	483.0	M1	-29.14	0.39
FC0802	481.0	M1	-29.46	0.85
D8	481.0	M1	-28.34	0.77
FC0815	476.0	M1	-29.09	0.41
FC0814	474.0	M1	-29.53	0.12
D7	472.0	M1	-28.62	0.42
D6	467.0	M1	-28.59	0.44
D5	457.0	M1	-28.34	0.32
D4	442.0	M1	-29.06	0.53
FC0801_2	438.0	M1	-27.64	3.43
FC0801_1	437.0	S2	-28.04	0.10
AD8	422.0	M1	-28.51	0.42
AD7	413.0	M1	-29.19	0.47
D3	410.0	M1	-28.64	0.65
D2A	408.0	S2	-27.46	0.17
D2	401.0	M1	-27.57	0.81
D1	327.0	S1	-28.68	1.17
A3	232.0	M2	-29.07	0.54
FC09A2b	202.0	M2	-28.80	0.62
AD5	134.0	M3	-29.28	0.53
AD0	49.0	M3	-28.10	0.53

APPENDIX B

High-resolution geochemical data from one sample interval containing intrastratal shrinkage cracks

Appendix B contains geochemical data obtained from the Bell Island sample FC0801 from Freshwater Cove (Parsonville). These data are presented in my second and thesis chapter. The table lists sample number, isotopic value ($\delta^{13}C_{org}$, ‰) and Total Organic Carbon TOC (wt%). TOC was measured using a Carlo Erba NA 1500 Series 2 elemental analyzer and $\delta^{13}C_{org}$ was measured using a Thermo Electron Delta V Plus mass spectrometer. The stratigraphic position of this sample is given in Appendix A.

Sample number	$\delta^{13}C_{org}$ (‰, PDB)	TOC (wt%)
FC0801-1	-24.41	0.51
FC0801-2	-27.61	1.18
FC0801-3	-27.65	2.08
FC0801-4	-26.41	0.57
FC0801-5	-26.97	0.72
FC0801-6	-24.92	0.36

APPENDIX C

High-resolution geochemical data from phycosiphoniform burrow elements (core and halo), as well as host sediment

Appendix C contains whole rock geochemical data obtained from sample ROS1 from the Pelican System (Rosario Formation). These data are presented in my fourth thesis chapter. The table lists sample number, isotopic value ($\delta^{13}C_{org}$, ‰) and Total Organic Carbon (TOC, wt%) content. TOC was measured using a Carlo Erba NA 1500 Series 2 elemental analyzer and $\delta^{13}C_{org}$ was measured using a Thermo Electron Delta V Plus mass spectrometer.

Sample name	$\delta^{13}C_{org}$ (‰, PDB)	TOC (wt%)
ROS_1_matrix	-24.28	0.75
ROS_1_matrix*	-24.00	0.72
ROS_1_halo	-23.69	0.61
ROS_1_halo*	-23.84	0.56
ROS_1_core	-24.44	1.80
ROS_1_core*	-24.44	1.76

*duplicate measurements

APPENDIX D

Sample locations for high-resolution geochemical analyses from phycosiphoniform burrow elements (core and halo), and host sediment from the Pelican System (Rosario Formation, Mexico)

This image contains the sampling locations for high-resolution (sub-mm) geochemical data analyses on sample ROS1 from the Pelican System (Rosario Formation). These data are presented in my fourth thesis chapter. The annotated image shows the sampling localitites and sample names for ICP-MS measurements. The sampling of sedimentary laminae and burrow elements core and halo was carried out using a Merchantek Micromill (New Wave) microsampling device (Electro Scientific Industries Inc., Portland, OR, USA), equipped with a 0.3 mm bit. Prior to drilling, linear spot trajectories were mapped out using the imaging software PXC (New Wave).

.

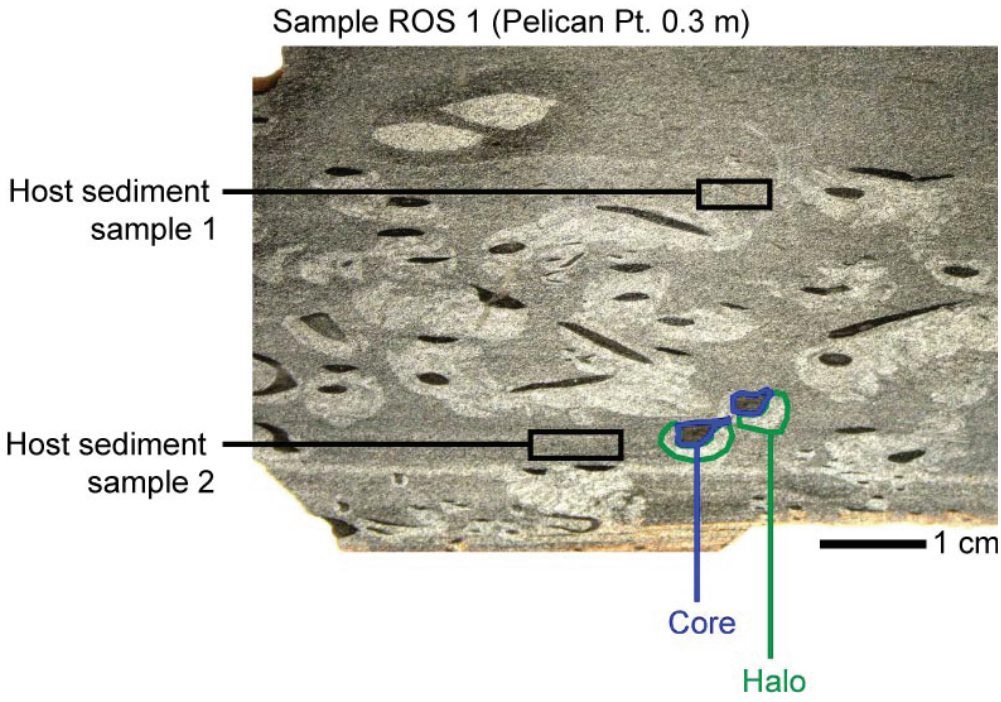
Sample ROS 1 (Pelican Pt. 0.3 m)
Host sediment sample 1
Host sediment sample 2
1 cm
Core
Halo

APPENDIX E

High-resolution geochemical analyses from host sediment and phycosiphoniform burrow elements (core and halo) from the Pelican System (Rosario Formation, Mexico)

This table contains high-resolution (sub-mm) trace element data obtained from host sediment, burrow halo and burrow core from sample ROS1. These data are presented in my fourth thesis chapter. The table shows trace element concentrations (in ppm). The data were obtained via ICP-MS measurements.

The sample (~0.1 g) was dissolved via HF and HNO_3 treatment (see Jenner et al. 1990). The sample solution was sprayed into the inductively coupled argon plasma (~8000°C) of a HP 4500 plus mass-spectrometer, allowing all analyte species to be atomized, ionized and thermally excited in order to be detected. Exact sampling locations are given in Appendix D.

Harazim , Environmental/Exploration RUN = 149; Apr08111
Sample ROS 1 Calculated on 08. Apr 2011 14:49:02

Name	Ca	Ti	V	Cr 52	Fe 54	Mn
	ppm	ppm	ppm	ppm	ppm	ppm
Host sediment, sample 1 (ppm)	15001.08	3886.38	110.77	67.85	22690.97	266.40
1 sigma (ppm)	2407.65	340.03	10.11	2.04	661.61	14.03
Host sediment, sample 2 (ppm)	14593.42	4229.96	134.62	82.24	26735.89	286.22
1 sigma (ppm)	2342.22	370.10	12.29	2.47	779.55	15.07
HALO (ppm)	15089.42	3896.93	107.73	62.72	22529.15	268.38
1 sigma (ppm)	2421.83	340.96	9.83	1.89	656.89	14.13
PHYCO CORE (ppm)	24746.18	5863.01	227.28	141.60	40077.11	372.07
1 sigma (ppm)	3971.73	512.98	20.74	4.26	1168.55	19.59
FER-4 standard average of 3 runs (ppm)	19748.7	370.8	12.5	9.4	268390.0	1585.2
FER-4 standard published (GeoREM, ppm)	15723.0	419.7	11.0	9.0	279690.0	1471.4
Host sediment average	14797.3	4058.2	122.7	75.0	24713.4	276.3
Host sediment average dev (ppm)	5506.5	1652.5	50.0	32.4	10689.7	116.6
Host sediment average dev (%)	37.2	40.7	40.8	43.2	43.3	42.2
Halo excess (ppm)	292.2	-161.2	-15.0	-12.3	-2184.3	-7.9
Core excess (ppm)	9948.9	1804.8	104.6	66.5	15363.7	95.8
Error calculation based on FER-4 published values						
Stdev (1 sigma, ppm)	**2846.58**	**34.58**	**1.07**	**0.28**	**7990.31**	**80.47**
Average (ppm)	17735.83	395.20	11.76	9.20	274040.00	1528.26
Stdev (1 sigma)	0.1605	0.0875	0.0913	0.0301	0.0292	0.0527
Stdev (1 sigma, %)	**16.05**	**8.75**	**9.13**	**3.01**	**2.92**	**5.27**

Appendix-12

Co	Ni	Cu	Zn	As	Se 77	Br 79	Ag 107	Cd	Sn	Sb	Te	I
ppm	ppm	ppm	ppm	ppm	ppm	ppm	ppm	ppm	ppm	ppm	ppm	ppm
62.27	25.58	41.80	74.72	11.74	-1.90	1178.32	0.28	0.96	2.80	1.30	0.36	23.45
2.18	2.14	9.37	49.64	0.32								
82.39	37.26	48.02	130.92	16.27	7.65	1059.26	0.42	1.44	2.95	1.46	3.22	13.84
2.89	3.12	10.77	86.99	0.45								
44.44	28.41	44.59	90.23	9.60	-13.45	1078.06	0.33	2.00	2.40	1.34	1.45	16.68
1.56	2.38	10.00	59.95	0.26								
137.33	56.58	72.43	138.57	25.98	1.64	1125.25	0.63	1.38	3.50	2.67	3.53	16.74
4.81	4.74	16.24	92.07	0.71					-8.20	2.84		
1.9	9.0	17.9	69.3	3.8	0.5	0.7	2.1	2.4	-4.0	9.0	14.5	1.7
2.0	8.0	13.0	25.0	4.0					1.0	1.3		
72.3	31.4	44.9	102.8	14.0	2.9	1118.8	0.3	1.2	2.9	1.4	1.8	18.6
31.2	13.0	15.8	30.5	6.1	4.8	59.5	0.1	0.2	0.1	0.1	1.4	4.8
43.1	41.4	35.2	29.7	43.4	166.1	5.3	20.2	19.9	2.5	5.5	79.9	25.8
-27.9	-3.0	-0.3	-12.6	-4.4	-16.3	-40.7	0.0	0.8	-0.5	0.0	-0.3	-2.0
65.0	25.2	27.5	35.8	12.0	-1.2	6.5	0.3	0.2	0.6	1.3	1.7	-1.9
0.07	**0.71**	**3.46**	**31.33**	**0.11**					**3.56**	**5.44**		
1.95	8.50	15.45	47.15	3.92					-1.52	5.11		
0.0350	0.0837	0.2243	0.6644	0.0275					-2.3443	1.0655		
3.50	**8.37**	**22.43**	**66.44**	**2.75**					**-234.43**	**106.55**		

Appendix-13

La	Ce	Pr	Nd	Er	Tm	Lu	W	Hg	Pb	Bi	Th	G/KG
ppm	ppm	ppm	ppm	ppm	ppm	ppm	ppm	ppm	ppm	ppm	ppm	
29.73	55.92	6.51	25.17	1.78	0.22	0.20	444.30	0.30	13.59	0.28	17.47	0.02
39.12	76.29	9.04	33.91	2.28	0.36	0.30	579.66	-0.24	14.26	0.40	12.46	0.02
29.72	57.84	6.88	25.89	1.82	0.27	0.22	369.81	-0.21	12.24	0.18	9.06	0.02
38.13	72.28	8.71	33.07	2.78	0.41	0.39	612.84	-0.19	17.48	0.58	15.78	0.02
0.15	95.04	11.70	45.85	3.49	0.24	0.53			4.11	0.00	6.77	
8.0	0.4	0.1	0.1	8.3	0.2	7.1	0.0	2.6	5.7	0.0	1.5	0.0
8.0	11.0	2.0	8.0	0.5	0.1	0.1			8.0		0.8	
34.4	66.1	7.8	29.5	2.0	0.3	0.3	512.0	0.0	13.9	0.3	15.0	
4.7	10.2	1.3	4.4	0.3	0.1	0.1	67.7	0.3	0.3	0.1	2.5	
13.6	15.4	16.3	14.8	12.5	22.6	19.6	13.2	1002.8	2.4	17.5	16.8	
-4.7	-8.3	-0.9	-3.6	-0.2	0.0	0.0	-142.2	-0.2	-1.7	-0.2	-5.9	
3.7	6.2	0.9	3.5	0.8	0.1	0.1	100.9	-0.2	3.6	0.2	0.8	
0.03	**7.49**	**1.38**	**5.60**	**5.52**	**0.10**	**4.93**			**1.61**		**0.49**	
8.02	5.70	1.03	4.04	4.40	0.17	3.58			6.86		1.15	
0.0041	1.3148	1.3434	1.3863	1.2537	0.5823	1.3747			0.2350		0.4291	
0.41	**131.48**	**134.34**	**138.63**	**125.37**	**58.23**	**137.47**			**23.50**		**42.91**	

PPM Rock
Run = 1026
FileName = Apr07121
Sample ROS - Calibration SRS-XRF point analyses

D.Harazim, Apr07121; RUN = 1026

Name	Li	Rb	Sr	Y	Zr	Nb	Mo	Cs
Host sediment, sample 1 (ppm)	28.82	143.67	221.55	14.54	48.67	8.50	1.25	5.99
1 sigma (ppm)	0.14	13.36	3.36	4.96	2.75	0.00	0.00	0.27
Host sediment, sample 2 (ppm)	35.39	143.52	235.36	20.55	65.75	9.38	0.99	7.36
1 sigma (ppm)	0.17	13.35	3.57	7.01	3.72	0.00	0.00	0.33
HALO (ppm)	28.89	119.94	222.67	15.79	44.70	9.76	0.97	5.78
1 sigma (ppm)	0.14	11.16	3.38	5.39	2.53	0.00	0.00	0.26
PHYCO CORE (ppm)	44.24	175.31	185.41	25.52	79.79	12.68	1.89	10.06
1 sigma (ppm)	0.22	16.31	2.81	8.71	4.51	0.00	0.00	0.45
FER-4 standard (4-run average)	6.95	18.25	63.34	4.89	19.50	1.61	1.70	0.66
FER-4 published (GeoREM)	7.00	16.00	62.00	8.00	18.00	1.50		0.70
Host sediment average (ppm)	32.104	143.597	228.458	17.544	57.214	8.942	1.120	6.673
Host sediment average dev (ppm)	3.282	0.076	6.906	3.003	8.540	0.441	0.132	0.684
Host sediment average dev (%)	10.2	0.1	3.0	17.1	14.9	4.9	11.8	10.2
HALO Excess (ppm)	-3.218	-23.660	-5.788	-1.751	-12.516	0.821	-0.151	-0.889
PHYCO CORE Excess (ppm)	12.133	31.710	-43.046	7.980	22.578	3.737	0.770	3.390
Error calculation based on FER-4 published values								
Stdev (1 sigma, ppm)	**0.03**	**1.59**	**0.95**	**2.20**	**1.06**			**0.03**
Average (ppm)	6.976	17.126	62.672	6.445	18.750			0.679
Stdev (1 sigma)	0.0049003	0.0930093	0.0151651	0.341252	0.0565593			0.0445749
Stdev (1 sigma, %)	**0.49**	**9.30**	**1.52**	**34.13**	**5.66**			**4.46**

07. Apr 2011 14:36

Ba	La	Ce	Pr	Nd	Sm	Eu	Gd	Tb	Dy	Ho	Er	Tm
992.12	29.01	55.09	6.61	24.74	4.53	1.08	3.80	0.56	3.27	0.60	1.66	0.24
24.82	0.65	0.00	0.00	0.00	0.09	0.00	0.00	0.00	0.00	0.00	0.00	0.00
1098.01	38.83	77.44	9.17	35.02	6.68	1.27	5.53	0.78	4.42	0.83	2.13	0.31
27.46	0.87	0.00	0.00	0.00	0.13	0.00	0.00	0.00	0.00	0.00	0.00	0.00
977.25	28.69	56.72	6.85	25.95	4.97	1.12	4.14	0.61	3.37	0.63	1.67	0.24
24.44	0.65	0.00	0.00	0.00	0.10	0.00	0.00	0.00	0.00	0.00	0.00	0.00
984.96	37.35	68.83	8.46	33.21	6.52	1.37	5.80	0.84	4.92	0.92	2.60	0.36
24.64	0.84	0.00	0.00	0.00	0.13	0.00	0.00	0.00	0.00	0.00	0.00	0.00
39.68	8.26	13.04	1.68	7.73	2.14	0.66	1.05	0.13	0.80	0.14	0.44	0.09
38.30	8.00	11.00	2.00	8.00	2.20	0.74	1.10	0.15	1.00	0.20	0.50	0.09
1045.064	33.918	66.268	7.891	29.880	5.605	1.175	4.667	0.669	3.845	0.711	1.895	0.275
52.946	4.908	11.173	1.278	5.142	1.076	0.099	0.865	0.110	0.574	0.114	0.231	0.033
5.1	14.5	16.9	16.2	17.2	19.2	8.4	18.5	16.4	14.9	16.1	12.2	12.2
-67.819	-5.228	-9.543	-1.041	-3.925	-0.638	-0.053	-0.524	-0.062	-0.475	-0.078	-0.220	-0.040
-60.102	3.431	2.566	0.570	3.326	0.917	0.195	1.136	0.172	1.075	0.207	0.703	0.085
0.98	**0.18**				**0.04**							
38.990	8.129				2.170							
0.02501283	0.0225273				0.0194377							
2.50	**2.25**				**1.94**							

Yb	Lu	Hf	Ta	Tl	Pb	Bi	Th	U	Dil(G/KG)
1.43	0.21	1.83	0.31	0.77	13.78	0.27	19.72	2.87	0.09
0.00	0.00	0.00	0.00	0.00	0.64	0.00	0.00	0.00	
1.80	0.26	2.10	0.35	0.77	13.82	0.30	13.15	3.04	0.10
0.00	0.00	0.00	0.00	0.00	0.64	0.00	0.00	0.00	
1.54	0.21	1.61	0.67	0.61	12.73	0.20	9.12	2.35	0.10
0.00	0.00	0.00	0.00	0.00	0.59	0.00	0.00	0.00	
2.23	0.36	2.64	0.41	0.95	15.97	0.73	15.63	4.42	0.09
0.00	0.00	0.00	0.00	0.00	0.74	0.00	0.00	0.00	
0.44	0.07	0.61	0.09	0.16	8.54	0.07	1.38	0.47	
0.60	0.10	0.50	0.11	0.80	8.00		0.80	0.50	FER-4 GeoREM
1.615	0.232	1.962	0.328	0.768	13.795	0.287	16.434	2.957	
0.187	0.025	0.136	0.023	0.002	0.020	0.016	3.285	0.085	
11.6	10.6	6.9	6.9	0.2	0.1	5.5	20.0	2.9	
-0.076	-0.026	-0.355	0.344	-0.156	-1.061	-0.088	-7.311	-0.605	
0.617	0.124	0.675	0.082	0.177	2.170	0.442	-0.808	1.462	

0.38
8.270
0.0461948
4.62

APPENDIX F

Chemical elemental maps obtained by Synchrotron Rapid Scanning X-ray Fluorescence (SRS-XRF)

This figure shows two-dimensional elemental maps of sample ROS1. These data are presented in my fourth thesis chapter. Non-destructive synchrotron X-ray fluorescence (SRS-XRF) imaging was performed at wiggler beam line 6-2 at the Stanford Synchrotron Radiation Lightsource (SSRL, CA, USA). Elemental maps were acquired with incident beam energies of 12 and 3.15 KeV for imaging of high and low atomic weight elements (respectively) and a beam spot size of 100 microns. For low atomic weight elements element imaging, samples are enclosed within a helium atmosphere to avoid the X-ray absorption and scattering effects of air at lower incident beam energy. Photon flux was within10^{10} and 10^{11} photons s^{-1}. Exact sampling locations are given in Appendix D.

.

Sample ROS 1 (Pelican Pt. 0.3 m)

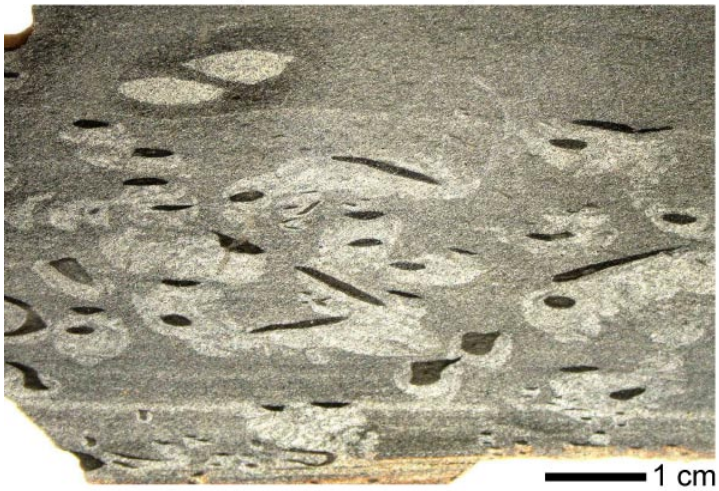

K
Ca
Zn
Ti KA
As
Ga
Mn
Cr
Fe

Ca
Cl
Si
S
Al
P

APPENDIX G

Elemental quantification of chemical elemental maps via Synchrotron Rapid Scanning X-ray Fluorescence (SRS-XRF)

This table contains point analyses parameters and calculated concentrations for trace elements obtained on wiggler beamline 6-2 at SSRL. Point analyses were obtained from host sediment, halo and burrow core of phycosiphoniform burrows by driving the rapid scanning stage to locations of interest defined by the previously acquired maps. The elemental maps have been quantified using a combination of ICP-MS analyses and SRS-XRF point analyses. The elemental concentration (ppm) of major and trace elements have been were claculated through curve fitting procedures using the freely available software PyMCA. Anorthite has been used as reference mineral to calibrate peak intensities of all measured elements, since it closely mirrors the original sediment composition of sample ROS1. Due to imprecision in detector distance as well as due to imperfect knowledge of the sediment matrix composition at each measurement point, total errors on the XRF point analyses tend to be larger than ICP-MS measurements. Only sulfur has been calculated via XRF point analyses, using an in-house barite standard (see Figure G-1 for exact measurement locations).

The quantification of individual point spectra has been performed post-scanning using the newly collected elemental images as a guide. Separate counts were obtained (~200 seconds) acquiring a full energy dispersive spectrum. Due to the significant compositional heterogeneity of most geological materials errors are ~30 % for high atomic number elements and ~50 % for light elements. This affects low atomic weight elements (i.e. Ca and below) in particular (see Appendix E).

Sample ROS1 (Pelican Pt. 0.3 m)

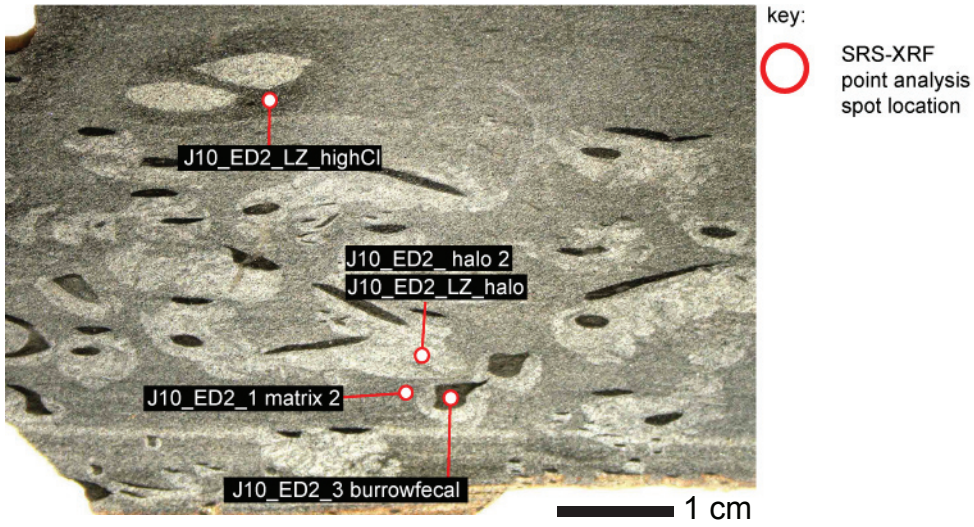

ICP-MS			Flux = 7e10, Detector Distance = 120mm
	Host sediment, sample 1	Host sediment, sample 2	ed2 matrix 2 (An)
Ca	15001.1	14593.4	3836.0
Ti	3886.4	4230.0	1195.0
V	110.8	134.6	66.7
Cr	67.9	82.2	0.0
Mn	266.4	286.2	73.4
Fe	22691.0	26735.9	20850.0
Co	62.3	82.4	-
Ni	25.6	37.3	95.2
Cu	41.8	48.0	30.6
Zn	74.7	130.9	77.3
As	11.7	16.3	16.6

Barite optimization		
	ed7 barite	Reference Concentration
Ba	438100.00	590000.00
S	160800.00	137400.00
		Uses recorded
	Barite HZ.cfg	Uses recorded
	Barite LZ.cfg	
	For HZ:	Barite HZ optimised.cfg
	Det. Dist. error	5.40%
	Flux error	14.30%
	For LZ (flux=1.	Barite LZ optimise.cfg
	Det. Dist. Error	Measured accurately
	Flux error	16.66%

Barite Optimised Parameters	Flux = 6e10, Detector Distance = 126.5mm	absolute error %
ed2 matrix 2 (An)	ed2 matrix 2 (An)	ed2 matrix 2 (An)
5333.0	1497.0	28.07
1614.0	419.0	25.96
87.5	20.8	23.81
0.0	0.0	
97.1	23.7	24.37
27410.0	6560.0	23.93
-		
124.4	29.2	23.50
40.0	9.4	23.39
100.8	23.5	23.29
21.6	5.0	23.27

	ICP-MS		Flux = 6e10, Detector Distance = 126.5mm Barite Optimised Parameters						
		Halo	ed2 halo 2 (An)		ed2 matrix 2 (An)		ed2 halo 2 (An)	ed2 halo 2 (An)	ed2 halo 2 (An)
Ca		15089.4	4870.0		5333.0		6769.0	1899.0	28.05
Ti		3896.9	1215.0		1614.0		1641.0	426.0	25.96
V		107.7	1.7		87.5		0.6	-1.1	23.32
Cr		62.7	0.0		0.0		0.0	0.0	-177.50
Mn		268.4	23.8		97.1		31.6	7.8	24.64
Fe		22529.2	20160.0		27410.0		22650.0	2490.0	10.99
Co		44.4	-		-		-	-	-
Ni		28.4	82.1		124.4		107.3	25.2	23.50
Cu		44.6	36.3		40.0		47.4	11.1	23.40
Zn		90.2	57.1		100.8		74.5	17.4	23.32
As		9.6	3.3		21.6		4.3	1.0	23.89

	ICP-MS		Flux = 6e10, Detector Distance = 126.5mm Barite Optimised Parameters						
		Phyco Core	ed2 burrowfecal (An)		ed2 halo 2 (An)		ed2 burrowfecal (An)	ed2 burrowfecal (An)	ed2 burrowfecal (An)
Ca		24746.2	1465.0		6769.0		2029.0	564.0	27.80
Ti		5863.0	1880.0		1641.0		2537.0	657.0	25.90
V		227.3	0.0		0.6		0.0	0.0	-
Cr		141.6	0.0		0.0		0.0	0.0	-
Mn		372.1	0.0		31.6		0.0	0.0	-
Fe		40077.1	34050.0		22650.0		44770.0	10720.0	23.94
Co		137.3	-		-		-	-	-
Ni		56.6	313.1		107.3		409.4	96.3	23.52
Cu		72.4	91.0		47.4		118.8	27.8	23.38
Zn		138.6	141.1		74.5		184.0	42.9	23.32
As		26.0	14.3		4.3		18.7	4.4	23.37

Barite optimization		
	ed7 barite	**Reference Concentration**
Ba	438100.00	590000.00
S	160800.00	137400.00
		Uses recorded
	Barite HZ.cfg	Uses recorded
	Barite LZ.cfg	
	For HZ:	Barite HZ optimised.cfg
	Det. Dist. error	5.40%
	Flux error	14.30%
	For LZ (flux=1.89e9)**:**	Barite LZ optimise.cfg
	Det. Dist. Error	Measured accurately
	Flux error	16.66%

Element	**Recorded Parameters**		**Barite Optimised Parameters**					
	Flux = 1.62e9, Detector Distance 9.28mm		Flux = 1.89e9, Det. Dist. = 10.33		Det. Dist. = 9.28 Optimized minus Recorded		% error	
S	ed2_lz_highcl (An)	ed2_lz_halo (An)	ed2_lz_highcl (An)	ed2_lz_halo (An)	ed2_lz_highcl (An)	ed2_lz_halo (An)	ed2_lz_highcl (An)	ed2_lz_halo (An)
	1139.0	41.3	976.6	35.4	-162.4	-5.9	-16.6	-16.7

APPENDIX H

Phase identification via X-Ray Diffractometry (XRD)

Appendix H contains the phases identified via X-ray diffractometry for phycosiphioniform halo and core as well as host sediment on sample ROS1 (see Appendix F). All samples were analyzed in triplicates. In order to identify the mineral phases present in different portions of the burrowed sediment, samples were obtained from the host sediment, halo and core and analysed with a Rigaku Ultima IV X-ray diffractometer (Rigaku Systems®, Tokyo, Japan) using monochromatic Cu–Kα radiation. The X-ray diffractometer was operated at 40 kV and 44 mA current, using a scintillation counter (1 mm divergent slit, 0.6 mm detector slit, 1.0 mm anti-scatter slit and a graphite monochromator). Samples were scanned with a step size of 0.02° and a count time of 2 s per step. All samples were analyzed in air-dried state.

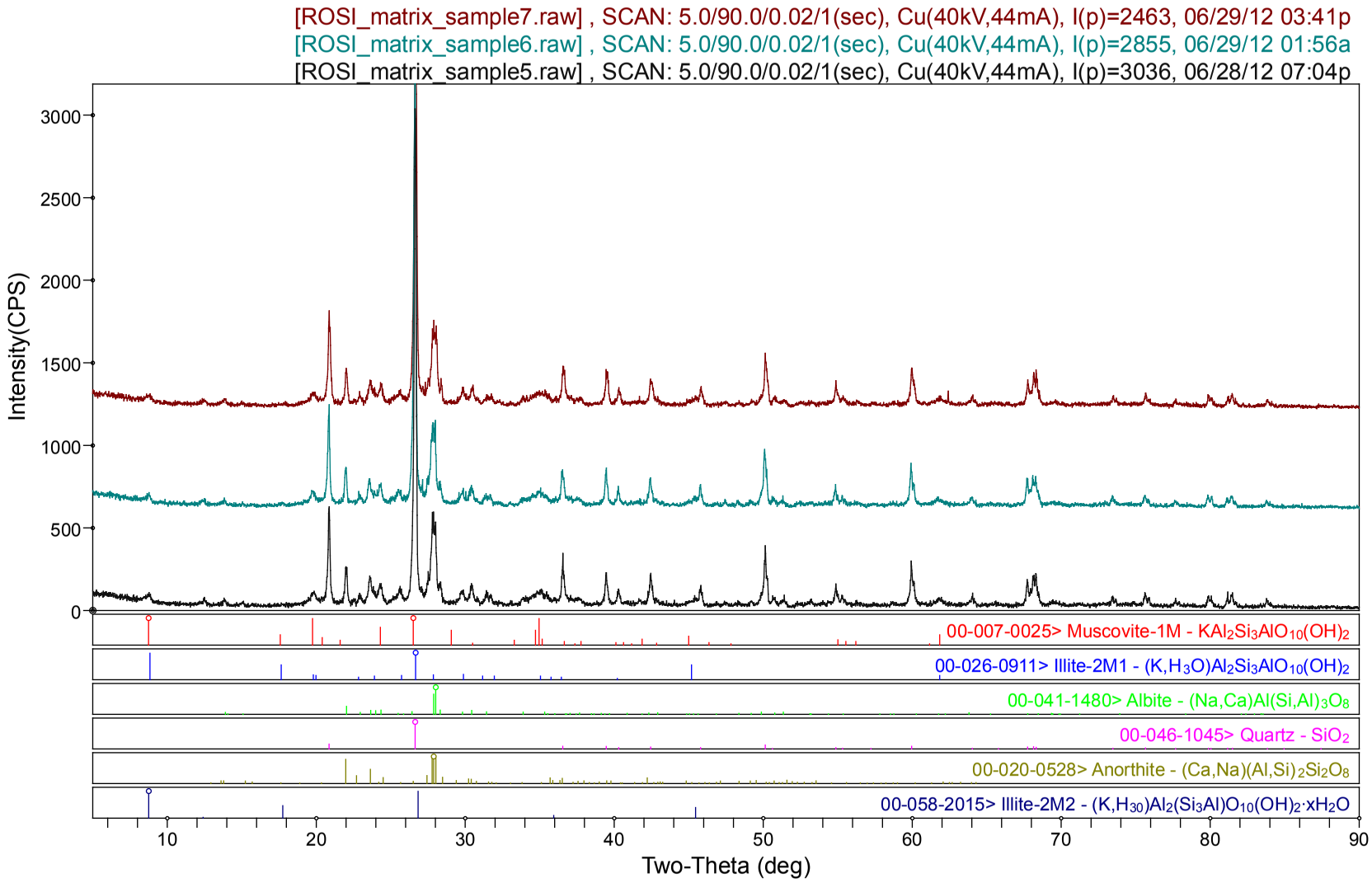
[ROSI_matrix_sample7.raw] , SCAN: 5.0/90.0/0.02/1(sec), Cu(40kV,44mA), I(p)=2463, 06/29/12 03:41p
[ROSI_matrix_sample6.raw] , SCAN: 5.0/90.0/0.02/1(sec), Cu(40kV,44mA), I(p)=2855, 06/29/12 01:56a
[ROSI_matrix_sample5.raw] , SCAN: 5.0/90.0/0.02/1(sec), Cu(40kV,44mA), I(p)=3036, 06/28/12 07:04p
Intensity(CPS)
3000
2500
2000
1500
1000
500
0
00-007-0025> Muscovite-1M - KAl2Si3AlO10(OH)2
00-026-0911> Illite-2M1 - (K,H3O)Al2Si3AlO10(OH)2
00-041-1480> Albite - (Na,Ca)Al(Si,Al)3O8
00-046-1045> Quartz - SiO2
00-020-0528> Anorthite - (Ca,Na)(Al,Si)2Si2O8
00-058-2015> Illite-2M2 - (K,H30)Al2(Si3Al)O10(OH)2·xH2O
10
20
30
40
50
60
70
80
90
Two-Theta (deg)

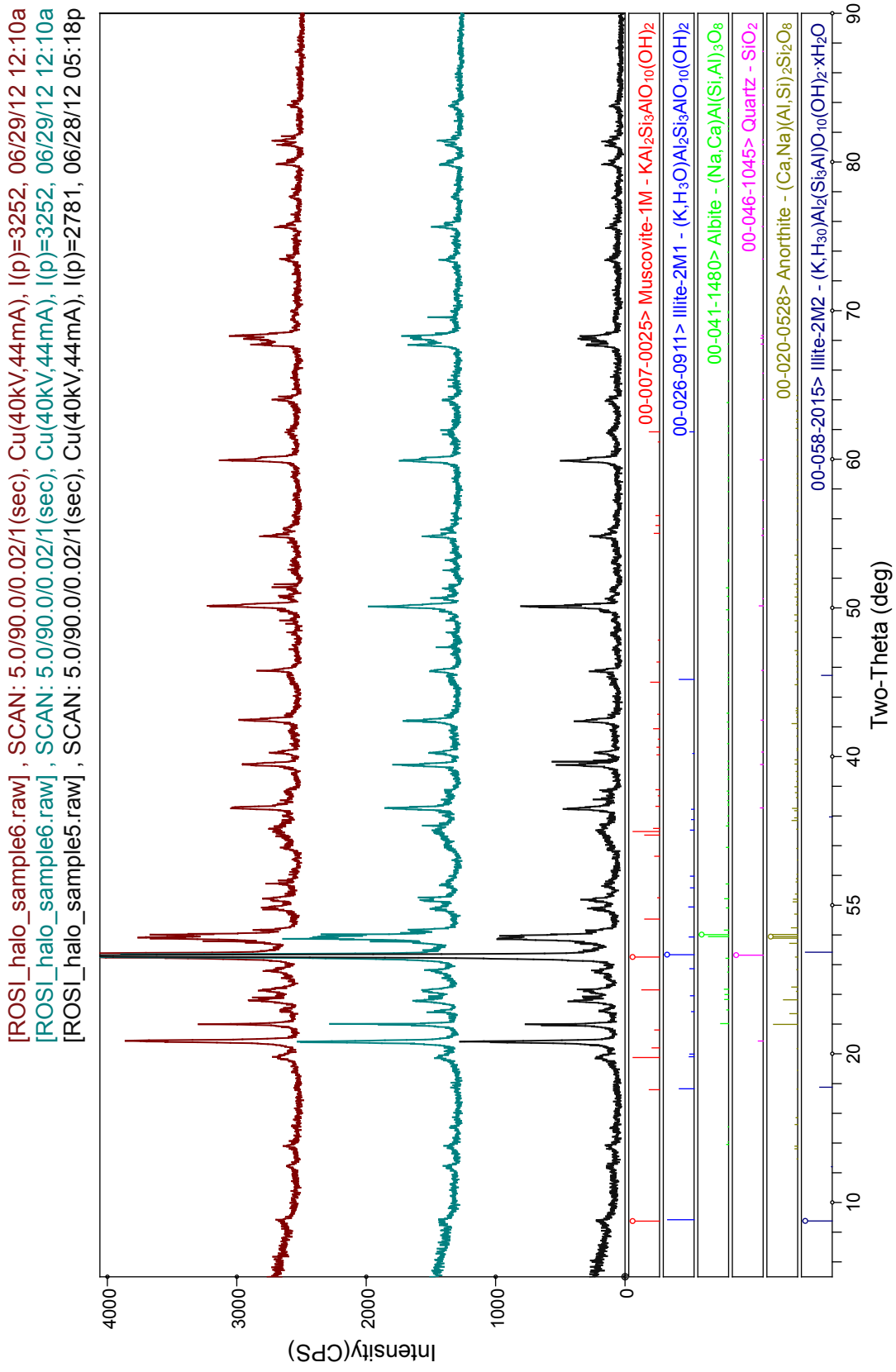
[ROSI_halo_sample6.raw] , SCAN: 5.0/90.0/0.02/1(sec), Cu(40kV,44mA), I(p)=3252, 06/29/12 12:10a
[ROSI_halo_sample6.raw] , SCAN: 5.0/90.0/0.02/1(sec), Cu(40kV,44mA), I(p)=3252, 06/29/12 12:10a
[ROSI_halo_sample5.raw] , SCAN: 5.0/90.0/0.02/1(sec), Cu(40kV,44mA), I(p)=2781, 06/28/12 05:18p
Intensity(CPS)
Two-Theta (deg)
00-007-0025> Muscovite-1M - KAl2Si3AlO10(OH)2
00-026-0911> Illite-2M1 - (K,H3O)Al2Si3AlO10(OH)2
00-041-1480> Albite - (Na,Ca)Al(Si,Al)3O8
00-046-1045> Quartz - SiO2
00-020-0528> Anorthite - (Ca,Na)(Al,Si)2Si2O8
00-058-2015> Illite-2M2 - (K,H30)Al2(Si3Al)O10(OH)2·xH2O

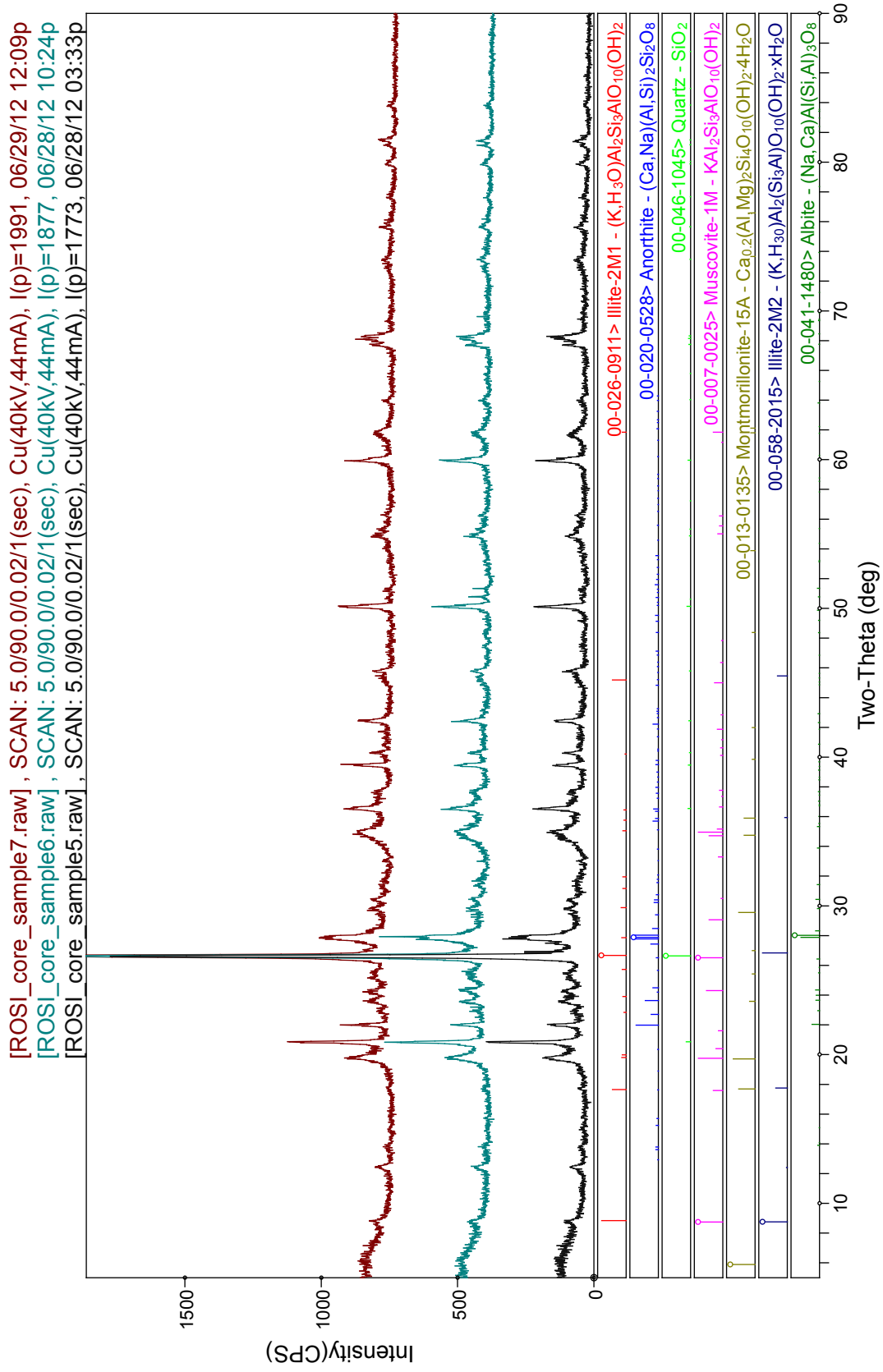
[ROSI_core_sample7.raw] , SCAN: 5.0/90.0/0.02/1(sec), Cu(40kV,44mA), I(p)=1991, 06/29/12 12:09p
[ROSI_core_sample6.raw] , SCAN: 5.0/90.0/0.02/1(sec), Cu(40kV,44mA), I(p)=1877, 06/28/12 10:24p
[ROSI_core_sample5.raw] , SCAN: 5.0/90.0/0.02/1(sec), Cu(40kV,44mA), I(p)=1773, 06/28/12 03:33p
Intensity(CPS)
1500
1000
500
0
Two-Theta (deg)
10
20
30
40
50
60
70
80
90
00-026-0911> Illite-2M1 - (K,H3O)Al2Si3AlO10(OH)2
00-020-0528> Anorthite - (Ca,Na)(Al,Si)2Si2O8
00-046-1045> Quartz - SiO2
00-007-0025> Muscovite-1M - KAl2Si3AlO10(OH)2
00-013-0135> Montmorillonite-15A - Ca0.2(Al,Mg)2Si4O10(OH)2·4H2O
00-058-2015> Illite-2M2 - (K,H30)Al2(Si3Al)O10(OH)2·xH2O
00-041-1480> Albite - (Na,Ca)Al(Si,Al)3O8

APPENDIX I

Phase identification via Fourier Transform Infrared Spectroscopy (FTIR)

Appendix I contains FTIR spectra for phases identified from host sediment, halo and core of sample ROS1. Samples were ground in an agate mortar for ~1 minute. The sample material was diluted with KBr (Sigma Aldrich, FTIR-grade). The sample-KBr mixture was then pressed at 10 tons to allow KBr and sample to crystallize as an IR transparent matrix (see Blanch et al. 2007 and Poduska et al. 2011). Infrared spectra have been obtained using a Bruker® Alpha FTIR Spectrometer (Bruker Corporation, Billerica, MA, USA). The FTIR measurements were carried out in transmission geometry (Nicolet 380, 4 cm^{-1} resolution).

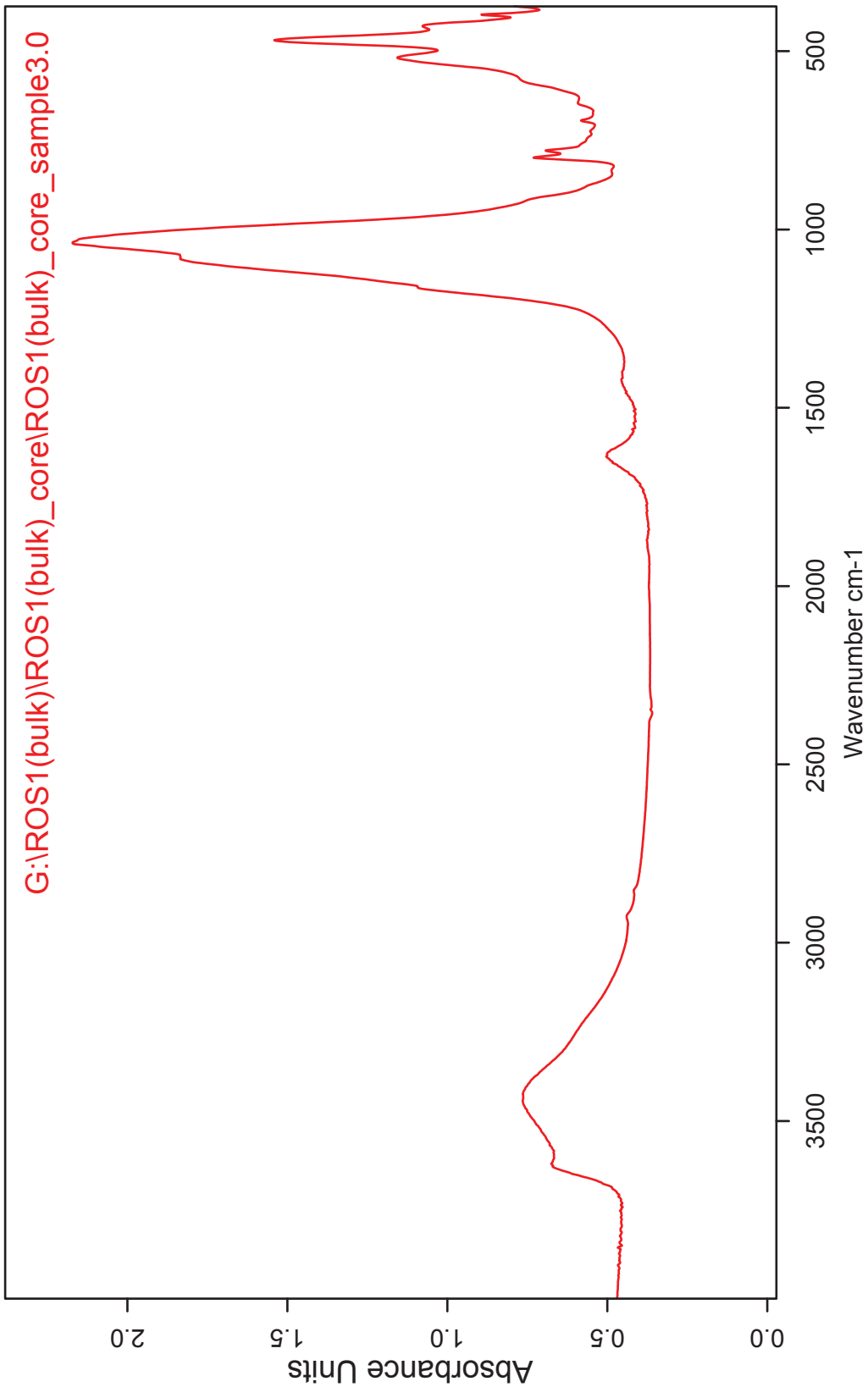
G:\ROS1(bulk)\ROS1(bulk)_core\ROS1(bulk)_core_sample3.0
Absorbance Units
0.0
0.5
1.0
1.5
2.0
Wavenumber cm-1
3500
3000
2500
2000
1500
1000
500

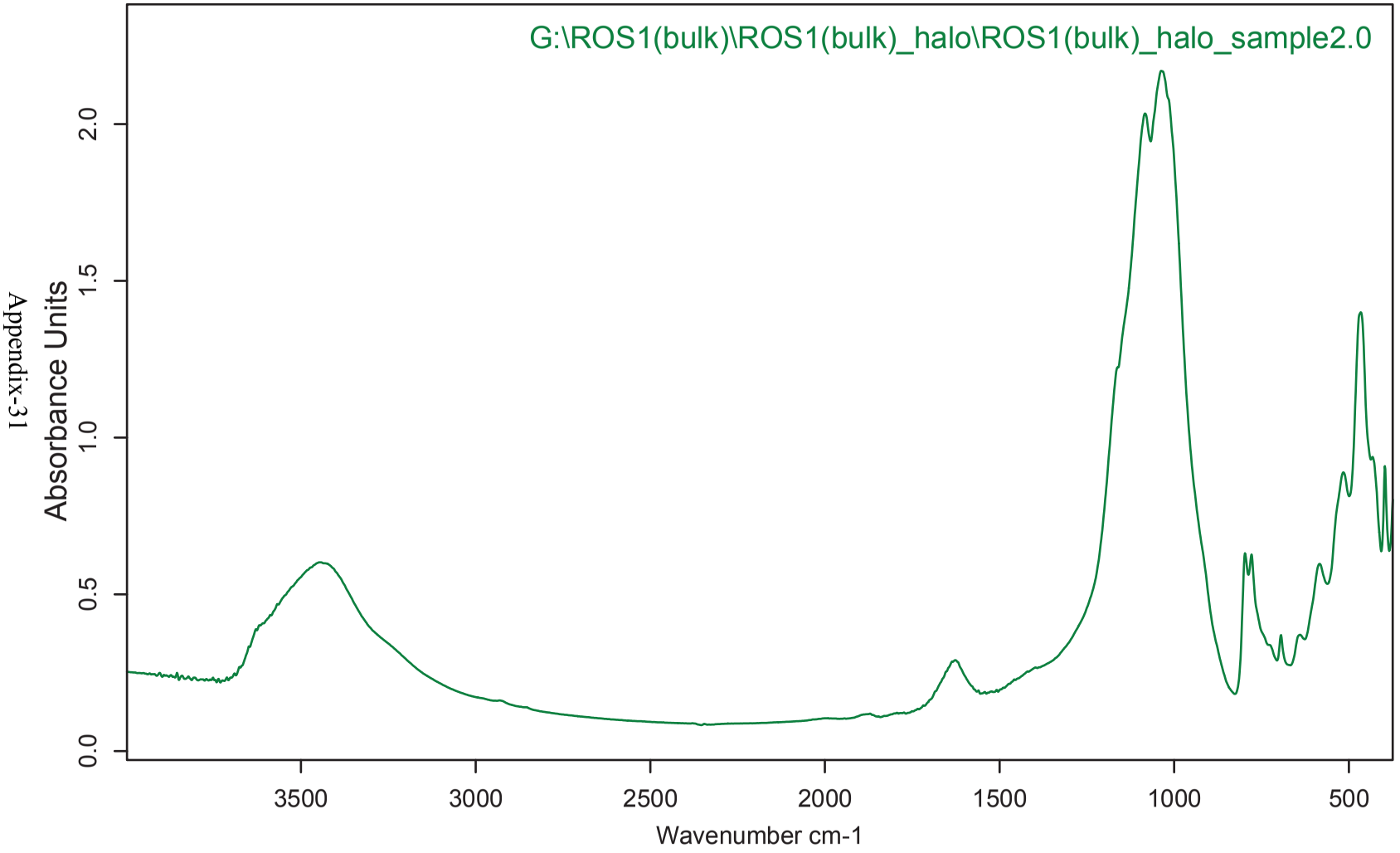
G:\ROS1(bulk)\ROS1(bulk)_halo\ROS1(bulk)_halo_sample2.0
Absorbance Units
0.0
0.5
1.0
1.5
2.0
3500
3000
2500
2000
1500
1000
500
Wavenumber cm-1

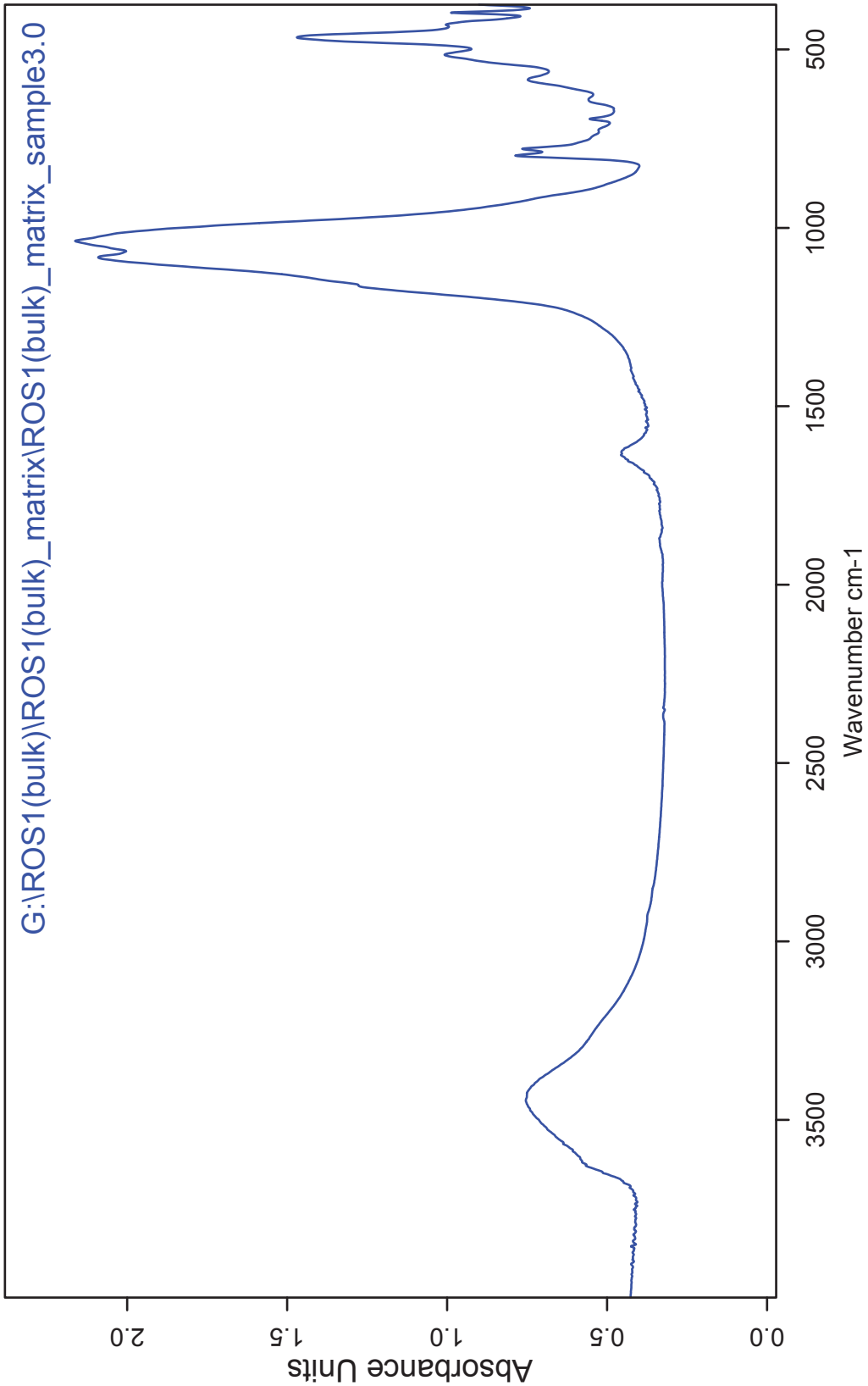
G:\ROS1(bulk)\ROS1(bulk)_matrix\ROS1(bulk)_matrix_sample3.0
Absorbance Units
0.0
0.5
1.0
1.5
2.0
Wavenumber cm-1
3500
3000
2500
2000
1500
1000
500